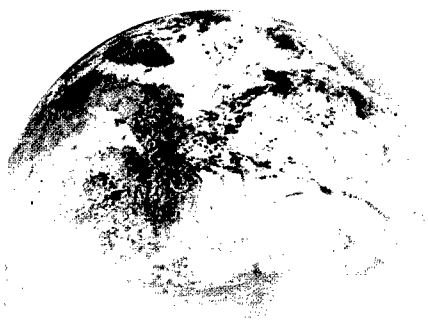


U.S. - RUSSIAN SECOND SPACE SURVEILLANCE WORKSHOP

4 - 6 JULY
1996

Poznań
Poland



Editors:

P. Kenneth Seidelmann
U.S. Naval Observatory

Iwona Wytryszczak
Adam Mickiewicz University

Bernard Kaufman
Naval Research Laboratory

DISTRIBUTION STATEMENT 2

Approved for public release
Distribution Unlimited

19961126 036

REPORT DOCUMENTATION PAGE

Form Approved OMB No. 0704-0188

Public reporting burden for this collection of information is estimated to average 1 hour per response, including the time for reviewing instructions, searching existing data sources, gathering and maintaining the data needed, and completing and reviewing the collection of information. Send comments regarding this burden estimate or any other aspect of this collection of information, including suggestions for reducing this burden to Washington Headquarters Services, Directorate for Information Operations and Reports, 1215 Jefferson Davis Highway, Suite 1204, Arlington, VA 22202-4302, and to the Office of Management and Budget, Paperwork Reduction Project (0704-0188), Washington, DC 20503.

1. AGENCY USE ONLY (Leave blank)		2. REPORT DATE August 1996	3. REPORT TYPE AND DATES COVERED Conference Proceedings, 4-6 July 1996	
4. TITLE AND SUBTITLE U.S. - Russian Second Space Surveillance Workshop			5. FUNDING NUMBERS CSP-96-1052	
6. AUTHOR(S) P. Kenneth Seidelmann, Iwona Wyrzyszcak, Bernard Kaufman				
7. PERFORMING ORGANIZATION NAME(S) AND ADDRESS(ES) Adam Mickiewicz University Poznan, Poland			8. PERFORMING ORGANIZATION REPORT NUMBER	
9. SPONSORING/MONITORING AGENCY NAME(S) AND ADDRESS(ES) EOARD PSC 802 BOX 14 FPO AE 09499-0200			10. SPONSORING/MONITORING AGENCY REPORT NUMBER CSP-96-1052	
11. SUPPLEMENTARY NOTES				
12a. DISTRIBUTION/AVAILABILITY STATEMENT Unlimited			12b. DISTRIBUTION CODE	
13. ABSTRACT (Maximum 200 words) Conference Proceedings for the U.S. - Russian Second Space Surveillance Workshop in Poznan, Poland, 4-6 July 1996.				
14. SUBJECT TERMS			15. NUMBER OF PAGES 255	
			16. PRICE CODE	
17. SECURITY CLASSIFICATION OF REPORT UNCLASSIFIED	18. SECURITY CLASSIFICATION OF THIS PAGE UNCLASSIFIED	19. SECURITY CLASSIFICATION OF ABSTRACT UNCLASSIFIED	20. LIMITATION OF ABSTRACT UL	

NSN 7540-01-280-5500

Standard Form 298 (Rev. 2-89)
Prescribed by ANSI Std. Z39-18
298-102

TABLE OF CONTENTS

Preface	4
<i>A. I. Nazarenko and G. M. Cherniavskiy</i>	
Evaluation of the Accuracy of Forecasting Satellite Motion in the Atmosphere	6
<i>A. I. Nazarenko</i>	
Technology of Evaluation of Atmosphere Density Variation Based on the Space Surveillance System's Orbital Data	18
<i>T. Amelina, G. Batyr, V. Dicky, N. Tumolskaya, and V. Yurasov</i>	
Comparison of Atmosphere Density Models.....	34
<i>V. F. Boikov</i>	
The Features of Prediction Procedures, Used in Low-perigee Satellites' Catalog Maintenance	42
<i>S. Coffey and H. Neal</i>	
Applications of Parallel Processing to Astrodynamics	56
<i>P. W. Schumacher and R. A. Glover</i>	
Analytical Orbit Model for U. S. Naval Space Surveillance: an Overview	66
<i>V. F. Boikov</i>	
Techniques of Orbit Determination Using Minimum Data, Accounting of the Features of Russian Space Surveillance System	106
<i>V. Andrewschenko, G. Batyr, V. Bratchikov, V. Dicky, S. Veniaminov and V. Yurasov</i>	
Reentry Time Determination Analysis for „Cosmos-398” and FSW-1-5	120
<i>V. Yurasov and A. Moscovsky</i>	
Geostationary Orbit Determination and Prediction	132
<i>R. I. Kiladze and A. S. Sochilina</i>	
On Orbital Evolution of Geostationary Satellites	150
<i>Z. Khutrovsky</i>	
Low-perigee Satellite Catalog Maintenance: Issues of Methodology	156
<i>P. Schumacher</i>	
Tracking Satellite Breakups	174

<i>V. Yurasov</i>	
Universal Semianalytic Satellite Motion Propagation Method	198
<i>P. J. Cefola and R. J. Prolux (Drape Lab.)</i>	
Current Development of the Precision Semianalytical Satellite Theory	212
Summary and Conclusions	252
List of Participants	254

PREFACE

Following some initial contact between the Naval Space Command and the Scientific Research Center "Kosmos" in Moscow in 1993, the first U.S. Russian Space Surveillance Workshop was hosted by the U.S. Naval Observatory in July 1994. This initial workshop led to the suggestion for the second workshop.

The second U.S. Russian Space Surveillance Workshop was planned and scheduled to coincide with IAU Colloquium 165 on the Astrometry and Dynamics of Natural and Artificial Celestial Bodies held in Poznań, Poland 1-5 July 1996. The workshop had a common program on 4 July and a separate program on 5 and 6 July. The proceedings of Colloquium 165 are being published separately by Kluwer Academic Publishers and edited by Drs. Wytrzyszczak, Lieske, and Mignard. The papers from this workshop are enclosed as separate proceedings. Special attention should be given to the summary and conclusions from the workshop.

Translations for the workshop were handled by astronomers Dr. Alexander Krivov of St. Petersburg University and Dr. Sergei Rudenko of the Main Astronomical Observatory of Kiev. The excellent performance of these translators significantly contributed to the success of the workshop and proved to be a major improvement over the professional translators used at the first workshop in Washington.

The excellent local arrangements and administrative matters for the workshop were handled by Dr. Iwona Wytrzyszczak. Particular thanks are due Mr. Marcin Gromadziński of the Astronomical Observatory in Poznań for the design and production of the cover for this proceedings volume.

We gratefully acknowledge the support of the Naval Research Laboratory, the United States Naval Observatory, the United States Air Force European Office of Aerospace Research and Development, the Office of Naval Research Europe, and the United States Army Research and Development Standardization Group, Europe, for their contribution to the success of this workshop.

These workshops have demonstrated a progression in improved communication, and the benefits both countries can achieve from learning from the other. As a Russian commented, "God has provided only one truth; the two countries are approaching that truth by different paths." The Russian delegation invited the participants to the next workshop in Moscow in 1997. The benefits of the continuation of the dialogue are hopefully evident to all, and subsequent workshops are strongly recommended.

P. K. Seidelmann

Evaluation of the Accuracy of Forecasting Satellite Motion in the Atmosphere

1. Introduction

The problem of increasing the accuracy of forecasting the motion in the atmosphere arose since the time of launching of the first Soviet AES in 1957. The practice of forecasting the motion of early satellites has shown high roughness of the upper atmosphere knowledge at that time (possible differences in the density amounted several times).

As early as at the end of fifties it was shown (M.L.Lidov, "ISZ", iss. 1, 1958; P.E.Elyasberg, "ISZ", iss. 1, 1958) that the upper atmosphere density (UAD) values can actually be updated from the satellite drag data. This fundamental result greatly influenced the methodology and results of constructing the UAD models. A further development of UAD models and an improvement of satellite motion models have occurred in parallel and interdependently. The increasing of UAD models accuracy gave rise to effective development of equations integration techniques and to the improvement of motion forecasting accuracy, which, in its turn, has allowed to rise a quality of UAD evaluations derived from the satellite drag.

The atmospheric drag is now taken into account in satellite motion forecasting by regular (in time) fulfillment of the following main operations:

- the use of the UAD model for calculating the drag (acceleration) of a satellite, w , at various points of trajectory

$$w = \rho \cdot k \cdot V^2, \quad (1)$$

where ρ is the atmospheric density, k is the ballistic factor, V is the satellite velocity with respect to air;

- the integration of the equations of satellite motion with taking into account the acceleration w ;

- the determination of ballistic factor k from the measurement data along with the six elements of the orbit.

There are some modifications and simplifications of the drag accounting technique, but they do not have principal character.

A noticeable feature of the development of UAD models and methods of forecasting the motion of low-altitude satellites is the fact, that, whereas considerable successes have been achieved in constructing the UAD models (the accuracy was increased by an order of magnitude), these "successes" are much more modest with respect to the models of motion. Even for two decades at least the generally accepted estimation of possible forecasting errors remains equal to 10 to 20 % of the atmospheric drag value over the

forecasting interval. What is the reason of such a delay in forecasting techniques development? This question may be answered by the detailed a priori and a posteriori analysis of forecasting errors. It is these issues, which are considered below in this report.

A characteristic feature of the applied technique of taking into account the atmospheric drag lies in the fact, that the estimation of factor k , obtained in orbit updating from measurement data, is in its essence the coefficient of concordance between the measurement data and the model (1). This circumstance is characterized by the following relationship:

$$\rho_{\text{real}} \cdot k_{\text{real}} \approx \rho_{\text{model}} \cdot k. \quad (2)$$

where the real and model values of quantities are marked by corresponding subscripts. This implies, that the estimation of k includes the influence of errors of the UAD model applied. It is also obvious, that the constant UAD model errors (i.e. the increase or decrease of the model density in comparison with the real one as much as several times) does not have any effect on the forecasting accuracy. These errors of the model are balanced by corresponding change in the estimation of k , so that equality (2) is hold. In the opposite case, i.e. when the $\rho_{\text{real}} / \rho_{\text{model}}$ ratio varies in time, equality (2) will not be hold, which will result in additional motion forecasting errors related with the inaccuracy of description of model density variation in time. So, the main attention in analyzing the forecasting errors for low-altitude satellites should be paid to the variability of atmospheric density in time.

2. *A posteriori accuracy estimation*

The below results have been outlined in papers [1, 2]. The accuracy estimation technique was as follows. The multiple forecasting of satellites motion was carried out. The initial and reference data were taken from the massif of orbital elements accumulated in the Russian Space Surveillance System. This massif was gathered in the year 1989 over the time interval from May 25 through September 20 during the PION satellites experiments. The massif consisted of 25000 sets of orbital elements determined for 64 satellites. The distribution of perigee heights of these satellites is given in Table 1.

Table 1. Distribution of the accumulated orbital data

Heights, km	150-200	200-250	250-300	300-350	350-400	400-450	450-500
Frequency	0.007	0.067	0.189	0.203	0.398	0.122	0.014

The geophysical situation over this time interval was characterized by the variation of solar activity factor $F_{10.7}$ within the range of 157 to 335 units and by the variation of three-hour geomagnetic activity indices k_p within the limits of 0 to 8 numbers.

The initial elements for predictions (including also the ballistic coefficient) were determined over the diurnal interval preceded the moment of

their estimation. With the use of the results predicted for 1 - 6 days' intervals discrepancies δt of the time of crossing the equator were estimated. Since the absolute meaning of discrepancies δt are changing within very broad limits (by 2 or 3 orders) depending on the prediction interval, the values of ballistic factors, altitudes and other factors, the errors were standardized in order to obtain a more homogenous bank of accuracy parameters:

$$\xi = \frac{\delta t}{\sqrt{2\sigma^2 + (0.1 \cdot \delta t_a)^2}} \quad (3)$$

Here σ^2 is the variance of errors of time determination under initial conditions, δt_a is disturbing influence of the atmosphere. Indicator (3) was chosen in such a way, that the values of σ_ξ were of the same order for various forecasting intervals.

For the forecasting intervals of the order of some days the condition $|0.1\delta t_a| \gg \sqrt{2} \cdot \sigma$ is fulfilled for low-altitude satellites. Since the error δt in the numerator of expression (3) has usually the order of 10 % of atmospheric disturbance δt_a , the variance of indicator (3) will not considerably differ from 1 in this case. Thus, under these conditions indicator (3) does not actually differ from the estimations expressed in fractions of atmospheric disturbance. The 10 % level of the root-mean-square (RMS) forecasting error corresponds to estimation $\sigma_\xi = 1$; the 20 % level of RMS error corresponds to $\sigma_\xi = 2$, e.t.c.

For short forecasting intervals, when $|0.1\delta t_a| < \sqrt{2} \cdot \sigma$, the estimation of σ_ξ will be of the same order, since in expression (3) the variance of a numerator is close to the square of a denominator: $E(\delta t^2) = 2\sigma^2$. This allows to avoid strong distortions of a traditional indicator for short forecasting intervals.

The forecasting of motion was performed with using the numerical-analytic algorithm developed by V.S.Yurasov [3]. This algorithm possesses rather high accuracy characteristics and high operation speed. This allowed to process a large orbital data mass for reasonable time. The atmospheric density was calculated in forecasting by using the dynamical model [4]. Three versions of techniques were applied for taking into account the solar and geomagnetic activity data, which correspond to different possibilities of taking into account the time variation of the atmospheric density. These versions are:
Version 1. Values of $F_{10.7}$ and k_p indices were supposed to be constant (the most widely spread technique).

Version 2. The current values of indices throughout the time interval were applied.

Version 3. Some corrections found by special technique [5, 6, 7] were added to the density calculated in accordance with point 1, namely:

$$\rho(t) = \rho_{\text{model}} \cdot \left(1 + \frac{\delta\rho}{\rho}(t)\right). \quad (4)$$

Each of three above-mentioned techniques was applied both on a forecasting interval and in updating the initial conditions (including the previous orbital data).

Let us consider the influence of forecasting interval within the range of 1 to 6 days on the indicator (3). The obtained experimental data (averaged over all considered satellites) are presented in Table 2.

Table 2. Values of indicator σ_ξ

Forecasting interval, days		1	2	3	4	5	6	On the average for 1 - 6 days
Technique	1	2.66	2.20	2.12	2.15	2.13	2.17	2.26
	2	1.52	1.27	1.17	1.19	1.20	1.23	1.27
	3	1.31	1.14	1.10	1.07	1.10	1.11	1.15
Number of implementations		858	914	774	814	658	714	4759

These data suggest, that the application of normalization (3) did not allow to exclude the influence of forecasting interval completely. However, the remaining influence is insignificant. Over the interval of 2 to 6 days the amplitude of scattering of indicator σ_ξ equals 2 to 4 % of the mean value. This deviation is more noticeable on the first day only: it reaches 15 to 20 % in this case. The applied technique strongly influences the level of errors. It is seen that for versions 2 and 3 the errors are 1.8 to 2.0 times lower than in version 1. This lowering is explained by taking into account the atmospheric density variations correlated with geomagnetic activity indices. It is also seen that the atmosphere model accuracy can be increased, if the variations are taken into account in a more complete manner.

Of considerable interest is to study, how does indicator σ_ξ depend on various factors. The analysis of experimental data has shown, that the main influencing factors are:

1. The satellite perigee height h . The influence of this factor follows from the well-known altitude dependence of atmospheric density variations correlated with indices $F_{10.7}$ and k_p [4].
2. The level of geomagnetic disturbances, which is proposed to be characterized by a sum of three-hour k_p - indices of geomagnetic disturbance $\sum k_p$ on a day interval preceded the moment of attributing initial conditions. The action of this factor is also associated with the well-known influence of geomagnetic disturbance on atmospheric density variations.

3. The relative time variability of satellites' ballistic factors. The influence of this factor is obvious in connection with the fact, that the drag force (1) is proportional to the ballistic factor. Quantitatively, this factor was characterized for each of considered satellites by the RMS value of relative discrepancies between current and mean values of ballistic factors:

$$\Delta = \frac{k - \bar{k}}{\bar{k}} - \frac{\delta p}{\rho}. \quad (5)$$

The σ_{Δ} values were found to be varied for various satellites within broad limits: from 0.001 to 0.30. This is explained by the diversity of geometric characteristics of satellites and by the variation of their position with respect to the velocity vector.

The obtained experimental data on forecasting errors in various conditions (for various values of influencing factors) were approximated by the dependence

$$\sigma_{\xi}(h, \Sigma k_p, \sigma_{\Delta}) = \bar{\sigma}_{\xi} \cdot f_{12}(h, \Sigma k_p) \cdot f_3(\sigma_{\Delta}). \quad (6)$$

The values of $\bar{\sigma}_{\xi}$ are presented in the right column of Table 1. Function $f_{12}(h, \Sigma k_p)$ were constructed for each of three versions of considered techniques. The $f_3(\sigma_{\Delta})$ function is common for all techniques. As a result, we have determined:

$$f_3(\sigma_{\Delta}) = 0.637 + 2.142 \cdot \sigma_{\Delta}. \quad (7)$$

The obtained estimations of coefficients of function (7) show that, as this factor varies within the aforementioned range of values the forecasting errors increase as much as 2 times.

The influence of first and second factors is characterized by the data of Table 3 which are calculated for the fixed value of the third factor ($\sigma_{\Delta}=0$).

Table 3 Values of factor $\sigma_{\xi}(h, \Sigma k_p) = \bar{\sigma}_{\xi} \cdot f_{12}(h, \Sigma k_p)$

Σk_p	Technique	Perigee height, km					
		160	200	240	280	320	360
10	1	0.58	0.73	0.87	1.02	1.17	1.31
	2	0.52	0.53	0.55	0.60	0.65	0.71
	3	0.57	0.48	0.46	0.51	0.63	0.81
25	1	1.01	1.25	1.51	1.78	2.01	2.27
	2	0.79	0.80	0.83	0.89	0.97	1.07
	3	0.73	0.62	0.59	0.65	0.80	1.04
40	1	1.58	1.97	2.36	2.76	3.15	3.55
	2	1.09	1.10	1.15	1.23	1.34	1.48
	3	0.98	0.83	0.79	0.87	1.07	1.39
55	1	2.07	2.59	3.11	3.63	4.15	4.66
	2	1.60	1.62	1.69	1.81	1.96	2.17
	3	1.32	1.12	1.07	1.19	1.46	1.88

The Table 3 data show that the RMS values of indicator (3) vary within broad limits: the maximum differs from the minimum 8; 4.2 and 4.0 time, respectively, for the techniques under consideration. It is natural, that the errors grow with the geomagnetic activity level (ΣK_p) and height h . The third version of techniques slightly declines from this rule. Here the altitude dependence has a minimum in the altitude range of 200 to 280 km, which is explained by a great amount of data on the variations at these altitudes and provides the highest effect: the three-fold increase of accuracy as compared to the first version of techniques.

At low altitudes and low solar activity level all techniques show about the same accuracy ($\sigma_\xi = 0.5 - 0.6$). Under these conditions the RMS forecasting error equals 5 to 6 % of the atmospheric disturbance value. At higher altitudes and for a considerable geomagnetic activity the difference between accuracies of techniques grows. The maximum values of factor σ_ξ are 4.7, 2.2 and 1.9 for the first, second and third technique, respectively. These quantities correspond to RMS estimations of forecasting errors equal to 47%, 22% and 19% of the atmospheric drag value, respectively.

3. *A priori estimation of accuracy*

The modern idea of the mechanism of appearance of the errors of forecasting the satellite motion in the atmosphere [1, 8] is based on the stochastic approach. As a source of errors, one considers the random process

$$\chi = \frac{\rho_{\text{real}} - \rho_{\text{model}}}{\rho_{\text{model}}}, \quad (8)$$

which reflects the deviations of actual density from the model one. The $\chi(t)$ process is usually assumed to be Gaussian, stationary one, which has a correlation function

$$K_\chi(t) = \sigma_\chi^2 \cdot \exp(-\alpha|t|), \quad (9)$$

where σ_χ^2 is the variance, α is the parameter, t is the time interval.

The content of known techniques of a priori estimation of the accuracy is reduced to re-calculating the influence of variations (8) on the time forecasting error. In so doing the determination of orbital parameters from the measurement data is carried out with using the well-known techniques (such as the least-square method, Kalman filter). In our opinion, this issue is outlined in the most compete manner in paper [1] of one of authors of this report. The main results of this paper are presented below.

In using three above-mentioned density calculation techniques, which differ in accounting the atmospheric density variations, the following values of

σ_χ and α parameters are recommended, which are determined from the a posteriori accuracy analysis:

Table 4. Values of parameter σ_χ

Σk_p	Technique	Perigee height, km					
		160	200	240	280	320	360
10	1	0.082	0.103	0.123	0.144	0.165	0.185
	2	0.073	0.075	0.078	0.084	0.092	0.100
	3	0.080	0.068	0.065	0.073	0.088	0.113
25	1	0.142	0.177	0.216	0.250	0.283	0.319
	2	0.111	0.116	0.118	0.125	0.136	0.150
	3	0.103	0.087	0.083	0.092	0.114	0.146
40	1	0.222	0.277	0.332	0.388	0.433	0.499
	2	0.154	0.156	0.162	0.173	0.188	0.208
	3	0.138	0.117	0.111	0.123	0.151	0.196
55	1	0.291	0.364	0.437	0.510	0.582	0.655
	2	0.225	0.228	0.237	0.254	0.275	0.305
	3	0.186	0.158	0.151	0.167	0.205	0.265

$\alpha = 0.24 \text{ 1/day} \approx 0.015 \text{ 1/revolution}$.

Some authors have successfully applied simplified equations of motion for evaluating the influence of disturbances on time parameters (the errors along the trajectory). In this case the state vector includes only the elements which characterize the motion in the plane of a near-circular orbit. Following this approach, we take the angular motion of a satellite in revolutions N as an argument, and as the state vector components we use the following elements: the time moment t_N corresponding to the trajectory point with the given latitude argument, and the period of revolution T_N . The following equations are valid for these variables:

$$\frac{dt_N}{dN} = T_N; \frac{dT_N}{dN} = \dot{T}. \quad (10)$$

Quantity \dot{T} has a meaning of period variation during one revolution. It is supposed to be associated with the atmospheric drag only. In this case (for constant k) the value of \dot{T} is proportional to the atmospheric density and, as follows from dependencies (1) and (8), may be presented as

$$\dot{T}(N) = \dot{T}_m \cdot (1 + \chi(N)), \quad (11)$$

where \dot{T}_m is the mean value, and $\chi(N)$ is the Gaussian random quantity having correlation function (9). The data source are supposed to be the direct measurements of time of trajectory points N_i :

$$z(N_i) = t(N_i) + v(N_i), \quad (i=1,2,\dots), \quad (12)$$

where the measurement error $\mathbf{v}(\mathbf{N}_i)$ (of discrete white noise type) is distributed according to the normal law with zero mathematic expectancy and variance σ^2 . The time interval between the measurement time moments is assumed to be constant and equal to ΔN (revolutions).

The above regularities of variation of time parameters (10), (11), the model of measurements (12) and statistic characteristics of random processes $\chi(\mathbf{N})$ and $\mathbf{v}(\mathbf{N}_i)$ allow to determine the correlation matrix of state vector errors and, in particular, the variance of errors of forecasting the time of intersection of the given latitude (the equator, for instance). The least errors are achieved with using the optimum algorithm of state vector estimation from measurements. In this case the Kalman-Bjucy discrete filter is optimal in the root-mean-square sense. Here, the forming filter

$$\frac{d\chi}{dN} = -\alpha \cdot \chi + \mathbf{w}, \quad (13)$$

is used for the "color" noise $\chi(\mathbf{N})$, where \mathbf{w} is the white noise. Here parameter α has the dimension of 1/revolution and equals ≈ 0.015 . Quantity $\chi(\mathbf{N})$ is assumed to be the third state vector component. As a result, the equations for a three-dimensional state vector \mathbf{x} are expressed as follows:

$$\frac{d\mathbf{x}}{dN} = \mathbf{A} \cdot \mathbf{x} + \mathbf{B} \cdot \mathbf{w}, \quad (14)$$

where $\mathbf{A} = \begin{bmatrix} 0 & 1 & 0 \\ 0 & 0 & 1 \\ 0 & 0 & -\alpha \end{bmatrix}, \mathbf{B} = \begin{bmatrix} 0 \\ 0 \\ \mathbf{T}_m \end{bmatrix}.$

The white noise intensity is determined by the relation $\sigma_w = \sqrt{2\alpha\sigma_\chi}$.

Now we shall apply for correlation matrices of vector $\mathbf{x}(\mathbf{N})$ at the $(i-1)$ th and i th steps of measurements processing the traditional designations: $\mathbf{P}_{i-1/i-1}$ and $\mathbf{P}_{i/i-1}$. These matrices are calculated from the well-known recurrent filter equations:

$$\mathbf{P}_{i/i-1} = \Phi(\Delta N)\mathbf{P}_{i-1/i-1}\Phi^T(\Delta N) + \int_{N_{i-1}}^{N_i} \Phi(N_i - \xi)\mathbf{B}\sigma_w^2\mathbf{B}^T\Phi^T(N_i - \xi) \cdot d\xi, \quad (15)$$

$$\mathbf{P}_{i/i} = (\mathbf{P}_{i/i-1}^{-1} + h^T\sigma^{-2}h)^{-1},$$

where $\Phi(\Delta N)$ is the fundamental matrix of solutions of equations (14), $h = \begin{bmatrix} 1 & 0 & 0 \end{bmatrix}.$

The correlation matrix of state vector at the correction time is determined from the condition of steady-state filtering regime

$P_{i/i} = P_{i-1/i-1} = P$. For convenience of subsequent analysis the normalization of P and $P_{i/i-1}$ matrices is applied:

$$K = \begin{bmatrix} k_{11} & k_{12} & k_{13} \\ k_{12} & k_{22} & k_{23} \\ k_{13} & k_{23} & k_{33} \end{bmatrix} = \frac{1}{\sigma^2} P, \quad (16)$$

$$K(\tau) = \frac{1}{\sigma^2} P_{i/i-1} = \Phi(\tau) K \Phi^T(\tau) + c^2 Q(\tau).$$

Here $\tau = \alpha \cdot \Delta N,$ (17)

$$\Phi(\tau) = \begin{bmatrix} 1 & \Delta N & \frac{1}{\alpha^2} [1 - \tau + \exp(-\tau)] \\ 0 & 1 & \frac{1}{\alpha} [1 - \exp(-\tau)] \\ 0 & 0 & \exp(-\tau) \end{bmatrix}, \quad (18)$$

$$c = \dot{T}_m \cdot \frac{\sigma_\chi}{\sigma}, \quad (19)$$

$$Q(\tau) = \begin{bmatrix} q_{11} & q_{12} & q_{13} \\ q_{12} & q_{22} & q_{23} \\ q_{13} & q_{23} & q_{33} \end{bmatrix}, \quad (20)$$

$$q_{11} = \left\{ 2\tau^3 / 3 - \tau^2 + 2[1 - \exp(-\tau) - \tau \exp(-\tau)] - [\tau - 1 + \exp(-\tau)]^2 \right\} / \alpha^4,$$

$$q_{12} = [\tau - 1 + \exp(-\tau)]^2 / \alpha^3,$$

$$q_{13} = [1 - 2\tau \exp(-\tau) - \exp(-2\tau)] / \alpha^2,$$

$$q_{22} = [2\tau - 3 + 4\exp(-\tau) - \exp(-2\tau)] / \alpha^2,$$

$$q_{23} = [1 - \exp(-\tau)]^2 / \alpha.$$

$$q_{33} = [1 - \exp(-2\tau)].$$

With taking into account the above normalization, the filter equation for matrix $P_{i/i}$ can be transformed to the form:

$$K = \begin{bmatrix} (1 + k_{11})^{-1} & 0 & 0 \\ -k_{12}(1 + k_{11})^{-1} & 1 & 0 \\ -k_{13}(1 + k_{11})^{-1} & 0 & 1 \end{bmatrix} \cdot K(\tau). \quad (21)$$

The convenience of application of a system of equations (16), (21) lies

in the fact, that its solution with respect to matrix \mathbf{K} depends only on three dimensionless parameters α , ΔN and c . Parameter α characterizes the system whose motion is investigated, ΔN - the measurement regime, c is the signal-to-noise ratio.

Equations (16) and (21) are easily solved with respect to matrix \mathbf{K} by means of iterations. Some approximation of matrix \mathbf{K} is used for calculating matrix $\mathbf{K}(\tau)$ based on relation (16). Then, the new approximation of matrix \mathbf{K} is determined by means of expression (21), etc. The required number of iterations depends on the value of parameter c . The process is well converged in cases of practical interest. And the convergence is slow at small values of parameter c only (i.e. for $c \ll 1$). In the limit, for $c \Rightarrow 0$, matrix \mathbf{K} also tends to zero.

Once matrix \mathbf{K} is determined, the variance of errors of forecasting for any number of revolutions n is easily calculated by means of relation (16) for $\tau = \alpha n$:

$$\sigma_t^2(n) = \sigma^2 \cdot K_{11}(\alpha n). \quad (22)$$

Here $K_{11}(\alpha n)$ is the corresponding element of matrix $\mathbf{K}(\tau)$.

The following quantities are used as initial data: \dot{T}_m , ΔN , α , σ_χ , σ and n . Two of these quantities, namely α and σ_χ , are associated with the main source of errors - the atmospheric density variations.

As an example of a priori accuracy estimations, we shall present the results of calculations similar to the data of Table 2. These results, as well as the initial values of σ_χ , are given in Table 5.

Table 5. A priori estimations of factor $\sigma_\xi(n)$

Forecasting interval, days		1	2	3	4	5	6	σ_χ
Technique	1	2.65	2.25	2.16	2.13	2.11	2.10	0.32
	2	1.50	1.28	1.23	1.22	1.21	1.20	0.18
	3	1.37	1.17	1.13	1.11	1.11	1.10	0.16

The comparison of these results with the Table 2 data shows their well coincidence. The discrepancies do not exceed 5 %.

Using the above technique of a priori estimation of accuracy, one can obtain the lower estimation of possible forecasting errors corresponding to ideal (hypothetical) conditions of absolutely accurate estimation of current density variations for the time of initial conditions used. In this case the equalities $\sigma=0$, $\mathbf{K}=0$ are met. The above expressions easily lead to the following formula:

$$\sigma_\xi = 20 \cdot \sigma_\chi \cdot (\sqrt{q_{11}(\alpha n)}) / n^2. \quad (23)$$

Table 6 below presents the results of calculations by this formula. These results are similar to those given above in Tables 2 and 5.

Table 6.

A priori estimations of factor $\sigma_{\xi}(n)$ for ideal conditions Forecasting

Interval, days	1	2	3	4	5	6	σ_{χ}
Technique 1	0.93	1.23	1.42	1.54	1.63	1.69	0.32
Technique 2	0.52	0.69	0.80	0.87	0.92	0.96	0.18
Technique 3	0.46	0.62	0.71	0.77	0.82	0.85	0.16

The comparison of these results with the data of Tables 2 and 5 indicates that essential reserves for increasing the accuracy exist for relatively short forecasting intervals only: from 2 to 3 days. For these conditions the accuracy can be potentially increased up to 2 - 3 times. For the 6-day forecasting interval and with using the most perfect techniques (No 2 and 3) the possible accuracy increasing reserve does not exceed 25 to 30%.

4. Conclusion

The materials presented in this paper lean mainly upon the results of studies carried out before the years 1990 - 91. We did not know any later results in this area. Therefore, the recommendations given here still remain to be topical.

Using the vast statistics on the forecasting the motion of low-altitude satellites, the authors have constructed the a posteriori empirical model of errors, which takes into account the technique applied in forecasting as well as the dependence of errors upon the satellite altitude, geomagnetic activity level and variability of ballistic factors. It is shown that, as compared to a widely-used technique that does not take into account the variation of geophysical conditions over the measurement data processing and forecasting interval, there exist realistic possibilities of increasing the accuracy up to 2 - 3 times. These possibilities are based on taking into account the atmosphere density variations correlated with solar and geomagnetic activity indices.

The theoretical model of forecasting the errors is constructed on the basis of a stochastic perturbation theory. The results of its application are shown to be in a rather well correspondence with the a posteriori analysis data. This model was used for estimating the forecasting errors under ideal hypothetical conditions, when the density variations at the given initial point are known accurately. For 2 to 3-day forecasting intervals the errors can be reduced down to 2 - 3 times. For the 6-day forecasting interval and with using the most perfect techniques the possible accuracy increasing reserve does not exceed 25 to 30 %.

5. References

1. А.И. Назаренко. Априорная и апостериорная оценка ошибок прогнозирования движения низковысотных ИСЗ. Космические исследования, вып. 4, 1991.
2. A.I. Nazarenko, S.N. Kravchenko, S.K. Tatevian. The space-temporal variations of the upper atmosphere density derived from satellite drag data. Adv. Space Res. Vol. 11, № 6, 1991.
3. В.С. Юрасов. Применение численно-аналитического метода для прогнозирования движения ИСЗ в атмосфере. Наблюдения искусственных небесных тел. № 82, Москва, 1987.
4. Модель плотности для баллистического обеспечения полетов искусственных спутников Земли. ГОСТ 25645. 115-84. Москва, Изд-во стандартов, 1984.
5. Ю.П. Горохов, А.И. Назаренко. Методические вопросы построения модели флуктуаций параметров атмосферы. Наблюдения искусственных небесных тел. № 80, Москва, 1982.
6. А.И. Назаренко, В.Е. Андреев, С.Н. Варнакова, Ю.П. Горохов, Р.В. Гукина, А.Г. Клименко, Л.Г. Маркова. Оценка точности модели атмосферы для баллистических расчетов ГОСТ 22721-77. Наблюдения искусственных небесных тел. № 81, Москва, 1984.
7. А.И. Назаренко, Т.А. Амелина, Р.В. Гукина, О.И. Кириченко, С.Н. Кравченко, Л.Г. Маркова, Н.П. Тумольская, В.С. Юрасов. Оценка эффективности различных способов учета вариаций плотности атмосферы при прогнозировании движения ИСЗ в периоды геомагнитных бурь. Наблюдения искусственных небесных тел. № 84, Москва, 1988.
8. Б.В. Кугаенко. Оценка влияния короткопериодических вариаций атмосферы на точность расчета орбит. Сб. Математическое обеспечение космических экспериментов. Москва, "Наука", 1978.
9. П.Е. Эльясберг. Влияние флуктуаций плотности атмосферы на точность определения и прогнозирования орбит искусственных спутников Земли. Космические исследования, вып. 6, 1981.
- 10 А.И. Назаренко, Б.С. Скребушевский. Эволюция и устойчивость спутниковых систем. Изд-во "Машиностроение", Москва, 1981.

Technology of evaluation of atmosphere density variation based on the Space Surveillance System's orbital data

1. Introduction

The analysis of numerous data on the atmospheric drag of various satellites has shown that these estimations vary synchronously in the most cases: they increase and decrease simultaneously. Obviously, such a synchronous variation of satellites' drag estimations is due to the same reason: the atmosphere density variations. That's why such estimations have been widely used for constructing the modern atmosphere density models [1].

The traditional use of drag estimations is characterized by the fact that they allowed to determine relatively slow atmosphere density variations correlated with the month cycle of solar activity and were not applied for determining short-periodic variations related with the change of geomagnetic indices. There are some reasons of such a situation, the main of which lies in the averaged character of traditional drag estimations, i.e. in their insufficient time resolution.

Since the very beginning of the existence of Russian Space Surveillance System (RSSS) the characteristics of satellites drag in the atmosphere (the change of a period for one revolution or the ballistic factor) were included into the set of parameters to be improved as the seventh element of the orbit. This allowed to decrease the level of a priori uncertainty of the atmospheric drag value and, as a result, - to increase the forecasting accuracy.

The detailed analysis of the RSSS satellite drag data has shown rather high time resolution of latters, which allows to estimate short-periodic atmosphere density variations (Figure 1). These possibilities arose as a result of a series of investigations aimed at updating the orbit improvement techniques using the measurements. In particular, the generalization of the Kalman filter for the case of "color" noise of a system was proposed [2, 3] and the numerical-analytical techniques of satellites motion forecasting were developed [4, 5]. This made it possible to increase the orbit determination accuracy for low-altitude satellites. It was the basis, on which the technique of constructing the atmosphere density variation model from the RSSS data was developed in the early eighties [6].

2. The technique of constructing the atmosphere density variations

2.1. General scheme of problem solution

The actual atmosphere density is presented as a sum of the value, calculated by the model ρ_{model} , and variation $\delta\rho$:

Figure 1. The relative variations of the atmosphere density

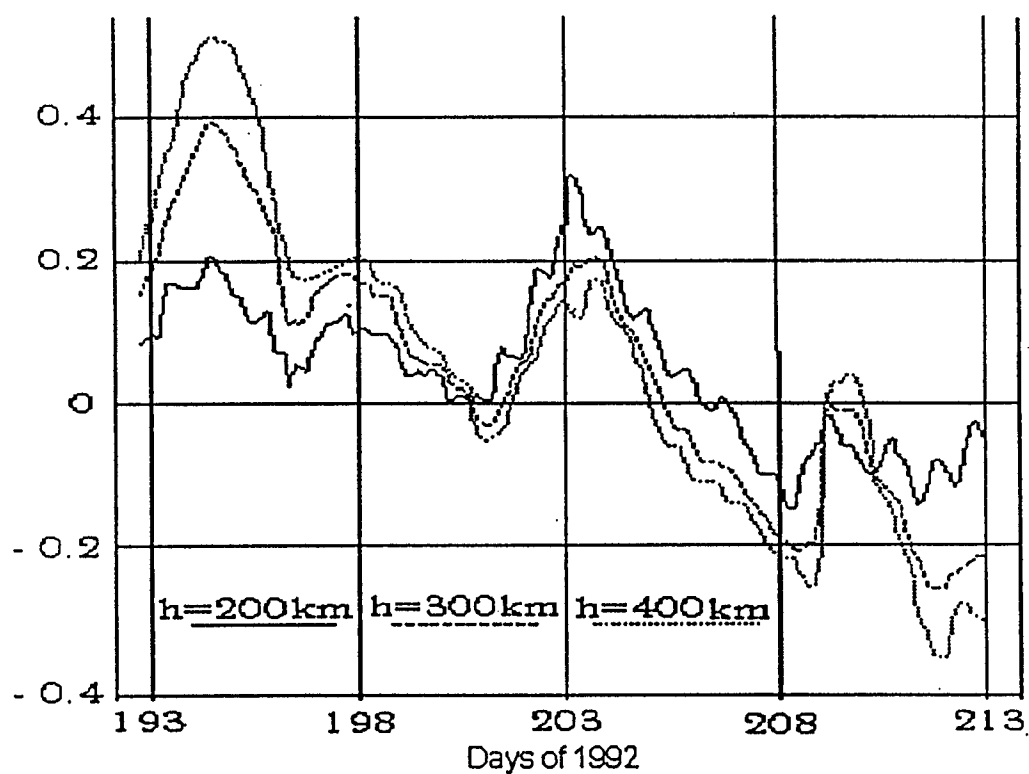
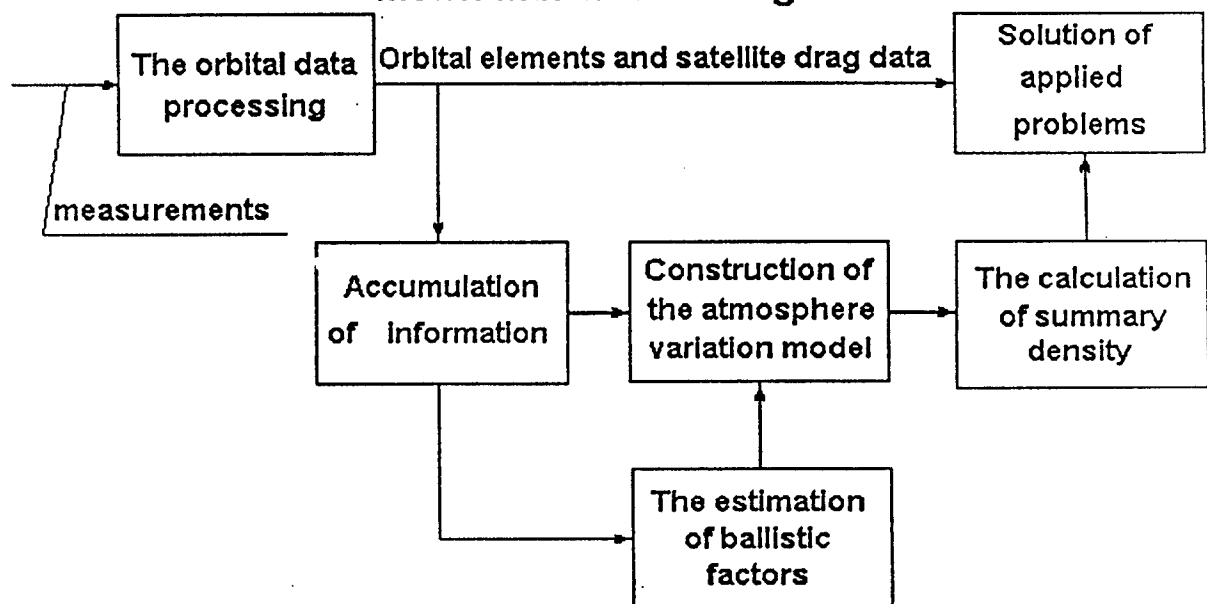


Figure 2. The interaction of the atmosphere variation model with the RSSS algorithms



$$\rho(t) = \rho_{\text{model}} + \delta\rho = \rho_{\text{model}} \cdot \left(1 + \frac{\delta\rho}{\rho_{\text{model}}}(t)\right). \quad (1)$$

Here the model density is calculated for constant indices of solar and geomagnetic activity. The principal scheme of obtaining the estimations $\delta\rho / \rho_{\text{model}}$ and their application is presented in Figure 2.

The orbital measurements of satellites come to an input of data processing algorithms. The orbital elements (Θ) and the estimations of drag characteristics (ballistic factor k , for instance) of various satellites are obtained at an output. These data, accumulated on some interval, are used for constructing the model of atmosphere density variations $\delta\rho / \rho_{\text{model}}$. The application of these estimations in accordance with formula (1) for calculating the density by integrating the equations of motion allows to take into account the found density variations during the process of forecasting the motion of objects and, thus, to increase the forecasting accuracy.

2.2 Basic relations

Let us consider the change of a satellite period \dot{T}^* for one revolution under the atmosphere effect to be the drag characteristics of a satellite. The real value of this quantity can be expressed as follows:

$$\dot{T}_{\text{real}} = k_{\text{real}} \cdot (\rho_p)_{\text{real}} \cdot f(\Theta). \quad (2)$$

Here k_{real} and $(\rho_p)_{\text{real}}$ are real values of ballistic factor and atmosphere density at the perigee of this satellite, respectively. $f(\Theta)$ is some function of orbital elements. The value of \dot{T} , determined from the data of improvement of orbital elements, differs from (2) in using the known estimations of quantities, rather than their real values:

$$\dot{T} = k \cdot (\rho_p)_{\text{model}} \cdot f(\Theta). \quad (3)$$

Quantity \dot{T} is, in essence, the estimation of the real drag characteristics (2). Introducing the relative error ε of estimation \dot{T} , the relation between quantities (2) and (3) can be written as follows:

$$\dot{T}_{\text{real}} = \dot{T} \cdot (1 + \varepsilon). \quad (4)$$

Expressions (1) - (4) give rise to the following relation for estimating the relative density variation $\delta\rho / \rho_{\text{model}}$ from the drag data of the i th satellite:

$$\left(\frac{k}{k_{\text{real}}}\right)_i - 1 = \frac{(\rho_p)_{\text{real}}}{\rho_{\text{model}}} - 1 - \left(\frac{k}{k_{\text{real}}}\varepsilon\right)_i = \left(\frac{\delta\rho}{\rho}\right)_{\text{real}} - \Delta_i. \quad (5)$$

*One should note that the choice of this particular characteristics is not a matter of principle.

If the real value of ballistic factor k_{real} were known, the quantity in the left-hand side of expression (5) could be considered to be the estimation of a current atmosphere density variation from the drag data of the i th satellite. Let us denote by \bar{k}_i the known estimation of a real ballistic factor of the i th satellite. Then the estimation of a current relative variation of density from the drag data of this satellite can be expressed as

$$\frac{\delta\rho}{\rho_{model}}(t)_i = \left(\frac{k}{\bar{k}}\right)_i - 1. \quad (6)$$

2.3. Construction of the model of density variations on the $(t_j, t_j + \tau)$ interval

Let the model of atmosphere density variations on the interval under consideration be presented as a function of the altitude of a point:

$$\frac{\delta\rho}{\rho}(h)_{real,j} \approx \frac{\delta\rho}{\rho}(h)_{model,j} = \sum_{q=0}^2 b_{qj} \cdot h^q. \quad (7)$$

On the interval τ the density variations are supposed to be constant. Then, in accordance with expression (5), the estimations (6) may be considered to be indirect measurements of parameters b_{qj} of the model of variations. The number of these measurements n_j is equal to a number of estimations k (for various satellites) on the $(t_j, t_j + \tau)$ interval. To estimate the parameters b_{qj} we shall apply the least-square method. The criterion to be minimized is written as

$$I(b_{qj}) = \sum_{i=1}^{n_j} p_i \cdot \Delta_{ij}^2, \quad (8)$$

where for discrepancies between estimations (6) at some time moment belonging to the $(t_j, t_j + \tau)$ interval and the values of variations calculated by the model (7) we apply the following designation:

$$\Delta_{ij} = \Delta_{ij}(b_{qj}) = \left(\frac{k}{\bar{k}}\right)_{ij} - 1 - \frac{\delta\rho}{\rho}(h_i)_{model,j}. \quad (9)$$

The values of these discrepancies depend on the unknown parameters b_{qj} of the model. To take into account the features of separate satellites, the weight coefficients p_i are introduced into the quadratic form (8).

The above approach to constructing the variations model has some assumptions and quantities which have to be clarified additionally.

Note that the value of interval $\tau \approx 3-6$ hours and the form of model representation as function (7) have been chosen as a result of numerous and protracted model experiments from the condition of minimizing the errors of estimation variations. The interval τ should be minimized for improving the

time resolution. However, this will result in decreasing the number of measurements n_j and in lowering the accuracy of estimations of parameters b_{qj} . These recommendations have a compromise character and reflect the features and operation conditions of RSSS algorithms. The issues related to the construction of estimations \bar{k}_i and to the choice of weight coefficients p_i will be discussed in the next Section.

The above technique is applied for operative evaluation of the atmosphere density variations. The appropriate program is actuated immediately after finishing the ordinary interval τ .

2.4. Use of the standard satellites for ballistic factors determination

The accurate enough a priori estimations of ballistic factors \bar{k}_i are known only for spherical-shaped satellites with known size, mass, and outer surface material. The orientation of such a satellite does not influence its ballistic factor.

The values of dimensionless drag coefficients C_x of these satellites are determined from theoretical calculations or by wind tunnel tests. We shall call these satellites standard ones. As a rule, the number of such satellites is small - about some units. As a result, the determination of atmosphere density variation (in a rather wide region of space and with acceptable time resolution) from standard satellites' drag data is unsolvable problem.

For constructing the density variations we have proposed to use the drag data for all objects, which exist in the altitude range up to 600 km for 1-2 months at least. Therefore, the problem of evaluating ballistic factors of all non-standard satellites arose. This problem can be solved "against the background" of standard objects only. If the latter are absent, the problem also becomes unsolvable.

The estimations of ballistic factors of all non-standard satellites are determined periodically: with the interval of about 1 month, as well as with the appearance of new satellites in the region under consideration. The essence of the algorithm is based on minimizing the quadratic form

$$I(\bar{k}_i, b_{qj}) = \sum_j I(b_{qj}) = \sum_j \sum_{i=1}^{n_j} p_i \cdot \Delta_{ij}^2. \quad (10)$$

Here, not only the values of parameters b_{qj} at each of τ intervals are unknown, but the estimations \bar{k}_i of all non-standard satellites as well. This problem is solved by means of successive approximations. The values of unknown estimates are updated after each "run" over whole time interval. As a result of this solution, the variances of residual discrepancies are formed for each of satellites:

$$\sigma_{\Delta i}^2 = \frac{1}{J_{\max}} \cdot \sum_{j=1}^{J_{\max}} \Delta_{ij}^2. \quad (11)$$

Weight factors p_i are formed as a quantity reciprocal to variance (11).

3. Some data on the atmosphere density estimations and application

3.1. Estimations of the atmosphere density variations

The above technique was applied for obtaining the current estimations of atmosphere density variations since the end of 1982. Some 200-250 estimations for various satellites have been processed every day. The obtained data have been analyzed in detail. In particular, various statistical characteristics of variations at different altitudes were determined. These characteristics include: mean values, variances, autocorrelation functions and mutual correlation functions. The regression analysis was also carried out. Some of results were published in papers [7, 8, 9].

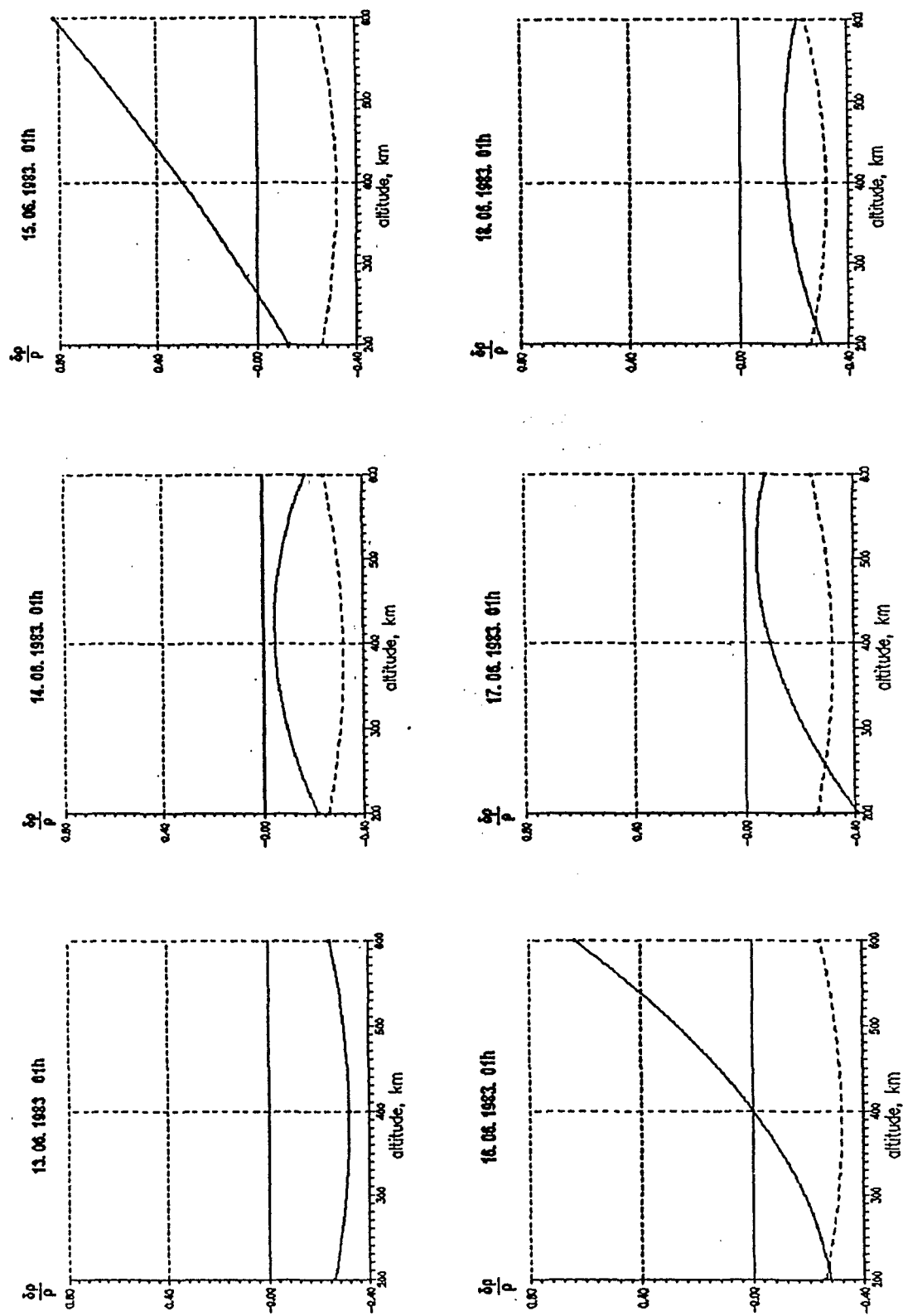
Figure 3 presents, as an example, the obtained data on the development of density variations at the 200-600 km altitudes during the geomagnetic storm of 13 June, 1983. The intensive growth of geomagnetic activity was observed at 00h UT on June 13. The values of K-indices increased from 3.3 to 6.3. At this time the corrections $\delta\rho / \rho_{\text{model}}$ were negative and equal to 0.26-0.32. The sum of 3-hour K-indices for a day was 42. In one day the geomagnetic indices returned to their initial level, and the density increased: the $\delta\rho / \rho_{\text{model}}$ corrections remained negative and were equal to 0.05-0.16. On the next day the density continued to increase, at high altitudes especially. The maximum of density was achieved at the evening on June 14. At altitudes of 200, 400 and 600 km the corrections were equal to 0.05%, 45% and 100%, respectively. During the period of June 15 through 17 the density has decreased. The initial level was achieved first for low altitudes (200 km in the morning on June 15) and only in the evening on June 17 - for high altitudes.

The obtained data were critically analyzed. In particular, the question on the value of time delay of obtained estimations with respect to actual density variations was investigated.

3.2 Determination of time delay of density variations estimations

Two approaches - experimental and theoretical - were applied for solution of this problem. In the first case the motion of various satellites was forecasted on the interval, where density variations have already been determined. The time delay Δt was introduced into the obtained estimates of variations at the moment t , i.e. the $\delta\rho / \rho_{\text{model}}(t-\Delta t)$ function was used in the drag calculation. The statistic characteristics of forecasting errors were determined from a great number of implementations for each of accepted delay values. That delay value, which provides the minimum of forecasting errors, was assumed as an

Figure 3. Evaluation of the atmosphere density variation after the geomagnetic storm at June 13, 1983



estimate. As a result, the quantity $\Delta t \approx 0.5$ days was determined (Figure 4). This estimate was used subsequently in making forecasts.

In the process of theoretic studies [10] the authors have developed the technique for constructing sensitivity characteristics of the program-algorithmic RSSS system as a tracking system. Some of obtained results are presented in Figure 5. One can see well coincidence of theoretic results with simulation modelling data.

3.3. "PION" satellites investigations

Small "PION" satellites were specially designed for investigating the atmosphere density variations. These satellites had spherical shape (33 cm in diameter), and their ballistic factor was well known from the a priori data. By this reason these satellites were taken as standard ones. 6 similar satellites were launched in 1989 and 1992 (see Table 1). The data on this experiment were published in a number of papers [11, 12, 13, 14]. 25000 sets of orbital elements and drag estimations were accumulated from 64 satellites with perigee heights ranging from 150 to 520 km during the period from May to September, 1989. Similar data were accumulated in 1992 as well. The detailed analysis of this information provided some interesting results.

				Table 1
Satellite №	Year of launching	Separation date	Weight, kg	Lifetime, days
1	1989	June 8	45.174	45
2	1989	June 9	44.570	45
3	1989	August 6	46.973	44
4	1989	August 7	47.250	43
5	1992	September 1	49.466	24
6	1992	September 2	49.434	23

Figure 6 presents current estimations of ballistic factors for "PION-5" and "PION-6" satellites. The synchronous variation of ballistic factors is clearly seen, which proves that it is caused by atmosphere density variations.

The data on the distribution of $\sigma_{\Delta i}$ values, which characterizes the level of residual discrepancies, are presented in Table 2.

Table 2							
Range $\sigma_{\Delta i}$, %	<1	1 - 3	3 - 6	6 - 10	10-15	15-20	>20
Frequency	0.07	0.15	0.23	0.38	0.07	0.07	0.03

It is seen that the $\sigma_{\Delta i}$ value lies within the range of 3 to 10% for the majority of satellites. For some objects is occurred to be *less than 1%*. One of such objects (the international № 80037-1) have a shape of smooth ball and rather big size (more than 1m in diameter). Therefore, a relative great number of measurements was obtained for this satellite. The number of accumulated orbital elements was about 500. The example of data for this object is given in Figure 7. Since the residual discrepancies were caused by the errors in ballistic

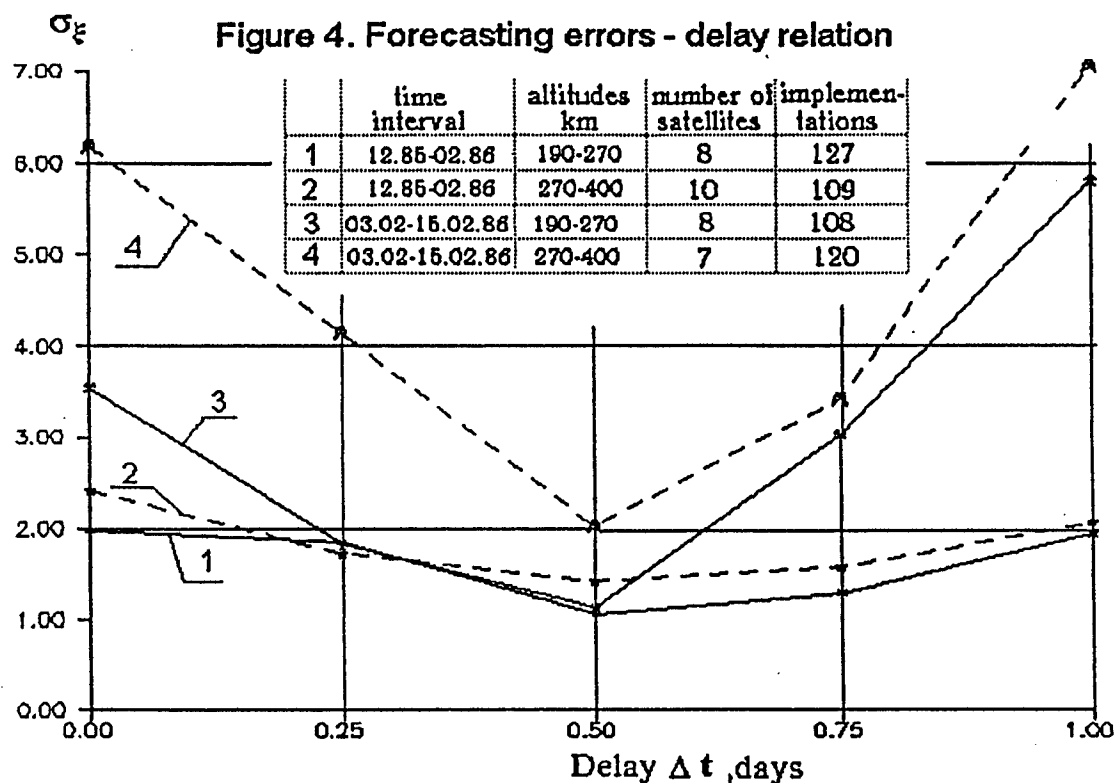
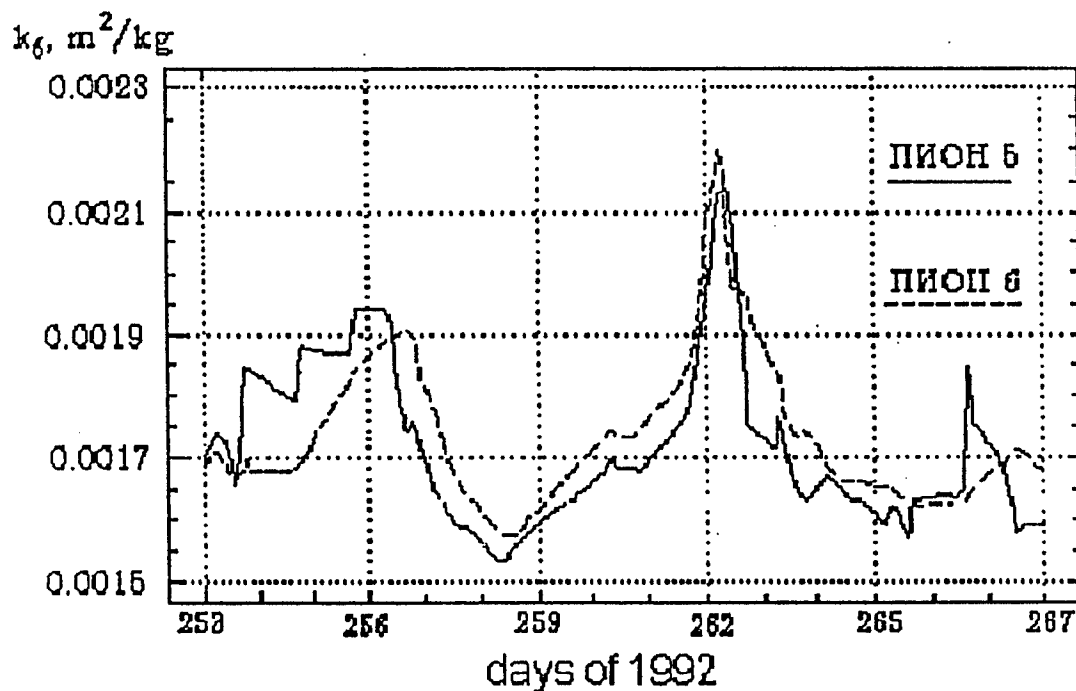


Figure 6. The variation of the ballistic factors of "ПИОН-5" and "ПИОН-6" satellites



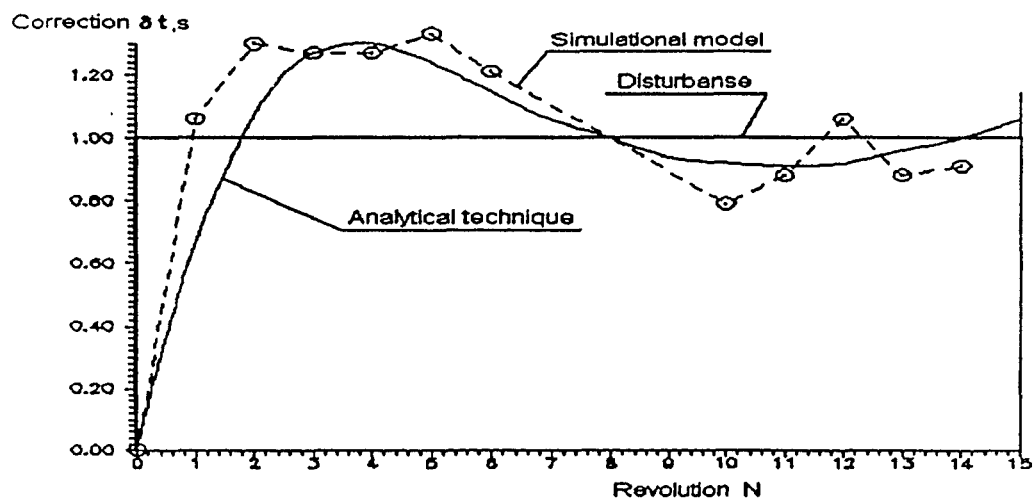
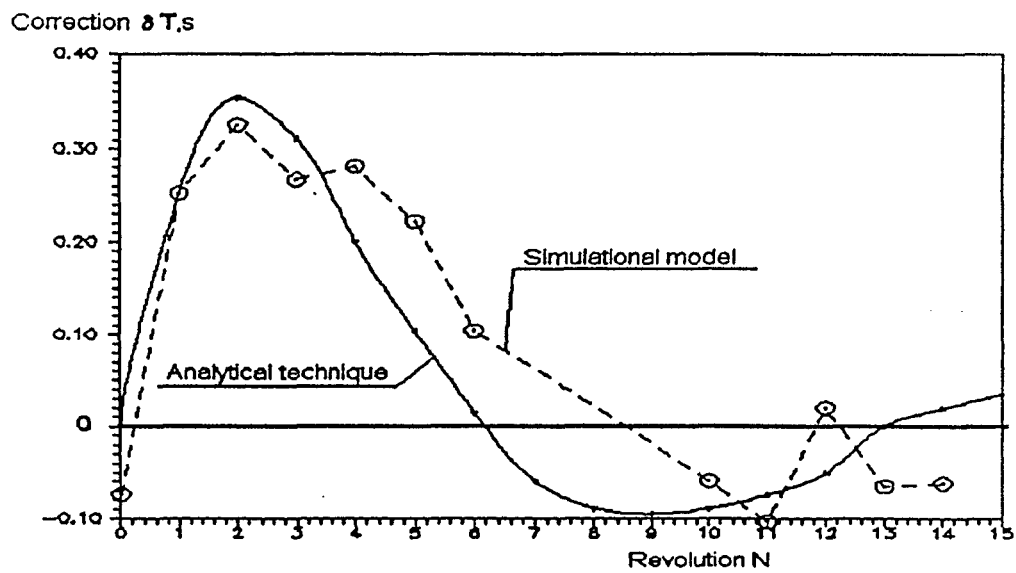
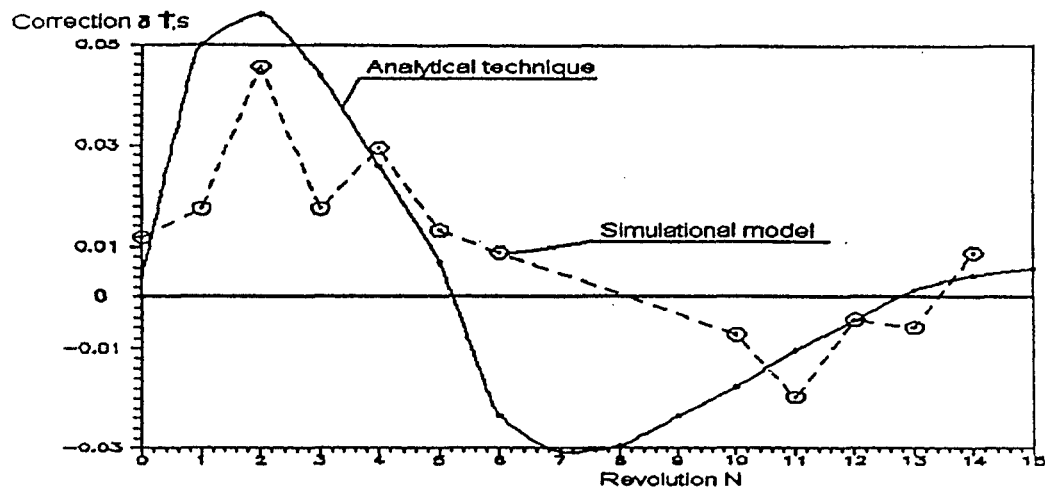


Figure 5. Effect of the time disturbance (1 sec) on the state vector estimations

factor estimations and in density variations, the presented estimation of discrepancies suggests, that *these quantities were determined with errors of the order of 1%.* This result is unique, in our opinion. The obtained estimation of errors is an order of magnitude lower, than traditional ideas on the level of atmosphere density determination errors.

The data accumulated during this experiment were used also for constructing the model of low-altitude satellites forecasting. The results of these studies were published in paper [15] and have also been presented in one of reports at our Workshop [16].

3.4. Determination of time and place of orbital complex "Salyut-7/Cosmos-1686" reentry

In determination and forecasting the motion of orbital complex (OC) at the last stage of its lifetime we have used the results of earlier investigations of the atmosphere density variations [17].

At the end of January, 1991, a very high solar activity level $F_{10.7}$ was observed. On January, 31 (7 days before the complex reentry) these values reached the highest level - 373 units. According to the variations monitoring data, it was found that at the high $F_{10.7}$ level the density model [18] gives overestimated density values. By this reason just on January 31, 1991, the correction was introduced into the model density calculations:

$$\rho(t) = \rho_{\text{model}} \cdot \{1 - 0.001[F_{10.7}(t) - 200]\}. \quad (12)$$

This resulted in updating the model density by 10-17% and contributed to increasing the motion forecasting accuracy.

In the night of February 5 to 6 the control of orbital complex orientation was performed; namely the longitudinal axis of OC was aligned with the velocity vector. At about 3hr on February 6 the complex again transferred into the uncontrolled flight. As a result of more correct determination, this was clearly revealed in a sharp and early synchronous decreasing of estimations of ballistic factor k from 0.003 down to 0.0027 m^2/kg , i.e. by 10%, and in subsequent restoring of initial estimation even in the evening of February 6. This result can serve as an experimental proof of the possibility of operative control of variations of satellites' ballistic factors and atmosphere density variations.

In the a posteriori analysis of orbital data of OC, obtained at the last stage of its existence, the OC lifetime determination errors were estimated with different methods (versions) of accounting the atmosphere density variations.

In the *first* of these versions the density was calculated for constant (mean) values of solar and geomagnetic activity indices.

In the *second* density calculation version the indices were supposed to be known.

As an accuracy indicator, the quantity

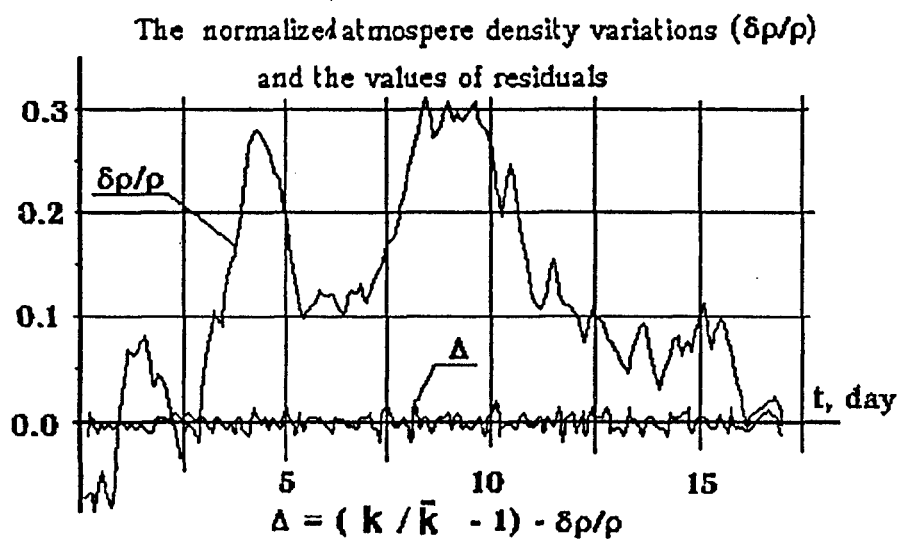
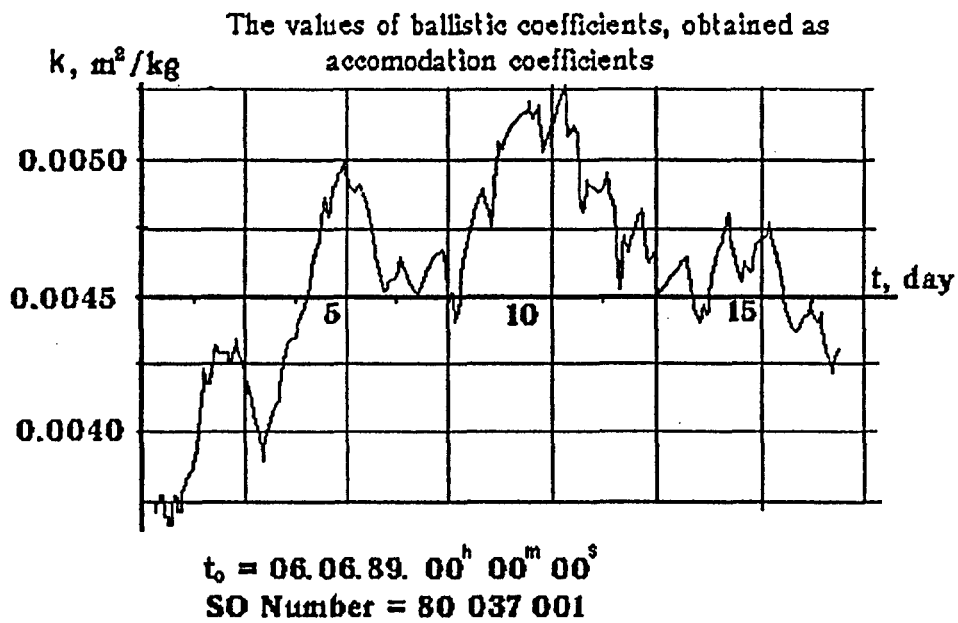


Figure 7. Values k estimated for the sperical satellite,
period 6 June - 23 June, 1989.

$$\varepsilon = \frac{\delta t}{t_r} \quad (13)$$

was used. Here t_r is the remaining lifetime of OC, δt is the reentry time determination error.

The obtained estimations of errors for these versions are given in Figure 8. 72 determinations were carried out for each of versions. The data show that, when the density variations correlated with solar and geomagnetic activity indices are taken into account, the level of errors is actually two times lower than without accounting these variations. This result confirms once again the conclusion about the considerable influence of density variations on the SO motion forecasting accuracy.

3.5. Development of the technique of density variation forecasting

In order to reveal space-time regularities of the change of atmosphere density variations, the technique of constructing the regression equations for stationary random vector processes was developed [19]. This technique has rather general character and, therefore, it is acceptable for time series of different nature.

In applying this technique for density variations investigation the four-dimensional state vector was chosen. The components of this vector consisted of density variations $\delta\rho / \rho_{\text{model}}$ at altitudes of 200, 250 and 300 km, as well as of 3-hour K-indices of geomagnetic activity. The links of this vector (also designated by z_t) with its values at preceding time moments z_{t-1} , z_{t-2} , etc. were studied. The interval between discrete time moments was assumed to be constant and equal to 3 hours.

Based on the analysis of accumulated data on variations, the following regression equation was constructed:

$$z_t = \Phi_1 \cdot z_{t-1} + \Phi_2 \cdot z_{t-2}, \quad (14)$$

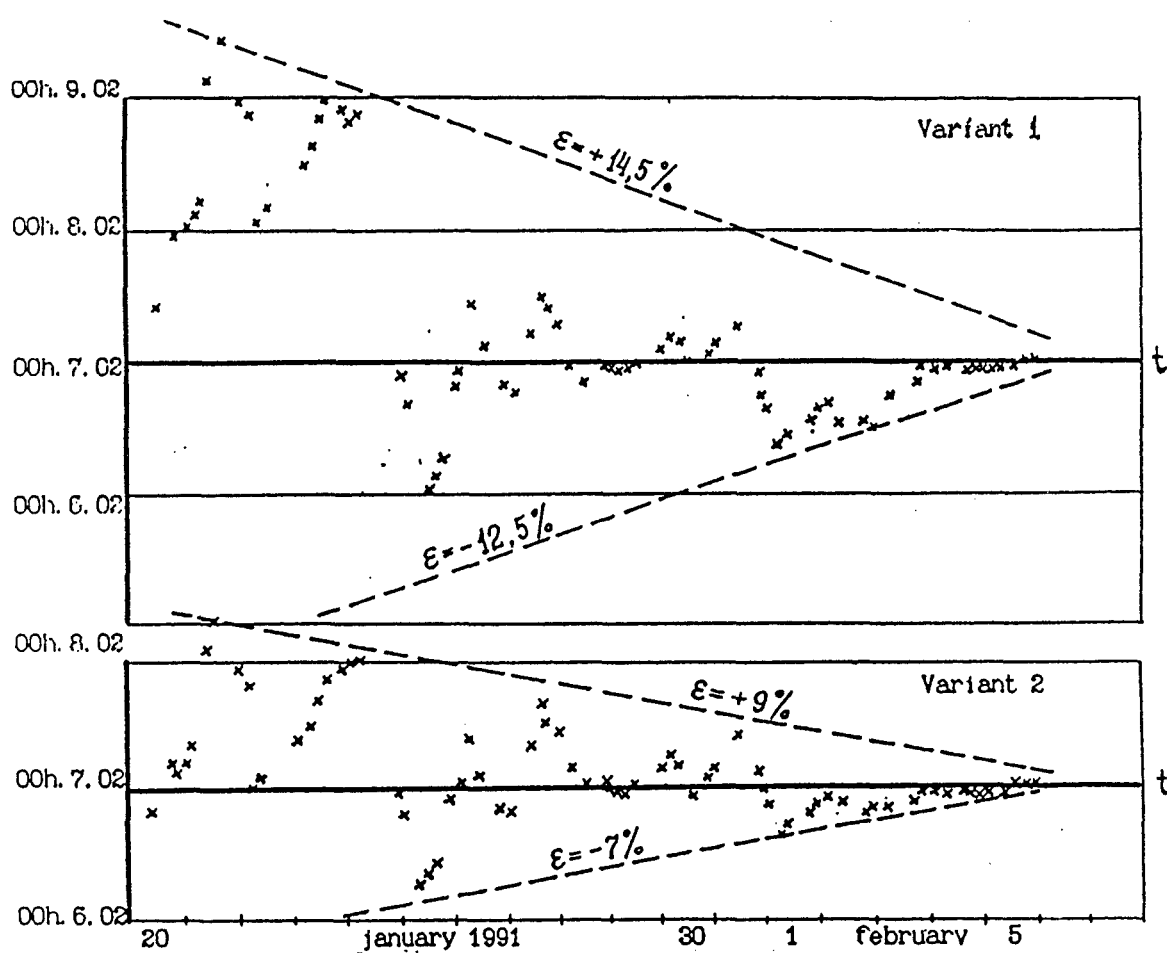
where

$$\Phi_1 = \begin{bmatrix} 1.273 & -0.198 & 0.489 & 0.039 \\ 0.134 & 1.131 & 0.460 & 0.025 \\ 0.079 & 0.215 & 1.292 & 0.032 \\ 0.233 & 0.153 & 0.579 & 0.710 \end{bmatrix}, \quad \Phi_2 = \begin{bmatrix} -0.307 & 0.057 & -0.351 & -0.023 \\ -0.100 & -0.410 & -0.245 & -0.005 \\ -0.070 & -0.189 & -0.359 & -0.007 \\ -0.224 & -0.039 & -0.569 & -0.006 \end{bmatrix}.$$

4. Conclusion

The aforementioned technique of operative estimation of atmosphere density variations with using the RSSS data allows to determine short-periodic density variations correlated with the geomagnetic activity indices. The extra results of this technique application are the estimations of ballistic factors of low-orbit satellites and characteristics of their variability. The technique was applied over the 10-year time interval: from 1982 to 1992.

Figure 8. Values of the time of space complex reentry with the various versions of the density calculation



A series of rather general techniques was developed for studying dynamical systems. These techniques were applied for studying the atmosphere density variations and include: 1) the Kalman filter generalization for the case of "color" noise of a system; 2) the method of studying the sensitivity of a system for tracking the motion of satellites; 3) the recurrent method of constructing the autoregression equations for vector processes.

Based on obtained density variation estimations, a number of applied investigations was carried out. The (2-3)-fold increase of satellite motion forecasting accuracy, as compared to a widely-applied technique not taking into account density variations, was demonstrated. The maximally achieved accuracy of determination of satellites' drag characteristics was found to be at the level of 1%, which is an order of magnitude better than commonly accepted estimations.

The materials of this work represent the review of a study of atmosphere density variations carried out over more than 10-year time interval by the author and his business colleagues: Yu.P. Gorokhov, V.D. Anisimov, L.G. Markova, R.V. Gukina, S.N. Kravchenko, V.S. Yurasov, V.A. Bratchikov and others. The retrospective analysis of these works, taking into account a more complete recent information on the state of this problem in Russia and other countries, indicates that the obtained results still remain timely. Moreover, in author's opinion, the possibility appeared for more extensive applying these results in the interests of increasing the accuracy of determination and forecasting the orbits of low-altitude satellites, as well as for the purpose upper atmosphere monitoring.

4. References

1. Jaccia I.G. Thermospheric temperature, density and composition: new models. SAO, spec. report № 375, 1977.
2. А.И. Назаренко, Л.Г. Маркова. Методы определения и прогнозирования орбит ИСЗ при наличии погрешностей в математическом описании движения. Сб. Прикладные задачи космической баллистики. Изд-во "Наука", Москва, 1973.
3. В.Д. Анисимов, Л.Г. Маркова, А.И. Назаренко, И.Г. Поздняков. Прогнозирование и определение орбит искусственных спутников Земли с учетом оценки флуктуаций атмосферного сопротивления. Сб. Определение движения космических аппаратов. Изд-во "Наука", Москва, 1975.
4. А.И. Назаренко, Б.С. Скребушевский. Эволюция и устойчивость спутниковых систем. Изд-во "Машиностроение", Москва, 1981.
5. В.С. Юрасов. Применение численно-аналитического метода для прогнозирования движения ИСЗ в атмосфере. Наблюдения искусственных небесных тел. № 82, Москва, 1987.
6. Ю.П. Горохов, А.И. Назаренко. Методические вопросы построения модели флуктуаций параметров атмосферы. Наблюдения искусственных небесных тел. № 80, Москва, 1982.
7. А.И. Назаренко, В.Е. Андреев, С.Н. Варнакова, Ю.П. Горохов, Р.В. Гукина, А.Г. Клименко, Л.Г. Маркова. Оценка точности модели атмосферы для баллистических

- расчетов ГОСТ 22721-77. Наблюдения искусственных небесных тел. № 81, Москва, 1984.
8. А.И. Назаренко, Ю.П. Горохов, Р.В. Гукина, С.Н. Крвченко, Л.Г. Маркова. Методика и некоторые результаты выявления пространственно-временных закономерностей крупномасштабных флуктуаций плотности атмосферы. Наблюдения искусственных небесных тел. № 82, Москва, 1987.
 9. А.И. Назаренко, Т.А. Амелина, Р.В. Гукина, О.И. Кириченко, С.Н. Кравченко, Л.Г.Маркова, Н.П. Тумольская, В.С. Юрасов. Оценка эффективности различных способов учета вариаций плотности атмосферы при прогнозировании движения ИСЗ в периоды геомагнитных бурь. Наблюдения искусственных небесных тел. № 84, Москва, 1988.
 10. В.А. Братчиков, А.И. Назаренко. исследование чувствительности системы слежения за движением искусственных спутников Земли. Автоматика и телемеханика, № 5, 1991.
 11. В.Д. Анисимов, В.П. Басс, И.Н. Комиссаров, С.Н. Кравченко, А.И. Назаренко, Ю.С. Пятницкий, А.П. Рычков, В.И. Сыч, Ю.Л. Тарасов, О.Г. Фридлиндер, В.М. Шахмистов, В.С. Юрасов. Результаты исследований аэродинамических характеристик и плотности верхней атмосферы с помощью пассивных спутников "ПИОН". Наблюдения искусственных небесных тел. № 86, Москва, 1990.
 12. Ю.Л. Тарасов, В.А. Акулич, Ю.Н. Горелов, И.Н. Комиссаров, Ю.С. Пятницкий, В.П. Червинский. Проектирование и конструкция комплекса "ПИОН". Наблюдения искусственных небесных тел. № 86, Москва, 1990.
 13. A.I. Nazarenko, S.N. Kravchenko, S.K. Tatevian. The space-temporal variations of the upper atmosphere density derived from satellite drag data. Adv. Space Res. Vol. 11, № 6, 1991.
 14. G.S. Batyr, V.A. Bratchikov, S.N. Kravchenko, A.I. Nazarenko, S.S. Veniaminov, V.S. Yurasov. Upper atmosphere density variation investigations based on Russian Space Surveillance System data. Proc. of First European Conference on Space Debris, Darmstadt, 5-7 April 1993.
 15. А.И. Назаренко. Априорная и апостериорная оценка ошибок прогнозирования движения низковысотных ИСЗ. Космические исследования, вып. 4, 1991.
 16. A.I. Nazarenko, G.M. Chernyavskiy. Evaluation of the accuracy of forecasting satellite motion in the atmosphere. Second UA-Russian Space Surveillance Workshop, Paznan, 1996.
 17. A.I. Nazarenko. Determination and prediction of the satellite motion at the end of the lifetime. Proc. International Workshop on Salyut-7/Kosmos-1686 reentry, ESOC, Darmstadt, 9 April 1991.
 18. Модель плотности для баллистического обеспечения полетов искусственных спутников Земли. ГОСТ 25645. 115-84. Москва, Изд-во стандартов, 1984.
 19. С.Н. Кравченко, А.И. Назаренко. Рекуррентный метод построения уравнений авторегрессии для векторных процессов. Техническая кибернетика. №1, 1992.
 20. *З.Н. Хуторовский и др. Оперативное уточнение орбит и времени существования космических объектов, испытывающих атмосферное торможение. Сб. Наблюдения искусственных небесных тел. М.: АС АН СССР, № 84, 1988.*

COMPARISON OF ATMOSPHERE DENSITY MODELS

T. Amelina, G. Batyr, V. Dicky, N. Tumolskaya, V. Yurasov

SRC "Kosmos", Moscow

The qualitative solution of many ballistic problems connected to determination and prediction of low-Earth orbit space objects motion, is impossible without use of precision models of the upper atmosphere density. The upper atmosphere is very dynamical. Under influence of short-wave and corpuscular solar radiation its density unregularly varies.

The modern atmosphere models take into account the most essential variations of atmosphere density and enable to determine its value in a given near-Earth space point for any moment of time if indexes of solar and geomagnetic activity are known. The well known foreign models of the upper atmosphere are CIRA-72, CIRA-86, MSIS, Jacchia, Barlier [1,2,3,4,5]. Practically all listed models are semi-empirical - for their development both physical laws of atmosphere components distribution and empirical data, obtained from direct and indirect measurements of its parameters were used.

In Russia the empirical atmosphere density models developed under the leadership of Professor Volkov I. I. - GOST 22721-77 [6] and GOST 25645.115-84 [7] have got the most wide circulation for the solution of ballistic problems. These models are constructed on the basis of processing large volume of long-term data on atmosphere drag and have been constantly updated by new information. In the last edition of model GOST 25645.115-84 atmosphere density is approximated by the following dependence

$$\rho = \rho_H K_0 K_1 K_2 K_3 K_4,$$

where

$$\rho_H = a_0 \exp[a_1 - a_2(h - a_3)^{1/2}],$$

$$a_0 = 9.80665 \text{ kg/m}^3,$$

$$K_0 = 1 + (l_1 + l_2 h + l_3 h^2)(F_{81} - F_0)K_F,$$

$$K_1 = 1 + (c_1 + c_2 h + c_3 h^2 + c_4 h^3) \cos^n \frac{\varphi}{2},$$

$$n = n_0 + n_1(h),$$

$$\cos \varphi = (z \sin \delta_{\odot} + \cos \delta_{\odot} (x \cos \beta + y \sin \beta)) / r,$$

$$\beta = \alpha_{\odot} + \varphi_1,$$

$$K_2 = 1 + (d_1 + d_2 h + d_3 h^2) A(D),$$

$$K_3 = 1 + (b_1 + b_2 h + b_3 h^2) (F - F_{81}) / F,$$

$$K_4 = 1 + (e_1 + e_2 h + e_3 h^2 + e_4 h^3) (e_5 + e_6 K_p + e_7 K_p^2),$$

h - altitude above surface of the Earth ellipsoid;

$\alpha_{\odot}, \delta_{\odot}$ - right ascension and declination of the Sun;

x, y, z - coordinates of a point of space;

$r = \sqrt{x^2 + y^2 + z^2}$ - distance from centre of the Earth to a point of space with coordinates x, y, z ;

ρ_H - density of night atmosphere;

F_0 - fixed level of solar activity for considered period of time;

F - daily mean value of index $F_{10.7}$;

F_{81} - value of $F_{10.7}$ averaged for 81 day, previous to a moment of account;

$$F_{81} = \frac{\sum_{i=1}^{81} k_i F_i}{\sum_{i=1}^{81} k_i},$$

$$k_i = 0.5 + 0.5(i-1) / (N-1), \quad N = 81, i = 1, 2, 3, \dots, 81.$$

$$F = F_{10.7}(t - \tau_F);$$

$$K_p = K_p(t - \tau_F);$$

$F_{10.7}$ - index of solar activity equal to 10.7 cm (2800 MHz) solar radiation flux density;

K_p - daily mean planetary index of geomagnetic activity;

K_0 - multiplier, describing change of atmosphere density, connected with a deviation of F_{81} from F_0 ;

K_1 - multiplier, taking into account daily effect in density distribution;

K_2 - multiplier, taking into account semi-annual effect;

K_3 – multiplier, describing change of atmosphere density connected with a deviation of F from F_{81} ;

K_4 – multiplier, taking into account dependence between atmosphere density and geomagnetic activity;

φ – the central angle between the point of space for which density is calculated and point of a maximum in its daily distribution;

φ_1 – the angle of delay of density maximum with respect to maximum of light flux;

$A(D)$ – multiplier, describing influence of semi-annual effect on atmosphere density;

τ_F, τ_K – factors, determining delay of reaction of atmosphere density to variation of indexes $F_{10.7}, K_p$;

D – days since the beginning of a year;

$a_1, a_2, a_3, b_1, b_2, b_3, l_1, l_2, l_3, c_1, c_2, c_3, c_4, d_1, d_2, d_3, e_1, e_2, e_3, e_4, e_5, e_6, e_7$,

n_0, n_1, φ_1 – coefficients used for account of atmosphere density at various values of F_0 and h . The values of these coefficients are tabulated.

The basic advantage of this model is its simplicity and feasibility for its computer realization. So, the calculation time for one value of density with help GOST 25645.115-84 is two order less than appropriate time when using foreign models. At the same time the accuracy of this model is comparable to that of more sophisticated semi-empirical models. In particular, more than twenty years of operation of the GOST models at the SSS, and also the results of a number of special experiments on studying of atmosphere density variations using satellite drag measurements [8-14] witness this. The RMS relative errors of atmosphere density determination when using the GOST model at altitudes of 200-500 kms make about 10 % in a quiet conditions and reach 30 % during geomagnetic storms [8-14].

During the space surveillance process exists the opportunity of reduction of influence of density calculation errors at altitudes of 200-500 kms for account of operative estimation and forecasting of density variations with the help of information on atmosphere drag of a group SO in proper area of space [12-14].

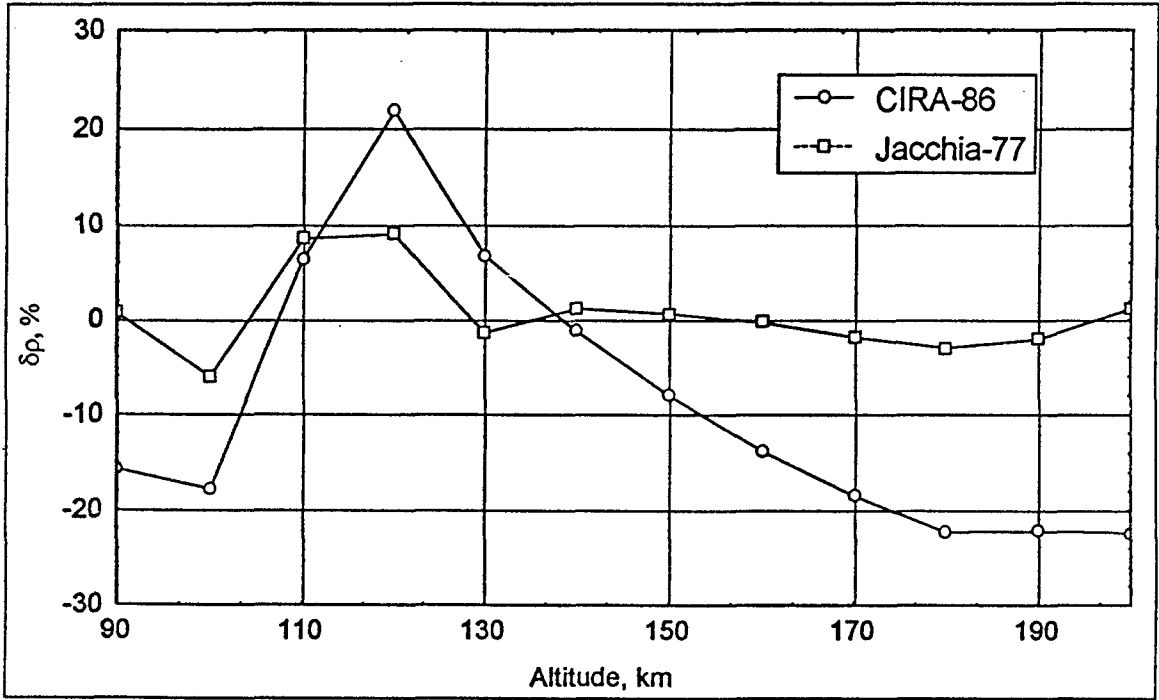
At smaller altitudes such opportunity is practically away because of short-term stay and small number of the satellites simultaneously being in this area. Here the atmosphere is more inertial and its density variations under changes of solar and geomagnetic activity emerge in a smaller degree.

However, the accuracy of knowledge of atmosphere density at low altitudes in many respects defines the accuracy of satellites reentry time determination on a final stage of their flight. Therefore, not less urgent is the problem of atmosphere density calculation accuracy increase at altitudes less than 200 kms. This, in particular, was confirmed by the results of the last works on satellite "Cosmos-398" and FSW-1-5.

Within the framework of research of this issue comparison of three atmosphere density models was made: GOST 25645.115-84, CIRA-86, Jacchia-77. For models CIRA-86 and Jacchia-77 within the range of altitudes of 90-200 kms relative deviations of atmosphere density values from those, calculated on GOST 25645.115-84 for $F_{10.7} = 70$ were determined.

The results of comparison of the models above at altitudes of 90-200 kms are submitted in figure 1.

Figure 1. Results of models comparison at altitudes of 90-200 kms



Given in this figure are two altitude dependences of relative deviations of atmosphere density values, calculated on models CIRA-86 and Jacchia-77 respectively, from the appropriate density on model GOST 25645.115-84 for

levels of activity $F_{10.7} = 70$. It can be seen, that the maximum differences between models GOST 25645.115-84 and Jacchia-77 at altitudes 130-200 km do not exceed 3 %, and at altitudes 110-120 km they reach 9 %. Thus, the difference between these models at small altitudes can be considered insignificant. At the same time CIRA-86 produced density differs from that of GOST 25645.115-84 almost by 25 %. These deviations have essential dependence on altitude. It is very important, as far as, if they had had systematic character and did not depend on altitude then their influence in process of orbit determination and prediction would have been difficult to find. In this case, inadequate description of the density distribution at small altitudes, if it takes place, can have an effect on accuracy of reentry time determination for LEO SO. To check this assumption calculations with use of real data on satellite "Cosmos-398" (71016A) and FSW-1-5 (930963H) were undertaken. The technique of them consists in the following.

On the base of orbital data, produced by US SSN and RSSS on the last revolutions before satellite reentry, on an interval of 7-9 revolutions by the least squares method orbit elements and ballistic coefficients were updated. The latter were the initial data for reentry time determination. The calculations were made with the use of two versions of atmosphere density models: CIRA-86 and GOST 25645.115-84

In figure 2 and 3 the diagrams of the satellites "Cosmos-398" and FSW-1-5 altitude variations at the orbit determination and prediction interval are presented.

It can be seen, that the both satellites have eccentric orbits and on the time intervals chosen for the analysis their altitude are in the range, where in a sufficient degree errors of atmosphere density models should be apparent. In table 1 values of prediction intervals and also absolute and relative values of reentry time determination errors of the satellites are presented.

From given data it follows, that use of model of CIRA-86 instead of GOST 25645.115-84 has resulted in reduction of reentry time determination error for satellite "Cosmos-398" by 5 times, and for satellite FSW-1-5 - by 1.8 time. Additional materials, evidently confirming these estimates, are the results of comparison of predicted and measured coordinates of "Cosmos-398", obtained on the prediction interval (see fig. 2). In table 2 differences between predicted and measured coordinates, corresponding to flight altitude 117-118 km are presented.

Figure 2. Satellite "Cosmos-398" altitude change

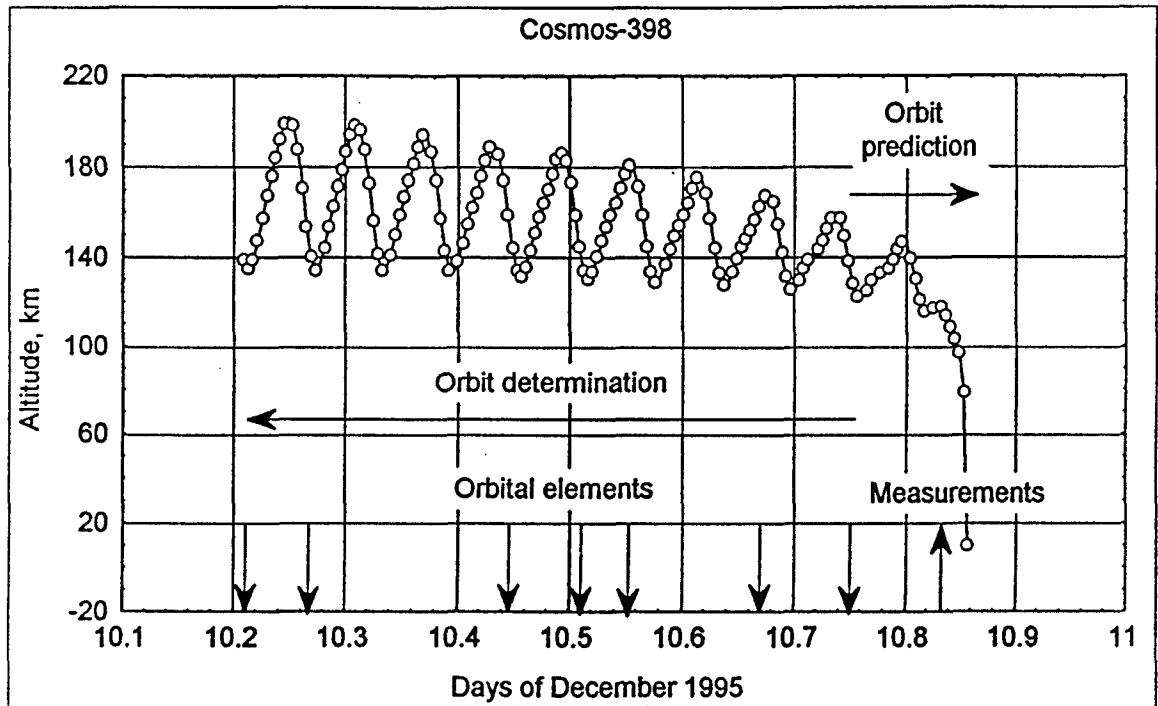


Figure 3. Satellite FSW-1-5 altitude change

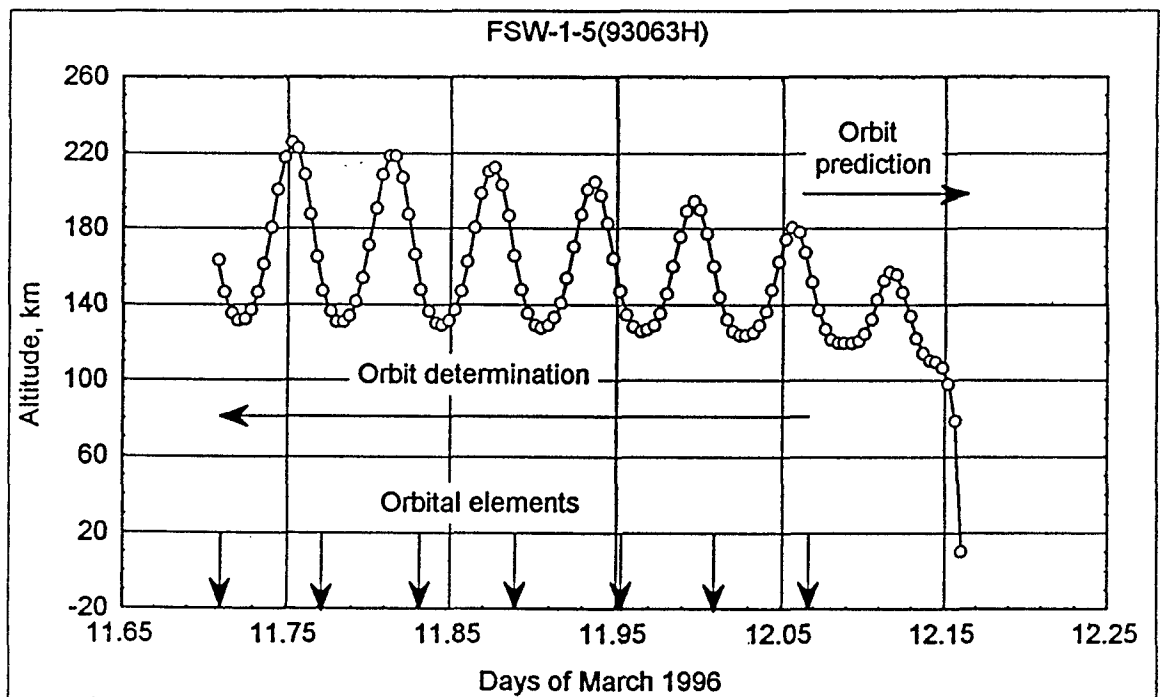


Table 1. Reentry time determination errors

Satellite	Prediction interval, min	Errors for CIRA-86, min(%)	Errors for GOST 25645.115-84, min(%)
Cosmos-398	152	6(3.9%)	31(20.9%)
FSW-1-5	140	14(10%)	26(18.6%)

Table 2. Residuals between predicted and measured coordinates of satellite "Cosmos-398"

Model Measurement	CIRA-86			GOST 25645.115-84		
	Δx , km	Δy , km	Δz , km	Δx , km	Δy , km	Δz , km
1	-0.25	-0.056	-0.307	2.511	-18.794	-9.661
2	0.025	-0.200	-0.273	3.258	-18.918	-10.187
3	0.185	-0.149	-0.005	3.891	-18.829	-10.486
4	0.748	-0.345	-0.285	4.936	-18.967	-11.337

It is obvious, that use of atmosphere model CIRA-86 in considered cases gives essential increase of satellite motion prediction accuracy at small altitudes. However, in view of limited amounts of actual data final conclusions apparently should be made later.

REFERENCES

1. COSPAR International Reference Atmosphere 1972 (CIRA-72). Akademik verlag, Berlin, 1972.
2. COSPAR International Reference Atmosphere 1986 (CIRA-86). Akademik verlag, Berlin, 1972.
3. Hedin A.E. A revised thermospheric model based on massspectrometer and incoherent scatter data. MSIS-83. J. Geophys. Res., № 88, 1983.
4. Jacchia L. G. Thermospheric temperature, density and composition: new models. SAO space report, № 375, 1977.
5. Barlier F. et al. A thermospheric model based on satellite drag data. Ann. Geophys., №34, 1978.
6. Model of the upper atmosphere for ballistic accounts. GOST 22721-77. Moscow, Publishing House of the standards, 1978.
7. Atmosphere of the Earth upper. Model of density for ballistic maintenance

- of flights of the artificial satellites of the Earth. GOST 25645.115-84, Moscow, Publishing House of the standards, 1984.
8. Volkov I.I., Yastrebov V.V. An estimation of models CIRA-72 and J-77 on satellite of a series "Cosmos" drag data. Supervision of artificial celestial bodies, USSR Academy of Sciences Astro council, №84, 1988.
 9. Volkov I.I. An estimation of model CIRA-86 on satellite of a series "Cosmos" drag data. Supervision of artificial celestial bodies, USSR Academy of Sciences Astro council, №86, 1990.
 10. Volkov I.I., Yastrebov V.V. Updating of atmosphere density model on on satellite of a series "Cosmos" orbit evolution data. Supervision of artificial celestial bodies, USSR Academy of Sciences Astro council, №86, 1990.
 11. Volkov I.I., Pankratiev O.V. Updating of atmosphere density model on accelerometer "CACTUS" data. Supervision of artificial celestial bodies, USSR Academy of Sciences Astro council, №86, 1990.
 12. Nazarenko A.I., Amelina T.A., Gukina R.V., Kirichenko O.I., Kravchenko S.N., Markova L.G., Tumolskaya N.P., Yurasov V.S. An estimation of efficiency of various ways of the atmosphere density variations account at satellite motion prediction during geomagnetic storms. Supervision of artificial celestial bodies, USSR Academy of Sciences Astro council, №84, 1988.
 13. Anisimov V.D., Bass V.P., Comissarov I.N., Kravchenko S.N., Nazarenko A.I., Rychkov A.P., Sych V.I., Tarasov Y.L., Fridlender O.G., Schackmistov V.M., Yurasov V.S. Results of research of the aerodynamic characteristics and the upper atmosphere density with the help of the passive satellites "PION". Supervision of artificial celestial bodies, USSR Academy of Sciences Astro council, №86, 1990.
 14. G. Batyr, V. Bratchikov, S. Kravchenko, A. Nazarenko, S. Veniaminov, V. Yurasov. Upper atmosphere density investigations based on Russian Space Surveillance System data. Proceedings of the First European Conference on Space Debris, Darmstadt, Germany, 1993.

THE FEATURES OF PREDICTION PROCEDURES, USED IN LOW-PERIGEE SATELLITES' CATALOG MAINTENANCE

V.F. Boikov

"Vympel" International Corporation, Moscow

Introduction

Prediction procedures [Ref. 1], used for maintenance of Russian satellite catalog are developed with account of requirements to the Space Surveillance Center and also have specific features, characterizing the time of their development. Currently, exchange of catalogs between US and Russian SSCs is organized and thus the community of Russian catalog users is extended. These new users are to be aware of these specific features and conditions.

[Ref.1] comprises formal description of the algorithms but does not treat the background of realized technical decisions. However, the customer is often more interested not in the formulae by themselves but in the understanding of the foundations for the choice of the algorithm.

These issues are the subject of this article. We are to mention our respect to the works [Refs. 2,3], that essentially influenced this paper.

Development of algorithms for satellites' motion prediction was undertaken in late 70-ies in research center of "Vympel" Corporation.

The following problems were posed.

1). To IMPROVE CALCULATIONS RATE to greatest extent possible, retaining the level of accuracy, achieved by algorithm-predecessor. Procedure, used as standard of accuracy was the algorithm developed by A. Nazarenko [Ref. 4] that used equatorial orbital elements.

2). To attain the possibility of rather simple enhancement of accuracy using perturbing factors, previously not taken into account.

3). The algorithm is to be feasible for producing computer codes.

Most of known techniques, proposed for modelling satellites' motion were analysed. The major are as follows (the authors of Russian models are mentioned).

1). Methods of integrating second order equations [Ref. 5].

The methods have certain advantages in calculations of short periodicals and are widely used in classical celestial mechanics (Laplace, Newcomb, Hansen and other techniques) Their limitations are accomplished computation of secular and long periodic perturbations.

2). Methods of consecutive approximations in Poisson form [Ref. 6].

Advantages - minimum knowledge, needed for understanding. Limitations - significant computer load (several functions are integrated) and difficulties in account of perturbations with complex character of secular evolution (atmospheric drag, for example).

3). Method of intermediate orbits [Ref. 7].

Advantageous for high orbits (an outstanding example - theory of the Moon by Hill and Brown). For low satellites intermediate orbit gives enhancement of accuracy for one order in comparison to Keplerian one, thus employment of special theory of intermediate orbit is not justified.

4). Method of consecutive canonic transforms (Delaunay-Zeipel)- [Ref. 8].

This method assumes transition from osculating elements to long-periodic and then from long-periodic to secular elements performed by similar procedures. Perturbations for all the elements are defined taking derivatives of one function. Finally, the method provides the shape for secular equations in complex cases (for example, account of atmospheric drag).

5). Averaging method in the form of calculating evolution of equatorial elements [Refs. 4,9].

Advantage is simple understanding of the technique. Limitation is the existence of two different procedures: calculation of evolution of the elements for a revolution and calculation of long-periodic evolution of these elements. Also, calculations of evolution for all equatorial orbital elements and evolution of the time of passing the equator are performed differently.

Detailed analysis of the methods resulted in the choice to use in development of algorithm (new model of satellite motion) the method of Delaunay-Zeipel in the form of Brouwer.

This solution was rather hard in many senses. The main issue was the fact that in this period all major satellite surveillance centers of the USSR used equatorial elements. These were "Russian" elements [Ref. 10].

So, having changed integration technique and thus rejecting "Russian" elements we became "bad guys" in the eyes of our colleagues (and the Customer). All the effort was taken to return us to the "right path".

It is interesting to mention that in course of these discussions we knew nothing of American models *SGP*, *SGP4*, *PP2*, and our opponents did not mention them as well.

1 Algorithms' package

1.1 Composition

We developed the package of interrelated prediction algorithms, comprising the following major procedures:

- analytical prediction algorithm (A),
 - analytical prediction algorithm with enhanced accuracy (AP),
 - numerical-analytical prediction algorithm (NA),
 - numerical-analytical prediction algorithm with enhanced accuracy (NAP),
 - numerical prediction algorithm (N),
 - numerical prediction algorithm with enhanced accuracy (NP),
- and a set of auxiliary procedures not to be treated here.

1.2 Considered perturbing factors

Uniform set of perturbing factors was accepted for all algorithms. It was considered important, that all the procedures take account of the perturbations **similarly** and with possible completeness. Otherwise,

analysis of discrepancies in propagating one satellite using different procedures becomes difficult.

For algorithms of general accuracy perturbations from zonal harmonics up to sixth order (included) were taken into account, i.e:

$$C_{20}, C_{30}, C_{40}, C_{50}, C_{60}.$$

Also in these procedures perturbations from sectorial harmonic

$$C_{22}, d_{22}$$

were included.

Algorithms with enhanced accuracy account of zonal harmonics up to the 8-th order i.e.:

$$C_{20}, C_{30}, C_{40}, C_{50}, C_{60}, C_{70}, C_{80}.$$

Tesserals are also included up to 8-th order, but to reduce CPU-time for analytical and numerical-analytical methods, in the series for perturbations from tesserals the most significant terms were retained so, that total error from truncation be of the order of 100 meters for satellites with orbital eccentricity not exceeding the threshold:

$$e \leq 0.05$$

In these expansions the terms with e^2 and higher are also ignored.

Precise numerical algorithm account of all the perturbations and also has the possibility to extend the order of included perturbations up to 16.

Atmospheric drag is taken into account in different ways for analytical, numerical and analytical-numerical algorithms.

Analytical algorithm assumes that atmospheric drag is small and can be taken into account via coefficients:

$$\ddot{M}, \ddot{\omega}, \ddot{\Omega}, \dot{L}, \dot{e}.$$

These coefficients are calculated using simplified formulas in dependence of night density of the atmosphere in altitude of satellite's perigee, that depends in its turn on solar radiation intensity $F_{10.7}$.

Numerical-analytical and numerical procedures calculate the density using complete dynamic model of the atmosphere.

Numerical-analytical algorithm calculates evolution of the elements under atmospheric drag by means of numerical integration of averaged equations of motion. This subject will be treated further.

1.3 Catalog elements

Input elements for all the procedures are non-singular orbital elements in the form, accepted for satellite catalog. Thus these elements will be called (as distinct from "Russian" elements ¹) *catalog elements (CEL)*. This set of elements comprise the following:

$$t, \lambda = M + \omega, L = \sqrt{\mu a}, \theta = \cos i, \Omega, h = e \sin \omega, k = e \cos \omega, S,$$

where:

t - reference epoch,

M - mean anomaly,

ω - perigee argument,

a - semi-major axis,

i - inclination,

Ω - longitude of ascending node,

e - eccentricity,

S - matching ballistic coefficient.

Together with orbital elements the *number of prediction procedure*, used in their updating is present in the catalog. The reason is: though similar in their form, orbital elements produced using different algorithms *differ*.

¹Widely known and frequently used in Russia so called "Russian" elements (REL) [Ref. 10], comprising the time of crossing the equator, draconic period, decline of period per revolution and Keplerian osculating elements for ascending node can be produced from catalog elements using special transformations' procedures. Certainly, the best accuracy of orbits' predictions can be achieved using catalog elements and the same prediction algorithm, that was used for updating of the elements; otherwise additional matching procedures and transformations are to be introduced, surely not enhancing prediction accuracy.

The differences are caused by various averaging techniques, employed in the algorithms.

In numerical algorithms no averaging is present, thus the elements have the meaning of *osculating*.

Analytical procedures are designed with account of double Brouwer averaging, thus the elements are *doubly averaged*.

Finally, design of numerical-analytical algorithm also uses Brouwer technique [Ref.11] to obtain equations, describing evolution of doubly averaged elements under atmospheric drag. These equations were further solved using averaging technique.

Thus, for numerical-analytical methods the input data are to be *averaged once, doubly averaged (Brouwer) elements*.

1.4 Special modes

Analysis revealed that the greatest part of time is consumed by the algorithms in course of updating the orbits with the measurements. With regard to prediction these tasks are rather specific. They require performing a set of predictions for various moments of measurements with one and the same initial data. That is why *special modes of on-going calculations* are used.

The sense of these modes is that once computed values are stored and used further in predictions for all the moments. For example, in analytical procedure coefficients of secular evolution and amplitudes of long-periodic inequalities are stored.

Also this is the reason to use formulae for fast computation of trigonometric functions, employing simple approximations, valid for small intervals of argument's variations.

For *critical inclination* the algorithms provide special mode, when corresponding additives of perturbations are transferred from long-periodic to secular and then are approximately integrated in the shape of polynomials of time. This technique has less accuracy than the known method of presenting solution as series in powers of square root of small parameter, but does not require essential accomplishment of algorithms.

2 Additional information on the algorithms

Analytical and numerical-analytical algorithms fulfill calculations of secular and long-periodic perturbations from zonal harmonics with accuracy $O(c_{20}^2)$ using the formulas, taking *complete* account of inclination and eccentricity dependences.

Expansion of hamiltonian in non-singular elements h, k is rather complex [Ref. 12], thus the algorithms use expansion of classical type in e, ω . Singularity in eccentricity is avoided, calculating $e\Delta(\omega)$ instead of $\Delta(\omega)$ and using modified functions of eccentricity.

Functions of inclination and eccentricity are calculated for these perturbations by means of special "diagonal" recurrent scheme.

Numerical-analytical algorithms use for integration of averaged equations Runge-Cutt third order technique.

The integration step is chosen using special empirical formulas depending on altitude and remaining orbital time. This step usually is 1-5 days, i.e. in orbits' updating numerical-analytical prediction performs one or two integration steps and in practice may be considered analytical.

To avoid fractioning of the step when one of the moments falls into it, *special new interpolation formula* is used. This formula is designed in such a way, that instead of unknown coefficients of Taylor series it involves known values of right sides for intermediate points of the step, computed by Runge- Cutt method.

For calculations of the right sides of averaged equations the values of the order of $O(e^3)$ and $O(e^2 \cdot \rho)$ are considered ignorable.

Derivation of equations for doubly averaged values the differences between averaged and osculating elements were taken into account only under exponent sign [Ref. 13].

For calculations of atmospheric density ρ special approximation of standard model of atmosphere FOCT 25645.115-84 was used, performing computing of the density in 150 operations.

For reference this model is presented in Appendix.

Numerical prediction algorithm uses Adams method, where special empirical rules are used to choose the order and the formula of the method

for the step.

Numerical method with enhanced accuracy uses Boullirsh technique.

3 The main characteristics of the package

The main characteristics of the package are presented in table 1.

Respectively:

first column - acronym of the algorithm,

second column - symbolically presents taken into account gravitational field,

third column indicates whether static or dynamic model of atmosphere is used,

fourth column presents *number of operations* for on-going calculations mode (in brackets - the main mode),

fifth column presents CPU-time for Elbrus-2 computer with average rate of 3500 000 operations per second,

sixth column gives prediction error along the track (in brackets - in normal direction).

Main theoretical characteristics of developed procedures are summarized in table 2.

Respectively:

first column - acronym of the algorithm,

second column gives the used catalog elements²,

third column presents symbolic notation of the main functions of employed method,

fourth column gives assessment of various errors.

²traditionally, the sign ' means averaging

The version of the package for PC (C language) is realized.

Currently preparation of needed user's documentation is being finished.

Table 1. Perturbation factors, number of operations, accuracy of different prediction procedures

Procedures	Earth	Atmosphere	Number of operations	CPU-time	Precision
A	6×2	static model $F_{10.7}$	1100 (2200)	0.0003s 0.0006s	1.5(0.5)km $e < 0.05$
AP	8×8	static model $F_{10.7}$	2800 (6300)	0.0006s 0.0015s	0.2(0.1)km $e < 0.05$
NAP	8×8	dinamic model	4200 (12000)	0.001s 0.003s	0.2(0.1)km $e < 0.05$, 3% atmospheric drag $e < 0.1$
N	6×2	dinamic model	10^6	0.16s/d	8km/d
NP	14×14	dinamic model	$(0.6 \div 2.7) \times 10^6$ (Earth $8 \div 8$)	$0.1 \div 0.45$ s/d	0.1km

Table 2. Methods and catalog element sets,
employed in prediction procedures

Proc	Catalog element set	Method	Precision: Δ
A	$W'' = \{\lambda'', L'', \theta'', \Omega'', h'', k'', S\}$	$W(t) = W''(t) + \delta\tilde{W}(t) + \delta W(t) + \delta W_{tes}(t)$	$\Delta W'' \sim o(c_{20}^2 t)$ $\delta\tilde{W}, \delta W \sim o(c_{20}), o(\frac{c_{n0}}{c_{20}})$ $\delta W_{tes} \sim o(\frac{c_{22}}{n_E} e^2)$
AP	$W'' = \{\lambda'', L'', \theta'', \Omega'', h'', k'', S\}$	$W(t) = W''(t) + \delta\tilde{W}(t) + \delta W(t) + \delta W_{tes}(t)$	$\delta W_{tes} \sim o(\frac{c_{nm}}{n_E} e^2)$
NAP	$W''' = \{\lambda''', L''', \theta''', \Omega''', h''', k''', S\}$	$\frac{dW'''}{dt} = \mathcal{F}(\frac{\partial W'''}{\partial W'''}(W''')) + \tilde{Q}_{atm}$	$Q \sim o(e^3, e^2 \rho)$ $\Delta \lambda_{rel} \sim 3\%$
N	$W = \{\lambda, L, \theta, \Omega, h, k, S\}$	base. $P_k E_1 C_{k+1} E_2 C_{k+1} (k = 6, 10)$ reserv. $P_k (E_1 C_{k+1})^2, t \leq 4$	$\Delta r \sim 1 \text{ km/d}$
NP	$W = \{\lambda, L, \theta, \Omega, h, k, S\}$	U	$\Delta r \sim 0.1 \text{ km/d}$

REFERENCES

1. V.Boikov, G.Makhonin, A.Testov, Z.Khutorovsky, A.Shogin, " Prediction Procedures Used in Satellite Catalog Maintenance", *Proc. of the US/Russia Orbit Determination and Prediction Workshop*, Washington, July 13-15, 1994.
2. A.I.Nazarenko, " Models of Motion Employed in Space Surveillance Activities: A Retrospective Analysis", *Proc. of the US/Russia Orbit Determination and Prediction Workshop*, Washington, July 13-15, 1994.
3. P.Schumacher, " Analytic Orbit Model for US Naval Space Surveillance", *Proc. of the US/Russia Orbit Determination and Prediction Workshop*, Washington, July 13-15, 1994.
4. "Основы теории полета космических аппаратов", Сб.под редакцией Г. С. Нариманова, "Машиностроение", Москва, 1972.
5. Ю. Г.Евтушенко, "Движение искусственных спутников в гравитационном поле Земли", Изд-во ВЦ АН СССР, 1967.
6. М.К.Тихонравов, И.К.Бажинов и др. "Основы теории полета и элементы проектирования ИСЗ", Москва, Машиностроение, 1974.
7. Е.П.Аксенов, "Теория движения искусственных спутников Земли", Наука, Москва, 1977.

8. М. Л. Лидов, "Полуаналитические методы расчета движения спутников", *Труды ИТА*, т.17, с.54-61, 1978.

9. Б. В. Кугаенко, П.Е. Эльясберг, "Эволюция почти круговых орбит под влиянием зональных гармоник", *Космические исследования*, т. 6, вып. 2, 1968.

10. A.I.Nazarenko, "Analysis and Comparison of Orbital Elements Used for Satellites Motion Prediction in Russia and in Space Surveillance Center", *Proc. of the International Workshop on Techniques for Cooperative International Satellite Orbit Determination and Maintenance*, Moscow, October 14-15, 1993.

11. D.Brouwer, G.Clemence, "Methods of celestial mechanics", *Academic Press*, New York and London, 1961.

12. D.Danielson, "Satellite Orbit Theories", *Proc. of the US/Russia Orbit Determination and Prediction Workshop*, Washington, July 13-15, 1994.

13. М.Л.Лидов, А.А.Соловьев, "Метод расчета атмосферных возмущений движения спутника по орбите с большим эксцентриситетом", *Препринт ИПМ АН СССР*, вып.37, Москва, 1976.

14. "Атмосфера Земли верхняя. Модель плотности для баллистического обеспечения полетов искусственных спутников Земли", ГОСТ 25645.115-84, Москва, 1985.

Appendix

Subroutine ATMOSPHERE

Subroutine ATMOSPHERE realizes approximation of the atmosphere density model [Ref.14].

The input parameters are :

h - satellite altitude over Earth surface,

$\sin u, \cos u$ - sine and cosine of the argument of latitude (under $P_{fl} = 0$),

$\sin i, \cos i$ - sine and cosine of inclination ,

Ω - longitude of ascending node ,

t - epoch time ,

P_{fl} - the flag of operation mode.

Subroutine uses two operation modes :

$P_{fl} = 0$ - calculation of density for required point

$P_{fl} = 1$ - calculation of "mean" density and parameters of solar bulging .

The flag $P_{fl} = 0$ is used for numerical integration of equations of motion. Access of the NA procedure to the subroutine is done with $P_{fl} = 1$

Calculations of density ρ , "mean" density $\bar{\rho}_0$ and solar bulging parameters F , $\cos u^*$, $\sin u^*$ are fulfilled using the formulas:

$$\rho = \rho_n K_0 K_1 K_2 K_3 K_4,$$

$$\bar{\rho}_0 = \rho_n K_0 K_2 K_3 K_4 (1 + 0.5 K_1' (U_1 + U_2)),$$

$$F = \frac{K_1' (U_1 - U_2)}{2 + K_1' (U_1 + U_2)},$$

$$\cos u^* = \kappa_1 / \kappa, \quad \sin u^* = \kappa_2 / \kappa,$$

where

$$K_0 = 1 + (l_1 + l_2 h + l_3 h^2) (\bar{F}_{135} - F_0) K_f,$$

$$K_2 = 1 + (d_1 + d_2 h + d_3 h^2) A(D),$$

$$K_3 = 1 + (b_1 + b_2 h + b_3 h^2) (\bar{F} - \bar{F}_{135}) / \bar{F}_{135},$$

$$K_4 = 1 + (e_1 + e_2 h + e_3 h^2 + e_4 h^3) (e_5 + e_6 \bar{k}_p + e_7 \bar{k}_p^2)$$

are multipliers, characterizing changes in atmosphere density due to: F_0 deviation from \bar{F}_{135} , half-year effect, \bar{F} deviation from \bar{F}_{135} , dependence of atmosphere density on geomagnetic perturbation respectively,

\bar{F} , F_0 , \bar{F}_{135} - are daily averaged, fixed and the mean for preceeding 135 days values of $F_{10.7}$,

$F_{10.7}$ - index of solar activity, equal to solar radio-emission flux density for the wavelength $10.7 sm$,

\bar{k}_p - daily averaged index of geomagnetic perturbations,

D - amount of days from the year beginning,

$\rho_n = \tilde{a}_1 P(z)$ - approximation of atmosphere night density :

$$z = \tilde{a}_2 \sqrt{h - \tilde{a}_3} - \tilde{a}_4 ,$$

$P(z)$ - polynomial approximat in of e^z :

$$P(z) = (1 + z(u_1 + z(u_2 + z(u_3 + zu_4))))^8,$$

$u_1 = -0.9998684/8$, $u_2 = 0.4982926/8^2$, $u_3 = -0.1595332/8^3$, $u_4 = 0.0293641/8^4$ - constants,

$K_1 = 1 + K'_1 \cos^n \varphi/2$ - factor, accounting for daily effect in density distribution:

$$K'_1 = c_1 + c_2 h + c_3 h^2 + c_4 h^3,$$

φ - central angle between the current point, where the density is calculated and the point with the maximum density, regarding its daily distribution:

$$\cos \varphi = \kappa_1 \cos u + \kappa_2 \sin u,$$

$$\kappa_1 = \sin i \sin \delta_{\odot} - \sin(\Omega - \alpha_{\odot} - \varphi_1) \cos i \cos \delta_{\odot},$$

$$\kappa_2 = \cos(\Omega - \alpha_{\odot} - \varphi_1) \cos \delta_{\odot},$$

$\alpha_{\odot}, \delta_{\odot}$ - angular coordinates of the Sun ,

$$\kappa = \sqrt{\kappa_1^2 + \kappa_2^2},$$

$$U_1 = (\frac{1}{2}(1 + \kappa))^{n/2},$$

$$U_2 = (\frac{1}{2}(1 - \kappa))^{n/2},$$

$K_f, \tilde{a}_1, \tilde{a}_2, \tilde{a}_3, \tilde{a}_4, b_1, b_2, b_3, l_1, l_2, l_3, c_1, c_2, c_3, c_4, d_1, d_2, d_3, e_1, e_2, e_3, e_4, e_5, e_6,$

e_7, n, φ_1 - coefficients of the model, stored in MKA array and used for calculating atmosphere density under different values of F_0 .

Unlike the [Ref.13] formula for night density calculations

$$\rho_n = a_0 \exp(a_1 - a_2 \sqrt{h - a_3}),$$

constants \tilde{a}_i , $i = 1 \div 4$, used for its polinomial fit, are specified not for three, as in [Ref.13], but for four layers :

$$120km \leq h \leq 180km, \quad 180km < h \leq 320km,$$

$$320km < h \leq 600km, \quad 600km < h \leq 1500km.$$

Their values are given. The values of other constants are not present here, one can find them in [Ref.14] .

$$F_0 = 75$$

$$\tilde{a}_1 = \{2488.5533, 40.293687, 0.4496995, 0.001213834\}$$

$$\tilde{a}_2 = \{0.7009, 0.8016, 0.8016, 0.2336\}$$

$$\tilde{a}_3 = \{115.3429, 86.3329, 86.3329, 491.2201\}$$

$$\tilde{a}_4 = \{1.512564, 7.758026, 12.25339, 2.43639\}$$

$$F_0 = 100$$

$$\tilde{a}_1 = \{2488.3927, 43.839081, 0.6731885, 0.002518119\}$$

$$\tilde{a}_2 = \{0.7000, 0.7675, 0.7675, 0.2417\}$$

$$\tilde{a}_3 = \{114.638, 77.1052, 77.1052, 490.7284\}$$

$$\tilde{a}_4 = \{1.620829, 7.785295, 11.96155, 2.52656\}$$

$$F_0 = 125$$

$$\tilde{a}_1 = \{2488.4695, 53.128673, 1.0484604, 0.005169129\}$$

$$\tilde{a}_2 = \{0.6419, 0.7362, 0.7362, 0.2654\}$$

$$\tilde{a}_3 = \{115.956, 70.5386, 70.5386, 479.9537\}$$

$$\tilde{a}_4 = \{1.290698, 7.702404, 11.62780, 2.90787\}$$

$$F_0 = 150$$

$$\tilde{a}_1 = \{2488.3167, 60.041084, 1.4225368, 0.009801573\}$$

$$\tilde{a}_2 = \{0.6124, 0.6805, 0.6805, 0.2911\}$$

$$\tilde{a}_3 = \{116.415, 80.4406, 80.4406, 461.9691\}$$

$$\tilde{a}_4 = \{1.159459, 6.789992, 10.53258, 3.42003\}$$

$$F_0 = 200$$

$$\tilde{a}_1 = \{2487.8713, 67.399254, 2.1926321, 0.027742197\}$$

$$\tilde{a}_2 = \{0.5974, 0.5797, 0.5797, 0.3492\}$$

$$\tilde{a}_3 = \{116.214, 100.9417, 100.9417, 399.0605\}$$

$$\tilde{a}_4 = \{1.162338, 5.154387, 8.57992, 4.95002\}$$

$$F_0 = 250$$

$$\tilde{a}_1 = \{2488.1558, 75.038546, 3.0883709, 0.060895223\}$$

$$\tilde{a}_2 = \{0.5772, 0.5095, 0.5095, 0.4130\}$$

$$\tilde{a}_3 = \{116.339, 115.2277, 115.2277, 284.6955\}$$

$$\tilde{a}_4 = \{1.104324, 4.100519, 7.29088, 7.35132\}$$

APPLICATIONS OF PARALLEL PROCESSING TO ASTRODYNAMICS

S. COFFEY

*Naval Research Laboratory
Washington, DC 20375-5355*

H. NEAL*

GRC International

July 17, 1996

Abstract. Parallel processing is being used to improve the catalog of earth orbiting satellites and for problems associated with the catalog. Initial efforts centered around using SIMD parallel processors to perform debris conjunction analysis and satellite dynamics studies. More recently, the availability of cheap super computing processors and parallel processing software such as PVM have enabled the reutilization of existing astrodynamics software in distributed parallel processing environments. Computations, once taking many days with traditional mainframes, are now being performed in only a few hours. Efforts underway for the US Naval Space Command include conjunction prediction, uncorrelated target processing and a new space object catalog based on orbit determination and prediction with special perturbations methods.

Key words: Parallel Processing, critical inclination, UCT, PVM, SIMD

1. Background

A decade ago parallel processing became available commercially from companies like Thinking Machines, MASPAC, INTEL, IBM and others. Since then many hardware and software environments have been available. In this paper we present an overview of problems to which we have applied parallel processing. The applications include the critical inclination problem in celestial mechanics and operational problems encountered by the US Naval Space Command (NSC), one of the primary US tracking organizations. The techniques we employed have varied; we have used SIMD (Single Instruction Multiple Data) Massively Parallel computers and Distributed Parallel Systems built on the PVM (Parallel Virtual Machine) environment.

There are several ways that parallel processing can benefit the user;

- provide improved turnaround time,
- enable the use of underutilized hardware,
- allow for the reuse of existing software.

In the applications we have built, many of these benefits have been realized.

* Naval Research Laboratory, Washington, DC 20375-5355

2. The Critical Inclination Problem

The Naval Research Laboratory (NRL) obtained a parallel processing computer, the Connection Machine 2 (CM-2) in 1987. Our first effort with this computer was to study the critical inclination problem for the theory of an artificial satellite. After averaging, the phase space for this problem is a 2 dimensional sphere which can be visualized graphically. We set out to develop a method for using the new parallel processor in our investigations. We started with a serial program called CCCP (Creative Color Contour Program) developed at NIST by Jonathan Aronson working in collaboration with Dr. André Deprit. This program, written for a LISP Machine, allowed one to display contours of a Hamiltonian by assigning colors to the Hamiltonian values. This eliminated the need for tedious numerical integrations producing a more complete picture than previously possible.

The Hamiltonian for the artificial satellite problem was constructed by averaging the short period terms when the perturbations were restricted to the zonal harmonics. We give here the Hamiltonian through J_4 ,

$$\begin{aligned} \mathcal{H} = & \left(\frac{G}{p}\right)^2 \left(\frac{\alpha}{p}\right)^2 \eta^3 \left(\frac{3}{4}s^2 - \frac{1}{2}\right) \\ & + J_2 \left(\frac{G}{p}\right)^2 \left(\left(\frac{\alpha}{p}\right)^4 \left(\xi_2^2 \eta \left(\frac{45}{32}s^2 - \frac{21}{16} \right) + \eta^5 \left(\frac{75}{128}s^4 - \frac{27}{32}s^2 + \frac{3}{16} \right) \right. \right. \\ & \quad \left. \left. + \eta^4 \left(-\frac{27}{32}s^4 + \frac{9}{8}s^2 - \frac{3}{8} \right) - \eta^3 \left(\frac{195}{128}s^4 - \frac{81}{32}s^2 + \frac{15}{16} \right) \right) \right. \\ & \quad \left. + \frac{J_3}{J_2^2} \left(\frac{\alpha}{p}\right)^3 \xi_2 \eta^2 \left(\frac{15}{8}s^2 - \frac{3}{2} \right) + \frac{J_4}{J_2^2} \left(\frac{\alpha}{p}\right)^4 \left(\xi_2^2 \eta \left(\frac{105}{32}s^2 - \frac{45}{16} \right) \right. \right. \\ & \quad \left. \left. + \eta^5 \left(-\frac{105}{128}s^4 + \frac{45}{32}s^2 - \frac{9}{16} \right) + \eta^3 \left(\frac{315}{128}s^4 - \frac{105}{32}s^2 + \frac{15}{16} \right) \right) \right). \end{aligned}$$

The variables in the Hamiltonian are given by

$$\xi_1 = \eta e s \cos g, \quad \xi_2 = \eta e s \sin g, \quad \xi_3 = \eta^2 - \frac{1}{2}(1 + H^2/L^2).$$

In these coordinates,

$$\xi_1^2 + \xi_2^2 + \xi_3^2 = \frac{1}{4}(1 - H^2/L^2)^2. \quad (1)$$

The remainder of the variables are e , the eccentricity, H the angular momentum, L the conjugate to the mean anomaly, $\eta = \sqrt{1 - e^2}$, and $s = \sin(I)$.

The Hamiltonian has one degree of freedom after averaging, with two integrals, H and L . Thus, interesting information was to be had by studying the evolution of the phase space under the control of the integrals.

Using CCCP as a guide, we wrote a new program for the CM-2, although with significant algorithms to enhance the details of the phase space. Conceptually, the idea is to assign different processors, from a pool of 64K processors, to the coordinates of a grid placed on the projection of the phase

space onto a plane, Figure 1. The parallel processor then computes simultaneously the Hamiltonian for all points in the grid. The Hamiltonian values are sorted and assigned colors which are used to paint the phase space. The initial idea was to construct a rectangular grid on the projection of the phase space. Thus, we first select an orientation then apply the coloring algorithms to paint the resulting projection. The full details behind this technique are provided in (Healy and Deprit, 1991). This technique provided a lot of information quickly that allowed us to gain an appreciation of the changing phase space. From these observations we drew conclusions that helped direct subsequent analytic investigations. The results of the research can be found in (Coffey, et al., 1994).

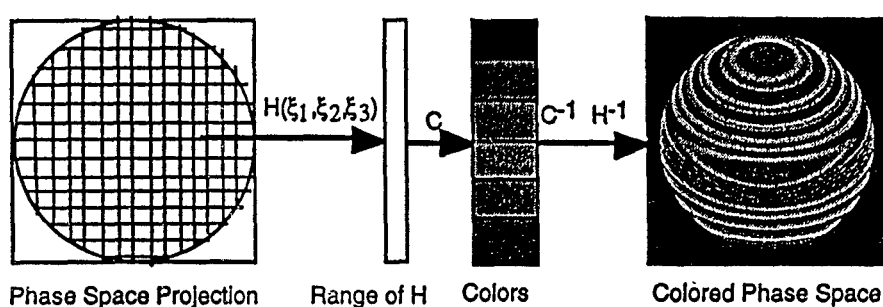


Figure 1. Coloring a Phase Space

Since the phase space is a sphere, it is important to see the image from different orientations. However, the CM-2 is not a good graphics engine. Using an icosahedral (nearly uniform) grid for the sphere (Baumgardner and Frederickson, 1985) we can compute the Hamiltonian on the sphere rather than on the projection of the sphere. This enables us to bring back the true 3 dimensional phase space for display on our Silicon Graphics workstations. This provides better visualization of the three dimensional images. We frequently use 40962 vertices for the true 3-d images.

A SIMD computer, like the CM-2, was a good choice for this problem. Here we were building a new computer program and were free to select the hardware best suited to the problem. For many subsequent problems we did not have this luxury in that we often have to reuse existing software, which carries with it the need to conform to certain hardware. SIMD stands for Single Instruction Multiple Data, which means that at each execution cycle every processor executes the same instruction. For the phase space problem we needed, at each grid point, to evaluate the Hamiltonian. The algebra is the same regardless of the coordinate. Only the coordinates which are the data are different. This program could therefore be written with huge

internal arrays to hold the Hamiltonian values. Each array element would be automatically mapped to a processor by the Connection Machine system. This computer system provides special hardware for efficiently broadcasting instructions to the processors and returning values to the control processor which is the front end computer.

3. Satellite Collision Prediction

Another problem that we applied our CM-2 computer to was COMBO, the Calculation of Miss Distance Between Objects in space. We wanted to determine when objects in space come close to each other. The Air Force and Naval Space Commands, which are part of US Space Command, have had for a number of years programs for computing the distances between a single object and the set of known objects in the space object catalog. We call this the one-to-all collision problem. We wanted to generalize this to determine when any two objects come close together, an all-to-all comparison of positions. This is useful for determining the probability of collisions in space which might lead to chain reactions of fragmentations of space objects.

Although we had access to the Naval Space Command's (NSC) COMBO software, we elected to build from scratch, a program we call CM-COMBO. The hardware of choice was again the Connection Machine. At first we used the CM-2. Later we converted to the Connection Machine 5E (CM-5). This computer runs similar to the CM-2, but is quite different in hardware. Its processors are 64 bit versions of the Vector Sparc Chip. There are fewer of them, 256 processors in our computer, with 16K possible. The technique on this computer is to allow each processor to act like a large set of virtual processors. That is, each processor cycles through arrays much like a serial computer does with a do-loop. This is transparent to the user, the programming being almost identical to that on the CM-2.

The concept behind CM-COMBO was to assign individual processors to the objects in space. Each processor starts with the initial conditions, called an element set, for its object. It applies a propagator to the elements to compute the new position. All objects are propagated to the same new time. We generally use the propagator PPT2, which is what NSC uses to construct the elements for the Navy's catalog. PPT2 is based on the analytic theory of Brouwer (1959). Since the propagator is analytic the same instruction set is used to compute the position of every object. Thus, once again we see the benefit of the SIMD computer. A fairly complex method for determining close approaches was developed, the details are available in (Healy, 1995). Although COMBO prints a report on the conjunctions, the most flashy output is a picture like that in Figure 2. This particular figure shows the

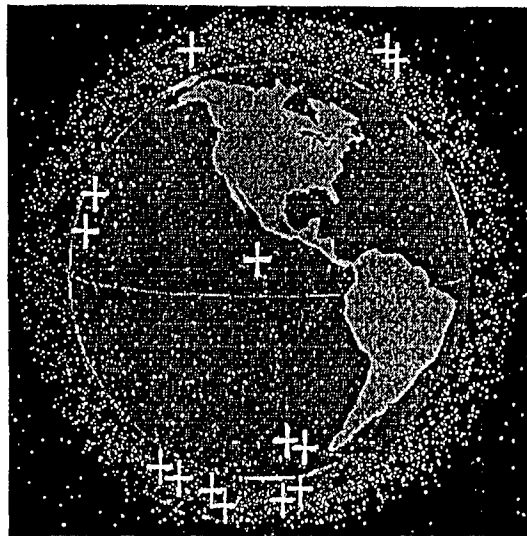


Figure 2. Conjunctions of Debris for catalog of 3 June, 1996. Catalog size of 8919 objects. Conjunction distance of 5 km.

instantaneous locations of all the objects in the catalog for December, 1995. The + marks, indicate two or more objects less than 5 km apart.

NSC runs COMBO remotely from an account on the CM-5. The element sets are automatically deposited in the account. NSC has used the program to confirm conjunctions with the shuttle which they obtain with their own software. They also run the program to obtain reports of coming conjunctions that might be photographed by ground based telescopes. One such event of TIROS 10 and NOAA 10 was photographed on May 21, 1993. COMBO computed a miss distance of 2.1 km. While the use of this program is not essential to their operations, it is believed to be the first significant use of external computing resources by NSC.

A SIMD computer is a natural choice for this problem because of use of the use of an analytic propagator. However, if for increased accuracy, a numerical integrator were substituted then the efficiency of the SIMD computer would suffer because the huge variation in the orbits represented in the catalog would require substantially different step sizes for the integrations. Thus the computer would run at the speed of the slowest integration.

SIMD computers are dropping in popularity and likely will be less of a factor for parallel processing in the future. As a result Dr. Healy recently ported most of COMBO to the PVM (Geist, A., et al., 1994) environment. PVM allows a group of heterogeneous computers to operate as a parallel computer. Unlike the SIMD method of broadcasting instructions, information in a PVM environment is passed by a message passing system. PVM proved an adequate system for this version of COMBO.

4. Uncorrelated Target Processing

US Space Command, in tracking space objects, frequently obtains observations that cannot readily be correlated to a known object. Often this results from an observation from an unknown object or from an object previously cataloged but later lost. Most often these observations come from fragments produced by explosions of rocket bodies and satellites. These observations, called uncorrelated targets (UCTs), present a serious problem for US Space Command. The Naval Space Command radar fence that stretches across the southwest United States is the largest detector of UCTs. This passive radar obtains returns for almost any object with an inclination above 30 degrees.

NSC developed a program called SAD (Search and Determine) to correlate UCTs which are kept for 60 days. The essence of the algorithm, when it is used for UCT processing, is to form every possible pair of observations from the UCT file and then determine what orbits could contain these two observations. For UCT processing the observation set is usually made up of earth-centered X-Y-Z observations. These observations are created by triangulating direction cosines from the NSC fence to create one X-Y-Z observation per orbital pass.

SAD is also used for processing fragmentation events. Here, the blast point of the fragmentation is used as the first observation in every pair. In this case the number of pairs processed decreases dramatically with a corresponding decrease in computer time.

NSC has never been able, with their 1970 vintage Cyber computers to process more than 5 days of observations, mainly because the computer time would take several days. Moreover, recent events at NSC eliminated any possibility of running the program. We undertook to rewrite this program for parallel processing (Coffey et al, 1996) with three objectives:

- reestablish the use of the SAD for UCTs,
- provide rapid turnaround performance,
- enable the processing of the full 60 day sets of observations.

This is an instance where we reused most of the existing program. We rewrote the program to run on top of PVM. PVM links distributed processors together in a parallel processing environment. Each processor completes an assigned task, receiving data and returning results to one or more computers. There are a number of nested loops in the original SAD program, starting with a loop through the pairs of objects called starter pairs, a loop over the direction of the orbits constructed and a loop on the possible solutions to Lambert's problem. Inside the starter pair loop there is a refinement step to include associated observations. We parallelized on the outermost starter pair loop. A master/slave design was implemented. The master program selects pairs of objects to construct orbits from. These pairs are sent to the slave processors along with the complete observation set. This code

was unchanged from the serial program. The master starts up the slave programs, one for each node in our "virtual machine." The virtual machine is the collection of processors on which the program executes. The master can auto-detect the number of nodes available eliminating the need to specify how many nodes to use. Because the master program does so little, a slave program is also set up on it.

The code internal to the starter pair loop was formed as a standalone program for the slave processors. The slave processors return the orbits found, providing a distinction for orbits presenting a high confidence of being a real object. These orbits are called superior orbits. The greatest dilemma in designing the parallel version of SAD was how to handle superior orbits. In the serial version of SAD, the discovery of a superior orbit affects the processing of all succeeding starter points because the observations linked to the superior orbit are removed from the observation set. In the parallel program, several starter points are processed concurrently, so when a superior orbit corresponding to a particular starter point is found in one slave program some of the observations supporting that superior orbit may have been already processed as starter points by other processors. In order to mimic the serial version of SAD, all starter points after the one for which a superior orbit was found would have to be reprocessed with the adjusted observations set. This would require greater complexity in the code to take care of the necessary bookkeeping, and the re-processing could severely diminish the efficiency of the parallel code, especially when a large number of nodes are present in our virtual machine.

We have some leeway in handling superior orbits. However, we still wish to remove the observations associated with superior orbits from the observation set. Leaving them in can result in extra orbits in the output. Our solution is to update the observation set on the master and all the slaves as soon as possible after it changes. The slave program in which the superior orbit is found returns the orbit and its associated observations which are removed immediately from the observation set. The updated observation set is then broadcast to all the slave nodes. The slave nodes will not receive this set, however, until they finish processing the starter point on which they are working. So, the change on all the slaves except the one with the superior orbit will be effective with the next starter point they process. The starter points that are being processed or have already been processed are not re-evaluated with the updated observation set.

One implication of updating the observation set in this manner is that if Parallel SAD is run multiple times with the same observation set, the number of orbits and their solutions will vary from run to run. This occurs because the starter points that have been processed when the observation set is updated will be different on each run, due to differences in the operating conditions on the nodes in the virtual machine. This behavior makes it

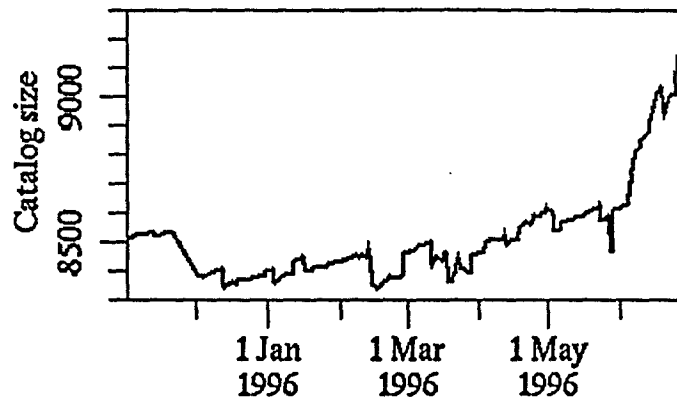


Figure 3. Increase in the Space Object Catalog

very difficult to test and debug the software, but it is acceptable from the analyst's point of view: any version of the output set will meet his needs. The program usually produces more orbits than the analyst can use. But, it generally does not miss real orbits.

Parallel SAD was installed at the US Air Forces's IBM SP2 parallel computer located at Kihei, Maui, Hawaii, where it became operational in May, 1995. Since then it has been used on average every two weeks by the operations group at NSC. Programs are submitted to the SP2 through batch queues, the largest allowing for 128 processors. The turnaround for a batched job can be as much as 24 hours. However, that is substantially less than it would take on a single workstation. The normal run time for 60 days of data is two to four hours on 128 processors. The programming time was approximately 3 man months. This is the second time that NSC has made significant use of external resources for operational activities.

Recently we installed the program at NSC on 14 little used workstations from their Finance Department. The installation took a day for PVM and Parallel SAD and 3 days to check out the program. However, interestingly, previous to installation it took 30 days to obtain approval to install the system. The normal execution takes about 16 hours on these computers.

On 3 June 1996 object 23106, a Pegasus rocket body launched in 1994, exploded in space. This has resulted in 539 fragments being cataloged, most of which will stay in orbit for hundreds of years. Parallel SAD played a significant role in cataloging these objects. As can be seen in Figure 3 the catalog now contains over 9200 objects. We can attribute significant credit for the growth in the catalog to the use of Parallel SAD.

We draw several conclusions about parallel processors from Parallel SAD,

- Many existing programs can be parallelized at little cost,
- Dedicated computers are not necessary for parallel processing,

- Proprietary concerns may exclude the use of existing resources for parallel processing,
- Distributed Parallel Processing is mature enough for operational use,
- Networking provides external computer resources for operational use,
- Parallel processing provides a means to run jobs that would be prohibitively long on a single serial machine.

5. Catalog Maintenance with Special Perturbations

Since the beginning of the Space Age, US Space Command has used analytic propagators to maintain their catalog. Recently we undertook a task to develop a catalog using special perturbations, that is with a numerical integrator. The reason is that numerical integrators can provide more accuracy through the use of better force models. Whether the radar data is sufficient to support the better accuracy needs to be determined.

Since this will require substantial computer time, we again are using parallel processing. Again we seek to adapt an existing program to run on top of PVM. The integrator itself is a variation of a Gauss-Jackson 8th order integrator already in use by US Space Command.

The concept here is fairly straight forward. The parallel system is written as a Master/Slave arrangement. The master computer organizes the I/O, starts up the slave nodes and sends them the initial state vector, and the correlated observations. The slave then integrates, differentially corrects the orbit state and sends it back to the master for cataloging.

This task illustrates the most primitive form of parallel processing. There is no communication between the slave processors, only between the master and the slaves, and then only for data transfer. The slaves are free to update their state vector in their own time. Once they complete one satellite, they return their state vector and receive a new one along with the observations. Synchronization is quite simple since the master controls everything.

6. Conclusions

One method of parallel processing we have not found useful is what is referred to as control decomposition where dissimilar parts of a program are sent to different processors for execution. In this form of parallelization great care must be exercised to maintain a high level of synchronization and utilization of the slave processors. We have not found this type of parallelization useful for our applications.

This should not be confused with the method used on SAD where a core module was extracted and duplicated for the slave computers. The slaves performed a large task to completion on each data set from the master.

For each of our applications, the data for the slave nodes has an identical structure and the programs on the slave nodes is always the same. In our SIMD application the synchronization was at the instruction level with each processor receiving a copy of an instruction to execute on the data. In the PVM applications the synchronization was more coarse, being at the program level. Here each processor received a complete yet identical program to execute on data possessing an identical structure. Thus, there is a great deal of similarity in our applications whether SIMD or distributed parallel processing under PVM. For the PVM applications the flexibility of processors completing tasks at different times produces better efficiency for problems that cannot be precisely synchronized.

The environment PVM is available for most computers. As we have indicated, we have made extensive use of it and have found it to be very robust. PVM has spawned a standardized language called MPI which is now available.

7. Acknowledgments

Many of the projects reported on here were supported by Naval Space Command under the direction of Drs. Steve Knowles and Paul Schumacher. Thanks to all members of NRL Code 8233 for their efforts in making the projects reported here successful. Special thanks to Dr. André Deprit who strongly advocated use of parallel processing when machines first became available.

Authors are listed in alphabetical order.

References

- Healy, L., and Deprit, E.: 1991, "Paint by number: uncovering phase flows of an integrable dynamical system," *Computers in Physics* Sep-Oct, 491-496.
- Coffey, S. L., Deprit, A. and Deprit, E.: 1994, 'Frozen Orbits for Satellites Close to an Earth-Like Planet,' *Celestial Mechanics and Dynamical Astronomy* 59, 37-72.
- Baumgardner, J. R. and Frederickson, P. O.: 1985, 'Icosahedral Discretization of the Two-Sphere,' *Siam Journal of Numerical Analysis* 22, 1107-1115.
- Healy, L.: 1995, 'Close Conjunction Detection on Parallel Computer,' *Journal of Guidance, Control, and Dynamics* 18, 824-829.
- Brouwer, D.: 1959, 'Solution of the problem of artificial satellite theory without drag,' *Astronomical Journal* 64, 378-397.
- Geist, A.: 1994, *PVM—Parallel Virtual Machine—A Users' Guide and Tutorial for Network Parallel Computing*, MIT Press, Cambridge, MA.
- Coffey, S. L., Jenkins, E., Neal, H. L., Reynolds, H.: 1996, 'Parallel Processing of Uncorrelated Observations Into Satellite Orbits,' AAS/AIAA Astrodynamics Specialist Conference, Paper No. 96-146, Austin, TX, 12-15 February.

Address for correspondence: (202)767-2818, shannon.coffey@nrl.navy.mil

ANALYTIC ORBIT MODEL FOR U.S. NAVAL SPACE SURVEILLANCE: AN OVERVIEW

Paul W. Schumacher, Jr.* and Robert A. Glover**

- Introduction
 - The PPT2 model (Brouwer theory, 1959)
 - Lyddane modification
 - Modification near critical inclination
 - Orbital decay modeling in PPT2
 - Use of PPT2 in orbit determination
 - The SGP4 model (Lane and Cranford theory, 1969)
 - The Brouwer part of SGP4
 - Orbital decay modeling in SGP4
 - Lunar/solar and resonance modeling in SGP4
 - Element conversion between PPT2 and SGP4
 - Improvements in the analytical model
 - Near term: the PPT3 model
 - Far term: advanced developments
- Appendix: The PPT3 Model of Satellite Motion

INTRODUCTION

For about thirty years, the catalog of Earth satellites has been maintained using analytic orbit models based mostly on Brouwer's 1959 artificial satellite theory. Satellite cataloging is one of the few space-related operations in which accurate special-perturbation (SP) orbit models have not yet replaced less accurate general-perturbation (GP) models. Until recently, the main reason was computing time: analytic models accurate to several kilometers execute one or two orders of magnitude faster than purely numerical models of similar accuracy. Moreover, the number of arithmetic operations for a GP prediction is nearly constant with respect to time from epoch, while the number of operations for an SP prediction is almost proportional to time from epoch. In the past, if SP models had been used exclusively, the available computers could not have kept up with the incoming observations on the entire catalog (currently about 8200 objects) while doing all the required data association, orbit determination and related analysis. Now the basic computing capacity does exist to maintain the catalog with

*U.S. Naval Space Command, 5280 Fourth Street, Dahlgren, Virginia 22448.

**General Research Corp., 985 Space Center Drive, Colorado Springs, Colorado 80915.

SP; however, for practical reasons, the catalog still consists of mean element sets derived with GP orbit models.

This paper describes the analytic orbit model, known as PPT2, that Naval Space Command (NAVSPACECOM) uses for space surveillance and related applications. (Ref.1) documents the software along with the basic theoretical background. The PPT2 model contains several modifications of Brouwer's original formulation, which are needed for Naval space surveillance operations but which may not be widely understood among users of cataloged elements. This paper also describes briefly how the model is used in orbit determination for catalog maintenance. Other components of U.S. Space Command use a different analytic model, known as SGP4, for space surveillance operations. We describe this model in comparison to PPT2 and outline the problem of converting element sets between these two models. Currently, the third-body and resonance models in SGP4 are being incorporated into PPT2 in order to create a new analytic model known as PPT3. (Ref.2) documents this effort to date, and (Ref.3) records some test results for both PPT2 and PPT3. The new model is being developed not only for improved accuracy for high-period orbits but also for improved compatibility between NAVSPACECOM and other components of U.S. Space Command.

PPT2 (Position and Partial as functions of Time 2)

PPT2 implements the complete 1959 Brouwer satellite theory⁴, together with certain modifications needed for operational orbit determination. The model was first created in 1964 by R.H. Smith of the Naval Space Surveillance System and is in use today in nearly its original form. The model does not include any third-body or resonance effects, mainly because the primary Naval concern at the time was to track near-Earth satellites. As discussed later, this modeling issue is now being revisited.

PPT2 includes all first-order zonal terms through $O(J_5)$, as derived by Brouwer⁴. Brouwer required no auxiliary expansions in eccentricity for the zonal satellite problem, so the theory holds for any eccentricity less than unity. PPT2 retains all long-periodic terms, including the ones with a zero divisor at the critical inclination. However, PPT2 handles these critical terms in a special way, as described below. All first-order zonal secular terms through

$O(J_5)$, and some second-order $O(J_2^2)$ zonal secular terms,

derived by Brouwer, are retained. A special feature of PPT2 is that the "mean" mean motion n'' (hereafter called simply the mean motion) is defined differently from Brouwer's quantity of the same name. Brouwer defined mean motion in terms of mean semimajor axis by essentially the Keplerian formula. However, for PPT2 it was decided for computational reasons to define the mean motion as the entire coefficient of time in the linear term in perturbed mean anomaly. That is, the PPT2 mean motion includes the zonal secular perturbation rate of mean anomaly that Brouwer derived. As a result, the expression for PPT2 mean motion explicitly contains perturbation parameters and functions of the other mean elements, similarly to the definition adopted by Kozai⁵ in a theory contemporary with Brouwer's. In fact, the numerical value of the PPT2 mean motion usually turns out to be closer to Kozai's value than to Brouwer's.

Three other important modifications of Brouwer's formulation have been incorporated into PPT2 in order to support operational orbit determination. These are (i) nonsingular variables to accommodate nearly circular or nearly equatorial orbits, (ii) a systematic way to accommodate orbits at or near the critical inclination, and (iii) a method of representing orbital decay due to drag. Each of these items will be discussed in turn.

The Lyddane Modification in PPT2

Because Brouwer's 1959 theory is developed in terms of Delaunay and classical elements, spurious singularities appear at zero eccentricity and zero inclination. In PPT2, these singularities are eliminated, without reformulating the entire theory, by introducing a set of auxiliary variables (essentially Poincare variables) suggested by Lyddane⁶. In short, Lyddane proposed to regroup Brouwer's terms to avoid the unwanted divisions. It must be admitted that the procedure does raise some conceptual difficulties, namely, inconsistencies in the definition of mean anomaly and argument of perigee at second order. Lyddane deliberately used "double-primed" values of these two elements in some places where Brouwer indicated "single-primed" values. The implications of this shortcut have been discussed not only by Lyddane but also by Lane and Cranford⁷. In practice, no real difficulties appear. Brouwer's theory is essentially a first-order theory, and minor inconsistencies at second order should be no cause for alarm. In fact, we have found that Lyddane's procedure, which also is a first-order approximation, produces entirely acceptable numerical results.

It is worthwhile to summarize Lyddane's method in the notation of this paper. Let

M = mean anomaly
 e = eccentricity
 I = inclination
 g = argument of perigee
 h = right ascension of the ascending node.

Then, using double primes to indicate mean elements and the δ operator to indicate perturbations of the elements, we consider the following combinations of classical elements:

$$\begin{aligned} e \cos M &= (e'' + \delta e) \cos(M'' + \delta M) \\ e \sin M &= (e'' + \delta e) \sin(M'' + \delta M) \\ \sin \frac{I}{2} \cosh &= \sin \frac{(I'' + \delta I)}{2} \cos(h'' + \delta h) \\ \sin \frac{I}{2} \sinh &= \sin \frac{(I'' + \delta I)}{2} \sin(h'' + \delta h) \end{aligned} \quad (1)$$

$$M + g + h = (M'' + g'' + h'') + \delta(M + g + h) = z'' + \delta z$$

Using angle-sum identities and keeping only first-order quantities, we have

$$e \cos M = (e'' + \delta e) \cos M'' - (e'' \delta M) \sin M'' \quad (2)$$

$$e \sin M = (e'' + \delta e) \sin M'' + (e'' \delta M) \cos M'' \quad (3)$$

$$\sin \frac{I}{2} \cosh = \left[\sin \frac{I''}{2} + \left(\frac{\delta I}{2} \right) \cos \frac{I''}{2} \right] \cosh'' - \left(\sin \frac{I''}{2} \delta h \right) \sinh'' \quad (4)$$

$$\sin \frac{I}{2} \sinh = \left[\sin \frac{I''}{2} + \left(\frac{\delta I}{2} \right) \cos \frac{I''}{2} \right] \sinh'' + \left(\sin \frac{I''}{2} \delta h \right) \cosh'' \quad (5)$$

$$z = (M'' + g'' + h'') + (\delta z) \quad (6)$$

For convenience, we also use the identity

$$\sin \frac{I''}{2} \delta h = \frac{(\sin I'' \delta h)}{2 \cos(I''/2)} \quad (7)$$

The groupings of quantities in parentheses above are numerically well-behaved for all values of eccentricity and inclination on elliptic orbits, including near-zero values. In several places, algebraic reductions of Brouwer's formulae are necessary. However, given the mean elements, we can evaluate the right-hand sides above with no loss of preci-

sion. Then we invert the equations to get the osculating classical elements:

$$e = \sqrt{(e \cos M)^2 + (e \sin M)^2} \quad (8)$$

$$M = \tan^{-1} \left(\frac{e \sin M}{e \cos M} \right) \quad (9)$$

$$\cos I = 1 - 2 \sin^2 \frac{I}{2} = 1 - 2 \left[\left(\sin \frac{I}{2} \cosh \right)^2 + \left(\sin \frac{I}{2} \sinh \right)^2 \right] \quad (10)$$

$$h = \tan^{-1} \left(\frac{\sin(I/2) \sinh}{\sin(I/2) \cosh} \right) \quad (11)$$

$$g = z - M - h \quad (12)$$

Poorly defined individual values of M , g or h always appear when eccentricity or inclination are small. However, as Lyddane discussed, errors of this type formally cancel in the calculation of position and velocity. PPT2 uses Lyddane's method for all orbits.

Critical Inclination in PPT2

Brouwer⁴ showed that the perturbation theory should remain valid for all inclinations except for an interval of about 1.5 degrees on either side of the critical inclination. Within this narrow range, special procedures are required in any implementation of a Brouwer-type theory. In PPT2, the procedure is as follows. First, we compute the critical factor

$$x = 1 - 5 \cos^2 I'' \quad (13)$$

This factor vanishes at about $I'' = 63.43^\circ$. Then all occurrences of $1/x$ are replaced by the approximation

$$\frac{1}{x} \approx \frac{1 - \exp(-100x^2)}{x} \equiv C(x) \quad (14)$$

Away from the critical inclination, $C(x)$ tends rapidly to $1/x$. But in the neighborhood of the critical inclination, $C(x)$ is bounded, and in fact vanishes at $x = 0$. It can be shown that $C(x)$ has a maximum amplitude of about 6.382.

There are two extrema having this amplitude, a minimum near $I'' = 61.86^\circ$ and a maximum near $I'' = 65.08^\circ$.

We do not compute the value of $C(x)$ directly from the above expression because of numerical ill-conditioning. Even the direct power-series expansion of the exponential function exhibits poor convergence because of the factor of 100. Both problems are avoided by repeatedly factoring the numerator of $C(x)$, expanding one factor in series and formally cancelling x from the denominator. In particular, we repeatedly factor the difference of squares to obtain the exact expression

$$C(x) = \frac{1}{x} (1 - \exp(-\beta x^2)) \prod_{m=0}^{10} (1 + \exp(-2^m \beta x^2)) \quad (15)$$

where $\beta = 100 / 2^{11}$. Then the first factor is computed by a series expansion truncated to a practical number of terms, which is feasible because of the smallness of β :

$$\frac{(1 - \exp(-\beta x^2))}{x} = \beta x \sum_{n=0}^{12} (-1)^n \frac{\beta^n x^{2n}}{(n+1)!} \quad (16)$$

No physical or analytical basis exists for handling the critical-inclination divisor in this manner. We have here merely a convenient numerical spline across the singularity. It is designed to limit the magnitude of the critical terms smoothly, producing a "soft" truncation that avoids omitting the terms entirely. The spline works well in practice mainly because the dynamical phenomena associated with the critical inclination happen on a time-scale that is longer than the interval over which the rest of the theory can be used in real orbit determination problems. Moreover, the number of product terms, the number of series terms and the value of the factor 100 are not highly refined values. They were obtained essentially by trial and error, the aim being to produce an acceptable combination of function amplitude and numerical smoothness near the critical inclination without excessive arithmetic. The approach has not received any critique in the open literature, though it has been mentioned in passing in (Ref.8). Recently, Coffey⁹ and co-workers had occasion to examine how well the approximation works far from the critical inclination. They have found

that the numerical results can be sensitive to the number of series terms in spite of the smallness of β , that the choice of only 12 series terms can lead to noticeable errors far from the critical inclination, and that the working formula for $C(x)$ needs to be tuned for the particular orbit model in which it is used.

Aesthetically, a better procedure than merely zeroing the critical terms would be to use a rigorous theory of the critical inclination. There is also some operational incentive to improve the handling of critical inclination because a large fraction of the catalog is in that regime. The problem of representing the motion analytically near the critical inclination has attracted considerable attention, though no operational models have been produced. The early theoretical contributions by Hori¹⁰ and Garfinkel¹¹ are only two of the many that could be cited. Recently Miller¹² made a fresh approach to the problem. Like its predecessors, Miller's theory is valid only in the neighborhood of the critical inclination, while a Brouwer-type theory is valid everywhere except at the critical inclination. It turns out that this feature is inherent in the problem. Recent investigations of the geometry of solutions in the phase space for the zonal-perturbed satellite problem^{13,14} have shown that the critical inclination is an essential singularity, so that one cannot construct a single perturbation solution that is valid for all inclinations. But this fact does not preclude developing an operationally useful model. The situation is reminiscent of the classical singular perturbation problem. There one tries to develop a composite perturbation solution by matching "inner" and "outer" asymptotic expansions in some overlap region near the singularity of the "outer" solution¹⁵. In the main problem of satellite theory the Brouwer solution is developed in powers of J_2 while the critical-inclination solution is developed in powers of $\sqrt{J_2}$, so a matching principle would be needed that can accommodate this difference. On the other hand, a simpler procedure would be to try to match the two solutions in an ad hoc way, perhaps using a spline approximation of the type we have just discussed. The result would be a homotopy mapping between the two theories, given as a function of the inclination. NAVSPACCOM has not yet tried either the singular-perturbation or the ad hoc approach for matching a critical-inclination theory with the Brouwer

theory. Even though the idea seems natural, we are not aware of any implementation of it.

Orbital Decay Modeling in PPT2

PPT2 models the along-track effect of atmospheric drag by assuming that the perturbed mean anomaly is given by at most a cubic polynomial function of time:

$$M'' = M_0'' + n_0'' (t - t_0) + \frac{\dot{n}''}{2} (t - t_0)^2 + \frac{\ddot{n}''}{6} (t - t_0)^3 \quad (17)$$

where t_0 is the epoch and M_0'' is the mean anomaly at epoch. The coefficients of the quadratic and cubic terms are determined empirically for each satellite by adjusting them along with the values of the mean elements in a differential correction against observations. In practice, it turns out that the cubic coefficient is almost always small and poorly determined. Orbital analysts sometimes use it for special purposes, but for all cataloged orbits the cubic coefficient is set to zero a priori. Hence, the mean anomaly is represented finally by a quadratic function of time. Of course, the empirical value of $\dot{n}''/2$ represents the combination of

all unmodeled secular along-track effects, not just atmospheric drag alone. But for most near-Earth orbits, drag is by far the dominant along-track effect. Then the main effects of orbital decay are represented by very simple formulae. The secular rate of change of mean semimajor axis is computed in terms of $\dot{n}''/2$ by assuming that Kepler's Third Law holds for the mean elements:

$$\frac{d}{dt} (n''^2 a''^3) = 0 \quad \rightarrow \quad \dot{a}'' = -\frac{4}{3} \frac{a_0''}{n_0''} \left(\frac{\dot{n}''}{2} \right) \quad (18)$$

where the zero subscript denotes an epochal value. The secular rate of change of mean eccentricity is computed in terms of \dot{a}'' as

$$\dot{e}'' = e_0'' (1 - e_0''^2) \frac{\dot{a}''}{a_0''} \quad (19)$$

Then the mean eccentricity and mean semimajor axis at the time of interest are computed as

$$e'' = e_0'' + \dot{e}''(t-t_0) \quad (20)$$

$$a'' = a_0'' + \dot{a}''(t-t_0)$$

Only these two mean elements, plus mean anomaly, receive explicit drag corrections when PPT2 is used in its usual prediction mode. Far enough from epoch, this decay modeling produces invalid eccentricity values that can cause trouble in other formulae and applications. There are many possible remedies, but the simplest ad hoc logic is used in practice. If the updated mean eccentricity is negative then the PPT2 model resets it to zero and if it is greater than 0.99999 then the model resets it to 0.99999. Similarly, if the updated mean semimajor axis is less than one Earth radius then PPT2 resets it to one Earth radius.

The formula (19) for the drag-induced secular rate in eccentricity requires some comment since it is not documented in the open literature. From the work of King-Hele¹⁶ and others, it is well known that the osculating semimajor axis and eccentricity obey the differential equations

$$\frac{da}{dE} = -B\rho a^2 \sqrt{\frac{1+e\cos E}{1-e\cos E}} (1+e\cos E) \quad (21)$$

$$\frac{de}{dE} = -B\rho a (1-e^2) \sqrt{\frac{1+e\cos E}{1-e\cos E}} \cos E \quad (22)$$

In these equations, E is the eccentric anomaly, ρ is the local atmospheric density, and B is the satellite ballistic coefficient. These are just Lagrange's planetary equations for the two elements in question, when the only perturbation is a drag force proportional to the square of the orbital speed and directed opposite to the velocity vector. Rotation of the atmosphere is therefore neglected. Assuming a static, spherically symmetric atmosphere with an exponential variation of density with height, the density at geocentric radius r is given by

$$\rho(r) = \rho_0 \exp[-(r-r_0)/H] \quad (23)$$

where ρ_0 is the reference density at radius r_0 and H is the scale height. With this simple model for the density, and assuming constant B and ρ_0 , one can derive the

first-order changes in semimajor axis and eccentricity over one revolution. Then the ratio of these changes turns out to be independent of ballistic coefficient and reference density. In particular,

$$\frac{\Delta e}{\Delta a} = \frac{e(1-e^2)}{a} F(a, e, H) \quad (24)$$

The function $F(a, e, H)$ is complicated, and the series expansions required in the averaging converge slowly at best. For example, to lowest order in eccentricity we obtain

$$F(a, e, H) = \frac{1}{2} \left(\frac{a}{H} + 1 \right) \quad (25)$$

which has an uncomfortably large value in any system of units. At this juncture in the development of the PPT2 drag model, the provisional agreement was to set $F = 1$, which explains the secular formula (19).

When PPT2 is used operationally for catalog maintenance, a value of $\dot{h}''/2$ is estimated for every orbit, not merely for decaying orbits, and the secular variations of eccentricity and semimajor axis (20) are always applied. Consequently, high-altitude orbits occasionally exhibit "negative decay" according to a least-squares update of the elements. This phenomenon is merely the aliasing of unmodeled effects (maneuvers, lunar/solar attraction, resonance, and solar radiation pressure) by the inadequate model. It causes no computational difficulties and usually produces acceptable short-time predictions as needed for most catalog maintenance. Of course, the secular eccentricity rate (19) is highly dubious if the value of $\dot{h}''/2$ is not caused by drag. A good case can be made for omitting the secular variation of e'' due to drag when $\dot{h}''/2$ is negative. But it has been clear for many years that better modeling is needed for high-period orbits, especially if longer-time predictions are to be made. This modeling issue is now being addressed, as discussed later.

The intention in the mid-1960s had been to try to develop a better decay model when the resources became available. In the meantime, it was found that this very simple decay modeling met all Naval space surveillance requirements after all, a rather surprising result in view of the severe approximations involved. Consequently, al-

though improved drag modeling has always been desirable, it has not been considered cost-effective to try to improve the general-perturbation (GP) treatment of drag for space surveillance operations. The more practical approach has been to change from the GP orbit model to a special-perturbation model when the analytic method becomes inadequate. We find that, under normal conditions, about 1.5% of the catalog requires continual attention from the operations analysts, mainly because of inaccurate GP decay modeling. Although a disproportionate share of the analysts' time is spent on these few orbits, the extra human effort involved rarely causes operational shortfalls.

USE OF PPT2 IN ORBIT DETERMINATION

For any particular PPT2 element set, the absolute prediction error at any time is not known quantitatively, especially when the error is conditioned on uncertain observations. As a result, there is no rigorous way to select either a data span for orbit determination or a deweighting factor for observations taken far from epoch. However, a set of nominal fit spans for orbit determination with PPT2 has been adopted to provide default values for the automatic catalog maintenance system. These time spans are purely empirical, the result of long experience with the catalog maintenance process using the PPT2 orbit model. They do not guarantee that optimum prediction accuracy will be achieved with any data set. They do represent informed opinion about how far from epoch a useful prediction accuracy can be maintained with PPT2 in a least-squares fit of data from the current space surveillance system. In this case, "useful accuracy" means that about 94% of all the data can be associated automatically with the correct satellite. (This percentage is not a design value, but merely reflects the current system performance.) A discussion of the association tolerances for catalog maintenance is beyond the scope of this paper, but they are typically on the order of 10 to several tens of kilometers in vector components of position. The operations analysts, who must deal manually with any unassociated or incorrectly associated data, are free to redefine the fit span for any particular satellite as needed for best maintenance of the orbit with the actual data available. However, they usually make only minor, if any, adjustments.

For satellites whose mean period is greater than or equal to 600 minutes, the nominal fit span depends on only the period:

PERIOD (minutes)	SPAN (days)
> 800	30
600 to 800	15

For satellites whose mean period is less than 600 minutes, the nominal fit span depends only on the rate of change of mean period as computed from $\dot{n}''/2$:

$$T_0'' = \frac{2\pi}{n_0''} \rightarrow \dot{T}'' = -\frac{4\pi}{n_0''^2} \left(\frac{\dot{n}''}{2} \right) \quad (26)$$

This dimensionless period rate is multiplied by 1440 minutes per day to obtain more practical working units. In particular:

PERIOD RATE (min/day)	SPAN (days)
> -0.0005	10
-0.001 to -0.0005	7
-0.01 to -0.001	5
< -0.01	3

In the NAVSPACECOM system, the fit spans, whether nominal or analyst-adjusted, are not always used explicitly in the least-squares update of the elements. In other words, PPT2 does not always have to predict the entire length of the fit span. To reduce the average processing time for each orbit, the system first attempts a sequential-batch least-squares update. This involves taking the most recent element set as an a priori estimate, establishing a new orbital epoch at the time of the most recent observation and incorporating only the data that have arrived since the last update. In principle, the a priori estimate contains all the information present in the previous observations, and hence PPT2 needs to predict only as far in time as the last update. In practice, the sequential process does not work indefinitely because of information being lost through model errors. As determined by various quality and consistency checks within the system, a more expensive, full-batch update of the elements may be required at irregular intervals in order to re-initialize the sequential process. But it is only in a full-batch update that the fit span explicitly conditions the new estimate of the elements, since only then must PPT2 predict the entire length of the fit span. It is also worth noting that each orbit is updated at least once per day, provided that new data are available, so

that PPT2 rarely needs to predict more than 36 hours from epoch if the sequential-batch update is successful.

SGP4 (Simplified General Perturbations 4)

The U.S. Air Force, under the aegis of U.S. Space Command, operates the primary space surveillance center at Cheyenne Mountain Air Station (CMAS), as well as most of the sensors in the space surveillance network. The analytic orbit model used at CMAS and at some sensors is known as SGP4, and it differs from PPT2 in several important ways. Since both SGP4 and PPT2 are used to maintain the entire space catalog, a brief comparison is in order. The main items to be mentioned are (i) differences in the Brouwer part of the model, (ii) differences in orbital decay modeling, and (iii) lunar/solar and resonance modeling in SGP4.

SGP4 is based on modifications, by Lane¹⁷ and Lane and Cranford⁷, of the theory developed by Brouwer and Hori¹⁸. The motivation for all these developments was to extend the original 1959 Brouwer theory to include atmospheric drag perturbations. Thus the theory of Lane and Cranford is a coupled zonal-drag perturbation solution of satellite motion. The realization of this theory as the present SGP4 model involved both truncations and additions in the underlying theory in order to meet Air Force operational requirements for space surveillance in the late 1970s.

The Brouwer Part of SGP4

In SGP4, all $O(eJ_2)$ and smaller short-periodic zonal terms have been omitted. All long-periodic zonal terms which contain a zero divisor at the critical inclination are omitted. All first-order secular zonal terms through $O(J_4)$ have been retained, as well as some second-order $O(J_2^2)$ terms, but all terms of any type containing J_3 have been omitted. These truncations in the model were accepted mainly to reduce the computational load on the original host computers. In effect, about 90% of the terms in the original Brouwer theory have been omitted, and no special procedures are necessary near the critical inclination. As with PPT2, singularities at zero inclination and zero eccentricity are avoided by using the auxiliary variables proposed by Lyddane⁶.

Orbital Decay Modeling in SGP4

The theory of Lane and Cranford⁷ assumes that atmospheric density is described by a power-law height profile and neglects the rotation of the atmosphere. The power-law density model was Lane's innovation¹⁷, and some exposition of it is also given in the textbook by Fitzpatrick¹⁹. The idea was to avoid an awkward shortcoming in the approach of Brouwer and Hori¹⁸. The latter authors had assumed an exponential density profile, essentially equation (23) above, with the result that cumbersome series expansions of the exponential function are required in order to obtain certain quadratures in closed form. Moreover, the series converge too slowly to be useful when the perigee altitude is low, so that the theory becomes inaccurate just when it is needed the most.^{***} Lane's idea was to replace the exponential function with a best-fit power function so that the quadratures could be obtained in closed form without any series expansions. For the most part, the complete theory⁷ treats drag as a numerically second-order $O(J_4)$ perturbation, though ultimately SGP4 retains one term in the secular variation of the node which contains the product of J_2 and the drag parameter. Even with these simplifying assumptions, the working formulae of the theory turn out to be lengthy and complicated, and extensive truncations of the drag terms were necessary for the original operational implementation. However, SGP4 does retain some terms for secular drag perturbations of every element except inclination. The drag parameter, known as B^* , is the one free parameter in all these terms. Formally, B^* is half the product of satellite ballistic coefficient and power-law reference density. In practice, its value is determined empirically for each satellite by adjusting it along with the mean-element values in a least-squares differential correction against observations, just as with the $\dot{h}/2$ value in the NAVSPACECOM system.

SGP4 models along-track drag effects by representing the perturbed mean longitude as a fifth-degree polynomial in time. However, the high degree of the polynomial causes the

^{***} These same shortcomings were felt by Smith at the Naval Space Surveillance System in 1964, which explains why the theory was not adopted for PPT2, either. In the mid-1960s, King-Hele offered the most practical approach.

prediction errors to be sensitive to errors in the initial conditions when the total drag perturbation rises above second order. Consequently, the fifth-degree polynomial is truncated to quadratic when the mean perigee altitude is below 220 kilometers. Many other formulae also are simplified when the mean perigee height is below 220 kilometers. In particular, the secular variation of semimajor axis reduces to a quadratic function of time, and the secular variation of eccentricity reduces to a linear function of time. Besides the simplifications below 220 kilometers, some secular terms containing B^* also contain the mean eccentricity as divisor. (The Lyddane modification does not help here.) These terms are omitted when the mean eccentricity is smaller than 0.0001.

Lunar/Solar and Resonance Modeling in SGP4

The requirement to track a growing population of satellites in Molniya-type and geosynchronous orbits motivated the addition of so-called "deep space" terms to the SGP4 model. U.S. Space Command classifies an orbit as "deep space" if its mean period is greater than or equal to 225 minutes, and SGP4 incorporates these additional terms only for such orbits. The perturbation solution was developed by Hujsak^{20,21} for immediate operational use, so the theory exists only in a truncated form. Lunar and solar point-mass perturbations were assumed to be second-order compared to

J_2 and were developed by restricting the direct part of the third-body disturbing function, expanded for the interior problem in the usual Legendre polynomials, to its leading term. All short-periodic effects are eliminated by averaging the disturbing function with respect to satellite mean anomaly and Earth rotation angle, so that the solution contains only long-periodic and secular third-body effects. Because the theory is developed in terms of classical elements, a spurious singularity appears in the secular rate of the node when the inclination is zero. This singularity is avoided by omitting the ill-defined terms whenever the inclination is less than 3° . The orbital elements of the Sun and Moon with respect to the equatorial plane at the epoch of the satellite orbit are obtained from a simple analytical model²².

The work of Hujsak^{20,21} also provides some limited modeling of resonance with the geopotential. The sectoral-tes-
seral perturbations of mean anomaly and semimajor axis are derived for orbits with mean periods near 1 day and 1/2 day. If the mean period is between 1200 minutes and 1800 minutes,

then geopotential terms of degree and order (2,2), (3,1) and (3,3) are included. If the mean period is between 680 minutes and 760 minutes, then geopotential terms of degree and order (2,2), (3,2), (4,4), (5,2) and (5,4) are included. The general form of the Kaula eccentricity functions²³ turned out to be impractical to implement in the operational software, and some kind of approximation had to be made. In the 1-day case, the series were simply truncated after the fourth power of the eccentricity. The resulting expressions are accurate only for small eccentricity. Most 1-day orbits are nearly circular, but the modeling is applied regardless of eccentricity. In the 1/2-day case, high-eccentricity Molniya orbits were of most interest. Polynomial approximations of the full eccentricity functions were developed for eccentricities greater than 0.5. These approximations are not adequate if the eccentricity is less than 0.5 and the modeling is not applied in that case. In both the 1-day and 1/2-day cases, the geopotential disturbing function has been averaged to eliminate short-periodic effects, which are subsequently neglected. The remaining perturbation is calculated using a simple second-order (Euler-Maclaurin) numerical integration with a 12-hour stepsize.

CONVERSION OF ELEMENT VALUES BETWEEN PPT2 AND SGP4

The differences between PPT2 and SGP4 lead to mean elements that are defined differently and are therefore incompatible. Even though both models are used to produce cataloged element sets in the same standard two-line format, it is not correct to compute predictions with one model using mean element values determined with the other model. The obviousness of this fact does not prevent difficulties from arising. For example, once a two-line element set has passed through several different communication systems, and possibly several agencies, it is not always easy for the user to tell which model produced it. The apparently straightforward, and ultimately correct, remedy of adopting one single analytic model for all space surveillance activities turns out to raise a host of logistical difficulties which are beyond the scope of this discussion. Meanwhile, the close coordination needed between the primary space surveillance center at CMAS and the backup center at NAVSPACECOM requires the continual interchange of element sets.

When SGP4 users must predict with mean elements determined with PPT2, the element values must be adjusted, and a value of B^* created, to produce the same ephemeris that PPT2 would have produced over some given time interval of interest. Likewise, when PPT2 users must predict with mean

elements determined with SGP4, the element values should be adjusted, and a value of $\dot{h}''/2$ created, to reproduce the SGP4 ephemeris over the specified time interval. This requirement does not imply that the orbit must be redetermined from observations. Instead, standard conversion methods which do not depend on observational data have been developed. But it should be obvious that any such conversion is only approximate, that there is always an accuracy penalty in predicting with converted elements, and that the conversion results can be guaranteed only in a statistical sense and not in individual cases. We have resorted to element conversion as expedient until the larger standardization problem can be solved.

NAVSPACECOM converts PPT2 element sets before they are issued to SGP4 users. The converted elements are intended for short-time predictions, nominally a day or less from epoch, as needed to support cataloging operations. The conversion method can be described in general terms as follows. Given a mean element set determined with PPT2, the epoch is changed from the PPT2 convention (time of last observation) to the SGP4 convention (time of last ascending node crossing). Then PPT2 is used to compute an ephemeris extending one nominal fit span prior to the epoch and one day beyond the epoch. SGP4 elements are differentially corrected against the ephemeris, using slightly modified PPT2 elements as starting values. An approximate starting value of B^* is computed in terms of $\dot{h}''/2$ by equating the coefficients of the quadratic terms in mean anomaly from the respective models. In many cases, this initialization alone is found to produce sufficiently accurate results. The reason is that many satellites are in low-eccentricity, low-to-moderate drag, near-Earth orbits. For this class of orbits, the modeling differences between PPT2 and SGP4 lead to relatively minor prediction differences. Full differential correction is required in the conversion for high-drag, resonant and deep-space orbits. The method is able to compensate for almost all the differences in drag modeling between PPT2 and SGP4. However, the conversion can only partly compensate for differences in deep-space predictions, since PPT2 does not model resonance or lunar/solar attraction.

IMPROVEMENTS IN THE ANALYTICAL MODEL FOR SPACE SURVEILLANCE

The most serious shortcoming of PPT2 in present operations is the lack of modeling for deep-space orbits. The shortcoming is really twofold. First, it degrades our pred-

iction accuracy, especially for geosynchronous orbits where the combined lunar/solar effect is almost as large as the Earth oblateness effect. Second, it represents an incompatibility between the primary operations center and the backup operations center that cannot be completely compensated by element conversion processing. NAVSPACECOM's response to this situation has also been twofold. First, in the near term the main compatibility problem can be solved, and an improvement in deep-space accuracy obtained, by adopting the same deep-space modeling that SGP4 uses. Second, in the long term, if the standardization issue of adopting a single orbit model for space surveillance is to be addressed competently, a more comprehensive analytic satellite theory must be developed and tested. These two responses will be described briefly.

Near Term

The PPT3 model, soon to enter an operational test phase, is essentially PPT2 with the addition of Hujsak's 1979 theory^{20,21}. There are two minor differences from the SGP4 implementation of the lunar/solar and resonance terms. First, the different definition of mean motion in PPT2 must be accommodated. Second, we have decided to retain all the lunar/solar terms for all orbits instead of omitting them for periods below 225 minutes. The perturbations are negligible for many near-Earth orbits, but we prefer to avoid an unnecessary discontinuity in the model. Also, omitting these terms merely to reduce the computational load is hardly justified with current computer systems.

Far Term

For several years, NAVSPACECOM has sponsored a research and development task in analytic orbit theory. Some notable advances have been made in this field since PPT2 and SGP4 were created. We believe that at least the major advances in theory formulation must be incorporated in one model and tested in orbit determination before an informed decision can be made to adopt a single analytic model for operations. Our current task deals with an improved treatment of the geopotential and third-body perturbations. A second-order theory, with partial derivatives, is being developed in nonsingular variables using algebraic manipulation software and automatic source-code generation. The basic analytical developments use canonical transformations proposed by Deprit. The elimination of the parallax²⁴ is used for the zonal problem and is a key to keeping the number of terms down to manageable levels. A more recent transformation, the

relegation of the nodes, allows a new formulation of time-dependent sectoral, tesseral and third-body effects.

Some general questions have been raised by this research. For a given host computer, an accuracy tradeoff exists between a second-order theory with a more limited force model and a first-order theory with a more extended force model. We often find that a second-order theory is more accurate far from epoch, while an extended first-order theory is more accurate close to epoch. The nature of this tradeoff is being examined. Also of interest are the tradeoffs between advanced general perturbation methods and special perturbation methods for orbit determination. For example, we have noticed in operations that orbit estimation using classical Gauss-type differential correction with one of the current GP models tends to be less accurate but more stable with respect to variations in the initial guess of the orbit, compared to the same orbit estimation method with a current SP model. This type of stability is important when one has only sparse, noisy data to work with: the solution accuracy hardly matters if one cannot obtain the solution in the first place. We would like to quantify this stability difference and find out whether it is inherent in the problem or is an artifact of our software implementation. Moreover, we would like to know how the picture changes when advanced GP or semianalytic models are compared with SP models in a variety of estimation procedures. We think that the traditional views of such tradeoffs may have to be revised in light of advanced computational techniques such as parallel processing. But NAVSPACECOM is only now beginning to consider these more subtle problems associated with maintaining an SP or advanced-GP catalog.

REFERENCES

- [1] "PPT2: The NAVSPASUR Model of Satellite Motion", NAVSPASUR Report 92-01, July 1992. Available from Commander, NAVSPACECOM, 5280 Fourth Street, Dahlgren, VA 22448-5300; attention: Logistics and Information Systems Division (Mail Code N4/6).
- [2] "PPT3: The NAVSPACECOM Model of Satellite Motion", draft NAVSPACECOM report, R.A. Glover, June 1995.
- [3] Robert A. Glover and Paul W. Schumacher, Jr., "Testing of Naval Space Command New Analytic Orbit Model", AAS Paper 95-430, AAS/AIAA Astrodynamics Specialist Conference, Halifax, Nova Scotia, 14-17 Aug 1995.

- [4] Dirk Brouwer, "Solution of the Problem of Artificial Satellite Theory Without Drag", *Astron. J.*, vol. 64, Nov 1959, pp. 378 - 397. Errata published in vol. 65, p. 108.
- [5] Yoshihide Kozai, "The Motion of a Close Earth Satellite", *Astron. J.*, vol. 64, Nov 1959, pp. 367 - 377, and "Mean Values of Cosine Functions in Elliptic Motion", vol. 67, June 1962, pp. 311 - 312.
- [6] R.H. Lyddane, "Small Eccentricities or Inclinations in the Brouwer Theory", *Astron. J.*, vol. 68, Oct 1963, pp. 555 - 558.
- [7] M.H. Lane and K.H. Cranford, "An Improved Analytical Drag Theory for the Artificial Satellite Problem", AIAA Paper 69-925, 20 August 1969.
- [8] Felix R. Hoots and Richard G. France, "An Analytic Satellite Theory Using Gravity and a Dynamic Atmosphere", *Celes. Mech.*, vol. 40, 1987, pp. 1 - 18.
- [9] Shannon Coffey, Liam Healy, Naval Research Laboratory, Washington, D.C.; Alan Segerman, Harold Neal, General Research Corp., McLean, Virginia. Private communication, Dahlgren, VA, 12 May 1995.
- [10] Gen-Ichiro Hori, "The Motion of an Artificial Satellite in the Vicinity of the Critical Inclination", *Astron. J.*, vol. 65, June 1960, pp. 291 - 300.
- [11] Boris Garfinkel, "On the Motion of a Satellite in the Vicinity of the Critical Inclination", *Astron. J.*, vol. 65, Dec 1960, pp. 624 - 627.
- [12] Bruce R. Miller, "Artificial satellite theory: analytical solutions at the critical inclination", unpublished manuscript, Nov 1993. National Institute of Standards and Technology, Computing and Applied Mathematics Laboratory, Gaithersburg, Maryland 20899.
- [13] Shannon L. Coffey, Andre Deprit, Bruce R. Miller, "The Critical Inclination in Artificial Satellite Theory", *Celes. Mech. Dyn. Astron.*, vol. 39, 1986, pp. 365 - 406.
- [14] Shannon L. Coffey, Andre Deprit, Etienne Deprit, "Frozen Orbits for Satellites Close to an Earth-like Planet", *Celes. Mech. Dyn. Astron.*, vol. 59, 1994, pp. 37 - 72.
- [15] Ali Hasan Nayfeh, Perturbation Methods, John Wiley and Sons, Inc., New York, 1973. Chapter 4.

- [16] Desmond King-Hele, Theory of Satellite Orbits in an Atmosphere, Butterworths, London, 1964.
- [17] Max H. Lane, "The Development of an Artificial Satellite Theory Using a Power Law Atmospheric Density Representation", AIAA Paper 65-35, 25 January 1965.
- [18] Dirk Brouwer and Gen-Ichiro Hori, "Theoretical Evaluation of Atmospheric Drag Effects in the Motion of an Artificial Satellite", *Astron. J.*, vol. 66, August 1961, pp. 193 - 225, and "Appendix to Theoretical Evaluation of Atmospheric Drag Effects in the Motion of an Artificial Satellite", vol. 66, August 1961, pp. 264 - 265.
- [19] Philip M. Fitzpatrick, Principles of Celestial Mechanics, Academic Press, New York, 1970.
- [20] R.S. Hujask, "A Restricted Four Body Solution for Resonating Satellites with an Oblate Earth", AIAA Paper 79-136, June 1979.
- [21] Richard S. Hujask, "A Restricted Four Body Solution for Resonating Satellites Without Drag", Special Astrodynamic Report No. 1, Project Space Track, Aerospace Defense Command, Peterson AFB, Colorado, November 1979. Available from AIAA Technical Information Service, New York, NY.
- [22] Explanatory Supplement to the Astronomical Ephemeris and American Ephemeris and Nautical Almanac, Her Majesty's Stationery Office, London, 1961. See page 98 for the solar elements and page 107 for the lunar elements.
- [23] William M. Kaula, Theory of Satellite Geodesy, Blaisdell Pub. Co. (Ginn and Co.), Waltham, MA, 1966.
- [24] A. Deprit, "The Elimination of the Parallax in Satellite Theory", *Celes. Mech.*, vol. 24, 1981, pp. 111 - 153.

APPENDIX: The PPT3 Model of Satellite Motion

Here we present the collection of formulae used to calculate position and velocity at any time of interest, given a set of mean elements determined with the PPT3 model for some epoch. Equations equivalent to the currently operational PPT2 model are recovered by omitting the lunar, solar and resonance terms. PPT2 has been documented in (Ref.1). Documentation of the PPT3 model exists in draft form² and will be available for general distribution sometime after operational testing of the software is complete. Besides the two references just cited, essential background on the lunar, solar and resonance modeling is contained in the paper and report by Hujsak^{20,21}, the book by Kaula²³ and (Ref.22). The zonal modeling in both PPT2 and PPT3 is based directly on the papers by Brouwer⁴ and Lyddane⁶. It is fair to say that trying to merge these different theories into a consistent model has exposed the weaknesses in all of them. There are still some unresolved questions about implementation details in PPT3, which will not be settled until testing is complete. However, even though the formulae presented here are subject to revision, we do not expect major changes. At least until PPT3 is adopted for operations, it is worthwhile to have a summary of the model in its current state of development.

The initial mean elements at epoch t_0 are

M_0''	mean anomaly
n_0''	mean motion
$\dot{n}''/2, \ddot{n}''/6$	empirical decay parameters
e_0''	eccentricity
I_0''	inclination
g_0''	argument of perigee
h_0''	right ascension of ascending node.

In present space surveillance practice, these elements are referred to the coordinate frame "mean equinox and true equator of date", the date being the epoch of the elements. This means that, for computational expediency, precession in right ascension has been accounted for up to the epoch of the elements but other precession effects and all nutation effects have been omitted. The resulting frame is assumed to be inertial to within the accuracy of the orbit model. Internally, PPT3 and PPT2 use a system of canonical units in which angles are in units of radians, distance is in units

of Earth radius (R_E), and the time unit is chosen so that the product of the Newtonian gravitational constant and Earth mass ($\mu_E = Gm_E$) is numerically equal to unity.

Dimensional zonal perturbation constants are

$$\begin{aligned} k_2 &= \frac{1}{2} J_2 R_E^2 = \frac{1}{2} \sqrt{5} (0.4841605) \times 10^{-3} R_E^2 \\ k_3 &= -J_3 R_E^3 = \sqrt{7} (0.95958) \times 10^{-6} R_E^3 \\ k_4 &= -\frac{3}{8} J_4 R_E^4 = \frac{3}{8} \sqrt{9} (0.55199) \times 10^{-6} R_E^4 \\ k_5 &= -J_5 R_E^5 = \sqrt{11} (0.65875) \times 10^{-7} R_E^5 \end{aligned}$$

For notational convenience, define

$$\theta = \cos I_0'' , \quad \eta = \sqrt{1 - e_0''^2}$$

Calculate mean semimajor axis a_0'' corresponding to the mean motion, remembering that the PPT2/3 mean motion contains the zonal secular perturbation of mean anomaly. By definition,

$$n_0'' = \sqrt{\frac{\mu_E}{a_0''^3}} (1 + \delta_z M)$$

Then we have

$$a_0'' = \left(\frac{1 + \delta_z M}{n_0''} \right)^{2/3} (\mu_E)^{1/3}$$

where dimensionless even zonal perturbation parameters are

$$\gamma_2' = \frac{k_2}{a_0''^2 \eta^4} , \quad \gamma_4' = \frac{k_4}{a_0''^4 \eta^8}$$

and

$$\begin{aligned} \delta_z M &= \frac{3}{2} \gamma_2' \eta (-1 + 3\theta^2) \\ &+ \frac{3}{32} \gamma_2'^2 \eta [-15 + 16\eta + 25\eta^2 + (30 - 96\eta - 90\eta^2) \theta^2 + (105 + 144\eta + 25\eta^2) \theta^4] \\ &+ \frac{15}{16} \gamma_4' \eta e_0''^2 (3 - 30\theta^2 + 35\theta^4) \end{aligned}$$

Iterate the a_0'' equation 5 times, using $a_0'' = (\mu_E / n_0''^2)^{1/3}$ as the initial guess in evaluating the right-hand side. Then the dimensionless odd zonal perturbation parameters are

$$\gamma_3' = \frac{k_3}{a_0^{1/3} \eta^6} , \quad \gamma_5' = \frac{k_5}{a_0^{1/5} \eta^{10}}$$

Secular rate of argument of perigee with respect to mean anomaly, due to zonals:

$$\begin{aligned} \left(\frac{dg''}{dM''} \right)_z &= \frac{1}{n_0''} \sqrt{\frac{\mu_E}{a_0^{1/3}}} \left\{ \frac{3}{2} \gamma_2' (-1+5\theta^2) \right. \\ &+ \frac{3}{32} \gamma_2'^2 [-35+24\eta+25\eta^2+(90-192\eta-126\eta^2)\theta^2+(385+360\eta+45\eta^2)\theta^4] \\ &\left. + \frac{5}{16} \gamma_4' [21-9\eta^2+(-270+126\eta^2)\theta^2+(385-189\eta^2)\theta^4] \right\} \end{aligned}$$

Secular rate of node with respect to mean anomaly, due to zonals:

$$\begin{aligned} \left(\frac{dh''}{dM''} \right)_z &= \frac{1}{n_0''} \sqrt{\frac{\mu_\odot}{a_0^{1/3}}} \left\{ -3\gamma_2'\theta + \frac{3}{8} \gamma_2'^2 [(-5+12\eta+9\eta^2)\theta + (-35-36\eta-5\eta^2)\theta^3] \right. \\ &\left. + \frac{5}{4} \gamma_4' (5-3\eta^2) (3-7\theta^2)\theta \right\} \end{aligned}$$

Secular rate of semimajor axis with respect to time:

$$\dot{a}'' = -\frac{4}{3} \frac{a_0''}{n_0''} \left(\frac{\dot{n}''}{2} \right)$$

Secular rate of eccentricity with respect to time, due to drag:

$$\dot{e}_D'' = \frac{e_0'' \eta^2 \dot{a}''}{a_0''}$$

Critical-inclination divisor:

$$\text{CRIT} = \frac{1 - \exp(-100x^2)}{x} \div \left[\beta x \sum_{n=0}^{12} \frac{(-1)^n \beta^n x^{2n}}{(n+1)!} \right] \left[\prod_{m=0}^{10} (1 + \exp(-2^m \beta x^2)) \right]$$

where $\beta = 100/2^{11}$ and $x = 1-5\theta^2$. The value CRIT is used in place of $1/(1-5\theta^2)$ wherever this factor appears.

Coefficients for long-periodic zonal terms:

$$\text{LPE1} = \eta^2 \sin I_0'' \left[\frac{\gamma_3'}{4\gamma_2'} + \frac{5\gamma_5'}{64\gamma_2'} (4+3e_0''^2) \left(1-9\theta^2 - \frac{24\theta^4}{1-5\theta^2} \right) \right]$$

$$\text{LPE2} = \frac{e_0'' \eta^2 \sin^2 I_0''}{1-5\theta^2} \left[\frac{\gamma_2'}{8} (1-15\theta^2) - \frac{5\gamma_4'}{12\gamma_2'} (1-7\theta^2) \right]$$

$$\text{LPE3} = -\eta^2 \sin I_0'' \left[\frac{7e_0''}{6} \left(\frac{5\gamma_5'}{64\gamma_2'} \right) \left(1-5\theta^2 - \frac{16\theta^4}{1-5\theta^2} \right) \right]$$

$$\text{LPI1} = -e_0'' \theta \left[\frac{\gamma_3'}{4\gamma_2'} + \frac{5\gamma_5'}{64\gamma_2'} (4+3e_0''^2) \left(1-9\theta^2 - \frac{24\theta^4}{1-5\theta^2} \right) \right]$$

$$\text{LPI2} = -\frac{e_0''^2 \theta \sin I_0''}{1-5\theta^2} \left[\frac{\gamma_2'}{8} (1-15\theta^2) - \frac{5\gamma_4'}{12\gamma_2'} (1-7\theta^2) \right]$$

$$\text{LPI3} = e_0'' \theta \left[\frac{7e_0''}{6} \left(\frac{5\gamma_5'}{64\gamma_2'} \right) \left(1-5\theta^2 - \frac{16\theta^4}{1-5\theta^2} \right) \right]$$

$$\begin{aligned} \text{LPH1} = e_0'' \theta & \left[\frac{\gamma_3'}{4\gamma_2'} + \frac{5\gamma_5'}{64\gamma_2'} (4+3e_0''^2) \left(1-9\theta^2 - \frac{24\theta^4}{1-5\theta^2} \right) \right] \\ & + 6e_0'' \theta \sin^2 I_0'' \left(\frac{5\gamma_5'}{64\gamma_2'} \right) \left[3 + \frac{16\theta^2}{1-5\theta^2} + \frac{40\theta^4}{(1-5\theta^2)^2} \right] \end{aligned}$$

$$\text{LPH2} =$$

$$-\sin I_0'' e_0''^2 \theta \left\{ \frac{\gamma_2'}{8} \left[1 + \frac{80\theta^2}{1-5\theta^2} + \frac{200\theta^4}{(1-5\theta^2)^2} \right] - \frac{5\gamma_5'}{64\gamma_2'} \left[3 + \frac{16\theta^2}{1-5\theta^2} + \frac{40\theta^4}{(1-5\theta^2)^2} \right] \right\}$$

$$\begin{aligned} \text{LPH3} = -\frac{e_0'' \theta}{3} & \left[\frac{7e_0''}{6} \left(\frac{5\gamma_5'}{64\gamma_2'} \right) \left(1-5\theta^2 - \frac{16\theta^4}{1-5\theta^2} \right) \right] \\ & - \frac{7}{9} e_0''^3 \theta \sin^2 I_0'' \left(\frac{5\gamma_5'}{64\gamma_2'} \right) \left[5 + \frac{32\theta^2}{1-5\theta^2} + \frac{80\theta^4}{(1-5\theta^2)^2} \right] \end{aligned}$$

$$\text{LPL1} = -\eta^3 \sin I_0'' \left[\frac{\gamma_3'}{4\gamma_2'} + \frac{5\gamma_5''}{64\gamma_2'} \left(1-9\theta^2 - \frac{24\theta^4}{1-5\theta^2} \right) (4+9e_0''^2) \right]$$

$$\text{LPL2} = \frac{e_0'' \eta^3 \sin^2 I_0''}{1-5\theta^2} \left[\frac{\gamma_2'}{8} (1-15\theta^2) - \frac{5\gamma_4'}{12\gamma_2'} (1-7\theta^2) \right]$$

$$\text{LPL3} = \eta^3 \sin I_0'' \left[\frac{7e_0''^{1/2}}{6} \left(\frac{5\gamma_5'}{64\gamma_2'} \right) \left(1-5\theta^2 - \frac{16\theta^4}{1-5\theta^2} \right) \right]$$

$$\begin{aligned} \text{LPS1} = & e_0'' \theta \tan \frac{I_0''}{2} \left[\frac{\gamma_3'}{4\gamma_2'} + \frac{5\gamma_5'}{64\gamma_2'} (4+3e_0''^{1/2}) \left(1-9\theta^2 - \frac{24\theta^4}{1-5\theta^2} \right) \right] \\ & + \tan \frac{I_0''}{2} \left\{ 6e_0'' \theta \sin^2 I_0'' \left(\frac{5\gamma_5'}{64\gamma_2'} \right) (4+3e_0''^{1/2}) \left[3 + \frac{16\theta^2}{1-5\theta^2} + \frac{40\theta^2}{(1-5\theta^2)^2} \right] \right\} \\ & + e_0'' \sin I_0'' \left\{ \frac{\gamma_3'}{4\gamma_2'} \left(\eta + \frac{1}{1+\eta} \right) + \frac{5\gamma_5'}{64\gamma_2'} \left(1-9\theta^2 - \frac{24\theta^2}{1-5\theta^2} \right) \left[\frac{\eta^2(4+9e_0''^{1/2})}{1+\eta} + 5(4+3e_0''^{1/2}) \right] \right\} \end{aligned}$$

$$\begin{aligned} \text{LPS2} = & \frac{\eta^3 \sin^2 I_0''}{1-5\theta^2} \left[\frac{\gamma_2'}{8} (1-15\theta^2) - \frac{5\gamma_4'}{12\gamma_2'} (1-7\theta^2) \right] \\ & - \frac{1}{2} \left\{ \frac{\gamma_2'}{8} \left[(2+e_0''^{1/2}) - 11(2+3e_0''^{1/2})\theta^2 - \frac{40(2+5e_0''^{1/2})\theta^4}{1-5\theta^2} - \frac{400e_0''^{1/2}\theta^6}{(1-5\theta^2)^2} \right] \right. \\ & - \frac{5\gamma_4'}{12\gamma_2'} \left[(2+e_0''^{1/2}) - 3(2+3e_0''^{1/2})\theta^2 - \frac{8(2+5e_0''^{1/2})\theta^4}{1-5\theta^2} - \frac{80e_0''^{1/2}\theta^6}{(1-5\theta^2)^2} \right] \left. \right\} \\ & - e_0'' \theta \left\{ \frac{\gamma_2'}{8} \left[11 + \frac{80\theta^2}{1-5\theta^2} + \frac{200\theta^4}{(1-5\theta^2)^2} \right] - \frac{5\gamma_5'}{64\gamma_2'} \left[3 + \frac{16\theta^2}{1-5\theta^2} + \frac{40\theta^4}{(1-5\theta^2)^2} \right] \right\} \end{aligned}$$

LPS3 =

$$\begin{aligned} & - \left[e_0'' \sin I_0'' \left(\frac{2}{3} + \eta + \frac{1}{1+\eta} \right) + \frac{1}{3} e_0'' \theta \tan \frac{I_0''}{2} \right] \left[\frac{7e_0''^{1/2}}{6} \left(\frac{5\gamma_5'}{64\gamma_2'} \right) \left(1-5\theta^2 - \frac{16\theta^4}{1-5\theta^2} \right) \right] \\ & - \frac{7}{9} e_0''^{1/3} \theta \tan \frac{I_0''}{2} \sin^2 I_0'' \left(\frac{5\gamma_5'}{64\gamma_2'} \right) \left[5 + \frac{32\theta^2}{1-5\theta^2} + \frac{80\theta^4}{(1-5\theta^2)^2} \right] \end{aligned}$$

Third-body elements and true anomalies at the satellite epoch are calculated in terms of the following fundamental quantities:

$I_{Le} = 5^\circ.145396374$ lunar inclination on the ecliptic
 $I_s = \epsilon = 23^\circ.4441$ solar incl. on the ecliptic (obliquity)
 $e_L = 0.05490$ lunar eccentricity
 $e_s = 0.01675$ solar eccentricity
 $n_L = 1.583521770 \times 10^{-4}$ lunar mean motion (rad/min)
 $n_s = 1.19459 \times 10^{-5}$ solar mean motion (rad/min)
 $\Omega_s = 0^\circ.0$ right ascension of solar node
 $\omega_s = 281^\circ.2208$ argument of solar perigee.

The two third-body perturbation parameters are given by

$$K_x = \frac{1}{4} \left(\frac{m_x n_x}{m_x + m_E} \right)$$

where m_x is the third-body mass and m_E is Earth mass. In particular,

$$\frac{m_s}{m_s + m_E} \approx 1 \quad \text{and} \quad m_L = \frac{m_E}{81.53}$$

so that

$$\begin{aligned}
 K_L &= 4.796806521 \times 10^{-7} \text{ rad/min} \\
 K_s &= 2.986479720 \times 10^{-6} \text{ rad/min}
 \end{aligned}$$

The initial third-body elements and other parameters are given at the epoch

$$t_{0x} = 1900 \text{ January } 0.5 = \text{JD } 2415020.0$$

For the epoch t_0 of the satellite orbit, calculate the right ascension of the lunar ascending node on the ecliptic as

$$\Omega_{Le} = (\Omega_{Le0} + \dot{\Omega}_{Le} \Delta t_0 + \ddot{\Omega}_{Le} \Delta t_0^2 + \ddot{\ddot{\Omega}}_{Le} \Delta t_0^3) \bmod 2\pi$$

where $\Delta t_0 = t_0 - t_{0x}$ and the coefficients are obtained from (Ref.22).

Lunar inclination with respect to the equator:

$$\cos I_L = \cos \epsilon \cos I_{Le} - \sin \epsilon \sin I_{Le} \cos \Omega_{Le}$$

$$\sin I_L = +\sqrt{1 - \cos^2 I_L}$$

Right ascension of lunar ascending node on the equator:

$$\sin\Omega_L = \frac{\sin I_{L\epsilon} \sin\Omega_{L\epsilon}}{\sin I_L} \quad \text{and} \quad \cos\Omega_L = +\sqrt{1 - \sin^2\Omega_L}$$

Then also

$$\sin\Delta = \frac{\sin\epsilon \sin\Omega_{L\epsilon}}{\sin I_L}$$

$$\cos\Delta = \cos\Omega_L \cos\Omega_{L\epsilon} + \sin\Omega_L \sin\Omega_{L\epsilon} \cos\epsilon$$

$$\Delta = \tan^{-1}(\sin\Delta/\cos\Delta)$$

Longitude of lunar perigee on the ecliptic:

$$\Gamma = u_{\epsilon 0} + \dot{u}_{\epsilon} \Delta t_0 + \ddot{u}_{\epsilon} \Delta t_0^2 + \ddot{\ddot{u}}_{\epsilon} \Delta t_0^3$$

where the coefficients are obtained from (Ref.22).

Argument of lunar perigee with respect to the equator:

$$\omega_L = \Gamma - \Omega_{L\epsilon} + \Delta$$

Third-body mean anomaly at satellite epoch:

$$l_x = (l_{0x} + \dot{l}_x \Delta t_0 + \ddot{l}_x \Delta t_0^2 + \ddot{\ddot{l}}_x \Delta t_0^3) \bmod 2\pi$$

where the coefficients are obtained from (Ref.22). The solution of Kepler's equation for third-body true anomaly at satellite epoch neglects $O(e_x^2)$ errors:

$$f_x = l_x + 2e_x \sin l_x$$

Special functions and parameters for third-body terms, which depend on the satellite elements e_0'' , I_0'' , g_0'' , h_0'' , and which are computed for each third body:

$$a_1 = \cos\omega_x \cos(h_0'' - \Omega_x) + \sin\omega_x \cos I_x \sin(h_0'' - \Omega_x)$$

$$a_3 = -\sin\omega_x \cos(h_0'' - \Omega_x) + \cos\omega_x \cos I_x \sin(h_0'' - \Omega_x)$$

$$a_7 = -\cos\omega_x \sin(h_0'' - \Omega_x) + \sin\omega_x \cos I_x \cos(h_0'' - \Omega_x)$$

$$a_8 = \sin\omega_x \sin I_x$$

$$a_9 = \sin\omega_x \sin(h_0'' - \Omega_x) + \cos\omega_x \cos I_x \cos(h_0'' - \Omega_x)$$

$$a_{10} = \cos\omega_x \sin I_x$$

$$a_2 = a_7 \cos I_0'' + a_8 \sin I_0''$$

$$a_4 = a_9 \cos I_0'' + a_{10} \sin I_0''$$

$$a_5 = -a_7 \sin I_0'' + a_8 \cos I_0''$$

$$a_6 = -a_9 \sin I_0'' + a_{10} \cos I_0''$$

$$X_1 = a_1 \cos g_0'' + a_2 \sin g_0''$$

$$X_2 = a_3 \cos g_0'' + a_4 \sin g_0''$$

$$X_3 = -a_1 \sin g_0'' + a_2 \cos g_0''$$

$$X_4 = -a_3 \sin g_0'' + a_4 \cos g_0''$$

$$X_5 = a_5 \sin g_0'' , \quad X_6 = a_6 \sin g_0'' , \quad X_7 = a_5 \cos g_0'' , \quad X_8 = a_6 \cos g_0''$$

$$Z_{31} = 12X_1^2 - 3X_3^2$$

$$Z_{32} = 24X_1X_2 - 6X_3X_4$$

$$Z_{33} = 12X_2^2 - 3X_4^2$$

$$Z_1 = 6(X_1^2 + X_3^2) + (1 + e_0'^2) Z_{31}$$

$$Z_2 = 12(X_1X_2 + X_3X_4) + (1 + e_0'^2) Z_{32}$$

$$Z_3 = 6(X_2^2 + X_4^2) + (1 + e_0'^2) Z_{33}$$

$$Z_{11} = -6X_1X_7 + 6X_3X_5 + e_0'^2 (-24X_1X_7 - 6X_3X_5)$$

$$Z_{12} = -6X_1X_8 - 6X_2X_7 + 6X_3X_6 + 6X_4X_5 + e_0'^2 (-24X_2X_7 - 24X_1X_8 - 6X_3X_6 - 6X_4X_5)$$

$$Z_{13} = -6X_2X_8 + 6X_4X_6 + e_0'^2 (-24X_2X_8 - 6X_4X_6)$$

$$Z_{21} = 6X_1X_5 + 6X_3X_7 + e_0'^2 (24X_1X_5 - 6X_3X_7)$$

$$Z_{22} = 6X_2X_5 + 6X_1X_6 + 6X_4X_7 + 6X_3X_8 + e_0'^2 (24X_2X_5 + 24X_1X_6 - 6X_4X_7 - 6X_3X_8)$$

$$Z_{23} = 6X_2X_6 + 6X_4X_8 + e_0''^2 (24X_2X_6 - 6X_4X_8)$$

Third-body secular rates with respect to time, computed for each third body:

$$(\dot{e}'')_x = - \frac{15 K_x n_x e_0'' \eta}{n_0''} (X_1 X_3 + X_2 X_4)$$

$$(\dot{i}'')_x = - \frac{K_x n_x}{2 n_0'' \eta} (Z_{11} + Z_{13})$$

$$(\dot{M}'')_x = - \frac{K_x n_x}{n_0''} (Z_1 + Z_3 - 14 - 6 e_0''^2)$$

$$(\dot{g}'' + \dot{h}'' \cos I_0'')_x = \frac{K_x n_x \eta}{n_0''} (Z_{31} + Z_{33} - 6)$$

$$\begin{aligned} (\dot{h}'' \sin I_0'')_x &= \frac{K_x n_x}{2 n_0'' \eta} (Z_{21} + Z_{23}) & \text{if } \sin I_0'' \geq \sin 3^\circ \\ &= 0 & \text{if } \sin I_0'' < \sin 3^\circ \end{aligned}$$

$$(\dot{h}'')_x = \frac{(\dot{h}'' \sin I_0'')_x}{\sin I_0''}$$

$$(\dot{g}'')_x = (\dot{g}'' + \dot{h}'' \cos I_0'')_x - \frac{\cos I_0''}{\sin I_0''} (\dot{h}'' \sin I_0'')_x$$

Secular update to time of interest, including zonal, drag and third-body effects:

$$\Delta M'' = n_0'' (t - t_0) + \frac{\dot{n}''}{2} (t - t_0)^2 + \frac{\ddot{n}''}{6} (t - t_0)^3 + (\dot{M}'')_L (t - t_0) + (\dot{M}'')_S (t - t_0)$$

$$M'' = (M_0'' + \Delta M'') \bmod 2\pi$$

$$e'' = e_0'' + \dot{e}'' (t - t_0) + (\dot{e}'')_L (t - t_0) + (\dot{e}'')_S (t - t_0)$$

$$e'' \leftarrow \min [\max (0.0, e''), 0.99999]$$

$$a'' = a_0'' + \dot{a}'' (t - t_0)$$

$$a'' \leftarrow \max (R_E, a'')$$

$$h'' = h_0'' + \left(\frac{dh''}{dM''} \right)_z \Delta M'' + \frac{(\dot{h}'')_L}{n_0''} \Delta M'' + \frac{(\dot{h}'')_S}{n_0''} \Delta M''$$

$$g'' = g_0'' + \left(\frac{dg''}{dM''} \right)_z \Delta M'' + \frac{(\dot{g}'')_L}{n_0''} \Delta M'' + \frac{(\dot{g}'')_S}{n_0''} \Delta M''$$

$$I'' = I_0'' + (\dot{I}'')_L (t - t_0) + (\dot{I}'')_S (t - t_0)$$

Solve Kepler's equation and calculate satellite true anomaly based on secularly updated mean elements:

$$M'' = E' - e'' \sin E'$$

$$\cos f' = \frac{\cos E' - e''}{1 - e'' \cos E'} \quad \text{and} \quad \sin f' = \frac{\sqrt{1 - e''^2} \sin E'}{1 - e'' \cos E'}$$

If the mean period $T_0'' = 2\pi/n_0''$ is between 1200 and 1800 minutes inclusive (the 1-day case), compute resonance corrections for mean anomaly and semimajor axis. The Kaula

(l, m, p, q) indices of interest are $(2, 2, 0, 0)$, $(3, 1, 1, 0)$, and $(3, 3, 0, 0)$. Several dimensionless geopotential constants, defined by

$$Q_{lm} = \sqrt{C_{lm}^2 + S_{lm}^2} \quad \text{and} \quad \lambda_{lm} = \frac{1}{m} \tan^{-1} \left(\frac{S_{lm}}{C_{lm}} \right)$$

where C_{lm} and S_{lm} are the sectoral/tesseral coefficients in the form of the geopotential adopted by Kaula²³, are independent of the satellite orbit. In particular, we use

$$\begin{aligned} Q_{31} &= 2.1460748 \times 10^{-6} & \lambda_{31} &= 0.13130908 \\ Q_{22} &= 1.7891679 \times 10^{-6} & \lambda_{22} &= 2.88431980 \\ Q_{33} &= 2.2123015 \times 10^{-7} & \lambda_{33} &= 0.37448087 \end{aligned}$$

The Kaula inclination functions $F_{lmp}(I)$ are closed expressions:

$$F_{220} = \frac{3}{4} (1 + \cos I_0'')^2$$

$$F_{311} = \frac{15}{16} \sin^2 I_0'' (1 + 3 \cos I_0'') - \frac{3}{4} (1 + \cos I_0'')$$

$$F_{330} = \frac{15}{8} (1 + \cos I_0'')^3$$

The Kaula eccentricity functions $G_{lpq}(e)$ are evaluated by omitting terms of the order indicated:

$$G_{200} = 1 - \frac{5}{2} e_0'^2 + \frac{13}{16} e_0'^4 + \dots O(e_0'^6)$$

$$G_{310} = 1 + 2 e_0'^2 + \dots O(e_0'^4)$$

$$G_{300} = 1 - 6 e_0'^2 + \frac{423}{64} e_0'^4 + \dots O(e_0'^6)$$

Special constants:

$$D_1 = \frac{3 n_0'^2}{a_0'^3} F_{311} G_{310} Q_{31}$$

$$D_2 = \frac{6 n_0'^2}{a_0'^2} F_{220} G_{200} Q_{22}$$

$$D_3 = \frac{9 n_0'^2}{a_0'^3} F_{330} G_{300} Q_{33}$$

Initial conditions for numerical integration:

$$\lambda(t_0) = M_0'' + g_0'' + h_0'' - \theta_g(t_0)$$

$$n(t_0) = n_0''$$

where $\theta_g(t_0)$ is the Greenwich sidereal time at the satellite epoch. The following pair of differential equations is integrated numerically:

$$\dot{\lambda} = n + \Lambda - \dot{\theta}_g$$

$$\dot{n} = D_1 \sin(\lambda - \lambda_{31}) + D_2 \sin(2\lambda - 2\lambda_{22}) + D_3 \sin(3\lambda - 3\lambda_{33})$$

where $\dot{\theta}_e$ is the Earth rotation rate. The constant Λ is the total secular perturbation rate in mean longitude, reckoned at the epoch. Recalling that, by definition, n_0'' already contains the zonal secular perturbation rate of mean anomaly, we have

$$\Lambda = (\dot{M}'')_L + (\dot{M}'')_S + n_0'' \left(\frac{dg''}{dM''} \right)_Z + (\dot{g}'')_L + (\dot{g}'')_S + n_0'' \left(\frac{dh''}{dM''} \right)_Z + (\dot{h}'')_L + (\dot{h}'')_S$$

The integration formula is

$$\lambda(t+dt) = \lambda(t) + \dot{\lambda}(t)(dt) + \ddot{\lambda}(t)(dt)^2/2$$

$$n(t+dt) = n(t) + \dot{n}(t)(dt) + \ddot{n}(t)(dt)^2/2$$

where the stepsize dt is initially equal to 12 hours. On the last integration step, dt is changed to meet the time of interest. The second derivatives are evaluated as

$$\ddot{\lambda} = \dot{n}$$

$$\ddot{n} = \dot{\lambda} [D_1 \cos(\lambda - \lambda_{31}) + D_2 \cos(2\lambda - 2\lambda_{22}) + D_3 \cos(3\lambda - 3\lambda_{33})]$$

Compute resonance-corrected mean anomaly and semimajor axis:

$$M'' = [\lambda(t) - g''(t) - h''(t) + \theta_e(t)] \bmod 2\pi$$

$$a'' = a'' + (\delta a)_R, \quad (\delta a)_R = -\frac{2}{3} \frac{a_0''}{n_0''} (\delta n)_R, \quad (\delta n)_R = n - n_0''$$

End of resonance corrections for 1-day case.

If the mean period $T_0'' = 2\pi/n_0''$ is between 680 and 760

minutes inclusive (the 1/2-day case), and the eccentricity is greater than or equal to 0.5, compute resonance correc-

tions for mean anomaly and semimajor axis. The Kaula (l, m, p, q) indices of interest are

$$(2, 2, 0, 1), (3, 2, 1, 0), (4, 4, 1, 0), (5, 2, 2, 0), (5, 4, 2, 1), \\ (2, 2, 1, 1), (3, 2, 2, 2), (4, 4, 2, 2), (5, 2, 3, 2), (5, 4, 3, 3).$$

Dimensionless geopotential constants:

$Q_{22} = 1.7891679 \times 10^{-6}$	$\lambda_{22} = 5.7686396$
$Q_{32} = 3.7393792 \times 10^{-7}$	$\lambda_{32} = 0.95240898$
$Q_{44} = 7.3636953 \times 10^{-9}$	$\lambda_{44} = 1.8014998$
$Q_{52} = 1.1428639 \times 10^{-7}$	$\lambda_{52} = 1.0508330$
$Q_{54} = 2.1765803 \times 10^{-9}$	$\lambda_{54} = 4.4108898$

Kaula inclination functions $F_{lmp}(I)$:

$$F_{220} = \frac{3}{4} (1 + \cos I_0'')^2$$

$$F_{221} = \frac{3}{2} \sin^2 I_0''$$

$$F_{321} = \frac{15}{8} \sin I_0'' (1 - 2 \cos I_0'' - 3 \cos^2 I_0'')$$

$$F_{322} = -\frac{15}{8} \sin I_0'' (1 + 2 \cos I_0'' - 3 \cos^2 I_0'')$$

$$F_{441} = \frac{105}{4} \sin^2 I_0'' (1 + \cos I_0'')^2$$

$$F_{442} = \frac{315}{8} \sin^4 I_0''$$

$$F_{522} = \frac{315}{32} \left[\sin^3 I_0'' (1 - 2 \cos I_0'' - 5 \cos^2 I_0'') + \sin I_0'' \left(-\frac{2}{3} + \frac{4}{3} \cos I_0'' + 2 \cos^2 I_0'' \right) \right]$$

$$F_{523} = \frac{105}{16} \sin I_0'' \left[1 + 2 \cos I_0'' - 3 \cos^2 I_0'' - \frac{3}{2} \sin^2 I_0'' (1 + 2 \cos I_0'' - 5 \cos^2 I_0'') \right]$$

$$F_{542} = \frac{945}{32} \sin I_0'' [2 - 8 \cos I_0'' + \cos^2 I_0'' (-12 + 8 \cos I_0'' + 10 \cos^2 I_0'')]]$$

$$F_{543} = \frac{945}{32} \sin I_0'' [\cos^2 I_0'' (12 + 8 \cos I_0'' - 10 \cos^2 I_0'') - 2 - 8 \cos I_0'']$$

The Kaula eccentricity functions $G_{lpq}(e)$ are approximated

by polynomials for $e_0'' \geq 0.5$ (primes omitted for clarity):

$$\begin{aligned} G_{211} &= +3.616 - 13.247 e_0 + 16.29 e_0^2, & e_0 \leq 0.65 \\ &= -72.099 + 331.819 e_0 - 508.738 e_0^2 + 266.724 e_0^3, & e_0 > 0.65 \end{aligned}$$

$$G_{201} = -0.306 - 0.44 (e_0 - 0.64) \quad \text{for all } e_0 \geq 0.5$$

$$G_{310} = -19.302 + 117.39e_0 - 228.419e_0^2 + 156.591e_0^3, \quad e_0 \leq 0.65$$

$$= -346.844 + 1582.851e_0 - 2415.925e_0^2 + 1246.113e_0^3, \quad e_0 > 0.65$$

$$G_{322} = -18.9068 + 109.7927e_0 - 214.6334e_0^2 + 145.5816e_0^3, \quad e_0 \leq 0.65$$

$$= +342.585 + 1554.908e_0 - 2366.899e_0^2 + 1215.972e_0^3, \quad e_0 > 0.65$$

$$G_{410} = -41.122 + 242.694e_0 - 471.094e_0^2 + 313.953e_0^3, \quad e_0 \leq 0.65$$

$$= -1052.797 + 4758.686e_0 - 7193.992e_0^2 + 3651.957e_0^3, \quad e_0 > 0.65$$

$$G_{422} = -146.407 + 841.88e_0 - 1629.014e_0^2 + 1083.435e_0^3, \quad e_0 \leq 0.65$$

$$= -3581.69 + 16178.11e_0 - 24462.77e_0^2 + 12422.52e_0^3, \quad e_0 > 0.65$$

$$G_{520} = -532.114 + 3017.977e_0 - 5740.032e_0^2 + 3708.276e_0^3, \quad e_0 \leq 0.65$$

$$= -1464.74 - 4664.75e_0 + 3763.64e_0^2, \quad 0.65 < e_0 \leq 0.715$$

$$= -5149.66 + 29936.92e_0 - 54087.36e_0^2 + 31324.56e_0^3, \quad e_0 > 0.715$$

$$G_{521} = -822.71072 + 4568.6173e_0 - 8491.4146e_0^2 + 5337.524e_0^3, \quad e_0 < 0.70$$

$$= -51752.104 + 218913.95e_0 - 309468.16e_0^2 + 146349.42e_0^3, \quad e_0 \geq 0.70$$

$$G_{532} = -853.66 + 4690.25e_0 - 8624.77e_0^2 + 5341.4e_0^3, \quad e_0 < 0.70$$

$$= -40023.88 + 170470.89e_0 - 242699.48e_0^2 + 115605.82e_0^3, \quad e_0 \geq 0.70$$

$$G_{533} = -919.2277 + 4988.61e_0 - 9064.77e_0^2 + 5542.21e_0^3, \quad e_0 < 0.70$$

$$= -37995.78 + 161616.52e_0 - 229838.2e_0^2 + 109377.94e_0^3, \quad e_0 \geq 0.70$$

Special constants, evaluated for each of the 10 (l, m, p, q) combinations of interest:

$$D_{lmpq} = \frac{3n_0^{//2}}{a_0^{//1}} F_{lmp} G_{lpq} Q_{lm}$$

Initial conditions for numerical integration:

$$\lambda(t_0) = M_0^{//} + 2h_0^{//} - 2\theta_0(t_0)$$

$$n(t_0) = n_0^{//}$$

The following pair of differential equations is integrated numerically:

$$\lambda = n + \Lambda - 2\theta_g$$

$$\dot{\lambda} = \sum_{(l,m,p,q)} D_{lmpq} \sin \left[(1-2p) g''(t) + \frac{m}{2} \lambda - \lambda_{lm} \right]$$

The sum is taken over the 10 (l,m,p,q) combinations of interest. The constant Λ is a combination of secular rates in mean anomaly and ascending node. Recalling that the initial mean motion already contains the zonal secular rate of mean anomaly, we have

$$\Lambda = (\dot{M}'')_L + (\dot{M}'')_S + 2n_0'' \left(\frac{dh''}{dM''} \right)_Z + 2(\dot{h}'')_L + 2(\dot{h}'')_S$$

The second differential equation requires the mean argument of perigee at any time since epoch:

$$g''(t) = g_0'' + \left[n_0'' \left(\frac{dg''}{dM''} \right)_Z + (\dot{g}'')_L + (\dot{g}'')_S \right] (t - t_0)$$

The numerical integration method is the same as for the 1-day case, and the stepsize is the same. The second derivatives needed in the method are

$$\ddot{\lambda} = \ddot{\lambda}$$

$$\ddot{\lambda} = \dot{\lambda} \sum_{(l,m,p,q)} \frac{m}{2} D_{lmpq} \cos \left[(1-2p) g''(t) + \frac{m}{2} \lambda - \lambda_{lm} \right]$$

Compute resonance-corrected mean anomaly and semimajor axis:

$$M'' = [\dot{\lambda}(t) - 2\dot{h}''(t) + 2\dot{\theta}_g(t)] \bmod 2\pi$$

$$a'' = a'' + (\delta a)_R, \quad (\delta a)_R = -\frac{2}{3} \frac{a_0''}{n_0''} (\delta n)_R, \quad (\delta n)_R = n - n_0''$$

End of resonance corrections for 1/2-day case.

Third-body long-periodic terms, evaluated for each third body:

$$F_2 = \frac{1}{2} \sin^2 f_x - \frac{1}{4}$$

$$F_3 = -\frac{1}{2} \sin f_x \cos f_x$$

$$(\delta_1 e)_x = - \frac{30 \eta e_0'' K_x}{n_0''} [F_2 (X_2 X_3 + X_1 X_4) + F_3 (X_2 X_4 - X_1 X_3)]$$

$$(\delta_1 I)_x = - \frac{K_x}{n_0'' \eta} [F_2 Z_{22} + F_3 (Z_{11} - Z_{13})]$$

$$(\delta_1 M)_x = - \frac{2 K_x}{n_0''} [F_2 Z_2 + F_3 (Z_1 - Z_3) - 3 e_x \sin f_x (7 + 3 e_0''^2)]$$

$$(\delta_1 g + \cos I'' \delta_1 h)_x = \frac{2 \eta K_x}{n_0''} [F_2 Z_{32} + F_3 (Z_{33} - Z_{31}) - 9 e_x \sin f_x]$$

$$(\sin I'' \delta_1 h)_x = \frac{K_x}{n_0'' \eta} [F_2 Z_{22} + F_3 (Z_{23} - Z_{21})]$$

$$(\delta_1 z)_x = (\delta_1 M)_x + (\delta_1 g)_x + (\delta_1 h)_x$$

$$= (\delta_1 M)_x + (\delta_1 g + \cos I'' \delta_1 h)_x + \tan \frac{I''}{2} (\sin I'' \delta_1 h)_x$$

Zonal long-periodic terms in Lyddane form:

$$(\delta_1 e)_z = \text{LPE1} \sin g'' + \text{LPE2} \cos 2g'' + \text{LPE3} \sin 3g''$$

$$(\delta_1 I)_z = \text{LPI1} \sin g'' + \text{LPI2} \cos 2g'' + \text{LPI3} \sin 3g''$$

$$(\sin I'' \delta_1 h)_z = \text{LPH1} \cos g'' + \text{LPH2} \sin 2g'' + \text{LPH3} \cos 3g''$$

$$(e'' \delta_1 M)_z = \text{LPL1} \cos g'' + \text{LPL2} \sin 2g'' + \text{LPL3} \cos 3g''$$

$$(\delta_1 z)_z = \text{LPS1} \cos g'' + \text{LPS2} \sin 2g'' + \text{LPS3} \cos 3g''$$

Auxiliary quantities for zonal short-periodic terms:

$$W17 = f' + e'' \sin f' - M''$$

$$W20 = ((e'' \cos f' + 3) e'' \cos f' + 3) \cos f'$$

$$W21 = 3 \sin(2g'' + 2f') + 3 e'' \sin(2g'' + f') + e'' \sin(2g'' + 3f')$$

$$W22 = (1 + e'' \cos f') (2 + e'' \cos f') / \eta^2$$

Zonal short-periodic terms in Lyddane form:

$$(\delta_2 a)_z = \frac{a'' \gamma_2'}{\eta^2} [(-1+3\theta^2) ((1+e'' \cos f')^3 - \eta^3) + 3(1-\theta^2) (1+e'' \cos f')^3 \cos(2g''+2f')]]$$

$$(\delta_2 e)_z = \frac{\gamma_2'}{2} \left[(-1+3\theta^2) \left(W_{20} + e'' \left(\eta + \frac{1}{1+\eta} \right) \right) + 3(1-\theta^2) (W_{20} + e'') \cos(2g''+2f') - \eta^2 (1-\theta^2) [3e'' \cos(2g''+f') + e'' \cos(2g''+3f')]] \right]$$

$$(\delta_2 I)_z = \frac{\gamma_2'}{2} \theta \sin I'' [3 \cos(2g''+2f') + 3e'' \cos(2g''+f') + e'' \cos(2g''+f')]]$$

$$(e'' \delta_2 M)_z = -\frac{\eta^3 \gamma_2'}{4} \{ 2(-1+3\theta^2) (W_{22}+1) \sin f' + 3(1-\theta^2) [(1-W_{22}) \sin(2g''+f') + (W_{22}+1/3) \sin(2g''+3f')] \}$$

$$(\sin I'' \delta_2 h)_z = -\frac{\gamma_2'}{2} \theta (6W_{17} - W_{21}) \sin I''$$

$$(\delta_2 z)_z =$$

$$-e'' (e'' \delta_2 M)_z \frac{1}{\eta^3} \left(\eta + \frac{1}{1+\eta} - 1 \right) - \frac{\gamma_2'}{4} (6(1+2\theta-5\theta^2)W_{17} - (3+2\theta-5\theta^2)W_{21})$$

Total periodic perturbations in Lyddane form:

$$\delta e = (\delta_1 e)_L + (\delta_1 e)_S + (\delta_1 e)_Z + (\delta_2 e)_Z$$

$$\delta I = (\delta_1 I)_L + (\delta_1 I)_S + (\delta_1 I)_Z + (\delta_2 I)_Z$$

$$(\sin I'' \delta h) = (\sin I'' \delta_1 h)_L + (\sin I'' \delta_1 h)_S + (\sin I'' \delta_1 h)_Z + (\sin I'' \delta_2 h)_Z$$

$$(e'' \delta M) = (e'' \delta_1 M)_L + (e'' \delta_1 M)_S + (e'' \delta_1 M)_Z + (e'' \delta_2 M)_Z$$

$$\delta z = (\delta_1 z)_L + (\delta_1 z)_S + (\delta_1 z)_Z + (\delta_2 z)_Z$$

Lyddane intermediate quantities:

$$DE = e'' + \delta e$$

$$DI = \sin \frac{I''}{2} + \frac{1}{2} (\delta I) \cos \frac{I''}{2}$$

$$DH = \frac{(\sin I'' \delta h)}{2 \cos \frac{I''}{2}}$$

$$DL = (e'' \delta M)$$

$$z = M'' + g'' + h'' + \delta z$$

$$a = a'' + (\delta_2 a)_z$$

Osculating elements by Lyddane method:

$$e = \sqrt{DE^2 + DL^2}$$

$$M = \tan^{-1} \left(\frac{DE \sin M'' + DL \cos M''}{DE \cos M'' - DL \sin M''} \right)$$

$$\cos I = 1 - 2 \sin^2 \frac{I}{2} = 1 - 2 (DI^2 + DH^2) \quad , \quad \sin I = \sqrt{1 - \cos^2 I}$$

$$h = \tan^{-1} \left(\frac{DI \sinh'' + DH \cosh''}{DI \cosh'' - DH \sinh''} \right)$$

$$g = z - M - h$$

Calculate position and velocity from osculating elements.
First, solve Kepler's equation and calculate true anomaly:

$$M = E - e \sin E$$

$$\cos f = \frac{\cos E - e}{1 - e \cos E} \quad \text{and} \quad \sin f = \frac{\sqrt{1 - e^2} \sin E}{1 - e \cos E}$$

Radius to the satellite:

$$r = \frac{a(1 - e^2)}{1 + e \cos f}$$

Unit radial vector:

$$\hat{u} = \begin{Bmatrix} \cosh \cos(g+f) - \sinh \sin(g+f) \cos I \\ \sinh \cos(g+f) + \cosh \sin(g+f) \cos I \\ \sin(g+f) \sin I \end{Bmatrix}$$

Unit transverse vector:

$$\hat{v} = \begin{Bmatrix} -\cosh \sin(g+f) - \sinh \cos(g+f) \cos I \\ -\sinh \sin(g+f) + \cosh \cos(g+f) \cos I \\ \cos(g+f) \sin I \end{Bmatrix}$$

Unit normal vector:

$$\hat{w} = \begin{Bmatrix} \sinh \sin I \\ -\cosh \sin I \\ \cos I \end{Bmatrix}$$

Satellite position:

$$\vec{R} = r \hat{u}$$

Satellite velocity:

$$\vec{v} = \frac{1}{\eta} \sqrt{\frac{\mu_E}{a}} [(e \sin f) \hat{u} + (1 + e \cos f) \hat{v}]$$

TECHNIQUES OF ORBIT DETERMINATION USING MINIMUM DATA, ACCOUNTING OF THE FEATURES OF RUSSIAN SPACE SURVEILLANCE SYSTEM

V.F. Boikov

"Vympel" International Corporation, Moscow

INTRODUCTION

Classical orbit determination techniques using minimum data have nearly two-centuries history and are developed to high level of perfection. However, specific features of Russian Space Surveillance System (SSS) require consideration of two issues significant for development of algorithms.

i) The measurements, acquired by Russian space surveillance radars comprise essentially not equally accurate components. In particular, elevation angle and its rate are subjected to significant errors.

ii) The SSS radars are located within the territory of the former USSR and thus the gaps between the observations of one satellite may range from several revolutions to several days (for small-sized objects).

Two types of orbit determination techniques using minimum data were developed respectively.

i) The set of methods for determination of Keplerian orbits using combined data which include both position and velocity components.

ii) Technique of orbit determination on the basis of two positions when secular evolution of orbit within the interval between two measurements is taken into account.

Let us treat these techniques in more detail.

1 Methods of orbit determination using combined data

Assume that tracking of one satellite by two radars (or by one radar for two intervals) produces observation vectors $\mathbf{f}_1 = (f_{11}, f_{12}, f_{13}, f_{14}, f_{15}, f_{16})$ and $\mathbf{f}_2 = (f_{21}, f_{22}, f_{23}, f_{24}, f_{25}, f_{26})$, related to the moments t_1 and t_2

respectively. Using six components (out of twelve) of these vectors and the temporal interval, Keplerian orbit can be determined.

We will deal with the class of orbit determination techniques requiring to solve the system of two non-linear equations.

Two classical orbit determination techniques exist.

i) Technique of orbit determination using phase vector (three components of position and three velocity components).

ii) Technique of orbit determination using two positions.

Thus, our generalizations of classical techniques will be called:

i) Technique of complementing to phase vector (TCPV).

ii) Technique of complementing to two positions (TCTP).

1.1 Technique of complementing to phase vector

The method is obvious.

Assume we know 4 components of phase vector \mathbf{f}_1 and two components of phase vector \mathbf{f}_2 . To be deterministic we take as known $f_{11}, f_{12}, f_{14}, f_{15}, f_{21}, f_{22}$.

Complementing the vector \mathbf{f}_1 with approximate values of components $\tilde{f}_{13}, \tilde{f}_{16}$, we obtain complete phase vector $\mathbf{f} = (f_{11}, f_{12}, \tilde{f}_{13}, f_{14}, f_{15}, \tilde{f}_{16})$.

Propagating this phase vector \mathbf{f} to the moment t_2 we can calculate two respective components of the second phase vector.

Denote these components as: $f_{21}^{cal}(\tilde{f}_{13}, \tilde{f}_{16}), f_{22}^{cal}(\tilde{f}_{13}, \tilde{f}_{16})$.

Thus TCPV algorithm means the search for solution of system (1).

$$\left. \begin{aligned} f_{21} &= f_{21}^{cal}(\tilde{f}_{13}, \tilde{f}_{16}) \\ f_{22} &= f_{22}^{cal}(\tilde{f}_{13}, \tilde{f}_{16}) \end{aligned} \right\} \quad (1)$$

1.2 Technique of complementing to two positions

Initial data for TCTP are four (out of six) components of two position vectors and two components of two velocity vectors. The unknowns to be determined are two components of two position vectors (to be deterministic: f_{13}, f_{23}).

Taking their approximate values we solve classical task of orbit determination using two positions. Equating the differences between thus calculated components of two velocity vectors and their given values we will obtain the system of two non-linear equations.

Taking into account non-linear equation of classical task of orbit determination using two positions we will have the system of three non-linear equations for three unknowns: two components of two position vectors and the variable of classical task of orbit determination using two positions.

Using special transformations one can obtain the system of two non-linear equations for two unknown components of two position vectors (to be deterministic: f_{13}, f_{23}).

Derivation of these equations is based on solution of auxiliary task presenting velocity vectors V_1, V_2 via position vectors r_1, r_2 and certain auxiliary quantities.

1.3 Auxiliary task

Denoting r_1, r_2, V_1, V_2 satellite's radius-vectors and velocity vectors in fixed geo-centric coordinate system for two moments, we have the first integrals of Keplerian motion:

i) areas integral

$$[r_1, V_1] = [r_2, V_2]; \quad (2)$$

ii) energy integral

$$V_1^2 - 2\mu/r_1 = V_2^2 - 2\mu/r_2; \quad (3)$$

iii) Laplace integral

$$(V_1^2 - \mu/r_1) \cdot r_1 - (r_1, V_1) \cdot V_1 = (V_2^2 - \mu/r_2) \cdot r_2 - (r_2, V_2) \cdot V_1. \quad (4)$$

Relationship of velocity vectors V_1, V_2 to measured velocity components we write in the form of linear equations :

$$(k_1, V_{p1}) = \psi_1, \quad (5)$$

$$(\mathbf{k}_2, \mathbf{V}_{p_2}) = \psi_2, \quad (6)$$

where p_1 and p_2 are equal 1 or 2.

The vectors \mathbf{k}_1 and \mathbf{k}_2 depend only on \mathbf{r}_{p1} and \mathbf{r}_{p2} respectively, and scalars ψ_1, ψ_2 in addition depend on measured first or second velocity components respectively.

Resolve velocity vectors into radial and transversal components:

$$\left. \begin{aligned} \mathbf{V}_1 &= \mathbf{V}_{1r} + \mathbf{V}_{1n} \\ \mathbf{V}_2 &= \mathbf{V}_{2r} + \mathbf{V}_{2n} \end{aligned} \right\} \quad (7)$$

As follows from areas integral

$$\left. \begin{aligned} V_{1n} &= (\mathbf{c}, \mathbf{n}, \mathbf{r}_1)/r_1^2 \\ V_{2n} &= (\mathbf{c}, \mathbf{n}, \mathbf{r}_2)/r_2^2 \end{aligned} \right\} \quad (8)$$

where \mathbf{n} - the vector, normal to orbital plane, determined using the formula

$$\mathbf{n} = [\mathbf{r}_1, \mathbf{r}_2]/(r_1 r_2 \sin \varphi), \quad (9)$$

φ - the angle between vectors \mathbf{r}_1 and \mathbf{r}_2 and $\mathbf{c} = [\mathbf{r}, \mathbf{V}]$.

As follows from equations (7),(8),(9) :

$$\left. \begin{aligned} \mathbf{V}_1 &= \mathbf{r}_1(V_{1r} - c \cot \varphi / r_1)/r_1 + \mathbf{r}_2 c / (r_1 r_2 \sin \varphi) \\ \mathbf{V}_2 &= \mathbf{r}_2(V_{2r} + c \cot \varphi / r_2)/r_2 + \mathbf{r}_1 c / (r_1 r_2 \sin \varphi) \end{aligned} \right\} \quad (10)$$

Equations (10) comprise three unknowns V_{1r}, V_{2r}, c . Equations (3), (4), (5), (6) can be used to determine them and it can be done in several ways.

a) System of three linear equations

Scalarly multiplying equation (4) over $\mathbf{V}_2 - \mathbf{V}_1$, we shall obtain equation

$$((r_1 \cdot \mathbf{r}_2 - r_2 \cdot \mathbf{r}_1), (\mathbf{V}_2 - \mathbf{V}_1)) = 0, \quad (11)$$

Substituting there equation (10), we will have linear with regard to V_{1r}, V_{2r}, c equation. The other equations are equations (5), (6), as mentioned above.

Yu. S. Savrasov was the first to propose this method to determine three unknowns V_{1r} , V_{2r} , c ¹

b) System of two linear and one quadratic equations.

In the previous system we will take equation (3) instead of equation (11), that will turn (after substituting expressions (10)) into:

$$c^2(1/r_1^2 - 1/r_2^2) + V_{1r}^2 - V_{2r}^2 + 2\mu(1/r_1^2 - 1/r_2^2) = 0. \quad (12)$$

System of equations (11), (4), (5) is simple to solve.

c) One quadratic equation.

Multiplying (4) respectively by r_2 , r_1 and using equations (10), we will obtain:

$$\left. \begin{aligned} V_1 &= r_1\mu(1 - \cos \varphi)/c \sin \varphi - c/(r_2 \sin \varphi) + r_2c/(r_1r_2 \sin \varphi) \\ V_2 &= r_2\mu(\cos \varphi - 1)/c \sin \varphi + c/(r_1 \sin \varphi) - r_1c/(r_1r_2 \sin \varphi) \end{aligned} \right\} \quad (13)$$

with one unknown c .

Substituting these expressions into one of measurements' equations, for example, into (5) we obtain quadratic equation for c :

$$c^2 + p \cdot c + q = 0, \quad (14)$$

где

$$p = -\frac{\psi_1 r_1 r_2 \sin \varphi}{(\mathbf{k}_1, (\mathbf{r}_2 - \mathbf{r}_1))}, \quad (15)$$

$$q = \frac{(-1)^{p_1} \mu r_1 r_2 (\mathbf{k}_1, \mathbf{r}_{p1})(1 - \cos \varphi)}{r_{p1}(\mathbf{k}_1, (\mathbf{r}_2 - \mathbf{r}_1))} \quad (16)$$

Having determined c from equation (14), from (13) we shall obtain relationship between velocity vectors \bar{V}_1 , \bar{V}_2 and position vectors \bar{r}_1 , \bar{r}_2 .

¹"Определение орбит по смешанным данным", Космические исследования, т. 10, вып. 4, с. 494-498.

1.4 Derivation of the main system of two equations

Having solved auxiliary task using one of mentioned techniques we will have formulas of the shape $V_1 = V_1(f_{13}, f_{23})$, $V_2 = V_2(f_{13}, f_{23})$, which are to be substituted into Kepler's equation (17) :

$$n \cdot (t_2 - t_1) - 2k\pi + [(\mathbf{r}_2, \mathbf{V}_2) - (\mathbf{r}_1, \mathbf{V}_1)]/a^2 n \mp \mp \arccos \{1 - [\mathbf{r}_1 \mathbf{r}_2 - (\mathbf{r}_1, \mathbf{r}_2)]/ap\} = 0, \quad (17)$$

where k -number of revolutions, n, p, a - are obtained using $\mathbf{r}_1, \mathbf{V}_1$.

Equation (17) together with one of equations not used in derivation of formulas for V_1, V_2 comprise the system of two equations for unknowns f_{13}, f_{23} .

1.5 Rationale for the choice of technique to solve auxiliary task

For all of techniques for solving auxiliary task, in the plane of independent variables f_{13}, f_{23} the points exist, where solution of auxiliary task degenerates.

For case a) the condition is $\det = 0$;

for case b) this is the condition when a system of two equations with three unknowns is not solvable with regard to arbitrary pair of unknowns;

for case c) this is the condition $[\mathbf{r}_1, \mathbf{r}_2] = 0$ of collinearity of vectors \mathbf{r}_1 and \mathbf{r}_2 .

More detailed analysis reveals that certain interesting for applications cases exist when *solution of auxiliary task using techniques a), b) is degenerated for the whole plane of independent variables f_{13}, f_{23}* . For example, assume one radar measures for two moments t_1, t_2 spherical angles $\alpha_1, \delta_1, \alpha_2, \delta_2$ and their rates $\dot{\alpha}_1, \dot{\alpha}_2$ with respect to not moving Earth. Since the Earth moves slowly (in comparison to the movement of low satellite), solution of auxiliary task using methods a), b) turns to be very poorly determined thus resulting in divergence in solving the main system of equations. Corresponding effect for linear equations brought to life optimal elimination techniques.

For TCTP, technique that does not degenerate was discovered to solve non-linear sub-system of three equations (i.e. degenerates only for practically not interesting case of collinear vectors \mathbf{r}_1 and \mathbf{r}_2).

1.6 Non-symmetrical task

The main system of TCTP equations comprise Kepler's equation (17) and rather simple equation for velocity measurements (5) (or (6)). Simplification of the algorithm can be achieved if equation (5) will be non-symmetrical: one component of the position will participate in essentially simpler way than the other. Then this component can be rather simply determined using this equation via the other one and from computations' point of view the task will be reduced to solving equation (17) for more complex component.

This idea is realized for non-symmetrical set of initial data

$$(R_1, R_2, \alpha_1, \alpha_2, \dot{R}_2, \dot{\alpha}_2),$$

where R_1, R_2 - ranges for respective moments.

Taking into account (10), (5), (6) lead to:

$$\left. \begin{aligned} \omega_1 c^2 + \gamma_1 \mu r_1 r_2 (1 - \cos \varphi) &= -\psi_1 r_1 r_2 \cos \varphi \\ \omega_2 c^2 + \gamma_2 \mu r_1 r_2 (1 - \cos \varphi) &= -\psi_2 r_1 r_2 \cos \varphi, \end{aligned} \right\} \quad (18)$$

where

$$\omega_i = (\mathbf{k}_i, \mathbf{r}_1) - (\mathbf{k}_i, \mathbf{r}_2), \quad \gamma_i = (\mathbf{k}_i, \mathbf{r}_2)/r_2, \quad i = 1, 2.$$

Eliminating c , we obtain:

$$(\mathbf{a}, (\mathbf{r}_1 - \mathbf{r}_2))^2 = \chi r_1 r_2 (1 - \cos \varphi) (\mathbf{b}, (\mathbf{r}_1 - \mathbf{r}_2)), \quad (19)$$

where

$$\chi = (\gamma_2 \psi_1 - \gamma_1 \psi_2)/\mu, \quad \mathbf{a} = \gamma_1 \mathbf{k}_1 - \gamma_2 \mathbf{k}_2, \quad \mathbf{b} = \psi_2 \mathbf{k}_1 - \psi_1 \mathbf{k}_2. \quad (20)$$

The values $\chi, \mathbf{a}, \mathbf{b}$ depend only on angular variable δ_2 .

Relationship of r_1 to angular variable δ_1 can be written as follows

$$r_1 = r_{10} + r_{1c} \cos \delta_1 + r_{1s} \sin \delta_1, \quad (21)$$

where quantities r_{10}, r_{1c}, r_{1s} depend only on angular variable δ_2 and do not depend on δ_1 .

Substituting (21) into (19) we obtain final equation, that is omitted here due to its unwieldy character. This equation replaces equation (5) for non-symmetrical versions of TCTP. Rather simple investigations demonstrate that equation (21) is algebraic equation of the eighth order in $\tan(\delta_1/2)$. Assuming small angles δ_1 (that is valid under our conditions), equation reduces to equation of the fourth order regarding the angle, that can be solved in radicals. Obviously, solving these equations poses much less difficulties in comparison to the primary task. Finally the task is reduced to solving equation (17) for δ_2 , and for each step of the process variable δ_1 is preliminary determined using equation (21).

1.7 Numerical methods and experiments

Proposed techniques were studied in the course of extensive set of numerical experiments. The findings of these experiments in brief are as follows. For real range of orbital parameters (only low orbits were considered) and radars' fields of view the problems turned to be essentially non-linear and having up to 6 roots. Special numerical technique is developed to obtain global solution (all the roots).

Outer module of this procedure organizes the movement along the lines of outer contour of the domain of two independent variables (in our experiments this domain is rectangular) and consequently finds all the intersections of the level line of the first equation (1) with the contour. In case such intersection is found the inner module starts operating.

The inner module arranges the movement along level line of the first equation until the boundary of the contour is reached. In case intersection with the level line of the second equation is found, the determined root is refined using Newton technique. Control of the step along the level

line is realized to make the steps far from the level line possibly greater, diminishing them in course of approaching the root.

All boundary problems, reduced to two non-linear equations using above mentioned techniques were solved for 10 typical orbits. Special numerical procedure did determine true root in course of the search for global solution in all the cases.

Reassuring results were obtained for non-symmetrical problems. Experiments produced one root, very rapidly refined by parabolas' method (the inner equation was solved using Newton's method). The rationale for different behaviour of symmetrical and non-symmetrical problems are not clear enough.

2 Orbit determination using two positions taking account of the evolution.

If the interval between two measurements is a day or more, the most informative for orbit determination set of components (among six of them) is a set of two positions. However, in this case orbit's evolution is to be taken into account. Let us consider Keplerian case first.

2.1 Non-degenerating case of orbit determination using two positions for Keplerian approximation

Deriving his classical technique Gauss used the system of two equations:

$$r_1 + r_2 = 2a \sin g^2 + \kappa \cos g, \quad (22)$$

$$\sqrt{\mu/a^3}(t_2 - t_1) = 2g - \sin 2g + \kappa a^{-1} \sin g, \quad (23)$$

where

$$g = (E_2 - E_1)/2, \quad \kappa = 2\sqrt{r_1 r_2} \cos f,$$

$2f = \theta_2 - \theta_1$ - angle between position vectors $\mathbf{r}_1, \mathbf{r}_2$.

E_1, E_2 - eccentric anomalies,

θ_1, θ_2 - true anomalies.

Gauss transformations of this system are intended to use hypergeometric functions in the shape of computationally efficient chain fractions. Thus the goal to develop well converging procedure (for small angles $2f$) was achieved. However, these transformations result in singularity rising for $2f = \pi$, and poor convergence for large and medium angles $2f$. Excellent study of this issue, together with technique to shift the singularity are presented in the paper R.H. Battin and R.M. Vaughan².

When orbital evolution is taken into consideration the equations are essentially accomplished and their reduction to any sort of known functions seems unrealistic. That is why our technique directly uses equations (22), (23).

The algorithm performs numerical solving of the equation:

$$Z(g) - Y(g) = 0, \quad (24)$$

where

$$Z(g) = \sqrt{\frac{\mu}{a_1}}, \quad Y(g) = \sqrt{\frac{\mu}{a_2}}, \quad (25)$$

a_1 and a_2 are determined from equations (22) and (23) respectively.

The search for $Z(g)$ and $Y(g)$ is fulfilled using Newton technique with modifications, limiting the step and ensuring convergence. Equation (24) is also solved using Newton technique.

After upgrades following experimental tests the method demonstrated convergence for all the problems.

2.2 Taking account of the evolution

We will take into account only secular evolution from second zonal harmonic since it predominates for long intervals.

²"An Elegant Lambert Algorithm", Journal of Guidance, Control, and Dynamics, 1984, v. 7, No. 6, pp. 662-670.

Secular evolution from second zonal harmonic is present only for angular parameters and is expressed by formulas:

$$\Delta\Omega = -\frac{3}{2} \frac{J_2 a_e^2 \theta}{p^2} \Delta t, \quad (26)$$

$$\Delta\omega = -\frac{3}{2} \frac{J_2 a_e^2 (1/2 - 5/2\theta^2)}{p^2} \Delta t, \quad (27)$$

$$\Delta l = -\frac{3}{2} \frac{J_2 a_e^2 (1/2 - 3/2\theta^2)}{p^2} \cdot \sqrt{1 - e^2} \Delta t, \quad (28)$$

where

$$\theta = \cos i, \quad \Delta t = (t_2 - t_1), \quad p = a(1 - e^2),$$

$\Delta\Omega$ - evolution of longitude of ascending node,

$\Delta\omega$ - evolution of perigee argument,

Δl - evolution of mean anomaly.

To calculate eccentricity using known a and g we have:

$$e^2 = \left(\frac{2a - r_1 - r_2}{2a \cos g} \right)^2 + \left(\frac{r_2 - r_1}{2a \sin g} \right)^2 \quad (29)$$

Denoting as \tilde{r} vector \bar{r} , turned for the angle $\Delta\Omega$, we have the formula:

$$\theta = \frac{(x_1 \tilde{y}_2 - \tilde{x}_2 y_1)}{(\sqrt{(y_1 z_2 - \tilde{y}_2 z_1)^2 + (x_1 z_2 - \tilde{x}_2 z_1)^2 + (x_1 \tilde{y}_2 - \tilde{x}_2 y_1)^2})}, \quad (30)$$

where

$$\left. \begin{aligned} \tilde{x}_2 &= \cos(\Delta\Omega)x_2 + \sin(\Delta\Omega)y_2 \\ \tilde{y}_2 &= \cos(\Delta\Omega)y_2 - \sin(\Delta\Omega)x_2. \end{aligned} \right\} \quad (31)$$

Taking into account evolution of perigee argument we obtain for the angle between position vectors \bar{r}_1, \bar{r}_2 :

$$2f = \theta_2 - \theta_1 + \Delta\omega. \quad (32)$$

Thus we have the formula:

$$\kappa = \sqrt{2r_1 r_2 [1 + \cos(2f - \Delta\omega)]}, \quad (33)$$

where:

$$2f = \arcsin \left(\frac{x_1 \tilde{y}_2 - \tilde{x}_2 y_1}{\theta} \right). \quad (34)$$

Finally, Kepler's equation with account of mean anomaly evolution l takes the form:

$$\sqrt{\mu/a^3}(t_2 - t_1) = 2g - \sin 2g + \kappa a^{-1} \sin g + \Delta l. \quad (35)$$

2.3 Procedure

The main equation (24) is the same as for Keplerian case.

The algorithm for solving it also does not change, but instead of equation (23) equation (35) is used.

Accomplishment is caused by varying coefficient κ and additional term in equation (35).

Let for certain iteration of equation (24) new approximations for a, g are obtained. Then determination of $\kappa, \Delta l$ is performed in the following succession.

1. Determine e using formula (29).
2. Solve equation (30) by iterations and determine θ .
3. Using (26), (27), (28) determine orbital evolution.
4. According to (33), (34) determine κ .

After these calculations we can proceed to determination of next approximation for equation (24).

3 Findings

Classical methods do not take into account specific features of data used for orbit determination in Russian Space Surveillance Center.

Rough components of position vectors do not allow to use the algorithms, based on Lambert problem and require employment of more sophisticated techniques.

The first part of the paper demonstrates that for extensive class of boundary conditions the problem can be reduced to solving the system of two non-linear equations.

This reduction can be done in various ways and presented study leads to recommendations for the choice of this way. Possibility of further simplification of the problem is demonstrated for non-symmetrical set of measured components and for this case one equation, comprising the root of algebraic equation in its coefficients is obtained to solve the problem.

Computation procedures for solving obtained equations are given without discussion.

The second part of the paper proposes modification of known Gauss technique, allowing to determine satellites' orbits using two positions, distanced for long temporal intervals, accounting of secular evolution of the orbit.

Fulfilled studies and their results lead to consideration that new, different from classical and computationally efficient algorithms can be discovered in the field of orbit determination problems.

REENTRY TIME DETERMINATION ANALYSIS FOR "COSMOS-398" AND FSW-1-5

**V.Andrewshchenko, G.Batyr, V.Bratchikov,
V.Dicky, S.Veniaminov, V.Yurasov**

SRC "Kosmos", Moscow

1. INTRODUCTION

Of late the Russian Space Surveillance System (RSSS) regularly cooperated with foreign space centers on monitoring space objects nearing the end of their orbiting. The last two such works were carried out in Nov.-Dec. 1995 and Feb.-Mar. 1996, on "Cosmos-398" and Chinese descent capsule FSW-1-5 respectively.

The "Cosmos-398" payload represented the Lunar Lander (1970-1974) designed to deliver a single cosmonaut to the lunar surface. After the launch in 1971 and the failure of the rocket program there emerged 5 fragments 4 of which burnt the same year.

The 5th fragment left in orbit consisted of the habitable pressure cabin with motors and the instrument compartment, having the total mass about 2000 kg and overall dimensions approximately 2.5m x 4m. The heat-proof mass made up less than 5% of the total mass.

The fragment was cataloged by both the RSSS and the US SSN (international number 71-016H), and the both systems had been continually tracking it since the launch on 26 Feb. 1971 till its reentry on 10 Dec. 1995.

FSW-1-5 ("China-40") was launched on 8 Oct. 1993 into 200km x 400km orbit (incl. 57 deg.). Of the 8 launch generated fragments 7 burnt the same October. The 8th one was a descent capsule (international number 93-063H) protected by a heat-proof shield, shaped like a cone approximately 1.3m x 1.7m, and had more than 500 kg estimated mass.

It should have been retrieved after 7-10 days of flight, but the failure of boost command put it into a highly elliptical 200km x 3000km orbit and let it exist till 12 Mar. 1996.

The SRC "Kosmos", having coordinated this work from Russian side together with Russian Space Agency, cooperated with the US SSC (via Kaman Sciences Corporation), Johnson Space Center, ESOC and other scientific centers.

The data exchange was regularly accomplished through the e-mail. We transmitted the data to NASDA and CNES as well.

The only sources of real measurements were the RSSS and the US SSN. These two systems not merely duplicate each other but they are profitably complementary. For example, the last day of "Cosmos 398" orbital existence the satellite was out of visibility of Russian radars during the 7 consecutive revolutions 45039-45045 and was tracked only by the US SSN. But the most essential for reentry prediction last two revolutions (45046 and 45047) were seen only by the RSSS facilities.

All the measurements were processed by the RSSS, the US SSN, SRC "Kosmos", Russian Mission Control Center, ESOC, Kaman Sciences Corporation, JSC, NASDA, CNES, FGAN, Braunschweig University and other scientific centers.

2.THE RESULTS OF MONITORING "COSMOS 398" REENTRY

Table 1 contains the "Cosmos-398" orbit determination data on the base of the RSSS measurements for the last two days of its orbital existence. Every day the orbit was updated at 6 or 7 revolutions. The last update was at 45046 revolution - one before the last. The last measurement was obtained about 20:00 GMT 10/12/95 at the 45047th revolution less than an hour before the reentry.

Alongside of the RSSS, only the US SSN tracked "Cosmos-398". For the last two days the US SSN transmitted us the element sets (TLE) at 8 different revolutions, recalculation of them into the Keplerian elements being presented in Table 2. The difference between Russian and American numeration systems accounts for discrepancy of the revolution numbers. So further on we will keep the RSSS numeration system.

The orbit and reentry time determination accuracy essentially depends on atmosphere perturbations due to short wave and corpuscular solar radiation. In atmosphere models these perturbations are taken into account via solar (F10.7) and geomagnetic (Kp) indices. Daily averaged meanings of them since 1 Dec. 1995 to 12 Mar. 1996 are depicted at Figs. 1 and 2.

Since 1 to 10 Dec. 1995 solar index variations were between 72.7 and 74.1. The geomagnetic activity level was rather low as well and till 8 Dec. had a trend to lowering (from 3 through 0.5). So at the end of orbital existence of "Cosmos-398" the solar and geomagnetic situation was rather still and its level was low enough.

The reentry time and site determination was carried out at RSSS and US SSN independently in their regular modes after every orbit update, each on the base of its own measurement information. ESOC, Russian Mission Control Center (RMCC)

and SRC "Kosmos" solved this task on one's own with the help of their own algorithms and programs and available information sources (ESOC and SRC "Kosmos" used the Russian and the US SSN element sets while RMCC - only the former).

The correlation of "Cosmos-398" reentry time estimates from different Centers and based on different initial data can be seen from Table 3. Its first column contains the last revolution number on which updated elements were used for calculation of the appropriate estimate. In the 2nd column the "author" of estimate is indicated, and in the 3d - the source of tracking data. The predicted reentry windows (if any) and expected reentry times are given in the 4th, 5th and 6th columns. The 7th column shows absolute residuals of estimates, the assumed standard being 20:40 GMT 10 Dec. 1995. In the 8th column there are prediction time intervals, and in the 9th - the relative errors of reentry time determination (as percents of the time remainder to reentry).

Fig.3 illustrates the data of Table 3. For every organization (except RMCC) which carried on calculations, it presents the deviations of reentry time estimates depending on the flight time remainder. For comparison there is shown the 10% level of error.

3.THE RESULTS OF MONITORING FSW-1-5 REENTRY

The FSW-1-5 orbit was updated daily in the RSSS at every of 9 revolutions. The results of its orbit determination for the last 2 days of its flight are given in Table 4. The last updating was conducted at the revolution number 11870 - 5 revolutions before its reentry. (After that the capsule was out of visibility of Russian radars.)

Table 5 presents the results of FSW-1-5 orbit determination at the US SSN.

The condition of tracking "Cosmos-398" and FSW-1-5 were very alike: the both orbits were eccentric, the solar and geomagnetic activity levels were rather low for the both satellites. However, for the last one the atmosphere perturbation was a little higher: since 1 till 9 Mar. the solar index decreased from 71.9 to 67.5 and then increased to 73.2 12 Mar. (see Fig.1); since 7 till 11 Mar. Kp increased from 0.5 to 3.8 (see Fig.2).

Table 6 and Fig.4 present comparative estimates of reentry time determination for FSW-1-5, obtained by different organizations on the base of different initial data, 04:05 UTC 12 Mar.1996 being assumed the real reentry time.

*

This paper deals predominantly with ballistic aspects of the works above. However, alongside of processing the measurements of motion parameters during tracking FSW-1-5, analysis of radar cross-section signatures was conducted for getting estimates of the design parameters and the attitude dynamics character. As the result it was settled that since Oct. 1993 through Feb. 1996 FSW-1-5 was destabilized and kept precession motion with variable period. The further analysis could perhaps clarify the observed leap of the FSW-1-5 ballistic coefficient early Feb. 1996 (approximately by 10%). This work is now under way, and a paper with detailed analysis of the signatures is being prepared.

4. FINDINGS

1. Almost all the reentry time determination errors by different organizations having taken part in the works on "Cosmos-398" and FSW-1-5 did not exceed the 10% level, which conforms to the accuracy of the atmosphere models used for quiet and moderately perturbed helio-geomagnetic situation.

2. For the last days of flight of the both satellites the relative errors of reentry time determination (except 1 or 2 last revolutions) did not basically exceed 5-6% level. At the very last revolutions the errors were about 10-22%. The aposteriori analysis conducted at "Kosmos" Center has shown that such high meanings could be accounted for by low accuracy of GOST 25645.115-84 atmosphere model at altitudes less than 150 km. Particularly, recalculation of the same estimates with the help of CIRA-86 model has lowered the errors to 3.9% for "Cosmos-398" and to 10% for FSW-1-5.

3. The large errors for FSW-1-5 at the very last interval of its flight seem to be accounted for by either the observed increase of solar and geomagnetic activity level, or by possible springing of the on-board active (explosive) sets, or by possible uncertainty of knowledge of the real reentry time.

4. International cooperation on monitoring the reentry stage of non-cooperative SO flight is very important from the point of view of both increasing the reentry time determination accuracy, and correlation and agreement of models, algorithms, programs and techniques used.

Table 1. "Cosmos-398" orbit updating results due to RSSS

N rev	Date	UTC, h, min	T ₀ , min	ΔT ₀ , min	I, deg	Ω, deg	l=e cos ω	l=e sin ω	Ha, km	Hp, km
45018	09/12/95	01.09	88.2418	-0.01933	51.3850	86.2450	0.00776	0.00356	256	143
45019	09/12/95	02.37	88.2215	-0.01975	51.3840	85.9030	0.00776	0.00354	254	142
45020	09/12/95	04.05	88.2018	-0.01978	51.3840	85.5660	0.00764	0.00354	253	142
45021	09/12/95	05.33	88.1828	-0.01976	51.3810	85.2140	0.00733	0.00356	250	143
45022	09/12/95	07.02	88.1625	-0.02019	51.3810	84.8680	0.00721	0.00354	248	143
45031	09/12/95	20.14	87.9347	-0.02635	51.3770	81.7670	0.00601	0.00336	230	140
45033	09/12/95	23.10	87.8735	-0.03140	51.3800	81.0780	0.00579	0.00321	225	138
45034	10/12/95	00.38	87.8406	-0.03283	51.3820	80.7300	0.00563	0.00314	222	138
45035	10/12/95	02.06	87.8052	-0.03472	51.3810	80.3820	0.00547	0.00311	220	137
45036	10/12/95	03.33	87.7668	-0.03737	51.3800	80.0390	0.00521	0.00304	216	137
45037	10/12/95	05.01	87.7288	-0.03876	51.3780	79.6890	0.00503	0.00298	213	136
45038	10/12/95	06.29	87.6888	-0.04080	51.3770	79.3400	0.00476	0.00292	209	136
45046	10/12/95	18.08	87.1251	-0.12590	51.3710	76.5460	0.00246	0.00177	165	125

Table 2. "Cosmos-398" orbit updating results due to US SSN

N rev	Date	UTC, h, min	T ₀ , min	ΔT ₀ , min	I, deg	Ω, deg	l=e cos ω	l=e sin ω	Ha, km	Hp, km
85213	09/12/95	01.09	88.2377	-0.01703	51.3831	86.2418	0.00782	0.00367	257	143
85216	09/12/95	05.34	88.1815	-0.01740	51.3809	85.2110	0.00745	0.00365	252	143
85220	09/12/95	11.26	88.0821	-0.02359	51.3806	83.8343	0.00684	0.00352	243	142
85228	09/12/95	23.10	87.9285	-0.15314	51.3783	81.0737	0.00572	0.00369	230	141
85236	10/12/95	10.52	87.5236	-0.02466	51.3765	78.2923	0.00411	0.00271	198	134
85237	10/12/95	12.19	87.4641	-0.04825	51.3775	77.9494	0.00367	0.00265	193	134
85238	10/12/95	13.46	87.4043	-0.05682	51.3797	77.6038	0.00357	0.00251	189	132
85240	10/12/95	16.41	87.1825	-0.09292	51.3765	76.9025	0.00302	0.00236	175	125

Table 3. Reentry time determination results for “Cosmos-398”

N rev	Estimate maker	El-set origin	Left boundary (10.12.95)	Right boundary (10.12.95)	Expected reentry time (10.12.95)	Deviation, min	Prediction interval, hours	Relative error, %
45020	SRC	RSSS			22.35	115	40.52	4.7
45021	SRC	RSSS			22.50	130	39.05	5.5
45022	SRC	RSSS			22.45	125	37.58	5.5
45022	SRC	USSSN+RSSS			22.35	115	37.58	5.1
45031	SRC	RSSS			22.14	94	24.37	6.4
45031	SRC	USSSN+RSSS			21.33	113	24.59	7.7
45037	SRC	RSSS			20.11	-29	15.59	-3.1
45037	SRC	RSSS			20.03	-37	15.59	-4.0
45038	SRC	USSSN+RSSS			20.06	-34	14.13	-4.0
45038	SRC	RSSS			20.05	-35	14.13	-4.1
45043	SRC	USSSN+RSSS			20.13	-27	6.84	-6.6
45046	SRC	USSSN+RSSS			20.07	-33	2.47	-23.0
45046	SRC	USSSN+RSSS	Aposteriori results		20.34	-6	2.47	-3.9
44994	ESOC	USSSN	16.37	10.58(11.12)	01.46(11.12)	306	78.83	6.5
45022	ESOC	RSSS			01.01(11.12)	261	37.58	11.6
45022	ESOC	USSSN+RSSS	18.01	04.49(11.12)	22.49	129	37.58	5.7
45025	ESOC	USSSN+RSSS	18.02	03.30(11.12)	21.02	22	33.18	1.1
45038	ESOC	USSSN+RSSS	19.16	22.28	20.52	12	14.13	1.4
45043	ESOC	USSSN			20.15	-25	6.84	-6.1
45010	USSSC	USSSN			21.31	51	54.73	1.6
45025	USSSC	USSSN	21.00	22.00	21.43	63	33.18	3.2
45038	USSSC	USSSN			20.49	9	14.13	1.1
45045	USSSC	USSSN			20.30	-10	3.93	-4.2
45006	RSSC	RSSS	15.30	17.30(11.12)	23.03	123	61.13	3.4
45020	RSSC	RSSS	18.00	02.00(11.12)	23.03	123	40.52	5.1
45031	RSSC	RSSS	18.00	04.44(11.12)	22.24	104	24.37	7.1
45037	RSSC	RSSS	17.25	23.24	19.54	-46	15.59	-4.9
45038	RSSC	RSSS	18.00	21.00	20.03	-37	14.13	-4.4
45046	RSSC	RSSS	19.58	20.28	20.09	-31	2.47	-20.9
45006	RMCC	RSSS	10.00	07.00(11.12)	20.00	-40	61.13	-1.1
45022	RMCC	RSSS	16.00	09.00(11.12)	23.12	132	37.58	5.9
45038	RMCC	RSSS	17.40	23.15	20.05	-35	14.13	-4.1
45046	RMCC	RSSS			20.19	-21	2.47	-14.2

Figure 1. Solar indices

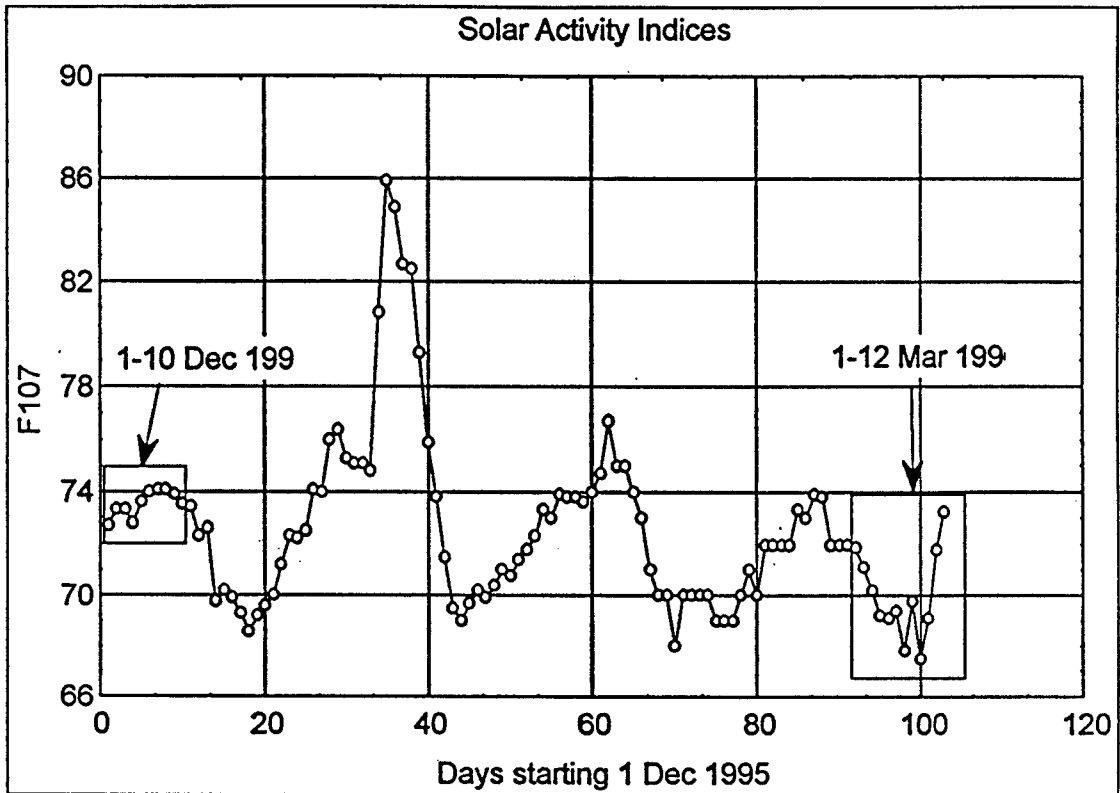


Figure 2. Geomagnetic indices

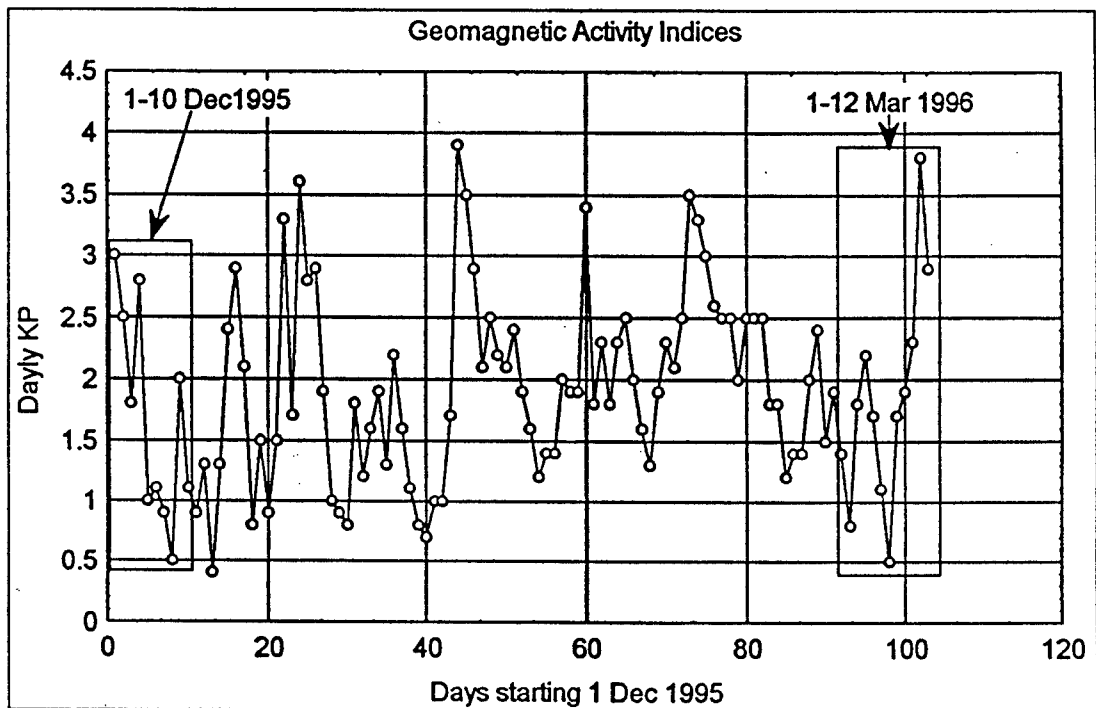


Figure 3. Correlation of "Cosmos-398" reentry time determination results

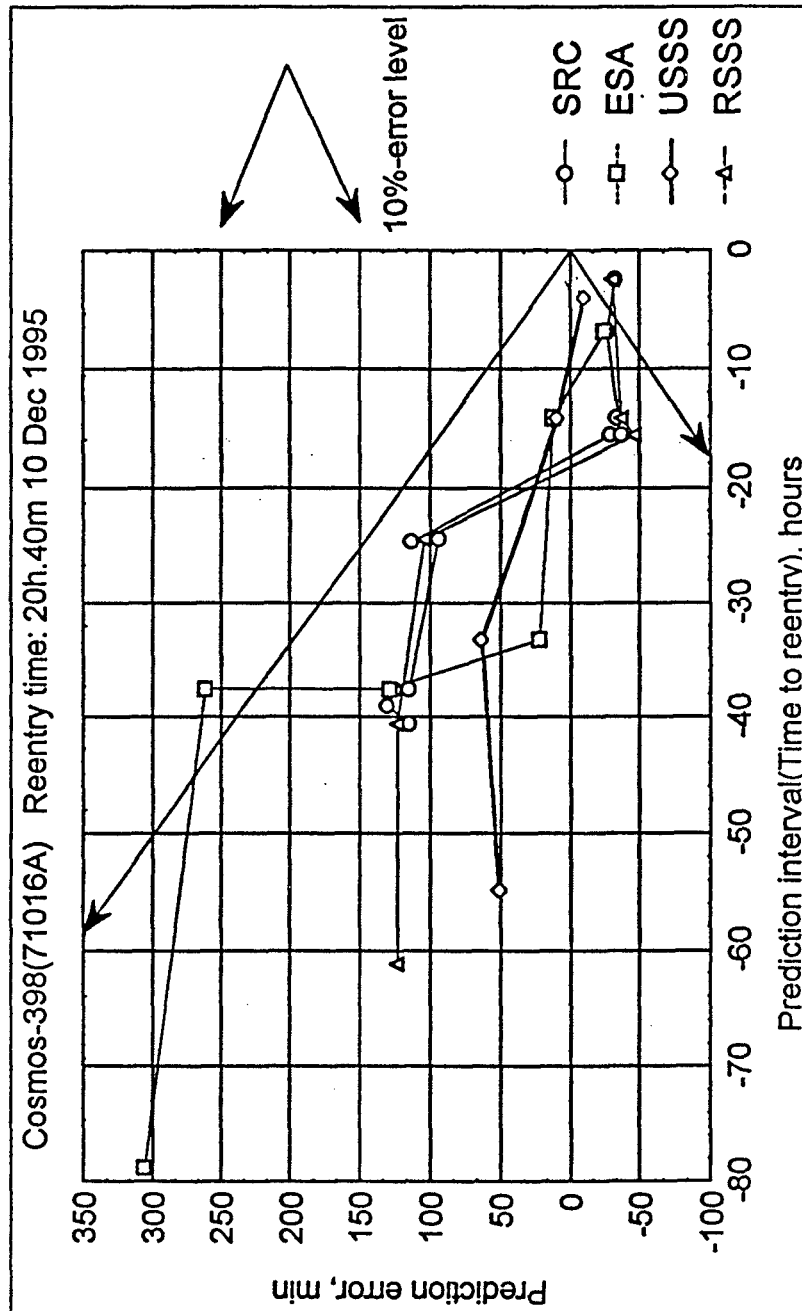


Table 4. FSW-1-5 orbit updating results due to RSSS

N rev	Date	UTC, h, min	T ₀ , min	ΔT ₀ , min	I, deg	Ω, deg	1-e cos ω	1-e sin ω	H _a , km	H _p , km
11847	10/03/96	10.07	88.59750	-0.02430	56.436	23.133	0.0027770	0.011924	308	132
11848	10/03/96	11.35	88.57551	-0.02461	56.435	22.824	0.0026790	0.011747	308	133
11849	10/03/96	13.04	88.54818	-0.02579	56.437	22.527	0.0027403	0.011664	304	132
11850	10/03/96	14.32	88.52088	-0.02686	56.437	22.225	0.0027677	0.011478	302	132
11851	10/03/96	16.01	88.49267	-0.02767	56.437	21.922	0.0027323	0.011312	299	131
11852	10/03/96	17.29	88.46395	-0.02814	56.437	21.612	0.0023488	0.011121	296	132
11853	10/03/96	18.58	88.43715	-0.02779	56.436	21.305	0.0023448	0.010967	294	131
11854	10/03/96	20.26	88.40888	-0.02852	56.434	21.002	0.0023240	0.010817	291	131
11855	10/03/96	21.54	88.37937	-0.02961	56.434	20.699	0.0022211	0.010644	288	131
11861	11/03/96	06.44	88.16205	-0.03850	56.435	18.878	0.0018963	0.009416	269	129
11863	11/03/96	09.40	88.07633	-0.04331	56.436	18.276	0.0020443	0.008861	261	128
11864	11/03/96	11.08	88.03105	-0.04575	56.437	17.969	0.0019184	0.008624	257	128
11865	11/03/96	12.36	87.98105	-0.04915	56.438	17.684	0.0019800	0.008356	253	127
11866	11/03/96	14.04	87.93034	-0.05196	56.438	17.360	0.0016505	0.008148	249	126
11867	11/03/96	15.32	87.87324	-0.05618	56.434	17.046	0.0016059	0.007833	244	125
11868	11/03/96	17.00	87.80923	-0.06205	56.433	16.742	0.0015807	0.007467	238	124
11869	11/03/96	18.28	87.74109	-0.06779	56.431	16.432	0.0016414	0.007065	232	123
11870	11/03/96	19.55	87.66784	-0.07423	56.430	16.123	0.0015434	0.006680	225	122

Table 5. FSW-1-5 orbit updating due to US SSN

N rev	Date	UTC, h, min	T ₀ , min	ΔT ₀ , min	I, deg	Ω, deg	1-e cos ω	1-e sin ω	H _a , km	H _p , km
11776	11/03/96	01.15	88.73399	-0.00190	56.4371	24.9547	0.0030663	0.012947	322	147
11779	11/03/96	05.41	88.65993	-0.02286	56.4334	24.0495	0.0030796	0.012313	314	147
11781	11/03/96	08.38	88.61554	-0.02262	56.4333	23.4433	0.0029583	0.012070	310	147
11787	11/03/96	17.29	88.46862	-0.02348	56.4352	21.6210	0.0027723	0.011278	297	145
11794	11/03/96	04.00	88.22093	-0.03590	56.4166	19.4725	0.0008897	0.009850	267	137
11801	11/03/96	14.04	87.91237	-0.05028	56.4297	17.3563	0.0016077	0.008135	248	140
11805	11/03/96	19.55	87.64798	-0.06628	56.4295	16.1196	0.001536	0.006642	225	136
11806	11/03/96	21.23	87.56886	-0.07757	56.4294	15.8096	0.001387	0.006294	219	135
11807	11/03/96	22.50	87.49947	-0.06988	56.4292	15.5002	0.0013898	0.005987	213	133
11808	12/03/96	00.18	87.34586	-0.09919	56.4293	15.1952	0.0015067	0.005435	202	129
11809	12/03/96	01.45	87.21859	-0.10748	56.4311	14.8970	0.0013367	0.005159	194	125
11810	12/03/96	03.12	86.95487	-0.16280	56.4332	14.5233	0.0007053	0.004177	174	119

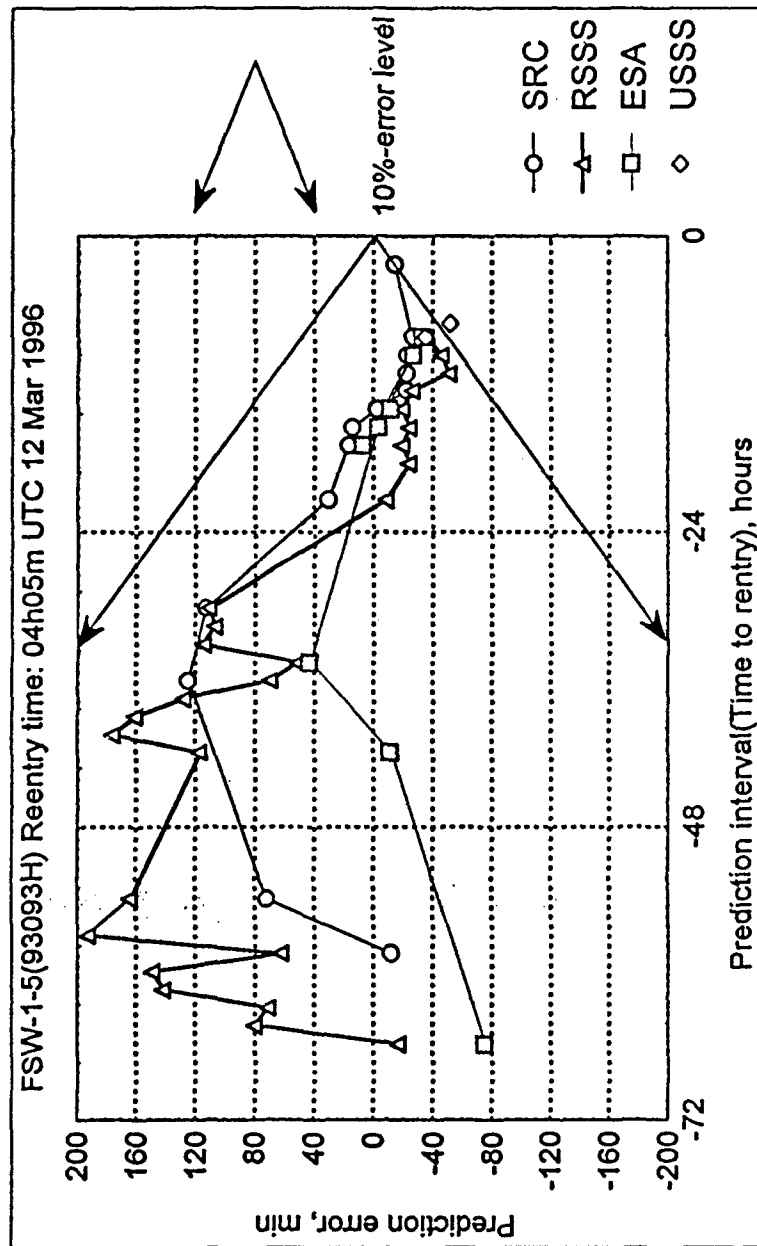
Table 6. Reentry time determination results for FSW-1-5

N rev	Estimate maker	El-set origin	Left boundary (12.03.96)	Right boundary (12.03.96)	Expected reentry time (12.03.96)	Deviation, min	Prediction interval, hours	Relative error, %
11831	ESA	RSSS			02.50	-75	65.64	-1.9
11847	ESA	Unknown			03.54	-11	41.96	-0.4
11852	ESA	Unknown			04.48	43	34.59	2.1
11865	ESA	Unknown			04.02	-3	15.47	-0.3
11864	ESA	RSSS	23.54	08.30	04.12	7	16.94	0.7
11866	ESA	RSSS	00.54	06.54	03.54	-11	14.01	-1.3
11869	ESA	RSSS	01.33	05.33	03.39	-26	9.62	-4.5
11870	ESA	RSSS	01.54	05.08	03.32	-33	8.16	-6.7
11831	RSSS	RSSS			03.48	-17	65.64	-0.4
11832	RSSS	RSSS			05.25	80	64.15	2.1
11833	RSSS	RSSS			05.16	71	62.67	1.9
11834	RSSS	RSSS			06.27	142	61.19	3.9
11835	RSSS	RSSS			06.34	149	59.71	4.2
11836	RSSS	RSSS			05.07	62	58.23	1.8
11837	RSSS	RSSS			07.18	193	56.75	5.7
11838	RSSS	RSSS			07.35	210	55.27	6.3
11839	RSSS	RSSS			06.49	164	53.79	5.1
11847	RSSS	RSSS	19.10(11.03)	16.54	06.02	117	41.96	4.6
11848	RSSS	RSSS			07.01	176	40.49	7.2
11849	RSSS	RSSS			06.46	161	39.01	6.9
11850	RSSS	RSSS			06.13	128	37.54	5.7
11851	RSSS	RSSS	20.03(11.03)	14.25	05.14	69	36.06	3.2
11852	RSSS	RSSS			04.56	51	34.59	2.5
11853	RSSS	RSSS			06.00	115	33.11	5.8
11854	RSSS	RSSS			05.52	107	31.64	5.6
11855	RSSS	RSSS			05.56	111	30.17	6.1
11861	RSSS	RSSS	00.28	09.18	03.56	-9	21.34	-0.7

Reentry time determination results for FSW-1-5 (continued Table 6.)

N rev	Estimate maker	El-set origin	Left boundary (12.03.96)	Right boundary (12.03.96)	Expected reentry time (12.03.96)	Deviation, min	Prediction interval, hours	Relative error, %
11863	RSSS	RSSS	00.40	08.05	03.41	-24	18.41	-2.2
11864	RSSS	RSSS	00.51	07.55	03.46	-19	16.94	-1.9
11865	RSSS	RSSS	00.57	07.21	03.41	-24	15.47	-2.6
11866	RSSS	RSSS	01.24	06.57	03.46	-19	14.01	-2.3
11867	RSSS	RSSS	01.39	06.30	03.39	-26	12.54	-3.5
11868	RSSS	RSSS	01.42	05.28	03.14	-51	11.08	-7.7
11869	RSSS	RSSS	01.59	05.12	03.20	-45	9.62	-7.8
11870	RSSS	RSSS	02.14	05.02	03.29	-36	8.16	-7.4
11836	SRC	RSSS			03.53	-12	58.23	-0.3
11839	SRC	RSSS			05.17	72	53.79	2.2
11851	SRC	RSSS			06.10	125	36.06	5.8
11855	SRC	RSSS			05.58	113	30.17	6.2
11861	SRC	RSSS			04.35	30	21.34	2.3
11864	SRC	RSSS			04.22	17	16.94	1.7
11865	SRC	RSSS			04.19	14	15.47	1.5
11866	SRC	RSSS			04.03	-2	14.01	-0.2
11867	SRC	RSSS			03.43	-22	12.54	-2.9
11868	SRC	RSSS			03.43	-22	11.08	-3.3
11869	SRC	RSSS			03.43	-22	9.62	-3.8
11870	SRC	RSSS+USSSN			03.39	-26	8.16	-5.3
11874	SRC	RSSS+USSSN	Aposteriori results		03.51	-14	2.33	-10.0
11870	USSC	USSSN			03.32	-35	8.16	-7.1
11871	USSC	USSSN			03.13	-52	7.0	-12.3

Figure 4. Correlation of FSW-1-5 reentry time determination results



GEOSTATIONARY ORBIT DETERMINATION AND PREDICTION

V. Yurasov, A. Moscovsky

SRC "Kosmos", Moscow

1. INTRODUCTION

Presently, fast growth of GEO population is observed. The geostationary orbits are widely used for meteorological surveillance, communication, telebroadcasting, monitoring and control of ground-based and space activities. The rate of space object population growth on these orbits are much higher, than on low orbits: annually the population on geostationary orbits grows on the average by 30-35 objects, that equals about 7 % of their total number (Figure 1). From new launched SO about 60 % are active. This tendency is explained by that many of functions having been realized earlier on low orbits are transferred now to GEO.

Now there are more than 600 large SO on geostationary orbits, from them more than 200 being active. The inclination and longitude distributions of geostationary SO are given in Figure 2. It is known, that the passive geostationary orbit planes gradually deviate from the equatorial plane up to 15 degrees. In Figure 2 early launched SO population is looked very well. It is objects with none-zero inclinations. At the same time the significant part of catalogued GEO has inclinations close to zero. It is active and recently launched space objects. All these objects are in the one orbit plane. It can be seen, that some longitude ranges are closely populated: mutual angular distance between some satellites in these ranges is equal less than one of tenth degree already. It is known, that the lifetime of geostationary SO is not limited. Therefore it is necessary to expect in future even more dense SO distribution in this area of space. It complicates and will complicate the solution of geostationary orbit determination and prediction problems.

The Russian SSS in comparison with US SSN has more limited opportunities for surveillance of GEO. The geostationary space objects monitoring in Russia are carried out by the optical and optical-electronic sensors. They are located on the territory of the former USSR. The locations of these sensors are given in Figure 3. In Russia it is Zvenigorod, Zelenchuk, Kourovka and Irkutsk, on Ukraine - Ughgorod and Simeiz, in Kazakhstan - Alma-Ata, in Georgia - Abastumani, in Tadjikistan - Dushanbe,

Fig. 1. Number of annual GEO launches

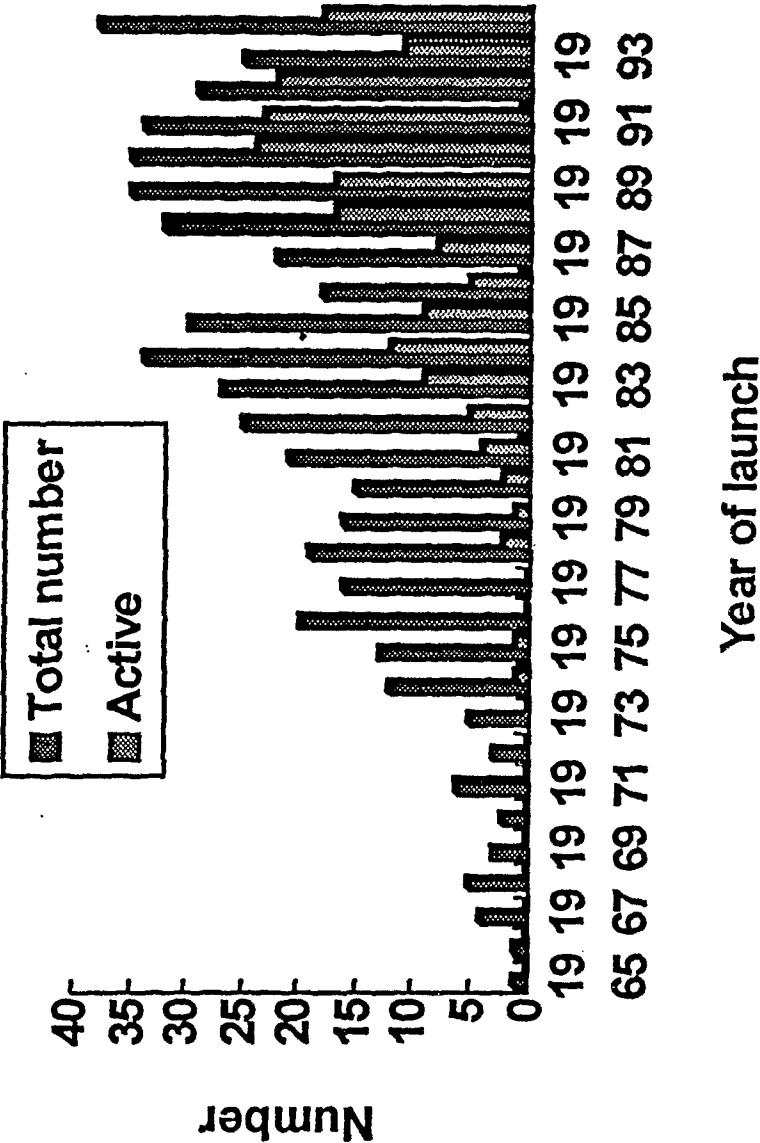


Figure 2. Inclination and longitude distribution of GEO

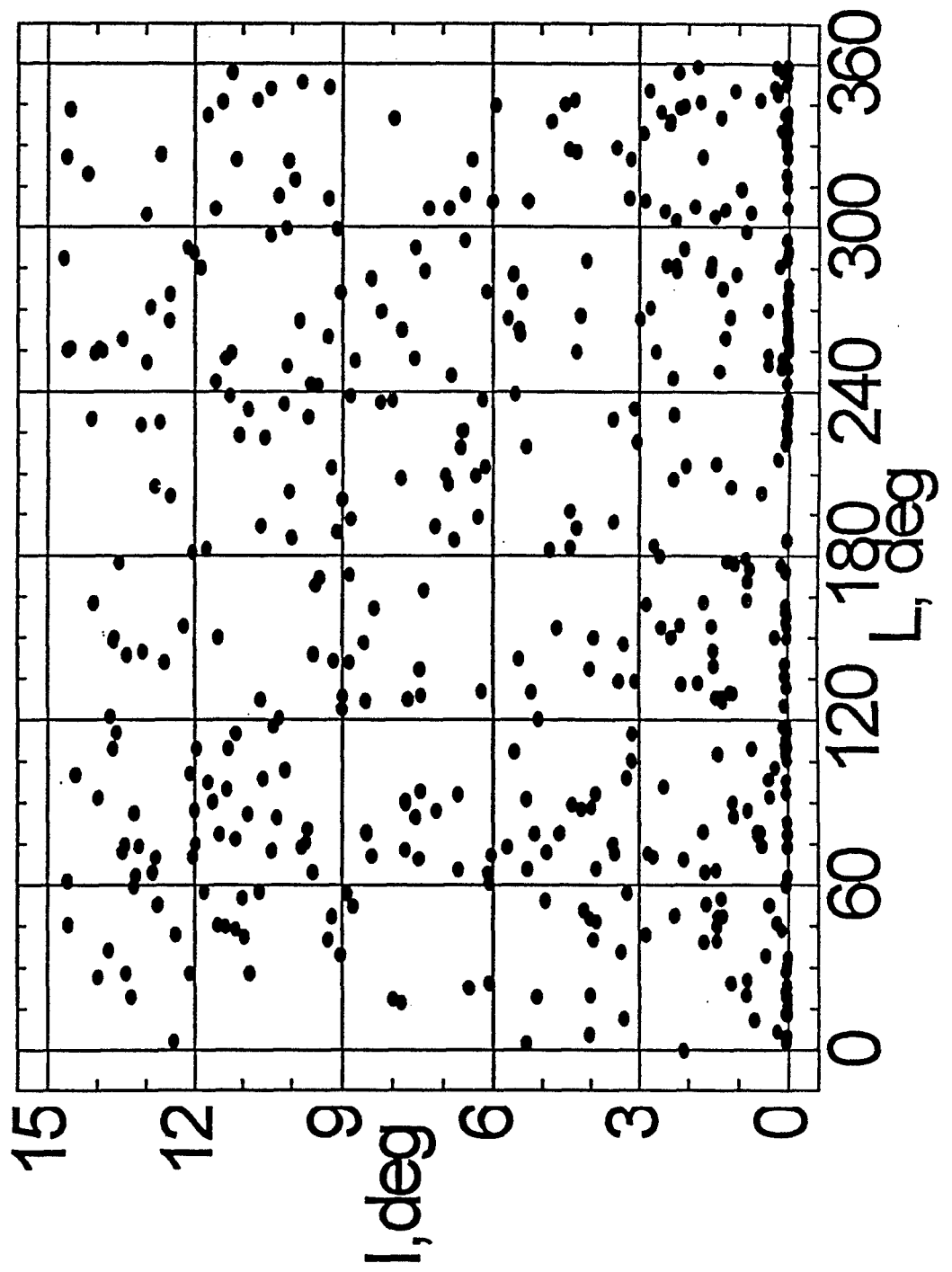
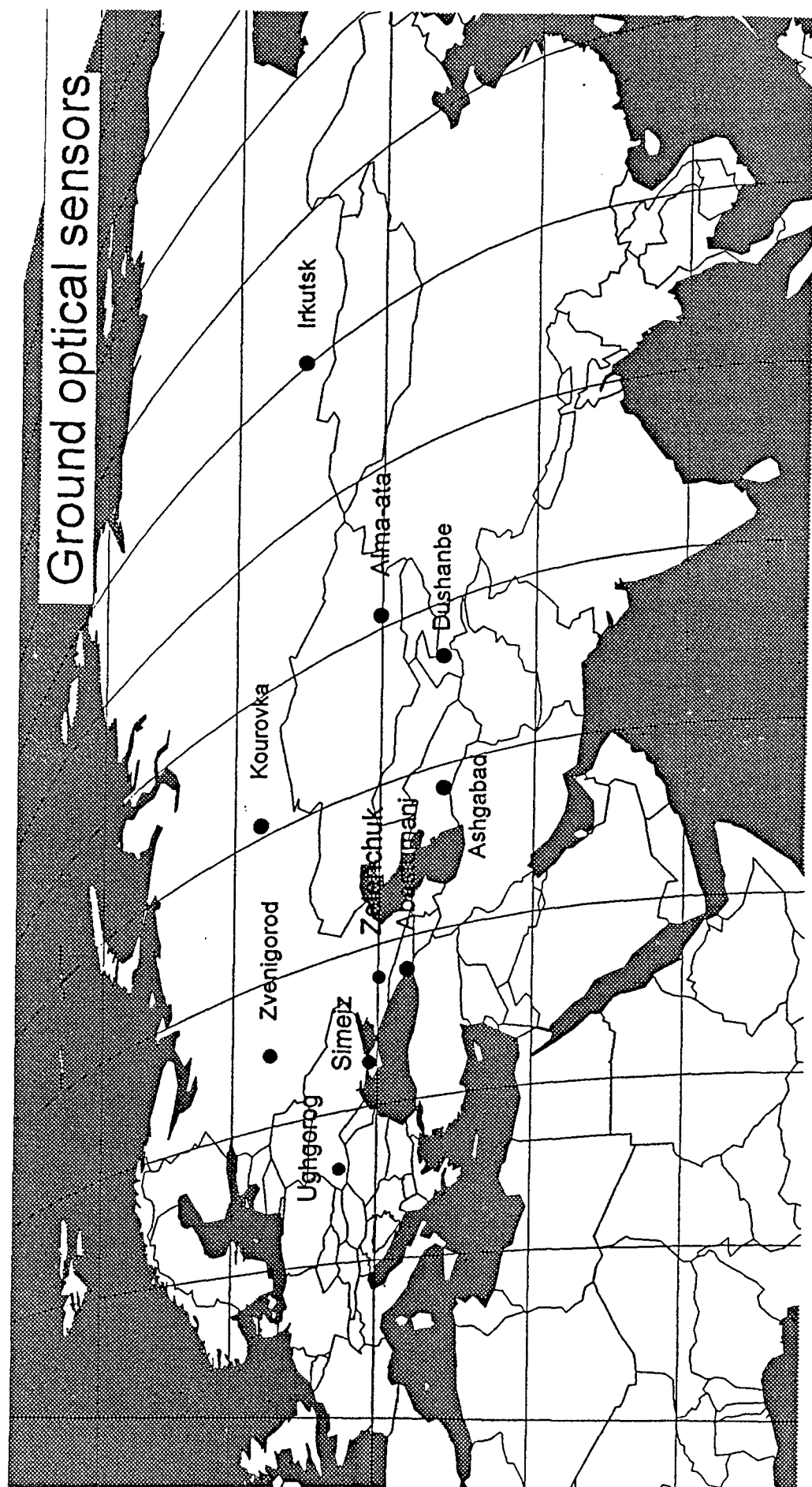


Figure 3. RSS optical sensors



in Turkmenia - Ashgabad. The accuracy of optical measurements of ground optical network sensors is sufficient high. The errors of individual measurements for the majority of sensors are equal to several angular seconds.

The characteristic property of RSSS is that in observation of the geostationary satellites large breaks are possible.

First, it is caused by the ground optical network sensors opportunities limitation. Figure 4 shows the controllable by each of sensor geographical longitude ranges. The ground optical network sensors can observe the geostationary satellites, being in a range of geographical longitudes from 30 degrees of western longitude up to 160 degrees of east longitude. Figure 5 shows the longitude drift distribution of 485 catalogued geostationary space objects. About 20 % of the geostationary satellites have drift more than 1 degree per day. These satellites during long time (a few months) can be in uncontrollable by Russian ground optical network longitudes area.

Secondly, the breaks in observation of geostationary space objects are may be caused by a unregularity of work of ground optical network sensors because of financial and political problems, connected with the USSR disintegration.

Urgent in this connection a problem of the passive geostationary satellites orbit determination on precision optical measurements distributed on large temporary intervals and long-time prediction of their motion is represented. In the given report some results of SRC "Kosmos" researches in in this direction are considered.

We shall consider in brief some questions connected to the decision of this problem. They are following:

- choice of optimum spatial coordinate system for GEO orbit determination and prediction and orbit estimation vector choice;
- the statistical method for the orbit determination choice;
- the account of non-uniformity of rotation of the Earth (correction between Universal Time UT1 and Universal Coordinated Time UTC);
- the geostationary satellite motion model choice.

Figure 4. Observation longitude range

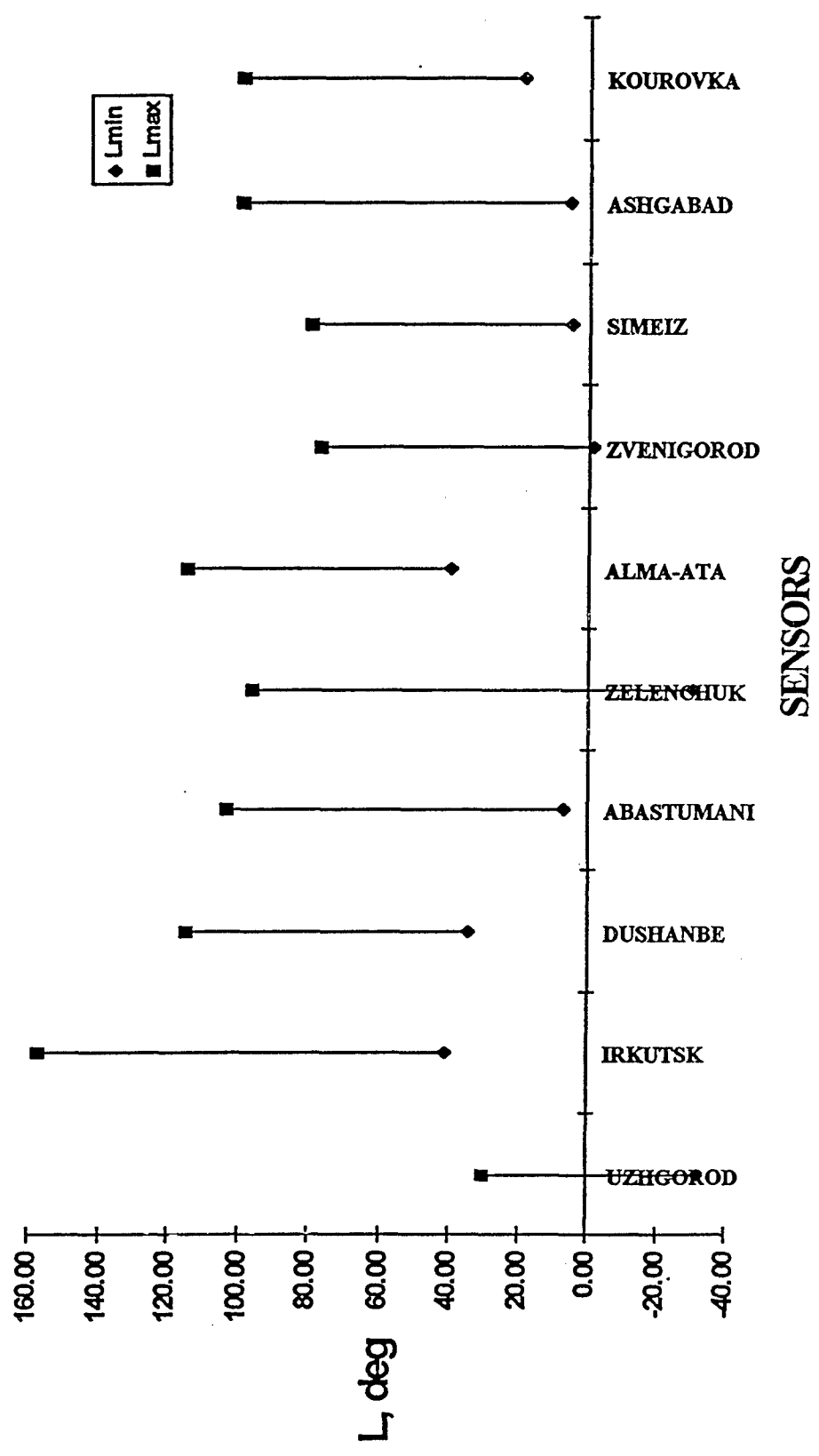
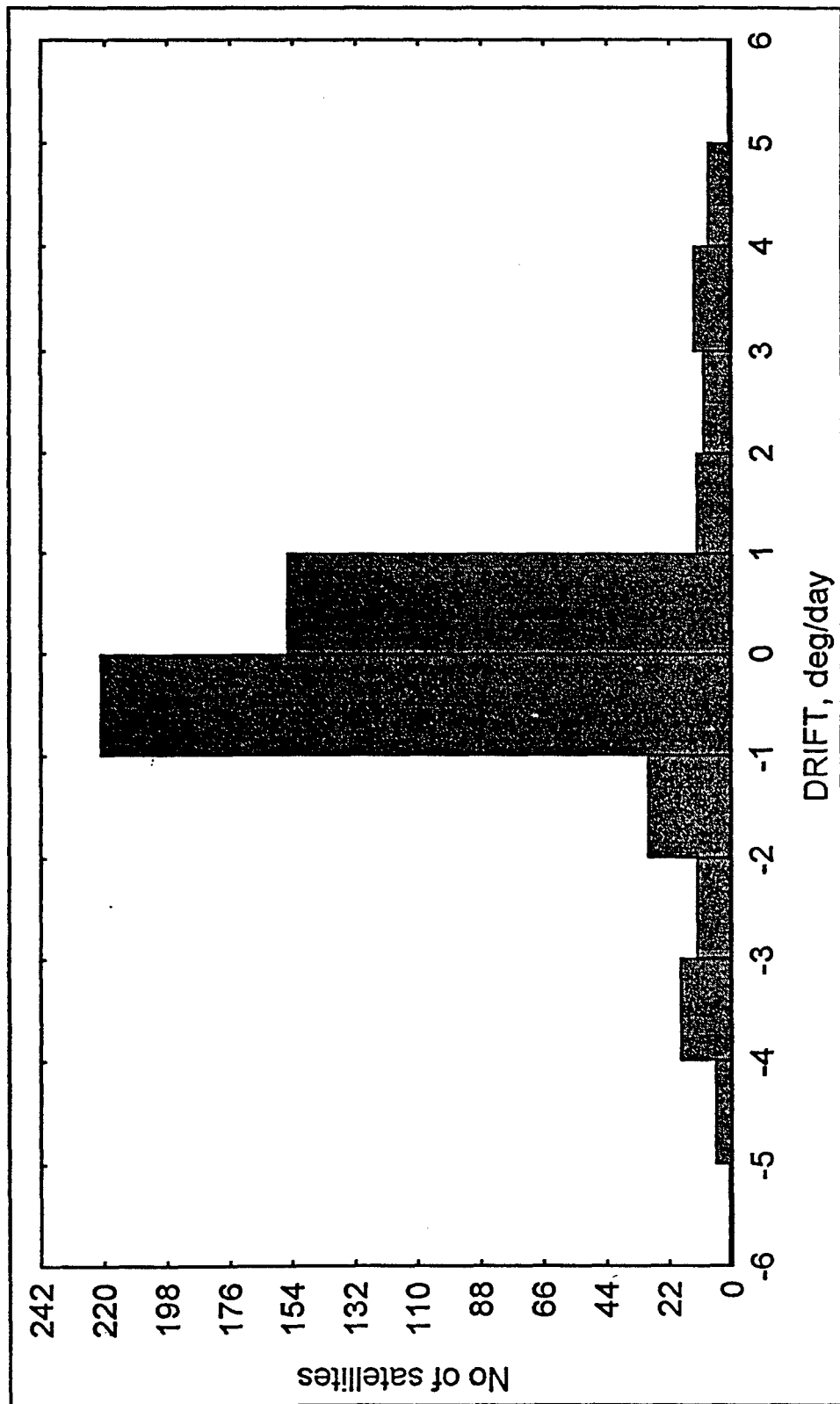


Figure 5. Drift distribution of GEO



2. COORDINATE SYSTEM AND TIME

For coordinate information processing in the RSSS, as a rule, is used coordinate system $Oxyz$, in which the axis Ox is directed to the mean equinox of current epoch t , the axis Oz is directed to the pole, and the axis Oy supplements system up to right. However, this system is not suitable for construction of the long-time precision analytical and semi - analytical satellite prediction theories because of terms caused by a precession and a nutation by its use. More preferable in this relation is the quasi-inertial system $Ox_0y_0z_0$, offered originally by Veis [1,2] and recommended according to RD-50-25645.325-89 [3] as basic for the satellite ballistic maintenance. This system is connected to the equinox of epoch T_0 and equator on the observation time moment. In this system the axis Ox_0 lays in the true equator plane of the current epoch t . It is directed to the point $\hat{\gamma}$, which is deviated to the east from the true equinox γ_{ucm} on a angle, equal to the sum of a precession in right ascension for the time interval between the epoch T_0 and the epoch t and a nutation in right ascension in the epoch t . The axis Oz_0 is directed on the instant Earth rotation axis of the to epoch t in the direction of Northern pole. The axis Oy_0 supplements system up to right.

It is necessary to note two moment concerning the above coordinate system:

- 1) noninertial of this system results to insignificant short-periodical perturbations in the SO motion theory;
- 2) the sidereal time, which connects this system with Greenwich system, is linear function of Universal Time UT1.

Taking into account these arguments, quasi-inertial system of coordinates $Ox_0y_0z_0$ was chosen as the basic coordinate system for geostationary space objects orbit determination and prediction on large temporary intervals.

By time unit accepted for registration of all time-dependent events and also independent variable at orbit determination in the RSSS is UTC (Universal Coordinated Time). In optical observations the direction "observer - satellite on a background of stars" is in essence fixed. For calculation of this direction it is necessary to know Universal Time UT1 connected with the Earth rotation.

The corrections $DUT1=UT1-UTC$ are transferred now by radio signals and are published in the bulletins by International Earth Rotation Service (IERS). However, at orbit determination of LEO these corrections are not

taken into account. At processing optical measurements on the geostationary satellites allocated on a large measure interval it is inadmissible. This can result in deterioration of orbit determination results because of arising errors which can be comparable or to surpass in some times measurement errors. Especially it can be displayed in a case, when on the measure interval there is the jump of Universal Coordinated Time UTC.

3. ORBIT ELEMENTS ESTIMATION AND MOTION MODEL CHOICE

For an orbit parameters estimation the least squares method with a consecutive rejection of abnormal measurements was chosen. If the measure interval is small gravitational perturbations influences are taken into account only and six elements of orbits are estimated. As estimation parameters the following system of nonsingular at small inclinations and eccentricities elements was chosen :

$$X = (a, \xi, \eta, P, Q, \lambda),$$

where a is axis,

$$\xi = e \cos \pi, \eta = e \sin \pi,$$

$$P = \sin \frac{i}{2} \cos \Omega, Q = \sin \frac{i}{2} \sin \Omega, \quad (1)$$

$$\lambda = \omega + \Omega + M,$$

$$\pi = \omega + \Omega,$$

i - inclination,

ω - argument of perigee,

Ω - longitude of ascending node,

M - mean anomaly.

For matrixes (transitive matrixes) $\partial X(t) / \partial X(t_0)$ calculation analytical formulas were used. At large intervals perturbations due to solar pressure are taken into account and the ratio of the satellite surface area (S) to its mass (m) is included to the estimation parameters. The transitive matrixes terms due to solar pressure are calculated numerically.

It is known, that the coordinate information processing quality depends on the characteristics of used SO motion model. In ideal variant the SO motion model used at the measurement processing should not bring an additional errors into orbit determination. In this connection the desire to maximize the measurement processing interval conflicts with the above

requirement.

For geostationary SO motion prediction the universal semi-analytical method [4] was used. The perturbations due to geopotential, including resonance perturbations, attraction of the Moon, Sun and solar pressure are taken into account. The methodical errors of the used semi-analytical method were estimated by the comparison with the results of numerical integration of the satellite motion equations. The maximum differences on fifty days prediction interval between results of the numerical and semi-analytical solution on radial and binormal directions are estimated as 40 m, along the track - 600 m. The analysis has shown that the deviations along the track have secular character and are connected with the transition from osculating to averaged elements in the semi-analytical method. At processing real measurements this coordination comes as a rule automatically.

4. ORBIT DETERMINATION AND PREDICTION RESULTS

We shall consider results of 69 real geostationary space objects orbit determination, based on processing of the optical information distributed on a large temporary interval.

In Table 1 the characteristics of the chosen satellites are presented. For each satellite in the first column is its number in the catalogue (number, smaller 30000, coincide with numbering in the US SSN catalogue), in second - international number, in third - name, in fourth - measure interval for the orbit determination, in fifth - RMS of residuals, appropriate to results of orbit determination on measurements, in sixth - number of measurements, in seventh - period, in eighth - inclination of an orbit.

Distribution histograms of periods, inclinations, intervals of orbit determination, number of measurements and RMS of residuals corresponding to the data of Table 1 are given in Figures 6-10. It is visible, that the selected realizations cover practically whole area of geostationary orbits. The measure intervals at orbit determination for the chosen satellites were in a range from 1 till 9 months. The minimum number of measurements was equalled 7, maximum - 54. The RMS of O-C residuals for the majority of orbits do not exceed 12 angular seconds.

For eight of given in Table 1 satellites, international numbers of which are labelled by asterisks, ephemeris on moment of new observation of these satellites were calculated. The maximum of ephemeris calculation interval reached two months. The residuals between observed and calculated values

TABLE 1. GEOSTATIONARY SATELLITE CHARACTERISTICS

Catalog number	COSPAR	Name	OD interval, days	RMS, “	Number of measurem ents	Period, min	Inclination, deg
7392	74 060001*	MOLNIYA 1-S	72.08	3.6	20	1437.02	14.366
8357	75 097001*	COSMOS 775	84.14	7.6	39	1437.17	14.078
10365	77 092001*	EKRAN 2	84.88	3.8	23	1435.20	13.418
10489	77 108001*	METEOSAT 1	58.02	3.0	37	1435.60	12.531
10778	78 035001*	INTELSAT 4A-F6	40.70	5.2	19	1437.72	8.154
11343	79 035001	RADUGA 5	262.03	5.0	20	1436.32	13.082
11440	79 062001*	GORIZONT 2	151.08	8.0	12	1436.25	11.776
12120	80 104001	EKRAN 6	145.99	6.2	14	1436.15	11.595
12618	81 069001	RADUGA 9	62.11	5.2	10	1437.19	11.166
13177	82 044001	COSMOS 1366	50.20	9.0	10	1436.19	11.045
13554	82 093001*	EKRAN 9	83.96	9.2	12	1436.54	10.254
13974	83 028001	RADUGA 12	144.19	11.8	18	1435.79	9.580
14114	82 044006*	SL-12 R/B(2)	61.01	2.0	37	1435.98	10.293
14158	83 065001	GALAXY 1	59.19	4.6	25	1438.33	0.738
14728	84 012003	JD 1	38.13	8.0	30	1435.69	8.601
14783	84 022001	COSMOS 1540	155.89	9.6	29	1435.83	9.332
15057	84 063001	RADUGA 15	173.13	3.0	15	1436.89	8.170

Catalog number	COSPAR	Name	OD interval, days	RMS, “	Number of measurements	Period, min	Inclination, deg
1518184 078006		SL-12 R/B(2)	123.07	3.6	26	1437.26	7.895
1548485 007001		GORIZONT 11	145.96	8.2	14	1436.33	7.373
1582485 048002		MORELOS 1	259.99	2.0	54	1447.63	1.688
1619985 102001		COSMOS 1700	264.02	8.0	27	1436.03	7.376
1625085 107001		RADUGA 17	58.84	3.2	21	1438.12	6.933
1652686 010001		CHINA 18 (STTW-1)	147.01	7.8	22	1436.22	5.621
1676986 044001		GORIZONT 12	173.99	4.2	17	1436.59	6.274
1712586 090004		SL-12 R/B(2)	34.10	3.2	13	1434.82	5.857
1857587 096001		COSMOS 1897	67.23	4.2	11	1435.26	5.608
1939788 071001		GORIZONT 16	41.24	3.8	14	1440.27	4.538
1940088 071004		SL-12 R/B(2)	55.96	2.0	9	1431.88	4.477
1977689 004006		SL-12 R/B(2)	80.95	1.6	7	1469.32	4.323
2008689 048004		SL-12 R/B(2)	81.06	4.0	9	1470.91	3.960
2026689 081004		SL-12 R/B(2)	67.87	1.8	9	1431.00	3.356
2036789 098001		RADUGA 24	89.18	3.4	15	1436.77	3.244
2069690 061004		SL-12 R/B(2)	179.15	7.2	11	1436.59	3.164
2101690 112001		RADUGA 26	56.12	2.2	8	1436.15	2.385
2101990 112004		SL-12 R/B(2)	56.09	0.6	5	1439.66	2.363
2104190 116004		SL-12 R/B(2)	41.08	2.4	8	1470.10	2.418

Catalog number	COSPAR	Name	OD interval, days	RMS, “	Number of measurements	Period, min	Inclination, deg
2104690 102004		SL-12 R/B(2)	83.20	4.2	15	1471.27	2.665
2111191 010001		COSMOS 2133	60.98	8.0	11	1436.15	1.703
2112991 010006		SL-12 R/B(2)	171.40	5.0	24	1437.92	1.126
2113591 014004		SL-12 R/B(2)	158.10	6.8	43	1392.07	2.267
2176291 074004		SL-12 R/B(2)	138.98	10.0	26	1444.24	0.973
2179291 079004		SL-12 R/B(2)	181.08	2.2	35	1460.05	2.101
2192592 017004		SL-12 R/B(2)	123.15	3.8	10	1424.29	1.237
2204492 043004		SL-12 R/B(2)	83.23	4.8	18	1471.80	1.140
2283993 062004		SL-12 R/B(2)	179.92	2.4	17	1434.43	0.434
2288393 069004		SL-12 R/B(2)	134.90	4.0	20	1432.77	0.459
2291093 072004		SL-12 R/B(2)	177.00	9.6	8	1395.70	0.287
2296694 002004		SL-12 R/B(2)	139.15	9.6	15	1447.60	1.110
2316894 038001		COSMOS 2282	86.05	19.4	12	1436.39	1.162
2317194 038004		SL-12 R/B(2)	141.28	8.6	12	1448.10	1.473
2332294 067004		SL-12 R/B(2)	99.93	2.4	18	1436.08	0.871
2333094 069004		SL-12 R/B(2)	100.45	4.6	12	1437.91	0.995
2342994 082004		LUCH R/B(2)	89.12	15.8	34	1428.38	1.841
2372095 063004			70.06	6.2	16	1437.27	0.109
50002			30.04	2.4	10	1436.00	3.305

Catalog number	COSPAR	Name	OD interval, days	RMS, “	Number of measurements	Period, min	Inclination, deg
50013			119.03	9.0	14	1435.65	6.976
50192			120.98	4.4	8	1446.00	2.851
50327			208.23	9.4	18	1444.06	1.765
51226			89.36	2.6	12	1441.28	2.231
51258			87.09	3.2	14	1436.73	2.722
51259			156.16	8.8	15	1436.99	2.718
51565			154.38	6.6	40	1437.29	1.125
51571			32.15	4.6	18	1435.88	8.953
51787			86.26	24.4	25	1435.64	14.788
51790			57.20	4.0	12	1439.30	3.452
51794			49.19	1.8	9	1439.21	0.594
51838			60.96	2.6	20	1435.12	0.173
52110			63.97	3.6	12	1436.09	1.965

Figure 6. Distribution of periods

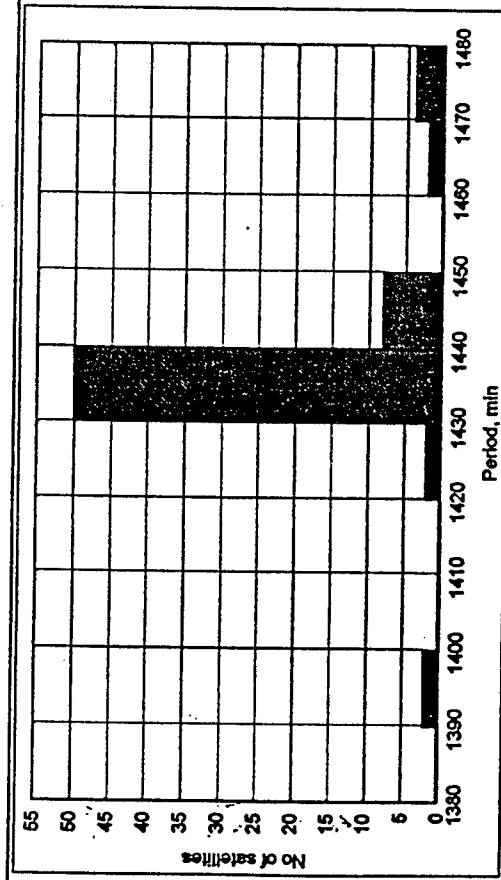


Figure 7. Distribution of inclinations

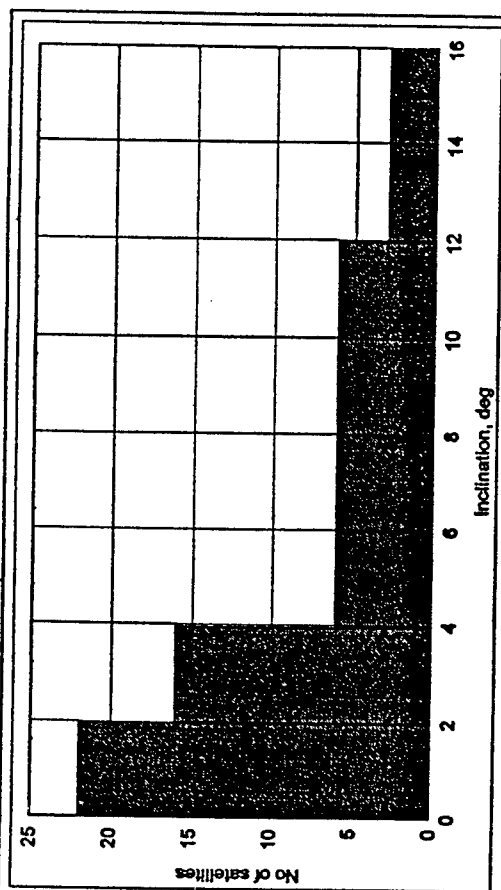


Figure 8. Distribution of OD intervals

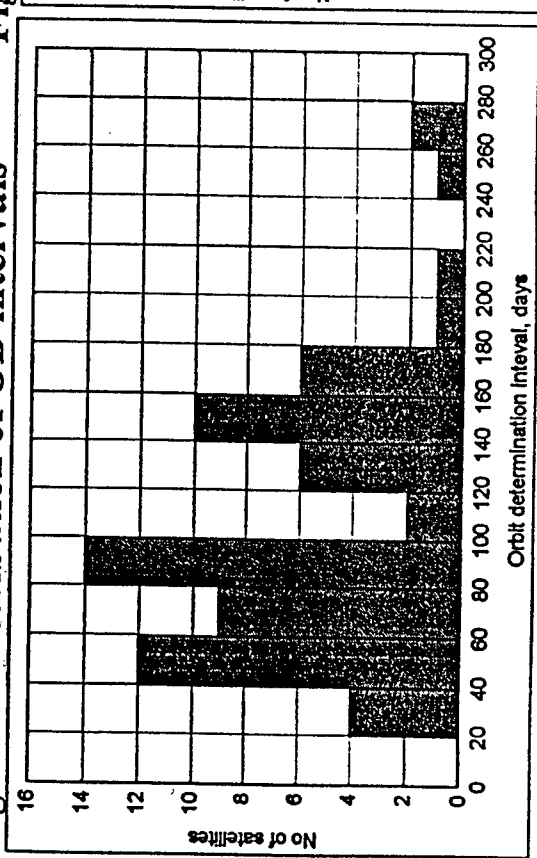


Figure 9. Distribution number of measurements

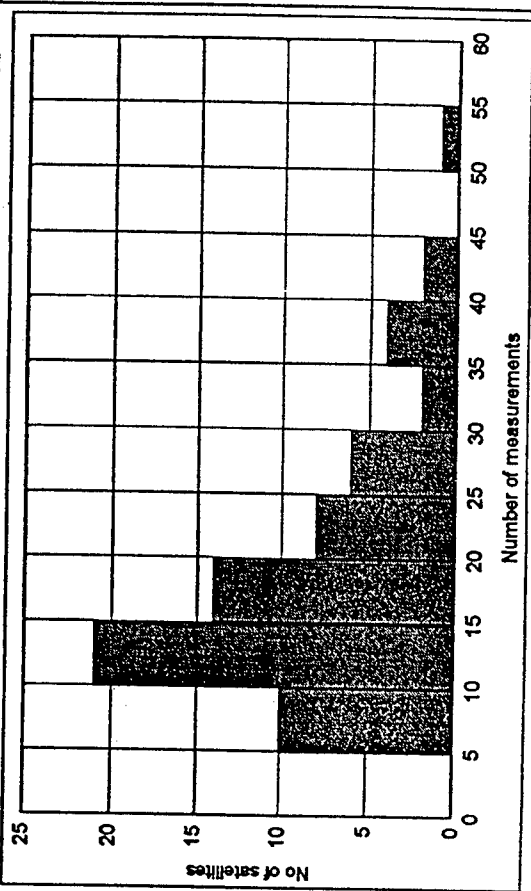


Figure 10. Distribution of RMS

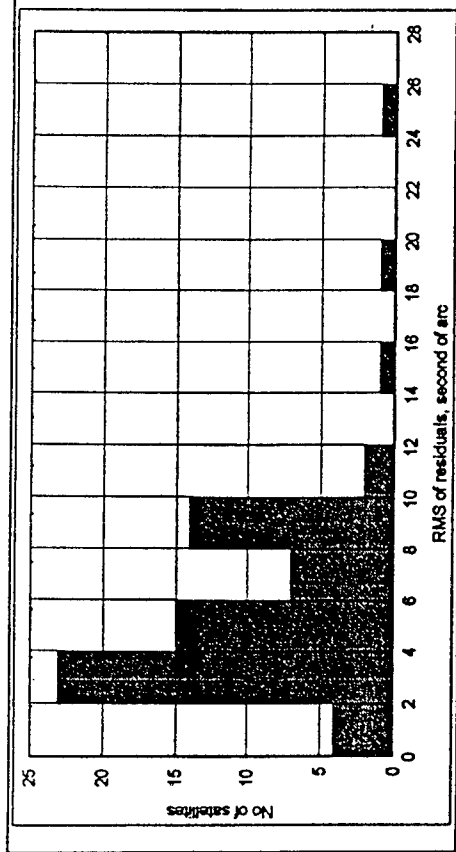


Figure 11. O - C on α and δ

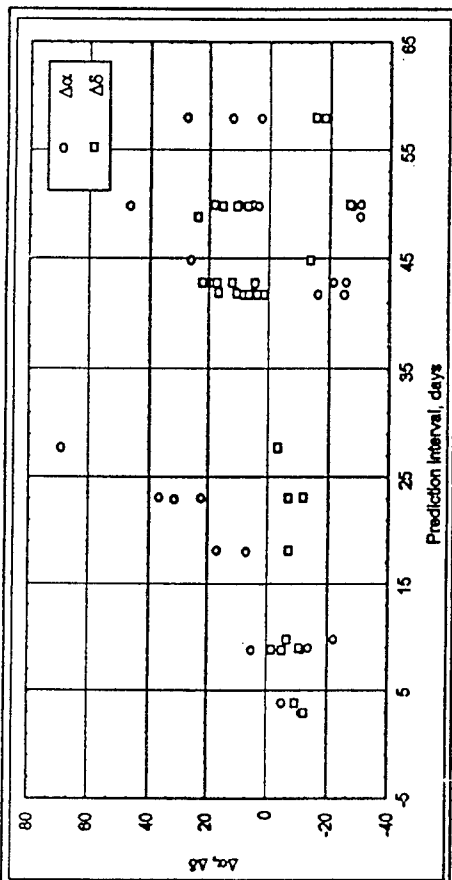


Figure 12. Deviations along the track

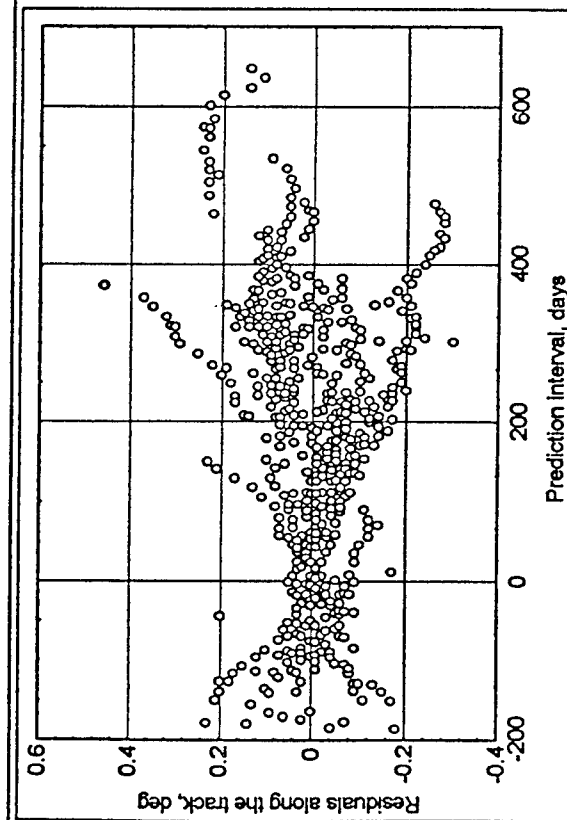
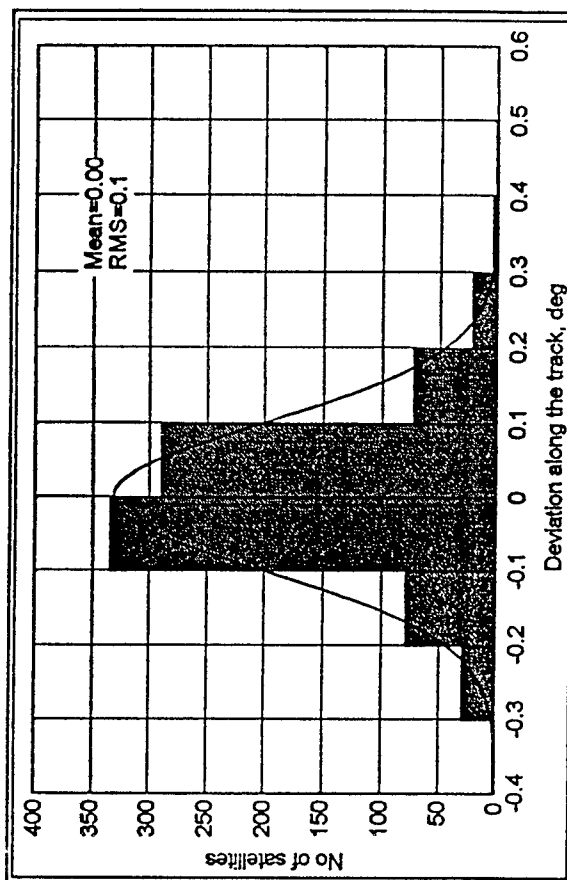


Figure 13. Distribution deviations along the track



of right ascension and declination are presented on Figure 11. The ephemeris errors on an interval till 60 days have not exceeded 30 arc second for the majority orbits. These accuracies are coordinated with the calculation ephemeris errors and they are sufficient for search, detection and identification of the geostationary satellites by optical sensors.

Orbits of 55 satellites from Table 1 were predicted to the moments of their updating by US SSN. Total prediction number was 829, that was 15 predictions for each of the satellites on the average. The prediction intervals laid in the range from 0 till 650 days. Figure 12 shows differences between predicted and updated satellites position along the track. In this Figure the negative values of the prediction interval correspond to the orbit determination on optical measurements interval. Figure 13 shows the distribution of these deviations. It is close to the normal with mean equal zero and RMS equal 0.1 degrees. From these data it can be seen that:

- the errors behaviour on a measure interval not differs from one on the prediction interval;
- the maximum errors on 650 daily prediction intervals do not exceed practically 0.3 degrees, the RMS of errors equal 0.1 degree;
- with increase of the prediction interval the common tendency of errors growth is observed though for the separate satellites an error can decrease.

The average level of errors is greater than expected one. Therefore the more detailed analysis of received results is required. In particular, one of the reasons of this may be that at calculation of osculating elements on TLE long-period perturbations due to resonance harmonics and also attraction of the Moon and Sun were not taken into account.

Nevertheless these results opens new opportunities in passive geostationary SO maintenance in conditions of the measurement deficit and large breaks in their observation.

Now in SRC "Kosmos" is formed archival database of the passive geostationary satellites observation. This database represents large interest as for the solution of geostationary satellites surveillance problem as for realization of fundamental researches.

5. REFERENCES

1. Veis G. Geodetic uses of artificial satellites, Smithsonian Contr. Astrophys., 3, 95-161, 1960.
2. Veis G. Precise aspects of terrestrial and celestial reference frames,

Smithsonian Astrophys. Obs. Special Rep.,123,1963.

3. Nazarenko A.I., Yurasov V.S, and other. The methodical instructions. Earth artificial satellites. The basic coordinate systems for ballistic maintenance of flights and technique of account of sidereal time. RD-50-25645.325-89. Publishing house of the standards, Moscow, 1990.

4. Yurasov V.S., Application of a semi-analytical method for satellite motion prediction in atmosphere. Supervision of artificial celestial bodies, USSR Academy of Sciences Astro council, N82, 1987.

IAU Colloquium 165
DYNAMICS AND ASTROMETRY OF
NATURAL AND ARTIFICIAL CELESTIAL BODIES
Poznan, Poland - July 1-5, 1996

ON ORBITAL EVOLUTION OF GEOSTATIONARY SATELLITES

R.I.Kiladze (Abastumani Astrophysical Observatory, Abastumani, Georgia)
A.S.Sochilina (Institute of Theoretical Astronomy, St.Petersburg, Russia)

INTRODUCTION

For the solution of many practical problems, connected with the ephemeris providing of observations of geostationary satellites (GS), it is necessary to have a rather simple and precise motion theory of these objects.

Because of remoteness of GS from both the centers of the Earth and the Moon, the short-period perturbations cause weak changes of orbital elements which do not exceed $1'$. Therefore it is preferable to construct the long-period motion theory, which should be also used as an intermediate orbit.

In our paper the resonant perturbations have been taken into account with the method, elaborated by Gedeon [1]. The introduction of the Laplacian plane [2] as fundamental one allowed to linearize Lagrange's equations with the luni-solar attraction function, because of a small change of the inclination i , and the linear changes of the longitude of node Ω and argument perigee ω . Here and further the orbital elements are referred to the Laplacian plane.

The developed theory and software were applied to the investigation of orbital evolution of GS at the long term intervals up to 10000 days and for improving their orbits, published in Catalogs [3-5]. The errors in GS positions as a rule do not exceed $10'$. One year of orbital evolution is calculated in 2 - 4 sec with PC - 386, depending on type of motion: libration or circulation.

THE BASIC EQUATIONS

In this investigation the following co-ordinate system has been adopted. Its origin is in the center of the Earth's mass. The fundamental plane coincides with the Laplacian plane, which crosses the equatorial and ecliptic planes. This plane forms with the equatorial one a dihedral angle Λ ($7^\circ 20'$). The X-axis is directed toward the mean vernal equinox of the date and Z-axis is perpendicular to the Laplace plane.

The principal difficulty of construction of GS motion theory consists in taking into account of resonant perturbations from the geopotential. These perturbations cause the largest variations in the stroboscopic longitude $\lambda = M + \omega + \Omega - S$, where M - mean anomaly, S - Greenwich siderial time.

The modified Gedeon's equation for λ , which includes the influence of resonant harmonics of geopotential and the luni-solar attraction [6] is written as:

$$\frac{d^2 \lambda}{dt^2} = -n^2 \sum A_{lmkpq} \sin(m\lambda - m\lambda_{lmkpq} + (k-m)\Omega_A) + LSP, \quad (1)$$

where n - mean motion of GS, coefficients A_{lmkpq} - depend on the Hansen coefficients, the inclination functions [7], parameters of the geopotential ($C_{lm}^2 + S_{lm}^2$) and on the relation of semi-major axis of GS orbit to the Earth's mean equatorial radius; LSP denotes the luni-solar perturbations.

Here the summation is fulfilled on resonant harmonics, when indexes l, m, p, q satisfy the following equality:

$$l - 2p + q = m. \quad (2)$$

INTEGRATION OF MOTION EQUATIONS

For the simplification of the further statement let us rewrite equation (1) as follows:

$$\frac{d^2 \lambda}{dt^2} = \sum A_i \sin(m_i \lambda - \phi_i - s_i \Omega) + LSP, \quad (3)$$

where

$$\begin{aligned} A_i &= -n^2 A_{lmkpq}, \\ \phi_i &= m\lambda_{lmkpq}, \\ s_i &= m - k. \end{aligned} \quad (4)$$

Choosing of the Laplacian plane as the reference one provides very slow changing with respect to time (almost constancy) of coefficients A_i , m_i , ϕ_i and s_i in (3).

If these coefficients and longitude of node Ω were constant, - in the case of absence of the luni-solar perturbations, - equation (3) would have the first integral:

$$\left(\frac{d\lambda}{dt}\right)^2 = C - \Pi(\lambda), \quad (5)$$

where C is the constant of integration, which is the analogue of Jacobi's constant in the restricted problem of three bodies, and

$$\Pi(\lambda) = 2 \sum \frac{A_i}{m_i} \cos(m_i \lambda - \phi_i - s_i \Omega). \quad (6)$$

In such case the problem could be resolved by means of quadrature:

$$t - t_0 = \int_{\lambda_0}^{\lambda} \frac{d\lambda}{\sqrt{C - \Pi(\lambda)}}. \quad (7)$$

The behavior of function $\Pi(\lambda)$ is shown on Fig.1. It is like to asymmetric sinusoid with two maxima of different heights. Accordingly to the value of parameter C in (5), GS may move in one of pits - simple libration near the stable point 75° E or 105° W, around both of these pits - complex libration or in the circulation regime.

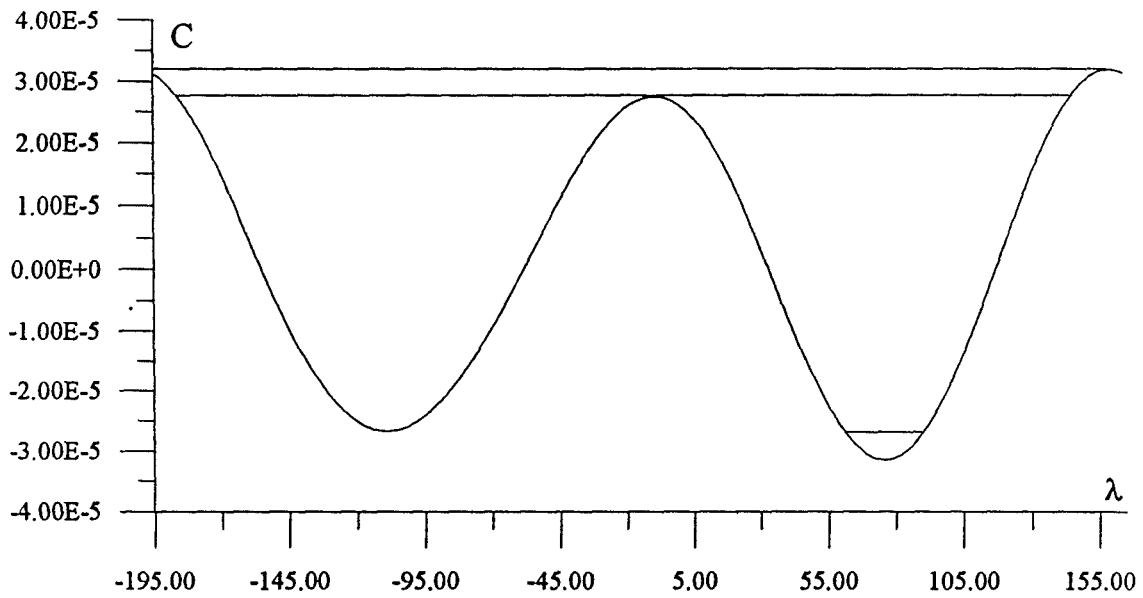


Fig. 1. Function $\Pi(\lambda)$.

However, because of smallness of $\dot{\Omega}$, the solution of (3) may be still expressed in form (5), if we consider C as a slowly changing function of the time.

As a result we shall have:

$$\frac{dC}{dt} = 2\dot{\Omega} \sum \frac{A_i s_i}{m_i} \sin(m_i \lambda - \varphi_i - s_i \Omega). \quad (8)$$

Introducing the new variable of integration $d\lambda$ instead of dt by means of (5), we obtain:

$$C = C_0 + 2\dot{\Omega} \int_{\lambda_0}^{\lambda} \frac{\sum \frac{A_i s_i}{m_i} \sin(m_i \lambda - \varphi_i - s_i \Omega)}{\sqrt{C - 2 \sum \frac{A_i}{m_i} \cos(m_i \lambda - \varphi_i - s_i \Omega)}} d\lambda. \quad (9)$$

The exact calculation of the right-hand side of equation (9) is impossible, because variables C and Ω have been unknowably depended on λ ; but with accuracy, enough for practical applications on short intervals of time, we may consider them as constants, equals to the middle values of \bar{C} and $\bar{\Omega}$, accordingly.

The variations of C and inexactitude in calculation of (7), connected with changing of Ω with the time, we can considerable reduce, introducing the oscillating system of co-ordinates, where the new variable X is determined by equation:

$$X = \lambda + 0.00821 \sin(\Omega - 0.0176) + 0.00007 \sin(2\Omega - 0.0362). \quad (10)$$

The introduction of variable X has the following geometrical sense. The tops of the function $\Pi(\lambda)$ (fig.1) are periodically shifting relative to their middle positions, accordingly to changing of Ω with the time. So, we receive the system of co-ordinates, oscillating synchronously with the tops of function $\Pi(\lambda)$.

This allows to increase the step of integration without the waste of accuracy.

CALCULATION OF QUADRATURES

The calculation of quadrature (7),- substituting X instead of λ , - may be realized by means of the numerical methods.

However, using of (7) for resonant GS is connected with some problems, because near the points of reverse the integrand becomes unlimited. Hence, the accurate calculations require very high range (many thousands) of approximating polynomial.

For this reason we have introduced in (7) a new variable of integration φ , connected with X as follows:

$$X = ((A - B)\sin \phi + A + B) / 2, \quad (11)$$

where A and B are some constants.

With the new variable φ the equation (7) becomes:

$$t - t_0 = \frac{A - B}{2} \int_{\varphi_0}^{\varphi} \frac{\cos \varphi d\varphi}{\sqrt{C - \Pi(X)}}. \quad (12)$$

We can choose constants A and B so, that in (12) the roots of $\cos \varphi$ and $C - \Pi(X)$ would coincide and at these points integrand becomes limited.

If one makes integration of (7) with the constant step of X , to the end of every half-period of librating GS the value of Δt must strongly grow, because at these points the derivative dX/dt tends to zero.

For obtaining of nearly equal intervals of time we use some method for choosing of step X , called as subroutine "Metka".

APPLICATIONS

Basing on the described mathematical method, the software for GS orbital calculations is elaborated. This software consist of two groups of procedures, which are called as "Evolution" and "Improvement".

The simplest one among them is the group of "Evolution", by means of which we may to investigate the evolution of GS orbital elements during tens of years, based on some initial conditions. The rate of calculation for one year of evolution with PC IBM-386 is equal to 2-4 sec. The accuracy of GS positions for 5 years of evolution is equal to some seconds of arc for ordinary GS and about a half minute for the GS, changing their moving regime; for 60-year evolution these errors grow to some minutes of arc or one degree, accordingly.

The another group of procedures permits to improve GS orbital elements by means of least square method, using all observations (made after the moment of last orbital correction).

Due to this software it is possible to calculate GS ephemerides for many years with the accuracy, enough for their identification and observation. It is also possible the identification of "old" GS, which were lost. By means of discrepancies in motion of some GS, moving on unstable orbits, it is possible to improve some low-order harmonics of the geopotential. For this purpose we have chosen 14 of such GS and their observational program "Resonance" have been created.

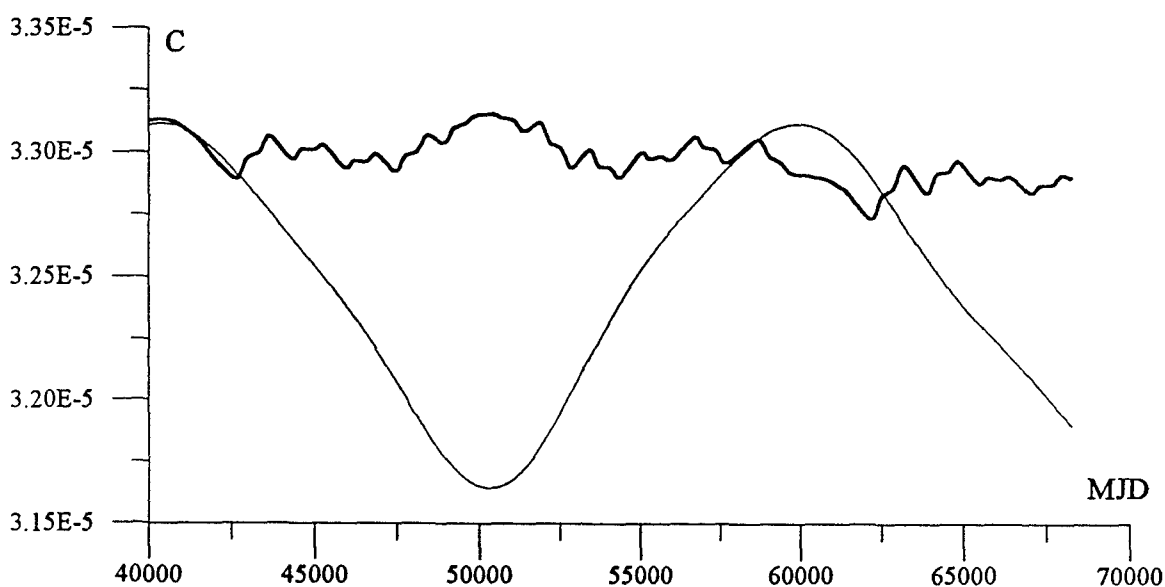


Fig 2. The C-parameter of 67001A and the "top" of $\Pi(\lambda)$.

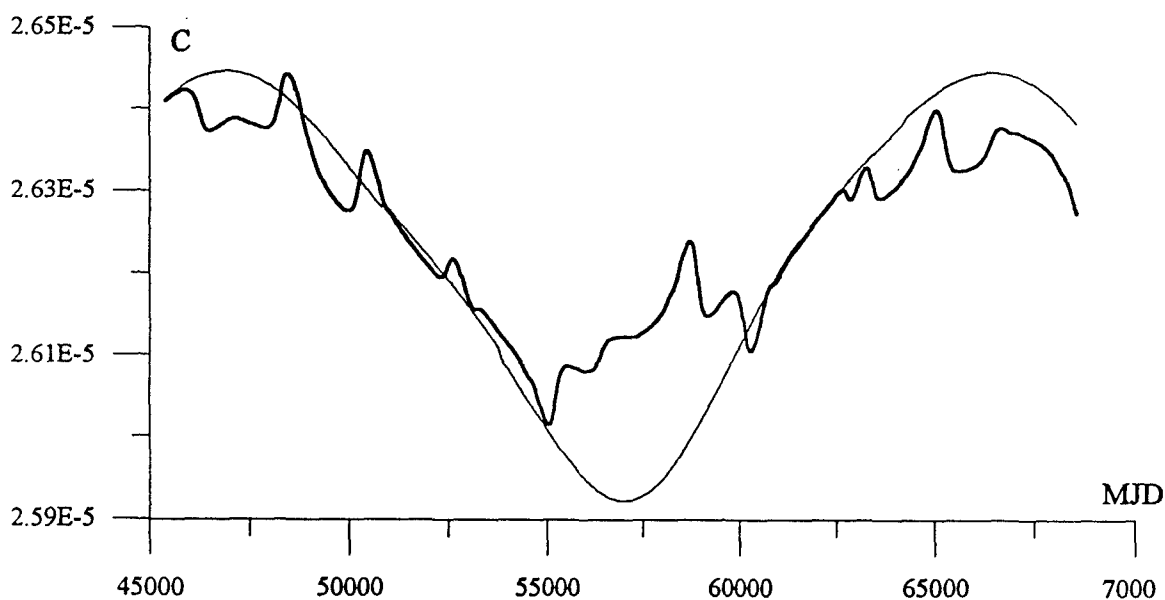


Fig 3. The C-parameter of 86027A and the "top" of $\Pi(\lambda)$.

On Fig. 2 and 3 there are shown the results of the long-period investigation of GS 67001A (Intelsat 2 f-2) and 86027A (Cosmos 1738) orbits. On these figures the values of C-parameter of GS (5) and the "tops" of potential hills, as functions of the time, are shown. The scale of time is about 60 years.

It is clear from Fig. 2 and 3 that the "tops" of potential function $\Pi(\lambda)$ are periodically moving up and down with the 54-year period. It is also shown, that both of these GS change their regime of motion: in 1974 GS 67001A from librating orbit had been passed to the circular one and in 1997 or 2000 GS 86027A will change the simple libration with the complex one.

REFERENCES

1. Gedeon G. S.. Tesseral resonance effects on satellite orbits. 1969. *Celestial Mechanics*, v.1, No.2, p.167-189.
2. Sochilina A. S.. The luni-solar perturbations and the motion of the high satellites. 1985. *Bull. ITA*, v.15, No.7(170), p.383-395.
3. Vershkov A. N., et al. 1994. *Catalogue of Improved Orbits of Uncontrolled Geostationary Objects*, v.1, 102 p.
4. Ibid, 1994. v 2, 94 p.
5. Sochilina A. S., et al. 1996. *Catalog of Orbit of Geostationary satellites*. 103 p.
6. Grigoriev K.V., et al. 1993. On catalogue of geostationary satellites. *Proc. First European Conf. on Space Debris*, Darmstadt, Germany, 5-7 April 1993, p.665-669.
7. Gaposchkin E. M.. 1973. *Smithsonian Standard Earth (III)*. *SAO Spec. Rep.*, No.353, 388 p.

LOW-PERIGEE SATELLITE CATALOG MAINTENANCE: ISSUES OF METHODOLOGY

Z.N.Khutorovsky

"Vympel" International Corporation, Moscow

In Russia the main source of information on orbital and ballistic characteristics of man-made Earth satellites is the catalog of these objects, maintained by the Space Surveillance System [Ref.1].

Maintenance of this catalog is performed in real-time scale by complex automatic system, which includes network of sensors and software tools for processing acquired data in automatic and interactive modes.

General composition and characteristics of this system with regard to satellites in low orbits were described in [Ref.2]. Here we will treat the architecture of the algorithms, forming the basis of the system. Our attention will be concentrated mainly not on the algorithms by themselves, but on the basic initial conditions and assumptions for their development, key methodological notions, character of the main tasks to be solved and considerations of principal possibilities to find necessary solutions.

Presented analysis is concluded by brief characterization of the main specific features of the algorithms employed in Russian Space Surveillance System for satellite catalog maintenance.

1. SENSORS

The main source of data for solving the task of satellites' catalogization are detection radars of the Early Warning and BMD systems. Certain characteristics of these sensors are presented in table 1 ([Refs.3,4]).

Note the main specific features of this network.

1. All sensors work in detection mode i.e. continuously observe the space within their fields of view and receive reflected signals, exceeding the threshold level, which form single measurements. Scanning is performed by each radar according to certain fixed programm. It means that on-site

detection process is not under the control of the Center, responsible for catalog maintenance.

Table 1. Characteristics of the sensors

location	coordinates	type	system	sector in azimuth	band
Irkutsk, Russia	103°W, 53°N	Dnepr	EWS	30°÷300°	VHF
Balkhash, Kazakh.	74°W, 45°N	Dnepr	EWS	30°÷330°	VHF
Murmansk, Russia	40°W, 68°N	Dnepr	EWS	295°÷355°	VHF
Riga, Latvia	22°W, 57°N	Dnepr	EWS	220°÷310°	VHF
Sevastopol, Ukraine	33°W, 44°N	Dnepr	EWS	140°÷260°	VHF
Uhgorod, Ukraine	23°W, 48°N	Dnepr	EWS	165°÷285°	VHF
Petchora, Russia	57°W, 65°N	Darial	EWS	300°÷0° 0°÷55°	VHF
Mingechaur, Azerb.	48°W, 41°N	Darial	EWS	105°÷215°	VHF
Moscow, Russia	37°W, 55°N	Dunai	BMD	255°÷305° 65°÷120°	UHF

2. All the sensors are located within the territory of the former USSR in boundary and central regions. Their geographic locations cover 12% of latitude and 22% of longitude ranges and sectors of view are limited in azimuth, elevation angle and range. Thus *complete surveillance of low-perigee satellites is not ensured*. Maximal gaps in observations of low orbit objects of meter size, moving in circular orbits with inclinations exceeding 30°, are 12 hours a day [Ref.1].

3. Only one of the sensors (Dunai radar, located in Moscow region) is a UHF radar, the others are VHF radars. Observation conditions for objects with sizes less than 20-30 cm ¹ are essentially different for UHF and VHF radars. Some of these satellites can be observed only by UHF radars. Thus, *satellites, observed by only one sensor, do exist*. In this case the range of latitude arguments *u* of observed parts of the orbit does not exceed 5°÷7°, i.e. covers 1.5÷2% of the range of *u*. If observation conditions do not let

¹The US satellite catalog comprises more than 2000 such objects.

the radar observe the satellite in ascending and descending revolutions, the total range of observed latitude arguments δu_{tot} may deviate from this value insignificantly.

2. MEASUREMENTS

Performing a set of single observations of the target the radar obtains the "marks" - **single measurements** of certain parameters along the track of a satellite. Usually a radar measures range D , azimuth ε , elevation angle γ and sometimes radial velocity \dot{D} in local radar's coordinate system [Ref.5].

Acquired single measurements are "smoothed" for the interval t_{tr} ($t_{tr} \leq 50 \div 100$ s [Ref.1]), producing as a result estimation of object's parameters or **measurement (observation)** $\mathbf{x} = (D, \varepsilon, \gamma, \dot{D}, \dot{\varepsilon}, \dot{\gamma})$.

Any radar measurement \mathbf{x} contains data on orbital parameters \mathbf{a} of the satellite, that produced it, since

$$\mathbf{x} = \mathbf{f}(\mathbf{a}) + \delta\mathbf{x}, \quad (1)$$

where $\mathbf{f}(\mathbf{a})$ - functional relationship between orbital parameters and parameters of the measurement, $\delta\mathbf{x}$ - observation's error.

Design of measurements' processing procedures most essentially depends on the accepted **model of measurements' errors**. The following model is used to describe real errors.

1. The value $\delta\mathbf{x}$ is presented as

$$\delta\mathbf{x} = \delta\mathbf{x}_{nor} + \delta\mathbf{x}_{an}, \quad (2)$$

where $\delta\mathbf{x}_{nor}$ and $\delta\mathbf{x}_{an}$ - are **normal** and **abnormal** components respectively.

2. *Normal* component $\delta\mathbf{x}_{nor}$ is present in each radar parameter of vector \mathbf{x} . It has Gaussian distribution with the mean \mathbf{m} and diagonal covariation matrix \mathbf{K} . Parameters \mathbf{m} and \mathbf{K} satisfy the conditions $\mathbf{m} \leq \mathbf{m}_{max}$, $\mathbf{K} \leq \mathbf{K}_{max}$.

3. *Abnormal* component $\delta\mathbf{x}_{an}$ satisfies the conditions $\delta\mathbf{x}_{an} \gg \delta\mathbf{x}_{nor}$, $|\delta\mathbf{x}_{an}| \leq \delta\mathbf{x}_{max}$. It is present only with certain probability $p_{an} \ll 1$ ($p_{an} = (p_D, p_\varepsilon, p_\gamma, p_{\dot{D}}, p_{\dot{\varepsilon}}, p_{\dot{\gamma}})$).

Real errors well correspond to this model. The model parameters m_{max} , K_{max} , δx_{max} were managed to be chosen so that the resulting error does not exceed 0.001, i.e. 99.9% of observations have errors, corresponding to accepted model. In this case

a) probability of abnormal error in any of "radar" components does not exceed 0.1 as a rule;

b) 21 combinations (out of 64 possible) of the six-dimensional vector x components can be abnormal simultaneously;

c) the number of abnormal components is not more than three.

Regarding the magnitudes of observation errors the following can be mentioned.

1. Different parameters are not equally accurate. The most accurate is the range. Errors in azimuth and elevation angle (transformed to linear measure) are as a rule much greater. Similar relationship is valid for velocity components.

2. Probabilities of arrival of abnormal errors are different for different parameters. The most consistent is the range. The least accurate components - elevation angle and its rate are subjected to distortions to the most great extent.

3. Among six orbital parameters three are determined most accurately on the basis of measurement: orbital inclination i , longitude of ascending node Ω and orbital period T . Approximate relationships for the errors δi , $\delta \Omega$, δT of i , Ω , T determination are as follows ²:

$$\begin{aligned}\delta i \{degree\} &\approx 0.75 \cdot 10^{-2} \cdot D \cdot |\delta D_0| + 0.6(D \cdot \delta \ddot{D} + 0.008 \cdot D \cdot |\delta D_0|) \cdot \cos u \\ \delta \Omega \{degree\} &\approx 0.75 \cdot 10^{-2} \cdot D \cdot |\delta D_0| + 0.6(D \cdot \delta \ddot{D} + 0.008 \cdot D \cdot |\delta D_0|) \cdot \sin u \cdot \sin i \\ \delta T \{minute\} &\approx 6 \cdot \dot{D} \cdot \delta \dot{D} + 3 \cdot D \cdot \delta \ddot{D} + 0.025 \cdot D \cdot |\delta D_0|,\end{aligned}\quad (3)$$

where u - argument of latitude for the point in orbit, in which vicinity the measurement is fulfilled; i - orbital inclination; $|\delta D_0|$ - error of

²These evaluations are obtained for satellites with orbital altitudes $h < 3000$ km and eccentricities $e < 0.1$, and also for observed by the radar at ranges $D < 2000$ km and radiation directions, deviating from the main (normal to antenna's plane) not more than for 30° . Their derivation uses known geometrical and dynamical relationships [Ref.5], [Ref.6].

evaluating direction to the object on the basis of measurement (error of the most roughly measured angular component); $\delta\ddot{D}$ - error in determining acceleration using the range, its upper limit evaluated using either the formula $\delta\ddot{D} = 2\cdot\delta\dot{D}/t_{tr}$, in case the radar measures \dot{D} ($\delta\dot{D}$ - maximal error of single measurements of \dot{D} not taking into account systematic component) or using the formula $\delta\ddot{D} = 16\cdot\bar{\delta}D/t_{tr}^2$, in case \dot{D} is not measured ($\bar{\delta}D$ - maximal error of D single measurements, not taking into account the component, linearly evolving with time).

It follows from (3) that the magnitude of errors of i, Ω, T determination on the basis of measurement for objects of meter size is 1% of the measured value, i.e. $\approx 1^\circ$ in i and Ω and ≈ 1 minute in T .

3. TRACKING

Key aspect is the notion of the trackability of a satellite. This notion formally is not to be dependent on the radars, since their operation is not under the control of the Center, maintaining the catalog.

We consider the object *trackable*, in case it is

- a) *observable*, i.e. its observations are fulfilled regularly;
- b) *separable*, i.e. its observations can be selected on the background of other measurements.

Thus, tracking of observed satellite is influenced by other also observed objects.

If the object is trackable, then it is principally possible to determine its parameters using all attributed observations' data, thus providing calculation of its position for arbitrary moment (with certain accuracy).

Regular tracking of a satellite means periodically repeating procedures of correlating new measurements with this satellite and updating its orbital parameters using these measurements. This will be called **tracking process**.

Now we will formulate condition of trackability (tracking) of a satellite. Its significance requires rather detailed consideration.

Assume, that all the measurements for given object are separated and on their basis the orbit is determined. Let a new observation x is

acquired for this object. Than to obtain correct correlation decision this measurement must be closer to the "own" object than to the others also having the orbits determined on the basis of measurements. "Distance" between the orbit and the measurement is determined by the differences between the measured and calculated using orbital parameters components of the observation.

Calculation of measurement's components on the basis of the orbit means propagation of the elset to the moment of measurement x and transformation of obtained data to parameters of the measurement.

If all the measurements and propagated elsets were not subjected to errors, the residuals of measurements with "own" orbits would be equal to zero and allocation of measurements to the objects won't pose any problems. Thus the residuals are determined by the errors of measurements and predicted orbit. Measurements' errors at least for one of measured parameters are essentially smaller than distances between neighbouring satellites, otherwise satisfactory selection of single measurements in course of on-site tracking and acquisition of measurements would become impossible. Thus, *the cause of mistakes in allocation of radar measurements to orbits of tracked satellites can be only the errors of predicted orbit.*

Orbital parameters for any object are obtained on the basis of the set of measurements, previously performed on this object by all the radars, participating in surveillance process. The employed for orbits' determination algorithms seek for the orbit, in certain sense, best to "inscribe" into these measurements. To calculate residuals with future measurements this orbit is propagated to their moments. Thus the errors of predicted orbit depend on

1. errors of determinating orbital parameters on the basis of measurements

2. errors of propagating this orbit.

These two sources of errors interact with each other, producing the *error of orbit's determination and prediction.*

So, condition of trackability assumes *small errors of orbits' determination and prediction in comparison with distances between them.* In other

terms *alien measurements are not to "inscribe" into satellite orbit*. We will call it **informativity condition**.

Let us evaluate accuracy of orbit's determination and prediction, ensuring fulfillment of informativity condition.

On one hand, maximal density of satellites, regularly tracked by US and Russian sensors, is $\approx 10^{-7}$ objects within km^3 [Ref.7], i.e. ≈ 1 one satellite within a volume of $10^7 km^3$, and density variations within altitude range 400-3000 km is three orders of magnitude. On the other hand, uncertainty domain, resulting from orbit's propagation, has the shape stretched along velocity vector, since the error in directions, normal to velocity vector is approximately e times smaller, where e - orbital eccentricity. For 90% of tracked satellites $e < 0.1$. Not taking into account objects with $e > 0.1$ and assuming that the volume of produced by propagation uncertainty domain is to be of the order of magnitude smaller than the volume, where one satellite can be found, we have the following condition for acceptable along the track prediction error δ_v : $0.1 \cdot 10^7 = (0.1 \cdot \delta_v) \cdot (0.1 \cdot \delta_v) \cdot \delta_v$. And hence $\delta_v \approx 500$ km. Transformed to time this is ≈ 1 minute along the track of a satellite. This estimation is obtained for most "populated" altitudes $\approx 800 \div 1000$ km and $\approx 1400 \div 1500$ km. For other altitudes acceptable errors are greater.

Let us evaluate how informativity condition is satisfied.

For propagating the orbit for M revolutions the error δ_v is evaluated using the formula:

$$\delta_v = M \cdot \delta T + 0.5 \cdot M^2 \cdot \delta(\Delta T), \quad (4)$$

where δT and $\delta(\Delta T)$ - errors of determination of orbital period T and its rate (per revolution) ΔT .

Understanding of the accuracy of T determination using one measurement is provided by formula (3). As we have mentioned earlier typical value of δT is 1 minute. In case we have several measurements, distanced in general for N revolutions, the upper limit for δT can be estimated, using the formula $\delta T = 2 \cdot \delta t_u / N$, where δt_u - maximal error of determining the moment t_u of satellite's passing the point with latitude argument u , calculated using one measurement. Usually the object is observed in

different revolutions with close latitude argument, thus the value of u can be chosen, for which δt_u is of the order of 1 s.

The value of ΔT depends on satellite's altitude over the Earth surface h and its ballistic coefficient k_b . The values of ΔT (in minutes) can be given by approximate formula $\log_{10}|\Delta T| \approx \log_{10}(\frac{k_b}{0.01}) - \frac{h}{100}$, where h - altitude in km, k_b - ballistic coefficient in m^2/kg (typical values are ≈ 0.01). The value of ΔT principally can not be determined as accurately as we desire since $\delta(\Delta T)$ is defined by the error of the used model of atmospheric density for prediction interval, that ranges from several percent up to several times (typical values are $\approx 10\%$) [8].

Analysis of this situation brings to the following.

1. The orbit, determined using one measurement, allows to track the object in case it is observed in each revolution. The sensors do not provide this possibility. Hence *estimation of orbital parameters for any satellite requires to combine the data acquired for different revolutions.*

2. *The orbit, determined using several measurements for different revolutions, allows to track satellites observed daily (with $h > 300$ km and $k_b < 1m^2/kg$).*

3. Observation conditions for satellite in near circular orbit depend on its altitude h . With increase of h the range of object's pass through radar's field of view usually increases and observation conditions become worse. On the other hand with the increase of h prediction errors decrease and acceptable prediction interval increases. In altitudes greater than 600 km (and $k_b < 1m^2/kg$) a satellite can be tracked even in case only one measurement a month is obtained. That is why *regularly (however, may be seldom) observed satellites in near circular orbits can be tracked.*

4. In case a satellite is in orbit with eccentricity, that can change observation conditions for various values of perigee argument, the measurements on this object may be irregular and long gaps in observations become possible. In this case tracking of satellite using the measurements may become impossible and **break of tracking** occurs. However this situation is temporary. When new data on this satellite arrive after a long gap, trackability condition for the set of measurements after the gap may be satisfied and the object principally, may be tracked again.

Above considerations treated "stationary" situation, when no new observed objects arrive in space.

Launches, separations, break-ups as well as arrival of new sensors and modernizations of existing ones also produce disturbances of informativity condition. Here disturbance of informativity condition is also of local (only for certain domain of parameters) and temporary (only for limited intervals) character. After certain time new objects will depart for significant distances and acquired observations will principally allow to determine their orbits with accuracy, required for tracking.

Here one more important notion is to be introduced. It will be treated in the next section.

Conclusions follow.

1. **Informativity condition is indispensable condition for tracking a satellite. For observed objects it is normally satisfied.**

2. **For certain satellites informativity condition may be disturbed for some intervals. Breaks of tracking may occur in this case for tracked satellites.**

3. **In case observations' data on new or not tracked (but tracked previously) satellite arrive, it must be stored until informativity condition is satisfied.**

4. PRIMARY DETERMINATION OF ORBITS

We already mentioned that the orbit determined using one measurement does not ensure satisfactory separation of future observations' data on this object. To obtain more accurate orbit we are to combine several measurements. In case the object is tracked this orbit is available. However its accuracy decreases with time. Therefore it is to be updated using new received observations. If the object is not tracked, principally new task is to be solved - **primary determination of the orbit or orbit's detection.**

Informativity condition must be satisfied to solve this task. This condition is satisfied in case the data, present in measurements of this object, principally allow to determine its orbit with accuracy making the errors of determination and prediction essentially smaller than the

distances to other observed objects so that "alien" measurements won't "inscribe" into the orbit.

For primary determination of orbit two measurements for different revolutions are not enough, since the chances to take two measurements produced by two objects are too great ³. We need to have at least *three measurements for three different revolutions (triplet)*. The orbit determined using these measurements is much more accurate than the orbit produced by one measurement and the chances that three measurements inscribed into one orbit are produced by different objects are essentially smaller than for two measurements.

In reality for primary determination of orbits we need:

- a) to find associating triplet among the measurements, not correlated to tracked objects;
- б) using discovered triplet, determine the orbit.

Let us analyze principal possibilities to solve this task⁴.

The main parameter, defining this possibility is the *uncertainty in the number of revolutions N between the boundary (with regard to reference moments) measurements of the triplet*.

Let $k_{ud} = [N \cdot \frac{|\delta\tilde{T}|}{\tilde{T}}] < 0.5 \cdot (p + q)$, where $\delta\tilde{T}$ - the error in period \tilde{T} , determined using one measurement; $[A]$ - entire of A , rounded-off; p and q - minimal integer positives, satisfying the condition $p/q = P/Q$; P - the number of revolutions between boundary and intermediate measurements, $Q = N - P$. Then no uncertainty exists. This condition will be called **unambiguity condition**.

When the unambiguity condition is satisfied for the set S_N of possible values of N (taking into account uncertainty coefficient k_{ud})⁵ the unique value \hat{N} exists, when parameters $t_u^{(1)}, t_u^{(2)}, t_u^{(3)}$ are matched ($t_u^{(1)}, t_u^{(2)}, t_u^{(3)}$ - calculated using the measurements of the triplet moments of satellite's

³Especially for multi-element launches and break-ups, when the orbits of different elements are close.

⁴For the task of primary orbits' determination the computation's aspects are also important, since decision making procedures are rather time-consuming. We won't deal with these issues here. Assume that arbitrary complex procedures are realizable.

⁵ $S_N = \{\tilde{N} + i, i = 0, \pm 1, \pm 2, \dots, \pm k_{ud}\}$, where $\tilde{N} = [|t_u^{(1)} - t_u^{(3)}|/\tilde{T}]$.

arrival at a certain latitude argument u for the revolutions, corresponding to these measurements).

The value \hat{N} is **true number of revolutions** between boundary measurements of the triplet and corresponds to the estimation \hat{T} of T , given by $\hat{T} = |t_u^{(1)} - t_u^{(3)}|/\hat{N}$, which accuracy exceeds accuracy of \tilde{T} by 1-2 orders of magnitude.

Consider the example. Let $|\delta\tilde{T}| < 1$ minutes and $T = 100$ minutes. Then for $N < 50$ ($|t_u^{(1)} - t_u^{(3)}| < 3.5$ days) $k_{ud} = 0$ and $\tilde{N} = \hat{N}$. Unambiguity condition is satisfied irrespectively of relative position of the intermediate measurement with regard to the boundary ones. Let now $N = 200$ (two weeks between boundary measurements) and $P = 100$. Then $k_{ud} = 2$, $p = q = 1$ and unambiguity condition is not satisfied. In this case $S_N = \{\tilde{N} - 2, \tilde{N} - 1, \tilde{N}, \tilde{N} + 1, \tilde{N} + 2\}$, step of uncertainty $p + q$ is two (corresponds to the step in period ≈ 1 minute) and within the set S_N two or three possible values of \hat{N} , when $t_u^{(1)}, t_u^{(2)}, t_u^{(3)}$ are matched, do exist. Each of them correspond to its own estimation \hat{T} with error $|\delta\hat{T}| \approx 0.01$ minute.

If uncertainty in the number of revolutions between boundary measurements of the triplet exists several primary orbits can be obtained, equally well inscribing into the measurements. In this case none of them can be found preferable and orbits' detection task won't be solved. Solution may be found some time after arrival of new measurements on the object. To be successful we need:

- a) informativity condition is to be satisfied for the interval of these observations;
- b) additional observations' data is to remove the uncertainty in the number of revolutions between boundary measurements.

Conclusions.

1. Possibility of solving the task of orbit's detection for certain satellite depends on its observability.
2. Detection of daily observed satellites is possible in case they are observed by at least one sensor.
3. Rarely (less than one time a day) observed objects

principally can be detected provided certain arrangement of measurements within the interval of observations and fulfillment of informativity condition.

5. IDENTIFICATION

After primary determination of orbit the origin of detected satellite is to be determined. This is the task of **identification**. Obtained orbit (in case it is enough reliable) may be either the orbit of new satellite, not previously tracked, or the orbit of the object tracked before, but lost due to break of informativity condition caused by absence of observations for a long time. In the first case the source of the object is to be determined, for example launch, break-up or separation. In the second case predecessor is to be identified.

Let us evaluate the possibilities to solve this task.

Accuracy of identification depends on delay $\tau_d = t_{det} - t_{in}$, where t_{in} - the time of newly detected object arrival in space or the time when previously tracked satellite was lost; t_{det} - the time of object's detection and start of its tracking.

If τ_d is small, identification with the origin does not pose serious difficulties, since first, rather complete information on space operations is published and second, the orbital data allows simple and accurate determination of satellite's parameters for the moment of its arrival t_{in} (for identification task parameters i, Ω and spatial position for this moment are of major interest).

With the increase of τ_d the error of determination of satellite's parameters for the moment t_{in} increases and we approach the moment, when correct determination of the origin immediately or after a short time after detection becomes difficult or impossible.

If *detected object is a "prolongation" of the old one*, then for making correct identification decision we need:

- a) parameters of detected object "inscribe" into the orbit of the old one;
- b) with regard to objects' parameters the "distance" (taking into account propagation errors) between the old and detected object is

essentially smaller than the distance between various previously tracked satellites.

Computation of this distance is fulfilled propagating parameters of the old satellite (it is more accurate since it was tracked for longer period) to the epoch of detected object. Prediction intervals may reach several years and we are to have prediction procedures good enough for such intervals. Principally this task is solvable in case old object was tracked for sufficiently long period and within the interval from its first detection up to its last loss rather complete pattern of orbital parameters' variations is available. In this case we can approximate temporal evolution of orbital elements with fragments of Fourier-Taylor series and perform predictions for the old object using this approximation. To fulfill these operations **global archive of orbital data** for all satellites, for which breaks of tracking are possible, is needed.

If detected object is not identified with any of the old ones and it can not be affiliated to recent launches and break-ups, most likely it is a fragment of one of old launches or break-ups. Possibilities of identification in this case mostly depends on accuracy of determination of Ω for the moment of assumed arrival (moments of launch or break-up). In its turn this accuracy is determined by duration of detected object's tracking. Sometimes several years of tracking are needed to determine the origin and the moment of satellite's arrival, that took place 20-30 years before the moment of detection. Here long-term prediction of Ω , similar to the cases of objects' loss, is performed using approximating functions, calculated on the basis of orbital data for new satellite for the whole interval of its tracking.

Conclusions.

1. To be successful in identification of detected orbits, corresponding to satellites, recently (from several days up to several months) arrived in space, we need the data on major orbital elements of the parent and on the time of arrival.

2. In case detected orbit is the orbit of satellite, residing in space for a long time, in addition we need global archive of orbital data for this satellite, stored for the interval, comparable to the

interval when the satellite was not tracked.

6. SPECIFIC FEATURES OF THE ALGORITHMS

Treated in the above sections initial conditions, input data and approaches to solving the task of satellite catalog maintenance lead to the following specific features of the algorithms used for this purpose [Refs.9,10].

Analysis of data sources and measurements of Russian network revealed the following. Certain limitations in observed altitudes, inclinations and orbital points do exist. Permanent control over low-perigee satellites is not ensured. Among the measurements of well observed meter-sized objects $\approx 10\%$ of abnormal and rough are present and for small-sized satellites this percent is greater. The orbit determined using one non-abnormal measurement is not enough accurate for trackability.

However, using temporally parted measurements and existing accurate and consistent components, integral amount of data, present in all the measurements principally allows to track the major part of observable objects regularly or with certain gaps.

The algorithms must use this principal possibility, i.e. extract this information from the measurements and "incorporate" it into the orbits without essential losses.

The algorithms, based on **statistical decisions theory** [Ref.11] are informationally efficient.

Characteristic feature of considered task is uncertainty in statistical description of observations' errors and the "noise" of the system⁶. Thus we are to use special methods of statistical decisions theory, developed for this case [Ref.12].

In the scope of statistical decisions theory the task of catalog maintenance is formulated as a task of estimating the amount of observed satellites and their parameters using measurements' data. In case informativity condition is satisfied unique solution of this task adequate to

⁶errors in prediction of orbital parameters caused mainly by atmospheric "noise".

real situation exists. Let us treat some features of the algorithm, realizing this solution.

1. Final decisions on allocation of measurements to objects and estimation of orbital parameters (for tracking as well as for primary determination) are made using analysis in points of minimum of quadratic functionals $\Phi(\mathbf{a})$, constructed on normalized residuals of measured and computed values in "radar" parameters $D, \varepsilon, \gamma, \dot{D}, \dot{\varepsilon}, \dot{\gamma}$ for various objects. Together with estimation of "main" parameters⁷ "interfering" parameters⁸ are evaluated. Here **adaptive Bayes approach** is used.

2. Selection of abnormal components of measurements is fulfilled using multi-pass minimization of $\Phi(\mathbf{a})$ with separation (in each pass) of abnormal components of all measurements using normalized residuals and with corrections of their weights⁹ in $\Phi(\mathbf{a})$. Using results of this selection hypothesis of non-predictable variations of orbital parameters¹⁰ is tested.

3. Decision regarding affiliating any measurement to a satellite is made using **minimax decision function**, providing acceptable probability of miss¹¹ under maximal values of errors in possible abnormal components. Parameters of this function are tuned to provide that in case informativity condition is satisfied probability of false decisions won't exceed the accuracy of the employed model of measurements' errors, i.e. 0.001. In particular, not greater than 0.001 in probability of unreliable decision¹² in tracking and in probability of miss.

4. For motion predictions we use procedures with methodical errors not exceeding the maximum of two values: stochastic components of observations' errors and potentially achievable real errors of prediction.

⁷satellites' orbital parameters.

⁸unknown parameters of measurements' errors for various sensors and propagation errors for various objects, subjected to essential atmospheric drag.

⁹coefficients of residuals' squares

¹⁰These variations may be caused, for example by ignition of satellite's engines, break-up of the satellite, significant geomagnetic storms or others

¹¹not affiliating of measurement to "own" object.

¹²The orbit is unreliable in case it is either not determined or it is determined but does not provide regular tracking of a satellite. Indispensable condition of reliability is the presence of at least three "inscribed" into the orbit measurements for different revolutions.

5. Minimization of $\Phi(\mathbf{a})$ functional uses specially developed techniques for making initial approximation and search for minimum, taking into account specific features of real measurements and providing determination of the minimum point under conditions of tracking and primary determination not less than in 99.9% and 90% of cases respectively.

6. For primary determination of orbits we realized the procedure ensuring (for a set of up to 20000 non-correlated with tracked objects measurements), *exhaustive search* of observations' triplets with analysis (for each triplet) of all possible values of coefficient of uncertainty in the number of revolutions between its boundary measurements, not exceeding 40.

7. Identification of detected orbit with lost objects is based on comparison with their last elsets. False identification of different objects and miss of identification are ensured to be of the level less than 0.1% and 10% respectively.

8. Various computation techniques, reducing CPU-time without losses in quality of decision making and allowing to have computer code capable of processing arriving observations in real time scale are employed.

The major are as follows:

a) preliminary allocation of arriving measurements to tracked satellites using *rough selection* of surely not correlating pairs (satellite-measurement) according to special three-step three pass scheme and *residuals with orbits* prior to their updating using these measurements ("input" residuals¹³);

b) preliminary selection of triplets of non-correlated measurements, surely not produced by one and the same object, using four parameters, most accurately calculated using individual measurements;

c) a set of techniques reducing CPU-time without loss of accuracy, employed in prediction procedures and minimization of functional $\Phi(\mathbf{a})$.

¹³contrary to residuals after minimization which can be called "output" ones and are used for making final decision regarding affiliation of measurements.

REFERENCES

1. А.А.Кузьмин, "Информационные возможности отечественной службы контроля космического пространства по наблюдению космического мусора", Проблемы загрязнения космоса (космический мусор), сборник научных трудов, Москва, Космоинформ, 1993.
2. З.Н.Хуторовский, "Ведение каталога космических объектов", Космические исследования, т.31, вып.4, стр.101-114, 1993.
3. G.Batyr, S.Veniaminov, V.Dicky, V.Yurasov, A.Menshikov, Z.Khutorovsky, "The Current State of Russian Space Surveillance System and its Capability in Surveying Space Debris", Proceedings of the First Conference on Space Debris, Darmstadt, Germany, 5-7 April 1993.
4. А.А.Курикса и др., Радиолокация космических целей (краткий обзор отечественных разработок), Радиопромышленность, вып. 1 (юбилейный), 1995.
5. Ю.С.Саврасов, Методы определения орбит космических объектов, Москва, изд-во Машиностроение, 1981.
6. I.I.Shapiro, The Prediction of Ballistic Missile Trajectories from Radar Observations, McGraw-Hill Book Company, Inc., New York-Toronto-London, 1958.
7. З.Н.Хуторовский, С.Ю.Каменицкий, В.Ф.Бойков, В.Л.Смелов, "Риск столкновения космических объектов на низких высотах", Столкновения в космическом пространстве (космический мусор), сборник научных трудов, Москва, Космоинформ, 1995.
8. Атмосфера Земли верхняя. Модель плотности для баллистического обеспечения полетов ИСЗ. ГОСТ-25645.115-84, Издательство стандартов, Москва, 1990.
9. V.Boikov, G.Makhonin, A.Testov, Z.Khutorovsky, A.Shogin, Prediction Procedures, Used in Satellite Catalog Maintenance, Proceedings of the Navspacom/Russia Orbit Determination and Prediction Workshop, Washington D.C., 13-15 July 1994.
10. З.Н.Хуторовский, В.Ф.Бойков, Л.Н.Пылаев, "Алгоритмические вопросы ведения каталога космических объектов на низких высотах", 1995 (в печати).
11. H.Cramer, Mathematical Methods of Statistics, Stockholm, 1946.
12. Репин В.Г., Тартаковский Г.П., Статистический синтез при априорной неопределенности и адаптация информационных систем, Советское радио, 1977.

TRACKING SATELLITE BREAK-UPS

Paul W. Schumacher, Jr.
Naval Space Command
Dahlgren, Virginia

INTRODUCTION

Satellite break-ups due to explosion or collision in space can instantly increase the trackable orbiting population by up to several hundred objects, temporarily perturbing the routine space surveillance operations at Naval Space Command (NAVSPACECOM) and Cheyenne Mountain Air Station.

This paper is a survey of some of the techniques and procedures used by NAVSPACECOM to respond to such events.

First, the overall space surveillance data flow at NAVSPACECOM is described, highlighting the places at which analysts may intervene with special processing.

Second, brief descriptions of some of the orbital analysis tools available to NAVSPACECOM analysts are given. These tools have been developed in-house over the past thirty years and can be used in a highly flexible manner. The basic design philosophy for these tools has been to implement simple concepts as efficiently as possible and to allow the analyst maximum use of his personal expertise.

Finally, several historical break-up scenarios are discussed. These scenarios provide examples of the types of questions that are fairly easy to answer in the present operational environment, as well as examples of questions that are very difficult to answer.

DATA FLOW FOR CATALOG MAINTENANCE

For the purpose of this discussion, the database of element sets and associated observations includes analyst satellites as well as regularly cataloged objects. Observations arrive at NAVSPACECOM from the tracking radars and telescopes operated mainly by Air Force Space Command and from the NAVSPASUR fence operated by NAVSPACECOM. The entire collection of sensors is called the Space Surveillance Network (SSN). We discuss the fence dataflow separately in more detail below because this sensor has special characteristics that are different from the tracking radars in the rest of the SSN.

The overall dataflow consists of the following steps:

- (1) verification of the sensor-level data associations ("tags");
- (2) identification of unassociated or mis-associated observations;
- (3) update of the database elements;
- (4) element-set generation and association for the remaining "uncorrelated targets" (UCTs);
- (5) release of updated elements to the SSN and external users.

When the Air Force sensors have recently updated elements to track on, they can associate at least 90% of their observations with database elements. The details of this sensor-level data association are different for each sensor and are beyond the scope of this discussion. The remaining 10% must be associated by central-level processing at Cheyenne Mountain Operations Center (CMOC) and at NAVSPACECOM.

All of the sensor-level associations are verified at the central level. This is a relatively fast process since only the element set indicated by the sensor needs to be retrieved from the database and propagated to the time of the observation. Well over 99% of the sensor-level associations agree with the central-level verification and are judged to be correct.

The few sensor-level mis-associations, plus the 10% of total observations that could not be associated at the sensor level, are passed to the identification process. Here some kind of comparison with the entire database of elements must be made for each observation. In practice, we retrieve and propagate element sets for only those orbits that come near the observed altitude. However, the identification process is still much slower (per observation) than the verification process. Usually about 94% of the observations presented for identification can be associated with objects that are already in the database, so the extra effort is worthwhile. The observations that fail the identification step are passed to the UCT (uncorrelated target) processing step.

As new observations become available, or at least once per day, an attempt is made to update each element set. The automatic update is a least-squares differential correction (DC) process using the most recent element values as the a-priori estimate. On average, about 98.5% of the element database is updated successfully without human intervention. The least-squares process may fail or produce poor results for a variety of reasons, so the analysts must examine about 1.5% of the database elements daily. The main tool that they use to do this is "manual differential correction" (MANDC), which gives them complete discretion over the least-squares fitting process. Using it, they can accept or reject individual observations, update only a subset of the complete element set, adjust the number of iterations, and so on. We find that new analysts acquire proficiency with MANDC only after considerable learning time, so that human expertise is an essential part of the cataloging system.

FENCE OBSERVATION PROCESSING

The NAVSPASUR fence operated by NAVSPACECOM is a continuous-wave multistatic radar interferometer deployed along a great-circle arc across the southern U.S. Raw signals detected at the receiver stations are sampled at an effective rate of 55 Hz for up to one second as the satellite passes through the fence beam, and then forwarded in real time to NAVSPACECOM.

Interferometric processing of each signal produces a pair of direction cosines reckoned at the time of peak signal strength at each individual receiver station. Then the cosines are associated with cataloged objects in real time by comparing them with pre-computed fence crossings of all objects in the database. This scheme is feasible because, by design, the fence beam is confined very near to the great-circle plane. Therefore it is possible to predict, to within nearly the accuracy of the element sets, when and where each satellite in the database will be detected by the fence.

Predictions based on the most recent element set for each satellite are computed for 36 hours into the future every time the element set is updated, or at least once per day. These predictions are then sorted in time order and merged with the predictions for all other satellites in a single prediction database. The fence data association then proceeds in time order as the observations arrive.

Normally, at least 97% of the fence observations can be associated with known satellites. This is a noticeably higher percentage than can presently be associated at the sensor level by the other tracking sensors in the SSN.

When fence observations (directions cosines) cannot be associated immediately with known satellites, an attempt is made to convert time-correlated lines of sight from all participating stations into a position fix for the object.

Additionally, a crude velocity estimate is available as a by-product of the interferometry. Therefore, a complete state vector can be passed to other SSN sensors if we want special tracking coverage of the object. Meanwhile, the position fix is passed to the automatic identification process.

UCT PROCESSING

"UCT" stands for "uncorrelated target", an observation or track that has not been associated with a known satellite. For this discussion, we consider UCTs to be those observations that fail to associate in the automatic identification process. Ultimately, we must dispose of UCTs either by (1) associating them with a cataloged element set or an existing analyst element set, or (2) creating a new analyst element set from the UCT data. Option (1) is still possible after the automatic identification step because the most recent element set may have been corrupted or because the element set has not been updated recently and no longer provides accurate predictions. Of course, it may be that no association will ever be made for some observation, perhaps because the data is corrupted or because the object has such low probability of detection that no element set can be maintained. The current practice is to retain all UCT data for up to 60 days for high-altitude orbits and up to 30 days for near-Earth orbits. Beyond these timespans, prediction accuracies have degraded so much that the chance of making correct associations is practically nil.

Whenever the automatic system cannot associate observations with known satellites, orbital analysts must use special software tools to make the proper data association. Although the analyst work is inherently slower than real-time, it is still essential to make the correct data associations as soon as possible. Human expertise built up through long experience has always been indispensable for this analysis. Moreover, satellite break-up events present special challenges because many unassociated observations and an unknown number of new satellites are involved. The number of association hypotheses that may have to be investigated always goes up exponentially with the number of unassociated observations and rapidly becomes unmanageable without human expertise to identify the most probable associations a-priori. Recently, advanced computation and parallel processing techniques have made it possible for the analysts to consider many more association hypotheses than in the past. Nevertheless, human expertise is still crucial in the overall management of the cataloging system.

When the automatic identification fails to make associations, the analysts usually try a "manual identification" first. This involves relaxing the association tolerances in some systematic way to account for known or expected inaccuracies in the element sets and observations. The tool SID

identifies position observations (including fence position fixes) by comparing all observations with each selected element set. The tool IDUAOB identifies angles-only observations (including fence direction cosines) by comparing all element sets with each selected observation. If any new associations can be made with these tools, the analysts may use MANDC to update the respective element sets in the database of known satellites.

If the manual identification cannot associate observations with known element sets, the analyst must generate new element sets from the UCT data. These candidate element sets are handled differently from the "analyst" element sets on known objects, because they have little statistical support. They are really only working hypotheses that may make it possible to associate data from different sensors or data that are widely separated in time. The candidate element sets are generated differently, depending on the sensor type.

For radar tracks with sufficiently many observations, it is relatively easy to generate a candidate element set. The main tool for creating single-track element sets is FORCOM. It can also compare other tracks and observations with predictions from the candidate element set, and can differentially correct the element set using observations that do associate with the predictions. Once FORCOM produces a candidate element set with reasonable statistical support, two other tools can be used to compare it with element sets on known objects or other candidate element sets. FNSORT compares two element sets by comparing their predictions. COMEL compares two element sets by comparing their element values directly. By one tool or the other, the analyst can usually decide whether two element sets belong to the same object. If they do, then the observations can be merged and a more refined element set produced via MANDC.

With fence position fixes and sparse radar tracks, it is not possible to generate sufficiently accurate single-track element sets. Therefore data that are widely separated in time must be associated before candidate element sets can be produced. In principle, one could consider generating all possible candidate element sets from the entire database of UCT observations. The tool SAD implements this approach. It takes a set of UCT observations selected by the analyst and generates an orbit through every possible pair of positions. Essentially, it solves Lambert's problem including secular perturbations. SAD also refines each candidate orbit in the same way that FORCOM does, so that finally some candidate orbits with reasonable statistical support are produced. These can be examined more closely with FNSORT and COMEL. Ultimately, the analyst may be able to produce some refined candidates via MANDC.

The only difficulty with SAD is that it generates a combinatorially large number of candidate orbits and compares each of these against the entire set of UCTs presented to it. In its original form, it required so much computation time that the analysts could not use it for the entire 30-day or 60-day collection of UCTs. The simple expedient of limiting the input to 5 days of UCT data (which still required several days of execution time!) did not work well. With such a short span of data, few orbits with reasonable statistical support could be produced. Instead, the analysts had to find ways to manually select UCT observations from the 30-day or 60-day time span that had high probability of originating from a small number of objects.

Several graphical tools were created to help with this selection job.

PLUME allows the analyst to select observations based on visual correlation in a plot of time differences relative to predictions from a reference (or "parent") element set.

TRIPLT allows the analyst to select fence position fixes based on visual correlation in a plot of fence data.

RAQUAD allows the analyst to group fence position fixes together by helping him find sequences of constant difference in right ascension with altitude constraints.

All of these tools have found some use, but none has provided a real solution of the problem. Of the three, PLUME finds the most use and works fairly well (in skilled hands) for finding pieces that have separated at low relative velocity from a parent satellite. But the real problem has always been that SAD inherently requires vast computations.

Recently, a parallel version of SAD was implemented at NAVSPACCOM on a cluster of 11 medium-performance workstations. It is able to process 30 days of UCT observations in about half a day and always produces a large number of candidate orbits with good statistical support. The reference by Coffey, et al., 1996, describes the parallel algorithm. As of July 1996, the tool is still being tested and qualified for operational use, but is already considered a breakthrough in UCT processing. It was used to process the Pegasus upper-stage break-up which occurred on 3 June 1996, a very timely application because that event turned out to be the largest satellite break-up to date (over 670 trackable pieces).

There are two other tools which are especially useful for satellite break-ups. COMBO finds the times and locations at which the distance between selected satellites is a local minimum. COMBO is used routinely when a break-up is suspected to see if the satellite in question could possibly have collided with a known object.

Similarly, BLAST computes the time and position of a satellite break-up once sufficiently many element sets for the pieces have been produced. It straightforwardly searches for the times at which the predicted positions cluster together and gives a statistical characterization of each cluster. Once the break-up time and position have been found, SAD can produce elements quite rapidly for all the remaining pieces that have been tracked. It does this by constraining all the candidate orbits to pass through the break-up position so that the number of candidate orbits is no longer combinatorially large.

Finally, some relatively new tools have been developed for historical analysis of the element set database. GOBS displays time histories of cataloged elements with analyst elements or UCT-derived elements superimposed. This allows the analyst to identify lost or mistagged objects. GOBS can also make reasonably accurate long-time predictions (on the order of years) for geosynchronous satellites, which aids UCT processing for that orbital regime.

HISTORICAL EXAMPLES OF SATELLITE BREAK-UPS

A few brief case histories are worth considering. More detailed information on all these case can be found in the reference by Grissom, et al., 1994.

1. TIROS N (11060)

This case illustrates the easiest possible break-up scenario. Single pieces separated from the parent satellite far apart in time so there was no uncertainty about which objects were the origin of the observations. Moreover, the orbits happened to be accurately represented by the current operational model. The satellite was operational from 13 October 1978 to 1 November 1980. At its altitude of over 800 km, it was expected to have a lifetime of about 350 years. Hence, any debris generated at this altitude could become an essentially permanent concern. Two pieces separated from the satellite in late 1987, on 28 September 1987, 1658 UT, and 4

October 1987, 2107UT, respectively. The analysts have high confidence in these times because the orbits were well determined and easy to predict. Interestingly, both pieces decayed during the winter of 1988-89, while the parent object still has a predicted lifetime over 300 years. This illustrates a common feature of break-ups, namely, that the fragments often decay much faster than the parent and consequently have very dissimilar body characteristics.

2. COBE (20322)

The Cosmic Background Explorer is in a sun-synchronous orbit similar to that of TIROS N. Beginning in January 1993, at least 12 well-defined single-piece separations were discovered over a 1-year period. Again, for the same reasons given above, the analysts have high confidence in the times of the separations.

Remarkably, however, the operators of the satellite noticed no anomalous behavior of the payload. By mid 1994, 40 pieces originating from COBE had been cataloged and were still in orbit, while the payload continued to function normally.

3. COSMOS 1823 (17535)

This was a geodetic satellite deployed at about 1500 km altitude. The break-up was especially interesting at the time because this type of satellite had few energy sources on-board that could explain the apparent explosion.

The break-up occurred on 17 December 1987. The first piece count was 22, made by the PARCS phased-array radar in Cavalier, North Dakota, in tracks taken between 2105UT and 2115UT. Between 2305UT and 2319UT, NAVSPASUR detected 35 pieces. Although the pieces remained relatively close together, analysis on 18 December 1987 produced 10 element sets and a probable "blast" point. NAVSPASUR analysts were also able to identify the main piece of the payload as that fragment with the orbit most similar to the parent object. By 3 weeks later, on 7 January 1988, 175 element sets had been generated and 33 had been cataloged. By mid-1994, 110 pieces had been cataloged and 44 were still in orbit.

4. COSMOS 1405 (13508)

This case presented some special difficulties for the break-up analysis that are typical of low-altitude break-ups. The satellite apparently exploded at 1214UT on 20 December 1983, at an altitude of 337 km. The "blast" point turned out to be relatively well-determined with a standard deviation of 6.5 km in position.

The first NAVSPASUR piece count showed 67 pieces crossing the fence between 1929UT and 1936UT on the same day, between 95 degrees and 102 degrees west longitude and between 247 km and 432 km altitude. However, it was difficult to generate orbits. All the pieces had high decay rates, and many re-entered before they could be adequately tracked. Moreover, the differential decay between pieces caused them to change their "parade order" between consecutive fence passes, making it difficult to make the correct associations.

By 2 weeks after the break-up, only 1 or 2 UCTs per day were being associated with this event, so it was not a serious operational problem. However, only 24 element sets were generated. Many of these were likely to have been spurious artifacts created by incorrect associations, and none of them were cataloged.

In the end, only 32 objects were cataloged and none remained in orbit by mid-1994.

5. EKRAN 2 (10365)

This case is revealing, because the break-up was first known to American personnel 14 years after it happened. EKRAN 2 apparently suffered an explosion on 23 June 1978 in geosynchronous equatorial orbit at 98.7 degrees east longitude.

The fact was communicated by Russian engineers and scientists in discussions with American space surveillance personnel in 1992. The SSN had been, and still is, unable to detect debris from the event.

6. TVSAT-1 and COSMOS 1646 (15653)

This case raised serious concern for the first time that a collision with untrackable debris had disabled a payload. In retrospect, such a collision appears very unlikely but the case is unusual nevertheless.

COSMOS 1646 broke up at 0131UT on 20 November 1987 at about 430 km altitude. By 21 November, the piece count was up to 50. Meanwhile, the payload TVSAT-1, an expensive joint European venture, was injected into geosynchronous transfer orbit at 0235UT on 21 November, at nearly the altitude of the COSMOS break-up.

The payload separated from the Ariane third stage at 0238UT and 30 seconds later crossed the plane of the COSMOS orbit. At 0244UT, the first payload anomaly appeared: a solar panel failed to deploy properly. Between 0530UT and 0726UT, the Ariane third stage was tracked by the ALTAIR radar on Kwajalein and was observed to have a very low thrust acting on it. The transfer orbit had been designed so that the upper stage would remain in orbit with a perigee altitude of about 179 miles. However, the low thrust caused the stage to make an unscheduled re-entry into the Pacific Ocean on the first revolution at 1249UT.

Some scientists speculated that small debris may have caused both the payload malfunction and the third-stage anomaly. NAVSPASUR analysts performed a COMBO analysis and found that both the payload and the rocket body did penetrate the envelope of the trackable COSMOS debris but did not come closer than 103 miles to any known piece.

24 pieces of the COSMOS were finally cataloged but all soon decayed, putting the whole case beyond further investigation. Of course, collision with small debris cannot be ruled out absolutely. However, it is considered very unlikely by all analysts who were involved in the analysis.

The payload eventually arrived on-station and was reported to be functioning normally. The Ariane vehicle had been suffering a series of technical problems at the time, but because the unscheduled re-entry caused no harm, the potential legal case about financial liability never materialized.

7. Clementine Rocket Body (22974)

The Clementine payload was injected into a circular parking orbit at 258 km altitude by a Titan II second stage on 25 January 1994. The payload itself proceeded on to the Moon successfully. However, the Titan stage broke up at 1719UT on 7 February 1994. The blast point was well determined with a standard deviation of 3.5 km, based on 26 orbits generated within 12 hours of the event. The early piece count by the fence was high: 364 pieces spread over altitudes of 200 km to 850 km, signifying an energetic event. Much concern was raised over the fact that both the Space Shuttle and the Mir space station passed through the debris cloud many times.

The Titan manufacturer initially reported that, although the second stage contained hypergolic propellants, the structural design precluded an inadvertent explosion. Some program officials alleged that a collision with untrackable debris was more likely than an explosion. No final report on the cause has reached NAVSPACCOM, and claims of collision have not been pursued, at least in the open literature. Meanwhile, 45 element sets were generated. None were cataloged, and no trackable pieces remain in orbit.

CONCLUSIONS

Based on the discussion thus far, we can make a few general conclusions. There are some tracking and cataloging problems that are readily solved by the current space surveillance system. It is relatively easy to determine the time and location of satellite break-ups by the orbital-mechanics techniques outlined here, and it is relatively easy to get a good piece count. Of course, we have to wait until the pieces have separated sufficiently, which usually occurs within a half a day to a day. But the fact remains that we can maintain the near-Earth catalog quite reliably, even when large break-ups occur.

On the other hand, there are some problems that we are not well equipped to handle with the current surveillance system.

- (1) It is very difficult to compute a reliable blast point immediately or within only several hours. The tracking coverage is not complete enough to produce the necessary observations that quickly, nor are the data association techniques good enough to produce reliable orbits for closely spaced pieces.
- (2) We do not have the tracking capacity, timeliness nor accuracy to support precise conjunction calculations.
- (3) We are unable at present to estimate the hazard to satellites of interest from untrackable debris. Efforts to extrapolate from the trackable population have not given satisfying results. It might be added that neither are we yet in a good position to assess the risk from trackable debris.
- (4) We have very limited capability to detect and track break-ups in geosynchronous equatorial orbit and geosynchronous transfer orbit.
- (5) We have never faced the situation in which we have multiple overlapping break-ups to catalog. It has always been possible for analysts to associate a UCT with the correct parent object once it has been determined that a break-up is in progress. With multiple simultaneous break-ups, this will no longer be true, especially if the break-ups occur in the same orbital plane.

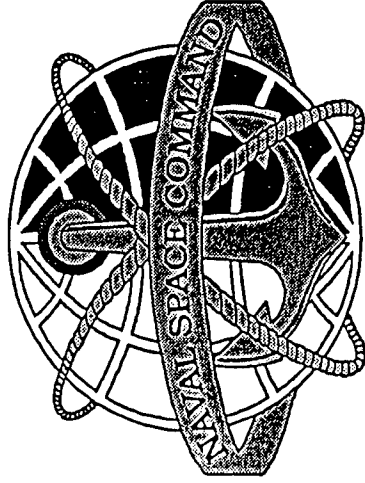
Naturally, this list is not comprehensive. But it does illustrate the fact that there is plenty of room for improvement in current space surveillance operations.

REFERENCES

Coffey, Shannon L.; Edna Jenkins; Harold Neal; Herbert Reynolds; "Parallel Processing of Uncorrelated Observations into Satellite Orbits". *American Astronautical Society (AAS) Paper 96-146, AAS/AIAA Astrodynamics Specialist Conference, Austin, Texas, 12-15 February 1996*. AAS Publications Office, P.O. Box 28130, San Diego, California 92198.

Grissom, I. Wayne; Robert P. Guy; David J. Nauer; "History of On-Orbit Satellite Fragmentations", *Eighth Edition. TBE Technical Report CS94-LKD-018, Teledyne Brown Engineering*, 1150 Academy Park Loop, Suite 111, Colorado Springs, Colorado 80910-3715. July 1994.

Tracking Satellite Break-Ups

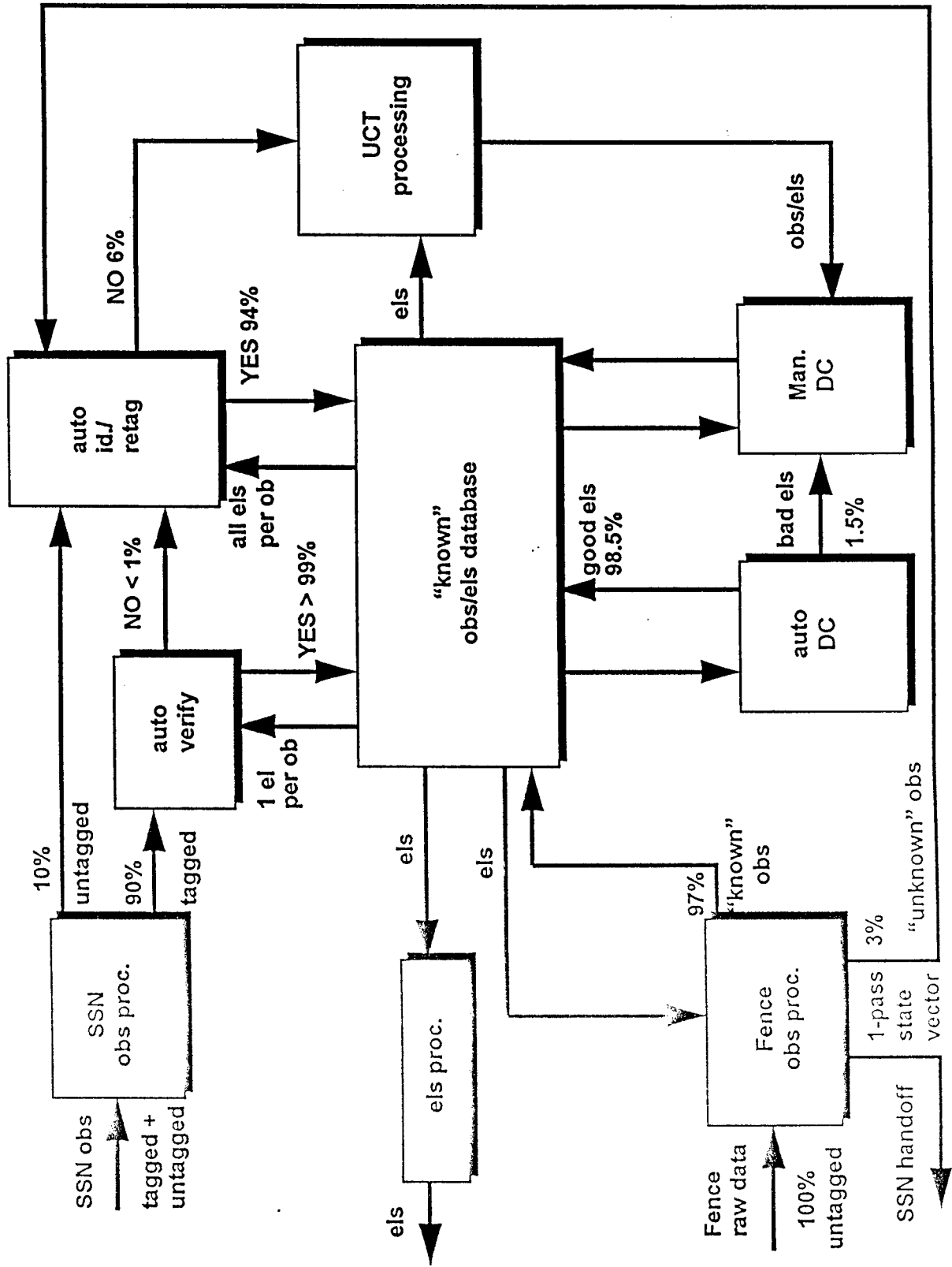


Paul W. Schumacher, Jr.
Naval Space Command
Dahlgren, Virginia

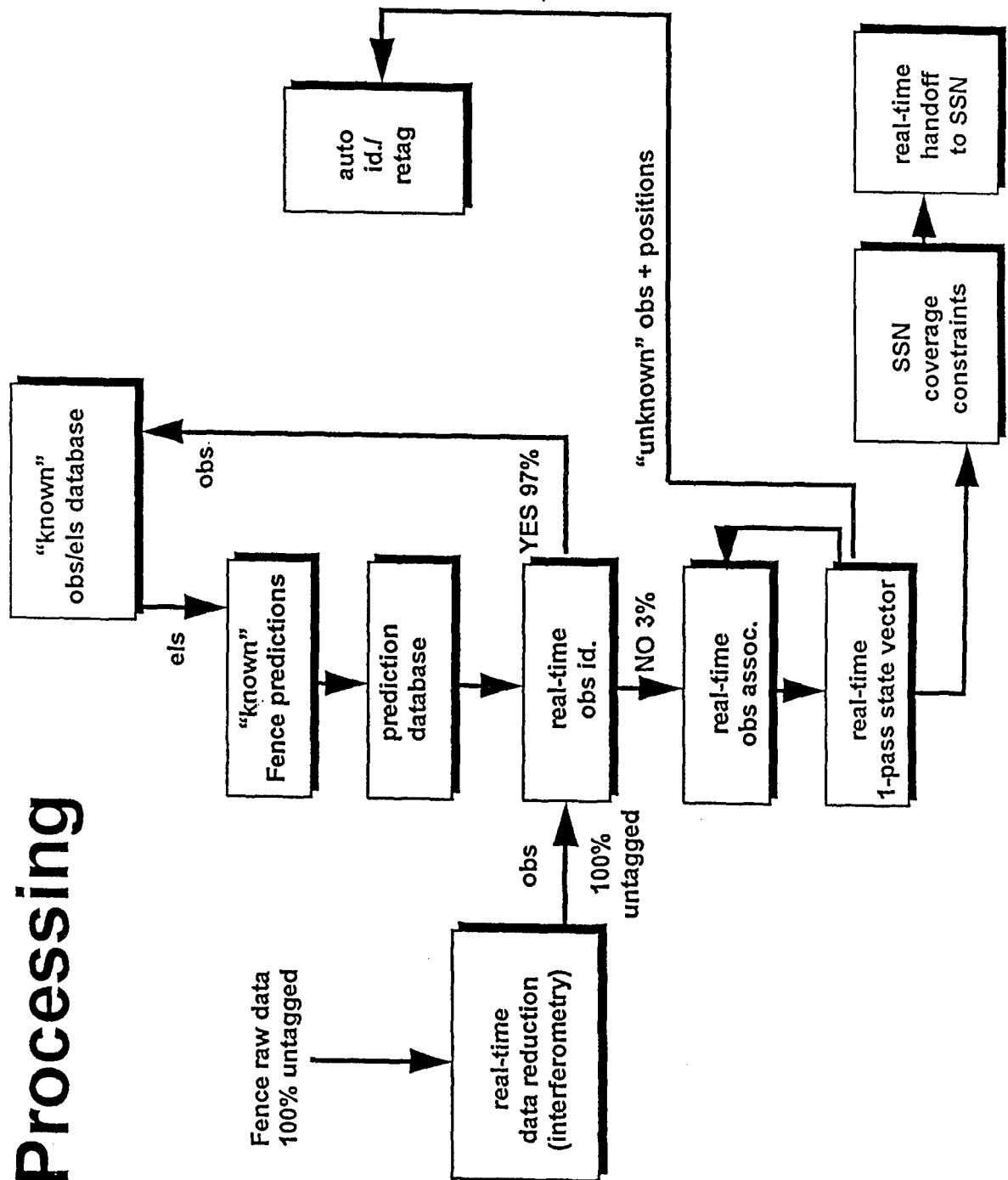
- **Space Surveillance Data Flow**
 - **Automatic Processing for Catalog Update**
 - **Analyst Tools for UCT/Break-Up Processing**
- **Historical Examples of Break-Ups**

Purpose: To understand which questions are easy, and which questions are hard, for the current surveillance system.

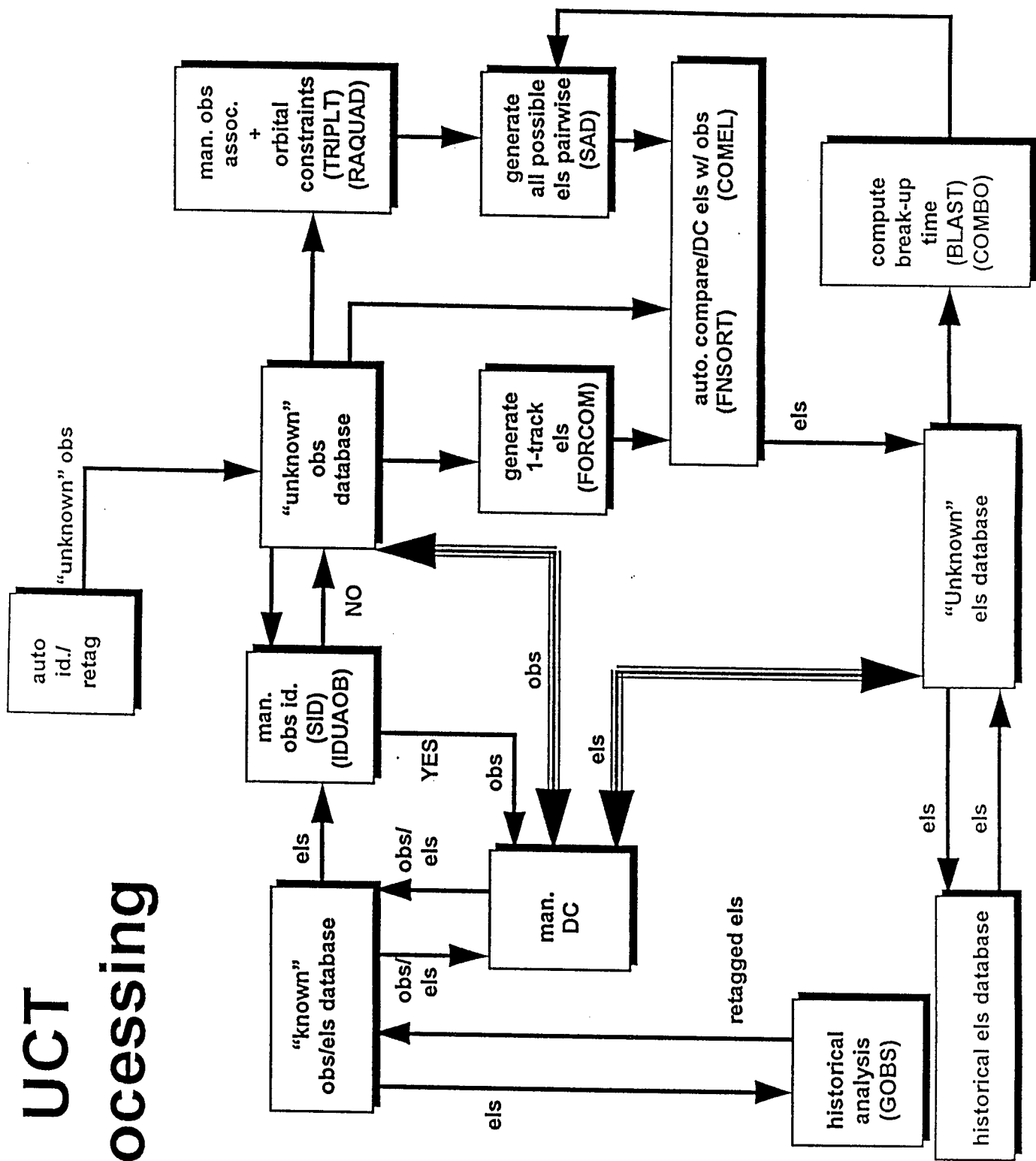
Dataflow for Catalog Maintenance



Fence Obs Processing



UCT Processing



Example: TIROS N (11060)

**835 x 855 km Altitude (350 Year Orbit Life)
99° Inclination**

- **Operational from 13 Oct 1978
to 1 Nov 1980**
- **Piece 1: 1658 UT 28 Sep 1987**
- **Piece 2: 2107 UT 4 Oct 1987**
- **Both Pieces Decayed During Winter 1988-89**

Example: COBE (20322)

871 x 886 km Altitude

99° Inclination

- **At Least 12 Well-Defined “Separation Events” Over a 1-Year Period Beginning Jan 1993**
- **40 Pieces Cataloged and Still in Orbit**

Example: COSMOS 1823 (Geodetic) (17535)

1454 x 1524 km Altitude
73.6° Inclination

- Break-Up on 17 Dec 1987
 - First Count: 22 Pieces
 - Second Count: 35 Pieces
 - Analysis on 18 Dec 1987
 - 3-Weeks Count : 175 el Sets (7 Jan 1988)
 - Final Count: 110 Cataloged
- 2105-2115 UT (Cavalier)
2305-2319 UT (NAVSPASUR)
- 10 el Sets and Blast Point
Id. Main Piece (Most Similar Orbit)
33 Cataloged
44 Still in Orbit (Mid-1994)

Example: COSMOS 1405 (13508)

311 x 335 km Altitude
65° Inclination

- Calculated Blast Point at 1214 UT 20 Dec 1983
23.7° S, 44.9° E, 337 km
(Std. Dev. = 6.5km)
- First NAVSPASUR Count: 67 Pieces
Between 1929 - 1936 UT
95° - 102° W
247 - 432 km Altitude
- High Decay; Variable “Parade Order”
- By T + 2 Weeks: 1-2 UCTs/Day
24 el Sets
None Cataloged
- Final Count: 32 Cataloged
None Remain in Orbit

Example: EKRA 2 (10365)

**35,790 km Altitude (Geosynchronous)
0.1° Inclination**

- **Break-Up on 23 June 1978
0.0° N, 98.7° E**
- **First Count: 1 Piece**
- **Final Count: 1 Piece (1992)**

Example: TVSAT-1 / COSMOS 1646 (15653)

- COSMOS: 400 x 433 km Altitude
65° Inclination
- Computed Blast Point: 0131 UT 20 Nov 1987
64.9° N, 60.3° W
Early Count: 50 Pieces
- TVSAT-1 / Ariane V20
21 Nov 1987
- Injection to GTO: 0235 UT
- Payload Separation: 0238 UT
- COSMOS Plane Crossing: 0238 UT+30 Sec.
- Payload Anomaly: 0244 UT
- 3rd Stage Anomaly: 0530-0726 UT
- 3rd Stage Re-Entry: 1249 UT

- NAVSPASUR COMBO Analysis
- Lockheed COMBO Analysis
- Final Count: 24 Cataloged
None Remain in Orbit

Example: CLEMENTINE Rocket Body (22974)

- **TITAN II 2nd Stage, Launched 25 Jan 1994**
258 km Altitude
67° Inclination
- **Break-Up Calculated at 1719 UT 7 Feb 1994**
59° S, 235° E
- **Std. Dev. 3.5km, Based on 26 Orbits Generated Within 12 Hours**
- **Initial Count (Fence): 364 Pieces**
200-850 km Altitude
- **Both Shuttle and Mir Passed Through the Debris Cloud Multiple Times**
- **Manufacturer's Conclusion About Cause**
- **Final Count: 45 el Sets Generated**
None cataloged
None Remain in Orbit

Conclusions

- **“Easy” Problems:**
 - Break-Up Time / Location
 - Piece Count (Trackable)
 - LEO Catalog Maintenance
- **Hard Problems:**
 - Immediate Answers
 - Precise Conjunctions
 - Untrackable Hazard to Other Sats
 - Tracking Break-Ups in GEO/GTO
 - Multiple Simultaneous or Overlapping Break-Ups

NAVSPOC Software Tools for UCT and Break-up Processing

SID	Position observation identification by comparing all observations with each selected element set.
IDUAOB	Angles-only observation identification by comparing all element sets with each selected observation.
TRIPLT	Association of "unknown" fence position estimates by visual correlation in a plot of selected data.
RAQUAD	Association of "unknown" fence position estimates by a search for sequences of constant difference in right ascension, with altitude constraints.
FORCOM	Orbit determination (element set generation) from single tracks of position observations, plus DC against selected "unknown" observations.
SAD	"Search and determine". Orbit determination (element set generation) from all possible pairs of selected "unknown" position observations (secular-perturbed Lambert solution), plus DC against all the remaining "unknown" observations.
FNSORT	Comparison of position observations with selected element sets, based on altitude constraints and closeness to each orbital plane. Optionally, compares element sets with element sets.
COMEL	Comparison of element sets to detect matches or duplicates in a selected list.
BLAST	Compute break-up time and position using predictions from selected element sets, by searching for times at which the predictions cluster together.
COMBO	"Computation of miss between orbits". Search for the times and locations of all close approaches between selected satellites, using predictions from two different lists of selected element sets.
GOBS	"Geosynchronous orbital belt study". Display historical plots of "known" element sets with "unknown" element sets superimposed, to try to identify lost, mistagged or "unknown" satellites.
MANDC	"Manual differential correction", in which the analyst has complete control over the least-squares fitting process. Data can be retained or rejected at will, any subset of a complete element set can be updated, arbitrary initial guesses for the solution can be used, and the convergence tolerances can be adjusted in any manner.

Glossary

SSN	Space Surveillance Network, made up of the fence operated by Naval Space Command, mechanical radars operated by the Army, and a variety of phased-array radars, mechanical radars and optical telescopes operated by Air Force Space Command.
obs	Metric observations of satellites (tracking data).
els	Orbital element sets (equivalent to state vectors).
fence	The NAVSPASUR multistatic continuous-wave radar interferometer, a unique space surveillance instrument whose fan beams lie in a great-circle plane inclined at about 33 degrees to the equator and extend across the southern United States. Coverage is continuous continent-wide, extending well out over both oceans and nominally to about 15,000 miles altitude.
DC	Differential correction, which produces updated orbital elements based on new tracking data by means of a least-squares estimation process.
UCT	"Uncorrelated target", an observation or trial element set which has not been associated with a "known" satellite.
"tag"	The satellite number in the space object catalog.
UT	Universal Time, formerly known as Greenwich Mean Time or "Zulu" time.
GEO	Geosynchronous equatorial orbit.
GTO	Geosynchronous transfer orbit.
LEO	Low Earth orbit.
NAVSPOC	Naval Space Operations Center at Naval Space Command, Dahlgren, Virginia, where Naval activities in space surveillance are headquartered.

UNIVERSAL SEMIANALYTIC SATELLITE MOTION PROPAGATION METHOD

V. Yurasov

SRC "Kosmos"

1. Introduction

The considered universal semianalytic method was developed and realized as a software on computer about 15 years ago. Basically it is used for testing specialized algorithms and programs for space object(SO) motion prediction in the RSSS. Besides it is applied for processing the measurement information on geostationary space objects, and also in works, connected with the ballistic maintenance of special important objects. Same examples of such work were the reentry of an orbital complex "Salyut-7" - "Cosmos-1686", satellites "Cosmos-398" and FSW-1-5. In this paper the basic principles of construction of a method are stated and estimations of the characteristics of its speed and accuracy are given.

The universality of the method is understood here as its suitability and flexibility for precision orbit prediction for various heights, eccentricity and inclination. The universality is achieved by choice of nonsingular orbit elements and taking into account perturbations from the Earth gravitational field, atmosphere drag, solar pressure, attraction of the Moon and Sun in the most general form.

The basic idea of semianalytic methods consists in separation slow and fast variables in the equations of space objects motion. Slow variables determine the form and orientation of an orbit in space. Fast variables characterize a movement of SO along the track and relative to the Earth. To separate fast and slow variables in the equations of motion a number of methods [1-3] are applied. Here an averaging method[1] was used.

2. Averaging method

The averaging method [1] is applied to the solving of systems of

ordinary differential equations, which are characterized by presence of slowly and quickly varying variables and periodicity of the right parts in relation to fast variable. More simple is the application of this method for systems with one fast variable. We shall consider this case as it is rather widespread: on account of zonal harmonics of geopotential, of atmosphere drag and both attraction of the Moon and Sun the SO motion is described by the equations with one fast variable:

$$\begin{aligned}\frac{dx}{dt} &= \varepsilon X_1(x, M) + \varepsilon^2 X_2(x, M) + \dots, \\ \frac{dM}{dt} &= n(x) + \varepsilon Y_1(x, M) + \varepsilon^2 Y_2(x, M) + \dots,\end{aligned}\quad (1)$$

where $x = (a, e, i, \omega, \Omega)$,

X_1, X_2, \dots – vector functions,

Y_1, Y_2, \dots – scalar functions,

ε – the small variable, for which is usually considered coefficient at the second zonal harmonic of geopotential.

In the method of averaging [2] with the help of replacement of a variable like

$$\begin{aligned}x &= \bar{x} + \varepsilon U_1(\bar{x}, \bar{M}) + \varepsilon^2 U_2(\bar{x}, \bar{M}) + \dots, \\ M &= \bar{M} + \varepsilon V_1(\bar{x}, \bar{M}) + \varepsilon^2 V_2(\bar{x}, \bar{M}) + \dots,\end{aligned}\quad (2)$$

the initial system of the motion equations (1) is reduced to the average system, containing no fast variable in the right parts:

$$\begin{aligned}\frac{d\bar{x}}{dt} &= \varepsilon A_1(\bar{x}) + \varepsilon^2 A_2(\bar{x}) + \dots, \\ \frac{d\bar{M}}{dt} &= n(\bar{x}) + \varepsilon B_1(\bar{x}) + \varepsilon^2 B_2(\bar{x}) + \dots\end{aligned}\quad (3)$$

The averaged system can be integrated analytically or numerically, but already with a much more large step, than initial system (1). Just due to this the semianalytic methods have gain in speed before numerical one.

The functions $A_1, A_2, B_1, B_2, U_1, U_2, V_1, \dots$ in the averaging method are defined in the following sequence:

$$\begin{aligned}
A_1(\bar{x}) &= \frac{1}{2\pi} \int_0^{2\pi} X_1 dM, \\
U_1(\bar{x}, \bar{M}) &= \frac{1}{n} \int (X_1 - A_1) dM + U_1^0(\bar{x}), \\
B_1(\bar{x}) &= \frac{1}{2\pi} \int (Y_1 + \frac{\partial \bar{n}}{\partial \bar{x}} U_1) dM, \\
V_1(\bar{x}, \bar{M}) &= \frac{1}{n} \int (Y_1 + \frac{\partial \bar{n}}{\partial \bar{x}} U_1 - B_1) dM + V_1^0(\bar{x}), \\
A_2(\bar{x}) &= \frac{1}{2\pi} \int (X_2 + \frac{\partial X_1}{\partial \bar{x}} U_1 - \frac{\partial U_1}{\partial \bar{x}} A_1 + \frac{\partial X_1}{\partial \bar{M}} V_1 - \frac{\partial V_1}{\partial \bar{M}} B_1) dM, \\
U_2(\bar{x}, \bar{M}) &= \frac{1}{n} \int (X_2 + \frac{\partial X_1}{\partial \bar{x}} U_1 - \frac{\partial U_1}{\partial \bar{x}} A_1 + \frac{\partial X_1}{\partial \bar{M}} V_1 - \frac{\partial V_1}{\partial \bar{M}} B_1 - A_2) dM + U_2^0(\bar{x}), \\
B_2(\bar{x}) &= \frac{1}{2\pi} \int (Y_2 + \frac{\partial Y_1}{\partial \bar{x}} V_1 - \frac{\partial V_1}{\partial \bar{x}} A_1 + \frac{\partial Y_1}{\partial \bar{M}} V_1 - \\
&\quad \frac{\partial V_1}{\partial \bar{M}} B_1 + \frac{1}{2} \sum_{j=1}^5 \sum_{k=1}^5 \frac{\partial^2 \bar{n}}{\partial \bar{x}_j \partial \bar{x}_k} U_{1j} V_{1k} + \frac{\partial \bar{n}}{\partial \bar{x}} U_2) dM,
\end{aligned} \tag{4}$$

and etc., where $U_1^0(\bar{x}), V_1^0(\bar{x}), U_2^0(\bar{x}), \dots$ - same functions, dependent from slow variables. It is possible to show that if these functions are identically zeros, the averaging method gives the same solution, as the Zeipel method [2]. However, unlike the last method an averaging method is applied not only to canonical systems of the differential equations.

Thus, the solution of the problem Cochi for system of the differential equations of SO motion (1) by use of a averaging method is made in three stages:

1. Calculation of mean elements $x(t_0), \bar{M}(t_0)$ from osculating elements $x(t_0), M(t_0)$, given in an initial moment of time t_0 , i.e. exception of short-periodical perturbations according to the formulas (2) in a moment t_0 is made.
2. By numerical integration of the averaged equations with a large step on an interval $[t_0, t_k]$ the mean elements $x(t_k), \bar{M}(t_k)$ at the moment of time t_k are determined.
3. With the help of formulas (2) osculating elements $x(t_k), M(t_k)$ are calculated on the base of of mean elements $x(t_k), \bar{M}(t_k)$, timed to the final moment t_k , i.e. calculation of short-

periodical perturbations for this moment t_k is made.

It should be noted, that if the mean elements are used instead of osculating elements as estimated parameters at orbit determination on measurements, the first stage of calculations is excluded. Thus, by use of semianalytical methods additional economy of computing expenses can be reached.

In [1] it is shown, that the solution 1-3 when using above algorithm of construction of the functions has an error of $O(\varepsilon^k)$ order with respect to the slow variables and $O(\varepsilon^{k-1})$ with respect to the fast variable on an interval of time $t \sim \frac{1}{\varepsilon}$, where ε^k - the order of terms, kept in the right parts of system (2).

3. Nonsingular orbit elements

As dependent parameters in the SO motion equations in the offered method nonsingular system of elements $x = (a, \xi, \eta, P, Q, \lambda)$ is used :

$$\xi = e \cos \pi, \quad \eta = e \sin \pi,$$

$$P = \sin \frac{i}{2} \cos \Omega, \quad Q = \sin \frac{i}{2} \sin \Omega, \quad (5)$$

$$\lambda = \pi + M,$$

where

a - axis,

i - inclination,

ω - argument of perigee,

Ω - longitude of ascending node,

M - mean anomaly.

As independent variable time t is used.

It is known, that the perturbation functions can be expressed directly through nonsingular elements of orbits (5). However in such a case the significant problems arrive with respect to getting effective fast algorithms. Therefore we decided to use the keplerian elements both in construction the relationships and in producing the software.

Let

$$\begin{aligned}\Lambda_1 &= \frac{da}{dt}, \quad \Lambda_2 = \frac{de}{dt}, \quad \Lambda_3 = \frac{1}{2} \cos \frac{i}{2} \frac{di}{dt}, \\ \Lambda_4 &= e \frac{d\pi}{dt}, \quad \Lambda_5 = \sin \frac{i}{2} \frac{d\Omega}{dt}, \quad \Lambda_6 = \frac{d\lambda}{dt} - n,\end{aligned}\quad (6)$$

$$\begin{aligned}\delta \Lambda_1 &= \delta a, \quad \delta \Lambda_2 = \delta e, \quad \delta \Lambda_3 = \frac{1}{2} \cos \frac{i}{2} \delta i, \\ \delta \Lambda_4 &= e \delta \pi, \quad \delta \Lambda_5 = \sin \frac{i}{2} \delta \Omega, \quad \delta \Lambda_6 = \delta \lambda,\end{aligned}\quad (7)$$

where n is the mean motion.

Then

$$\begin{aligned}\frac{da}{dt} &= \Lambda_1, \quad \frac{d\lambda}{dt} = n + \Lambda_6, \\ \frac{d\xi}{dt} &= \Lambda_2 \cos \pi - \Lambda_4 \sin \pi, \quad \frac{d\eta}{dt} = \Lambda_2 \sin \pi + \Lambda_4 \cos \pi, \\ \frac{dP}{dt} &= \Lambda_3 \cos \Omega - \Lambda_5 \sin \Omega, \quad \frac{dQ}{dt} = \Lambda_3 \sin \Omega + \Lambda_5 \cos \Omega.\end{aligned}\quad (8)$$

$$\begin{aligned}\delta a &= \delta \Lambda_1, \quad \delta \lambda = \delta \Lambda_6, \\ \delta \xi &= \delta \Lambda_2 \cos \pi - \delta \Lambda_4 \sin \pi, \quad \delta \eta = \delta \Lambda_2 \sin \pi + \delta \Lambda_4 \cos \pi, \\ \delta P &= \delta \Lambda_3 \cos \Omega - \delta \Lambda_5 \sin \Omega, \quad \delta Q = \delta \Lambda_3 \sin \Omega + \delta \Lambda_5 \cos \Omega\end{aligned}\quad (9)$$

4. Perturbations account

Common information about the considered perturbation factors are presented in table 1.

It is known that the basic advantage of semianalytic methods against numeric ones is large speed and high enough accuracy. At the development the universal semianalytical method this advantage is not so simply attainable. For this purpose it is required to receive special representation of expressions for the right parts of the averaged equations and short-periodical perturbations.

Table 1. The characteristics perturbations considered

Perturbations	Short-periodical perturbations	Averaging equations
Second zonal harmonic(C_{20})	<ul style="list-style-type: none"> • First order linear terms in $\xi, \eta, \dot{P}, Q, \lambda;$ • second order terms in α. 	First and second order terms relative to C_{20}
Harmonics lm of geopotential($2 \leq l \leq l_{max}$ $0 \leq m \leq l, lm \neq 20$)	Linear terms in general form	Linear terms, including resonance effects in general form
Attraction of Moon and Sun	Linear terms in general form	Linear terms in general form
Atmosphere drag (density model GOST 25645.115-84)	No	Linear and cross with C_{20} terms
Solar pressure	No	Linear terms of direct solar pressure[4]

These expressions have the following structure:

- for a case of the account of zonal harmonics

$$\Lambda_j = n \sum_{k=0}^{l-1} Q_k^{(j)}(a, e, i) J(k\omega); \quad (10)$$

- for a case of the account of resonance perturbations

$$\Lambda_j = n \sum_{r=1}^l \sum_{m=1}^l \sum_{q=r-l}^{r+l} C_{rmq}^{(j)}(a, e, i) S_{rmq}^{(j)}(\omega, \Omega, M, \Theta); \quad (11)$$

- for a case of the account of perturbations from the Moon and Sun

$$\Lambda_j = n \sum_{l=2}^{l_k} \sum_{m=0}^l \sum_{p=0}^l D_{lmp}^{(j)}(a, e, i) S_{lmp}^{(j)}(\omega, \Omega, F_k); \quad (12)$$

- for a case of perturbations from atmosphere drag and solar pressure $\Lambda_j = n \sum_k f_k^{(j)}(a, e, i) S(\omega, \Omega), \quad (13)$

For all perturbation forces expressions for calculaton of the right parts of the averaged equations are given as a sum of products of functions, dependent on a axis, eccentricity and inclination, and of trigonometrical functions, dependent on argument of perigee, ascending node and mean anomaly. As the axis, eccentricity and inclination do not experience perturbations of the first order relative to

C_{20} , the functions from these variables will be changed slowly. Use of spline approximation for these functions instead of labourious calculation of their values by complex formulas at each step of computation of the right parts of the averaged equations gives significant labour-saving effect.

The similar representation is used also for calculating account of short-periodical perturbations. So, the formulas for calculation of perturbations from a geopotential of the Earth look as follows

$$\delta\Lambda_j = \sum_{q=-q}^q \sum_{m=0}^l \sum_{k=q-l}^{q+l} (C_{qmk}^{(j)}(a, e, i) \cos \varphi + D_{qmk}^{(j)}(a, e, i) \sin \varphi), \quad (14)$$

$$\varphi = k\omega + (k + q)M + m(\Omega - \Theta).$$

5. Accuracy and speed estimation

The estimation of accuracy and speed of the method was carried out for five categories of SO orbits. The description of these categories of orbits is given in table 2. In the same table data on amount of estimations chosen for realization of orbits and their inclinations, eccentricities and heights ranges are resulted. All elements of orbits for realization of estimations were chosen from the real catalogue of space objects.

Table 2. Categories of orbits

Category number	Name	Eccentricity	Inclination, deg	Perigee and apogee altitudes, km	Number of orbits
1	Low Earth Orbit	0.00-0.03	25-98	175-420 206-580	34
2	Medium Earth Orbit	0.00-0.09	23-115	450-1200 550-1900	353
3	Half-day Period Circular	0.00-0.02	53-65	19340-20250 20220-20700	30
4	Half-day Period Eccentric	0.50-0.74	16-70	700-6400 34000-41000	114
5	Geostationary	0.00-0.02	0-16	34500-36000 35500-36600	432

The estimation of the characteristics of the universal semianalytical method was carried out on the basis of comparison of prediction results with results of numerical integration of the motion

equations in cartesian coordinates by the method Everchart [5,6]. The prediction interval for all realizations was chosen equal to 50 revolutions and the comparison of results was spent on the fiftieth revolution in ten points, in regular intervals distributed on orbits. The methodical errors of a semianalytic method were estimated in orbital system of coordinates. The radial (R) and binormal (W) errors were expressed in kilometers, temporary errors along the track (t) - in seconds. As for low-earth-orbital objects of an error along the track much depend on a atmosphere drag, for reception of similar statistical data, allowing to receive a more objective estimation of correctness of the account of perturbations due to atmosphere drag, normalized nondimensional parameter was used

$$\xi = \frac{\delta t}{\Delta t} 100\%, \quad (14)$$

where Δt - value of perturbation of a SO motion along the track due to the atmosphere drag.

The data on distribution of methodical errors of a semianalytic method are submitted on figure 1 - 5:

- On fig. 1 - for low-earth-orbital space objects;
- On fig. 2 - for medium-earth-orbital space objects;
- On fig. 3 - for half-day period circular space objects;
- On fig. 4 - for half-day period eccentrical space objects;
- On fig. 5 - for geostationary space objects.

Maximum values of universal semianalytic method errors and its run time evaluation are resulted in table 3. From submitted data follows:

- The methodical errors of the account of atmospheric perturbations by use of a semianalytical method do not exceed 5%. It is a quite allowable level of errors, as accuracy of account of density of atmosphere for modern atmosphere models density makes 10-30 %.
- As for medium-orbital, and for high-orbital circular space objects the maximum prediction errors on a radial and binormal direction have approximately one level and make about 30-50 meters. The errors along an orbit for these space objects reach 0.1-0.3 second and have linear character from an interval of

forecasting. They are explained first of all by incomplete exception of short-periodical perturbations at transition from osculating elements to average (2). At processing real measurements this maintenance is compensated at the expense of the appropriate correction of estimated parameters.

- For eccentric orbits a level of errors in 2-3 times more. This fact is explained by that in a universal semianalytic method decomposition on average anomaly is used which poorly converges at large eccentricities.

The universal semianalytic method at long-term motion prediction of circular orbits is ten times as fast than the numerical method. For eccentric orbits the gain in speed much less and makes 2-3 times.

Table 3. Characteristic of maximum methodical errors and speed

Category number	$\max \delta R $, km	$\max \delta W $, km	$\max \delta t $, sec	$\max \xi $, %	Gain in run time
1	0.10	0.05	-	4.5	≈ 25
2	0.02	0.03	0.10	-	≈ 15
3	0.010	0.005	0.012	-	≈ 10
4	0.15	0.08	0.56	-	≈ 3
5	0.02	0.04	0.30	-	≈ 10

6. References

1. Grebenikov E.A., Y.A. Ryabov. Constructive methods of nonlinear systems. Moscow, "Science", 1979.
2. Brouwer D., Clemence G. Methods of celestial mechanics. Academic Press, New York and London, 1961.
3. Nazarenko A.I., Skrebushevsky B.S. An evolution and stability of satellite systems. Moscow, "Mechanical Engineering", 1981.
4. Kozai Y. Effects of solar radiation pressure on the motion of an artificial satellite. Smithsonian Contr. Astrophys., vol. 6.
5. Everhart E. Implicit Single Sequence Methods for Integrating Orbits. Celestial Mechanics, vol. 10, 1974.
6. Sorokin N.A., Tatevjan S.K. The program "Forecast" for calculation of geodetic satellite orbits. "Satellite supervision", N 20, 1980.

Figure 1. Distribution of methodical errors on a radial, binormal directions and along the track for low-earth-orbital SO

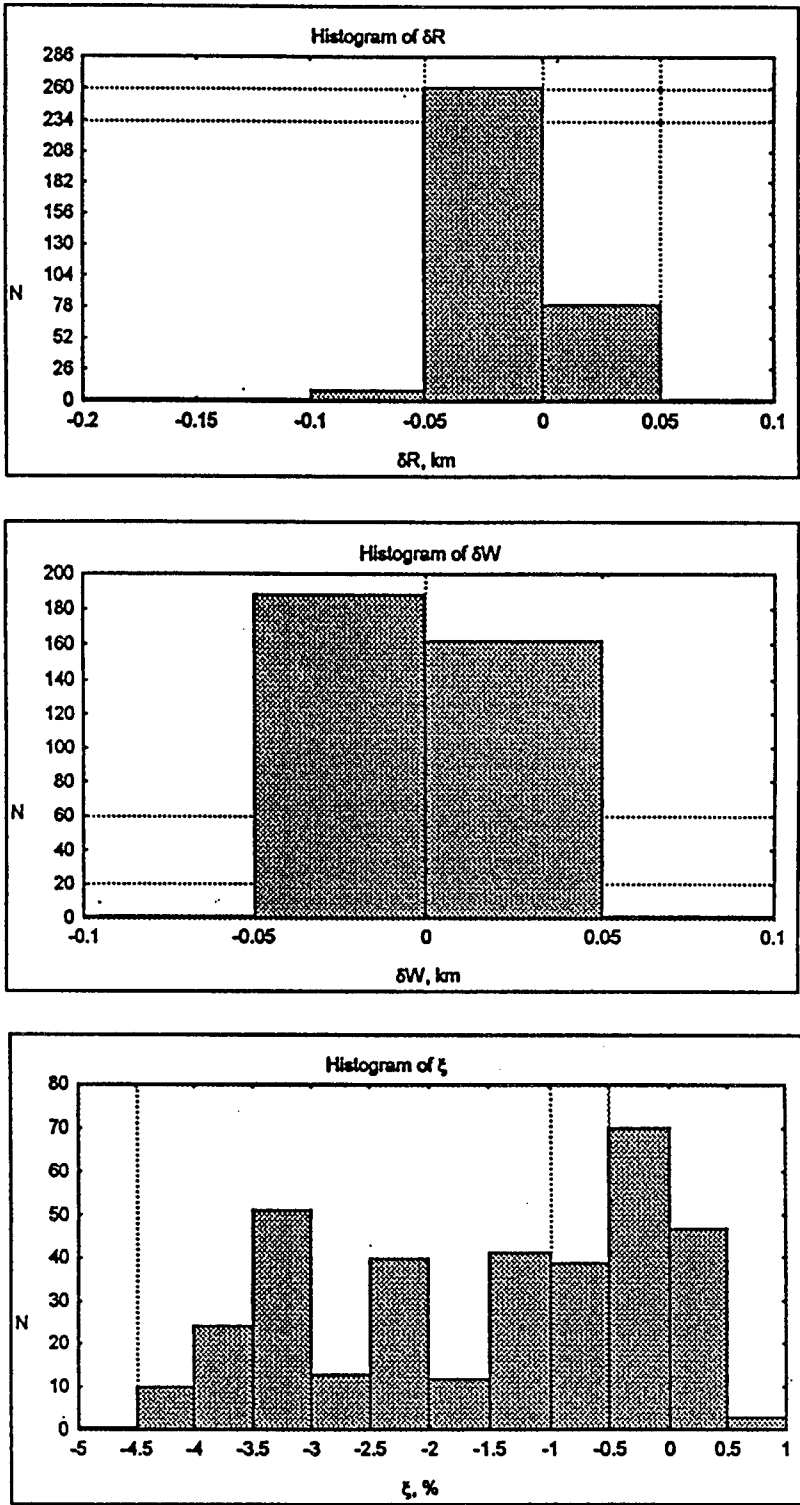


Figure 2. Distribution of methodical errors on a radial, binormal directions and along the track for medium-orbital space objects

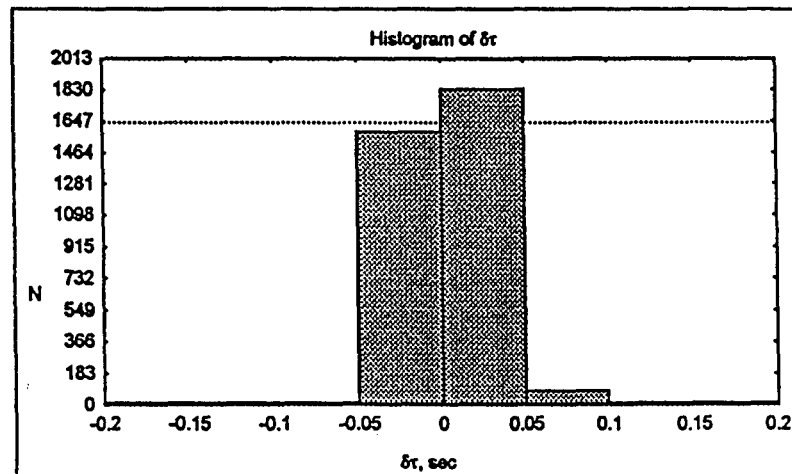
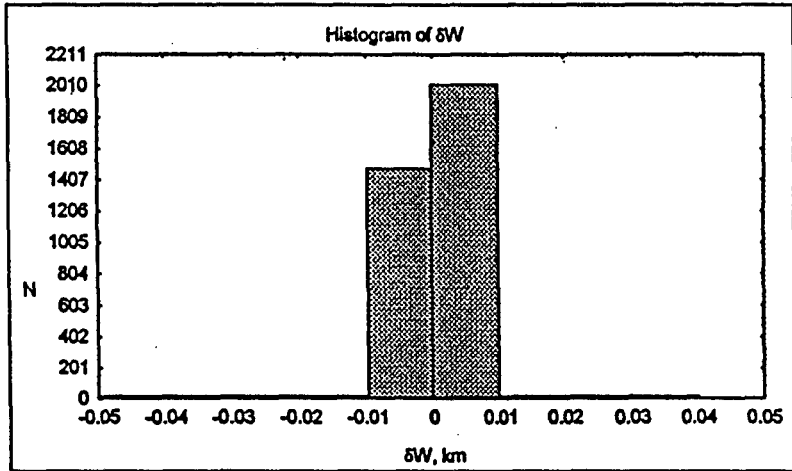
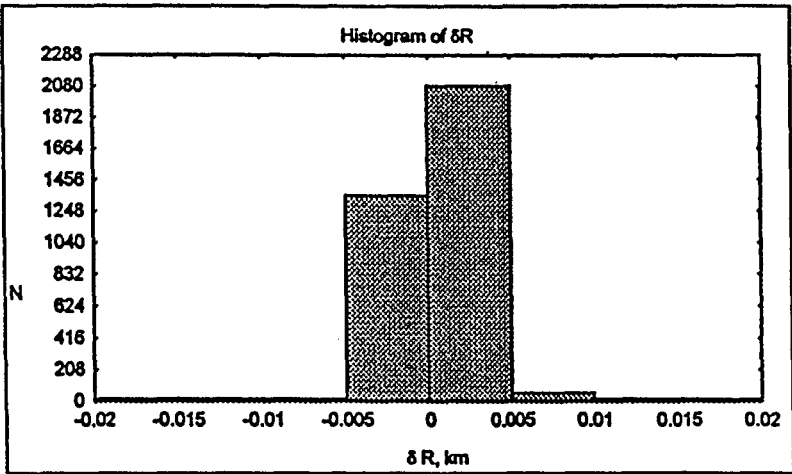


Figure 3. Distribution of methodical errors on a radial, binormal directions and along the track for half-day period circular space objects

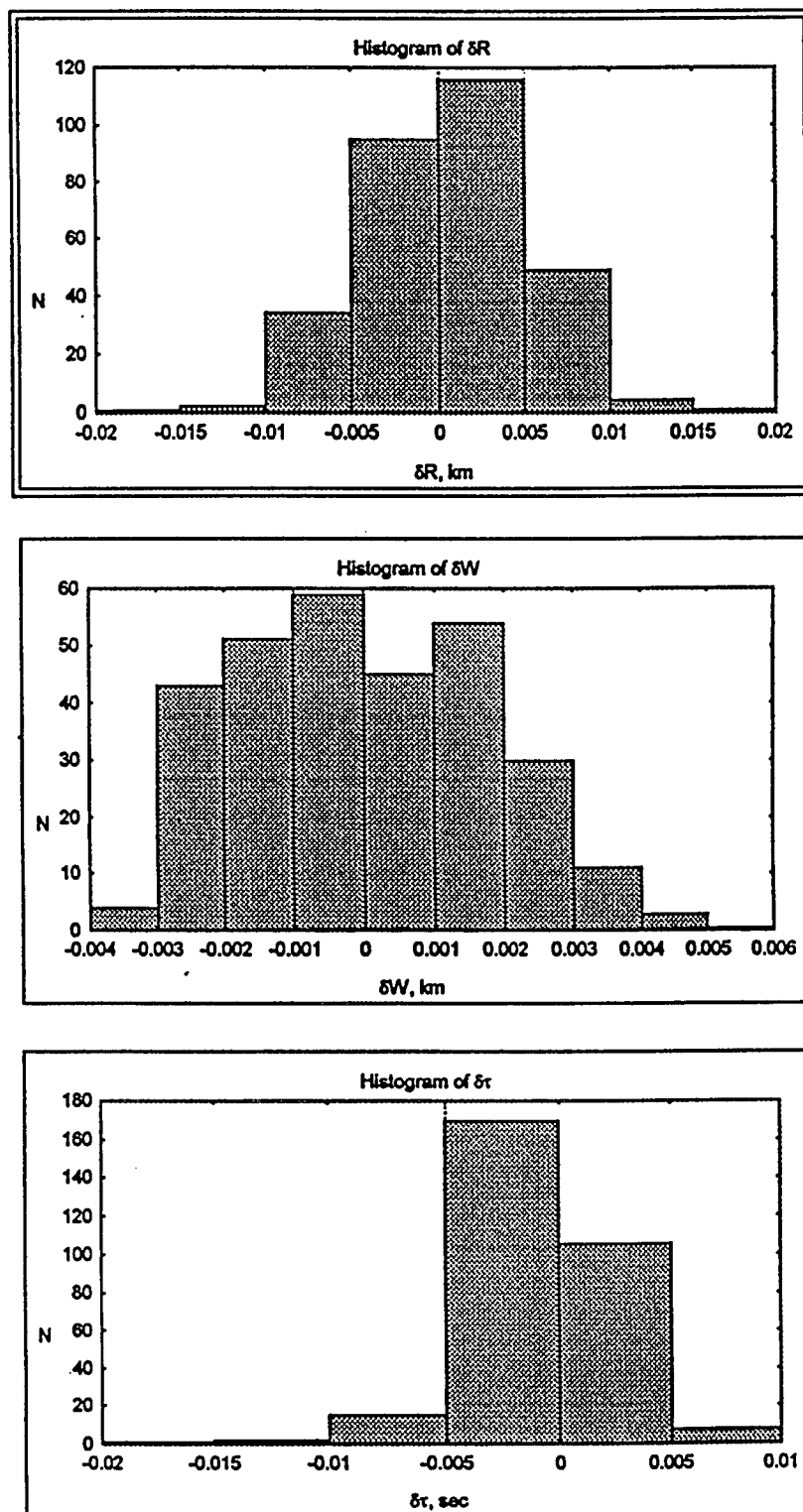


Figure 4. Distribution of methodical errors on a radial, binormal directions and along the track for half-day period eccentrical space objects

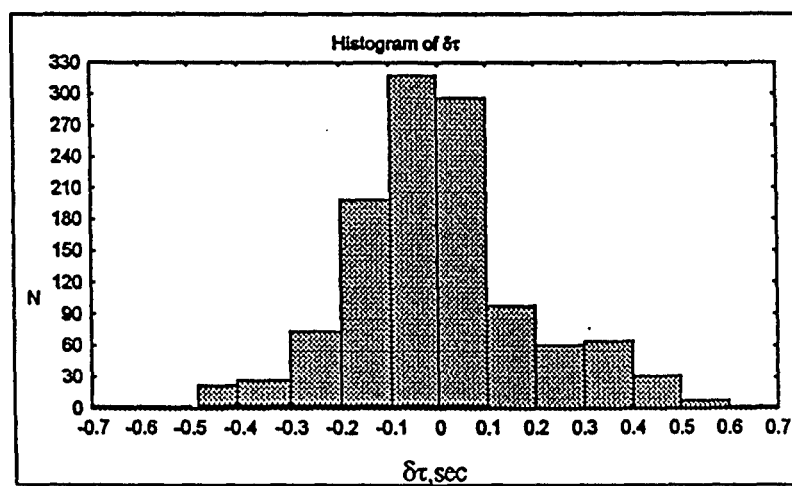
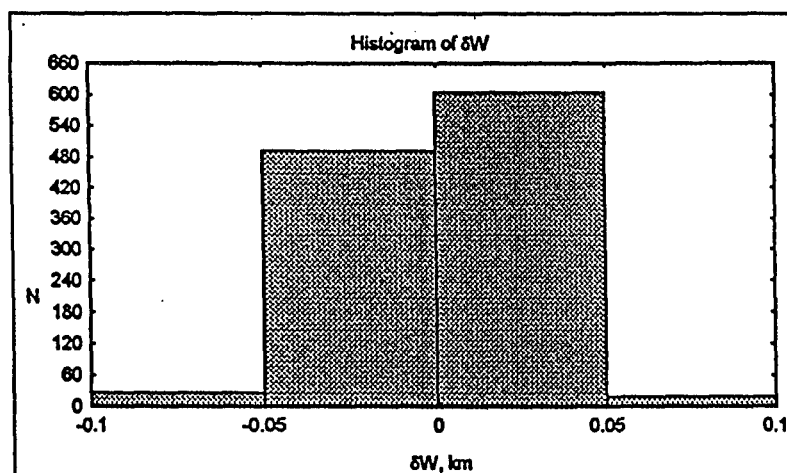
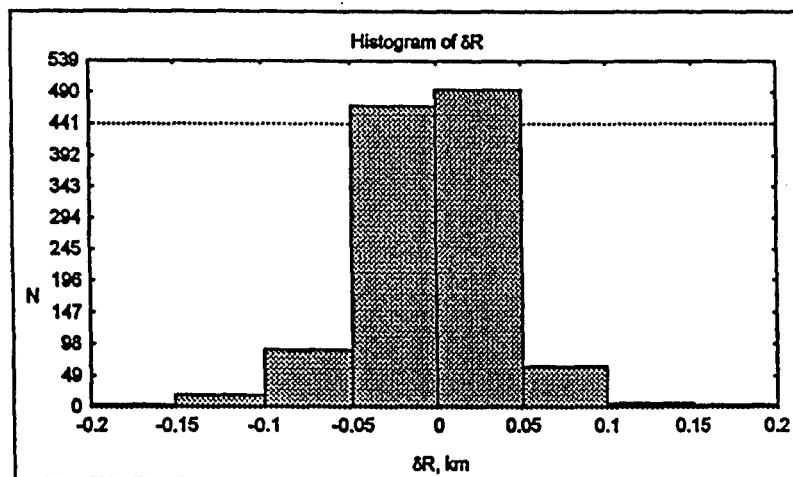
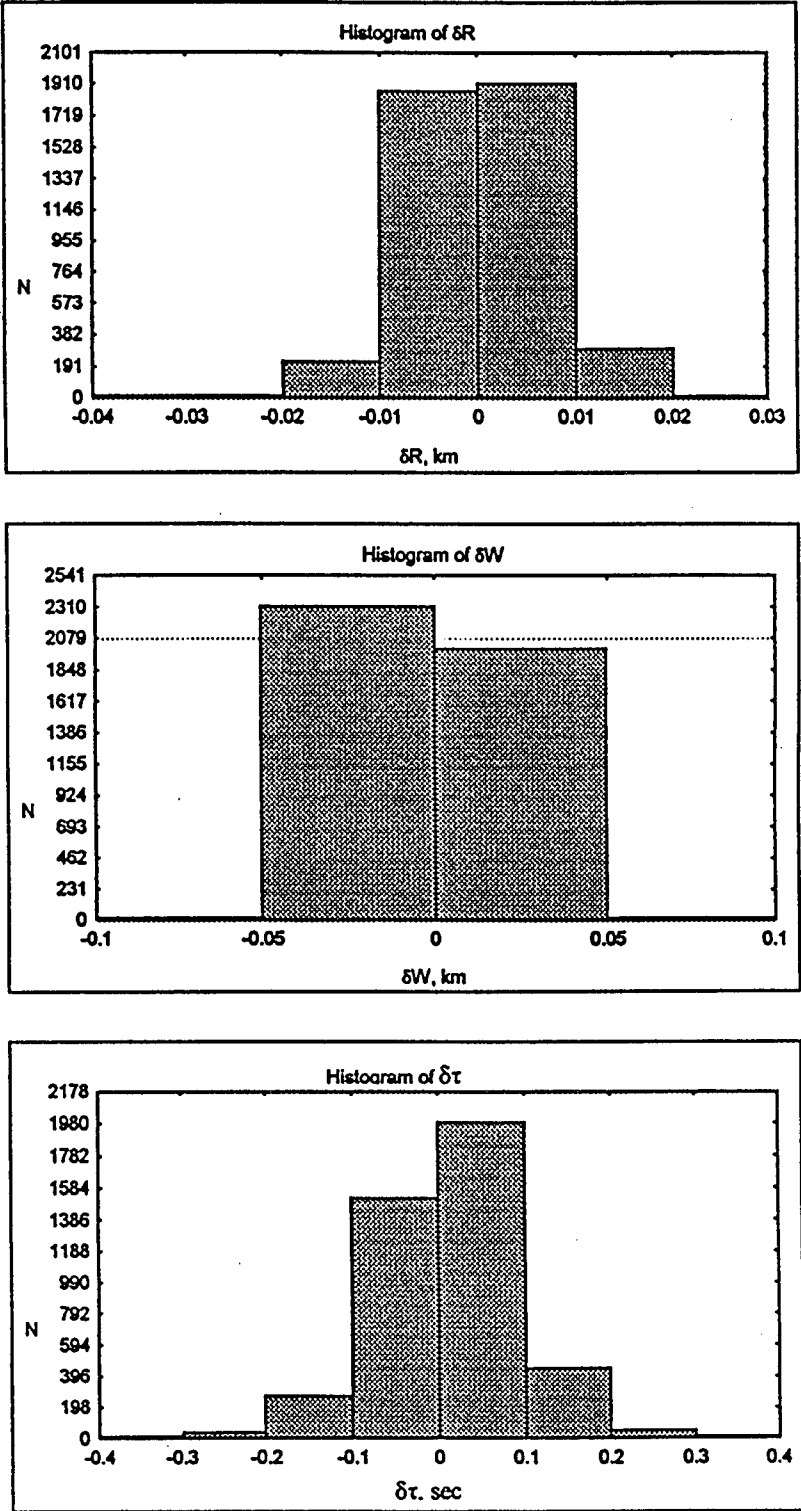


Figure 5. Distribution of methodical errors on a radial, binormal directions and along the track for geostationary space objects



CURRENT DEVELOPMENT OF THE PRECISION SEMIANALYTICAL SATELLITE THEORY

P. J. Cefola and R. J. Proulx

**The Charles Stark Draper Laboratory
Cambridge, MA, USA**

**3rd US / Russian Space Surveillance Workshop
4 - 6 July 1996 / Poznan, Poland**

OUTLINE

- Historical Perspective
- Initial Developments of Semianalytical Satellite Theory
- Expansion of the Geopotential in Equinoctial Elements
- Generalized Method of Averaging
- Semianalytical Satellite Theory Models
- Architecture of the Semianalytical Satellite Theory Implementation
- Comparison with External Reference Orbits
- Relationship between Semianalytical Theory Models and Canonical Satellite Theory
- Opportunities for Parallel Processing

HISTORICAL PERSPECTIVE, CIRCA 1973

- **Analytical Theories**

- Brouwer, Kozai, Vinti theories based on low degree geopotential (J2 thru J5)
- Extensions to include Atmospheric Drag
 - Brouwer-Hori, Vinti-Sherrill, Lane and Cranford
- Brouwer-Lyddane modification for small eccentricity, inclination
- Operational implementations of Brouwer, Kozai
 - SGP, SGP4, PPT2
- Higher Order Developments via Computer Symbolic Algebra and different perturbation formalism
 - Deprit

- **Numerical Satellite Theories**

- Higher degree and order geopotential (21 x 21)
- lunar-solar point masses
- atmospheric drag
- solar radiation pressure
- Multistep predictor-corrector numerical integration and interpolation techniques
- mainframe computer programs: DELTA, AOES, GTDS, TRACE, CELEST



INITIAL DEVELOPMENTS OF SEMIANALYTICAL SATELLITE THEORY

- Initial developments
 - low degree geopotential, lunar-solar point masses, atmospheric drag
 - long term motion of the mean Keplerian elements
 - mission analysis applications
 - Kaufman, Uphoff
- Developments employing the equinoctial elements
 - reformulated the disturbing potentials directly in the non-singular elements
 - numerical averaging for the non-conservative perturbations
 - same limited physical models as employed in the Keplerian semianalytical theories
- Arthur Fuchs' (NASA GSFC) question (1974):
 - Can we have a nonsingular, semianalytical theory that combines some of the best characteristics of Numerical and Semianalytical Satellite Theories?
 - comprehensive physical models
 - detailed model configuration at execution time
 - inclusion of short periodic motion
 - computational efficiency

EXPANSION OF THE GEOPOTENTIAL IN EQUINOCTIAL ELEMENTS

- Expression in spherical harmonics relative to the ECI frame
 - radial distance, latitude, and longitude
- Rotation of the spherical harmonics to the equinoctial orbital frame
 - Jacobi polynomials replace the Kaula inclination functions
 - stable recursion formulas are available in the mathematical literature
- Products of radius to a power times \sin or \cos of true longitude (and multiples) are expanded as a Fourier series in the mean longitude
 - Modified Hansen coefficients replace the Kaula eccentricity functions
 - stable recursion formulas due to Hansen (1855) were rediscovered in the astronomical literature

ROTATION OF THE SPHERICAL HARMONICS

- Generating function

$$P_{nm}(\sin \phi)e^{jm\alpha} = \sum_{r=-n}^n \frac{(n-r)!}{(n-m)!} P_{n,r}(0) S_{2n}^{(m,r)}(p,q)e^{jrL}$$

- where (for $m \geq 0$)

$$S_{2n}^{(m,r)}(p,q) = (1+p^2+q^2)^r (p-jq)^{m-r} P_{n+r}^{(m-r,-m-r)}(\gamma) \qquad r \leq -m$$

$$S_{2n}^{(m,r)}(p,q) = \frac{(n+m)!(n-m)!}{(n+r)!(n-r)!} (1+p^2+q^2)^{-m} (p-jq)^{m-r} P_{n-m}^{(m-r,r+m)}(\gamma) \qquad -m \leq r \leq m$$

$$S_{2n}^{(m,r)}(p,q) = (-1)^{m-r} (1+p^2+q^2)^{-r} (p+jq)^{r-m} P_{n-r}^{(r-m,r+m)}(\gamma)$$

- and $\gamma = \cos i$ $r \geq m$

MODIFIED NEWCOMB OPERATOR EXPANSION

• Standard Expansion

$$X_t^{n,s} = e^{|t-s|} \sum_{i=0}^{\infty} X_{i+a,i+b}^{n,s} e^{2i}$$

• New Expansion

$$X_t^{n,s} = (1 - e^2)^{n+3/2} e^{|t-s|} \sum_{i=0}^{\infty} Y_{i+a,i+b}^{n,s} e^{2i}$$

Convergence for the set of Hansen coefficients $X_t^{n,s}$ at $e = 0.7$ with relative accuracy 1.0D-5

$$a = \frac{|t-s| + t - s}{2}$$

$$b = \frac{|t-s| - (t-s)}{2}$$

n	s	t	N	Y
-3	0	1	17	6
-3	2	1	9	9
-4	-1	1	20	7
-4	1	1	20	7
-5	0	2	22	6
-5	2	2	23	7
-6	-1	1	25	6
-6	1	1	26	5
-6	-1	2	25	7
-6	1	2	25	7

GENERALIZED METHOD OF AVERAGING ASSUMPTIONS

- Osculating Element equations of motion:

$$\dot{a}_i = n\delta_{i,6} + \varepsilon F_i(a, \lambda)$$

- Mean Element equations of motion:

$$\dot{\bar{a}} = \bar{n} + \delta_{i,6} + \varepsilon A_{i,1}(\bar{a}) + \varepsilon^2 A_{i,2}(\bar{a})$$

- Expansion of the Osculating Elements in terms of mean:

$$a_i = \bar{a}_i + \varepsilon \eta_{i,1}(\bar{a}, \bar{\lambda}) + \varepsilon^2 \eta_{i,2}(\bar{a}, \bar{\lambda})$$

- Boundary Condition:

$$\int_0^{2\pi} \eta_{i,j}(\bar{a}, \bar{\lambda}) d\bar{\lambda} = 0$$

FIRST ORDER AVERAGED POTENTIALS AND GENERATING FUNCTIONS

- Definitions

$$\bar{R} = \frac{1}{2\pi} \int_0^{2\pi} R d\lambda$$

- Averaged Potential:

$$\tilde{R} = R - \bar{R}$$

- Short-Periodic Potential:

$$S = \int \bar{\lambda} \tilde{R} d\bar{\lambda}$$

- Generating Function:

$$\Delta a_i = a_i - \bar{a}$$

- Short-Periodic Variation:

$$\dot{\bar{a}}_i = \bar{n} \delta_{i,6} - \sum_{j=1}^6 (\bar{a}_i, \bar{a}_j) \frac{\partial \bar{R}}{\partial \bar{a}_j}$$

• Mean Element Equations of Motion

$$\Delta a_i = -\frac{1}{\bar{n}} \sum_{j=1}^6 (\bar{a}_i, \bar{a}_j) \frac{\partial S}{\partial \bar{a}_j}$$

• Short-Periodic Motion

MEAN ELEMENT EQUATIONS OF MOTION

- Central-body gravitational spherical harmonics of arbitrary degree and order (zonals and tesseral resonance)
- J2-squared second order effect (explicit analytical expression, truncated on eccentricity)
 - J2-squared eccentricity-squared terms are neglected at present
- Third-body point mass effects (both single and double averaging theories)
- Atmospheric drag with J2 / drag coupling
- Solar radiation pressure with eclipsing

SHORT-PERIOD MOTION MODELS

- Central-body gravitational zonal harmonics of arbitrary degree
- Central-body gravitational m-daily sectoral and tesseral harmonics of arbitrary degree and order
- Central-body gravitational high-frequency sectoral and tesseral harmonics of arbitrary degree and order
- J2-squared and J2 / m-daily second order short-periodic variations
- Third-body point mass effects [both single (including WTD) and double averaging theories]
- Atmospheric drag
- Solar radiation pressure

SHORT-PERIOD MOTION FORMULAS

- Zonal Harmonics (closed form)

$$\Delta a_i = C_{i,0} + S_{i,0}(L - \lambda) + \sum_{k=1}^{2N+1} [C_{i,k} \cos(kL) + S_{i,k} \sin(kL)]$$

- Tesseral m-Dailies (closed form)

$$\Delta a_i = \sum_{k=1}^M [C_{i,k} \cos(k\theta) + S_{i,k} \sin(k\theta)]$$

- Tesseral Linear Combination Terms

$$\Delta a_i = \sum_k \sum_t [C_{i,t,k} \cos(t\lambda - k\theta) + S_{i,t,k} \sin(t\lambda - k\theta)]$$

- Lunar-Solar Point Masses (closed form)

$$\Delta a_i = C_{i,0} + \sum_{k=1}^{N+1} [C_{i,k} \cos(kF) + S_{i,k} \sin(kF)]$$

OTHER SEMIANALYTICAL SATELLITE THEORY MODELS

- Short-periodic models for the non-conservative perturbations
 - Atmospheric Drag
 - Solar Radiation Pressure
- Integration Coordinate Systems
 - True of Reference Date
 - Mean of 1950
- State Transition Matrix
 - Partial derivatives of position and velocity at arbitrary time with respect to epoch mean elements are required
 - State transition matrix for the mean element equations of motion
 - linear variational equations are integrated numerically
 - RHS's of v.e.'s are evaluated either analytically, or by finite differences, or by quadratures
 - Short-Periodic partial derivatives
- Weight Least Squares Estimation (Differential Correction)
- Hybrid Extended/Linear Kalman Filter

IMPLEMENTATION ARCHITECTURE

- Initialization of the Interpolator
 - Integration of the Mean Element Eqs of Motion
 - Low Order Hermite interpolator for the Mean Elements
 - Evaluation of slowing varying short periodic coefficients at selected points in the Mean Element interpolator interval
 - Low Order Lagrange interpolators for the short-periodic coefficients and perturbation phase angles (e.g. GHA)
- Output at Requestion Time
 - Evaluation of Mean Element interpolator
 - Evaluation of short-periodic coefficients and perturbation phase angles
 - Assembly of short-periodic variations
 - Assembly of the osculating equinoctial elements
 - conversion to position and velocity
- Refreshment of Interpolators
 - adjacent interpolator interval
 - 'seperated' interpolator interval

RECENT EXTENSIONS TO THE SEMIANALYTICAL THEORY

- **Modification of SST software to handle 50 x 50 geopotentials**
 - generalized array structure where the size of the geopotential is a parameter set at compile time
 - extensive stability tests of the recursive computations for the 50 x 50 case; initial testing for 70 x 70 case
 - need to implement normalized coefficient formulation at future time
- **Solid Earth Tide Model for the Mean Element Equations of Motion**
 - frequency independent Love number term
- **J2000 Integration Coordinate System Options**
 - Mean of J2000
 - True of Reference compatible with J2000
- **Instantaneous True of Date Output Option**
 - compatible with J2000
- **Earth Albedo Pressure model (in progress)**
- **Modified Newcomb operator database for moderate eccentricity orbits ($e = 0.35$)**

EXTERNAL REFERENCE ORBITS

- Intensive tracking
 - Satellite laser ranging
 - Differential GPS
 - DORIS on-board device (TOPEX)
- Very precise force models
 - JGM-2 70x70 Gravity Field
 - Lunar-Solar Point Masses
 - Solid Earth Tides
 - Atmos. Drag (Jacchia-Roberts)
 - Solar Radiation Pressure (Conical Model)
 - Earth Radiation Pressure
 - Ocean Tides
 - Rotational Deformation
- 15 cm maximum error, over the whole orbit (TOPEX)
 - NASA Goddard, University of Texas, CNES

LEAST SQUARES FIT OF SST THEORY TO TOPEX EXTERNAL REFERENCE ORBIT -- RADIAL FIT ERRORS

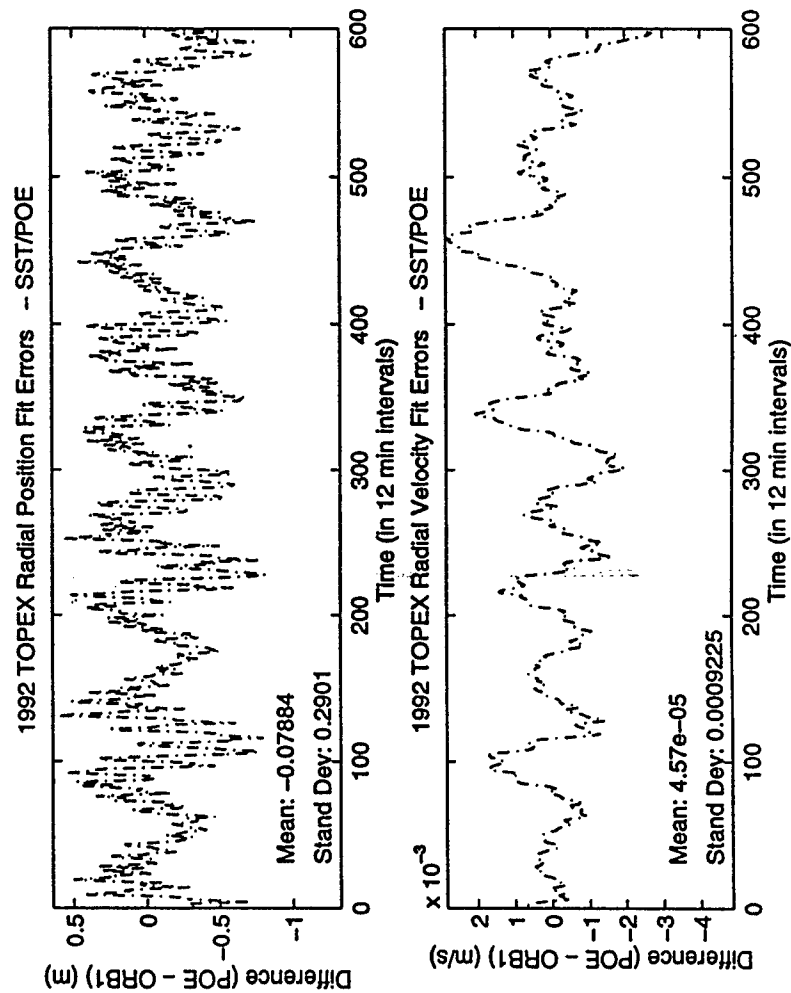


Figure 1. Radial Differences, Best Fit SST vs. TOPEX POE

LEAST SQUARES FIT OF SST THEORY TO TOPEX ORBIT -- CROSS-TRACK FIT ERRORS

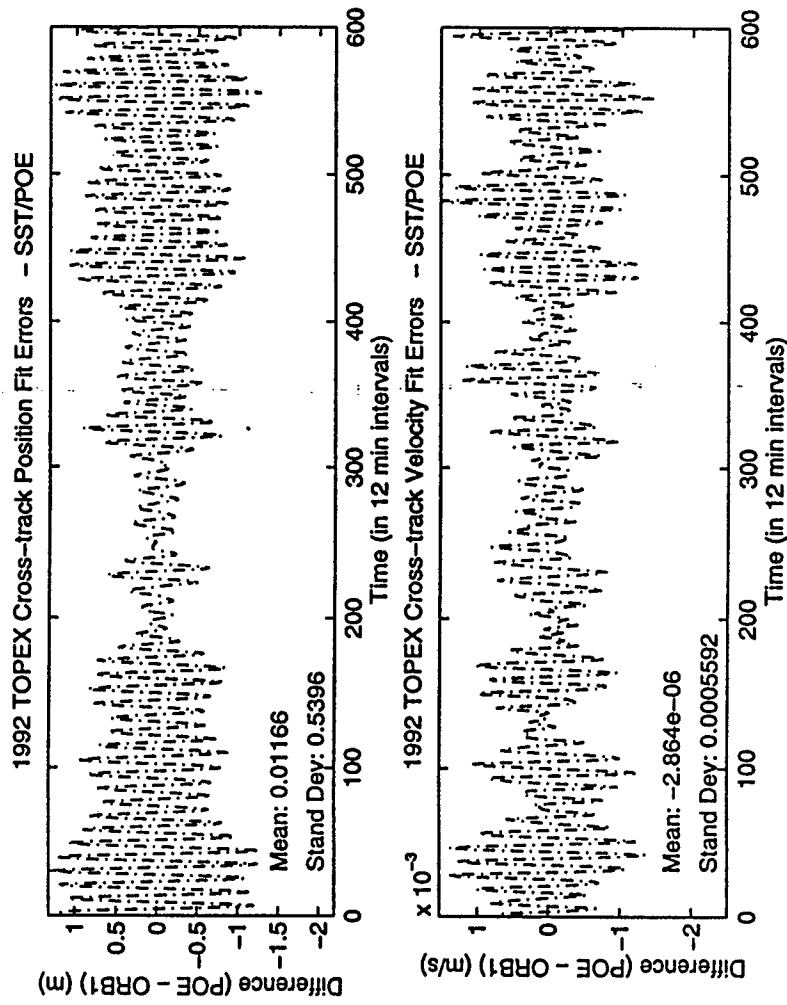


Figure 2. Cross Track Differences, Best Fit SST vs. TOPEX POE

LEAST SQUARES FIT OF SST THEORY TO TOPEX ORBIT -- ALONG-TRACK FIT ERRORS

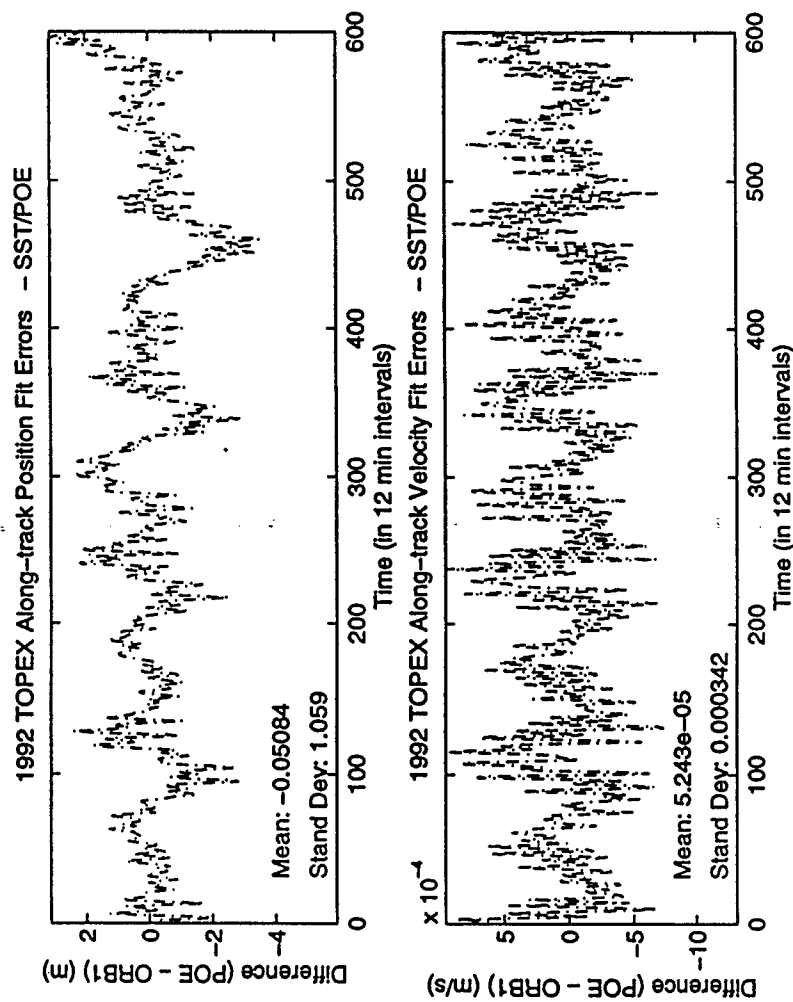
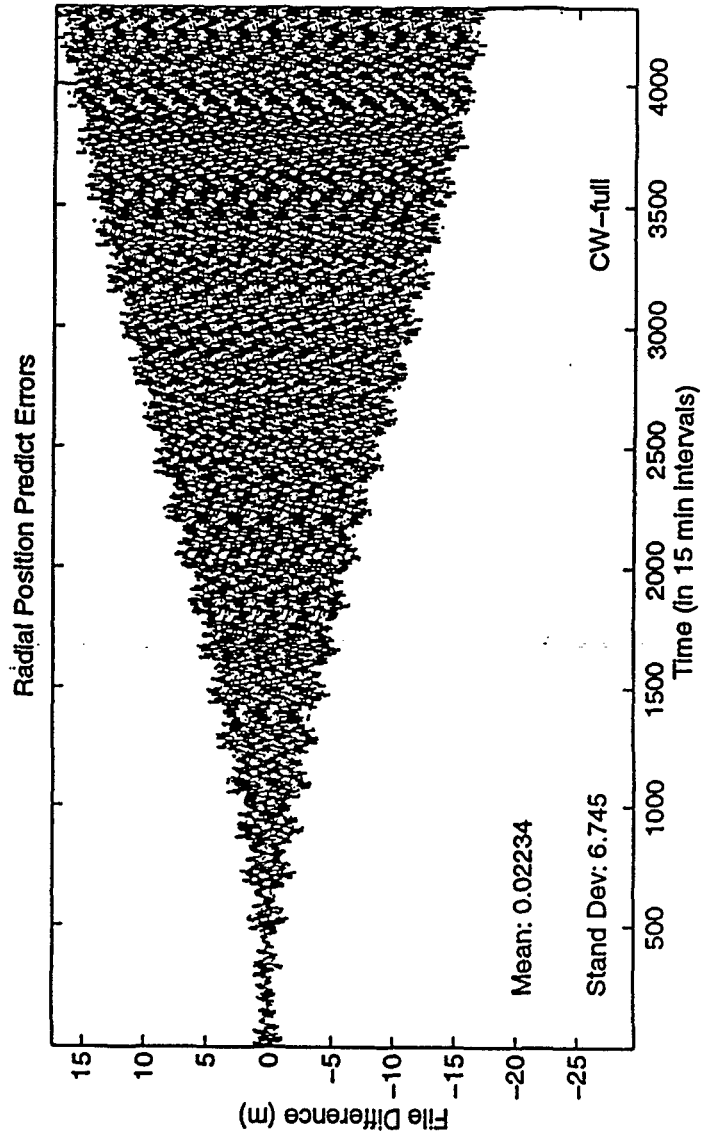


Figure 3. Along Track Differences, Best Fit SST vs. TOPEX POE

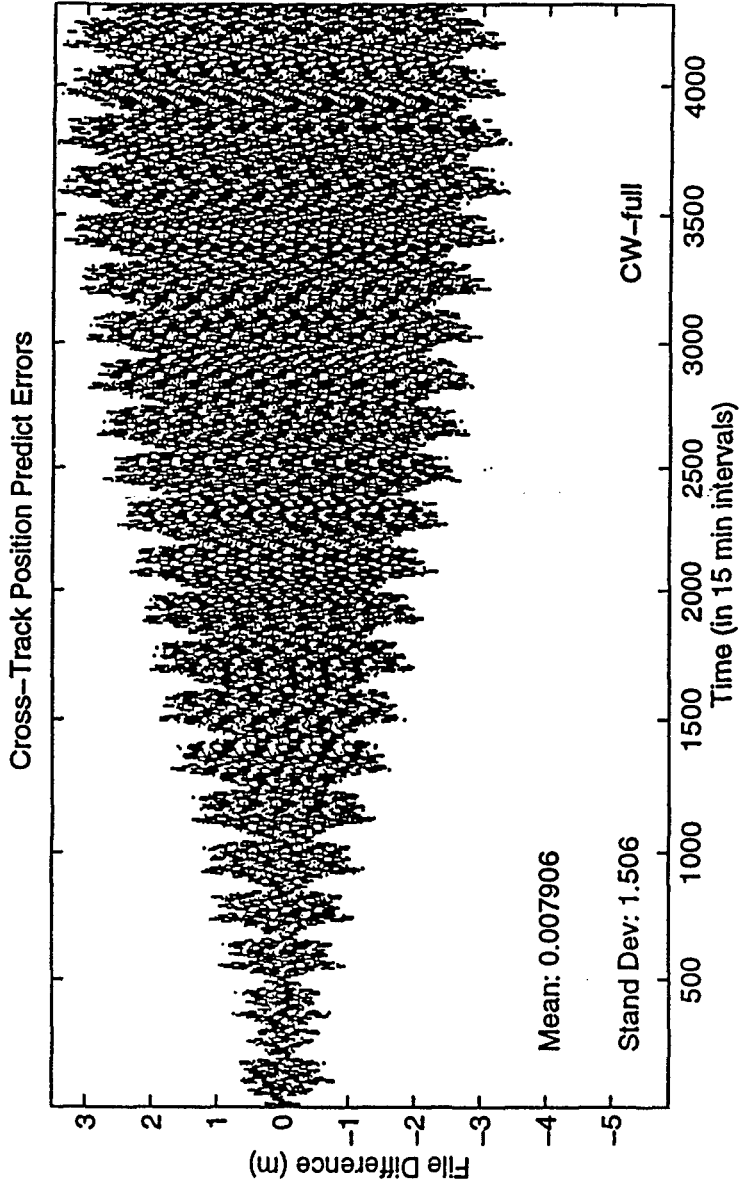
LONGER ARC TEST CASE

- **Cowell Truth Orbit**
 - Near Circular, Frozen Orbit at 1400 km
 - Inclination of 52 degrees
- **Truth force model**
 - 50 x 50 geopotential
 - Lunar-Solar point masses
 - Solar radiation pressure
 - Solid earth tides
 - Atmospheric drag (JR 71 with smoothed Schatten data base)
- **Scenario**
 - Truth orbit is 45 days long
 - Weighted least squares determination of the epoch mean elements (5 day fit)
 - 40 day prediction
 - Comparison of SST prediction with Cowell truth

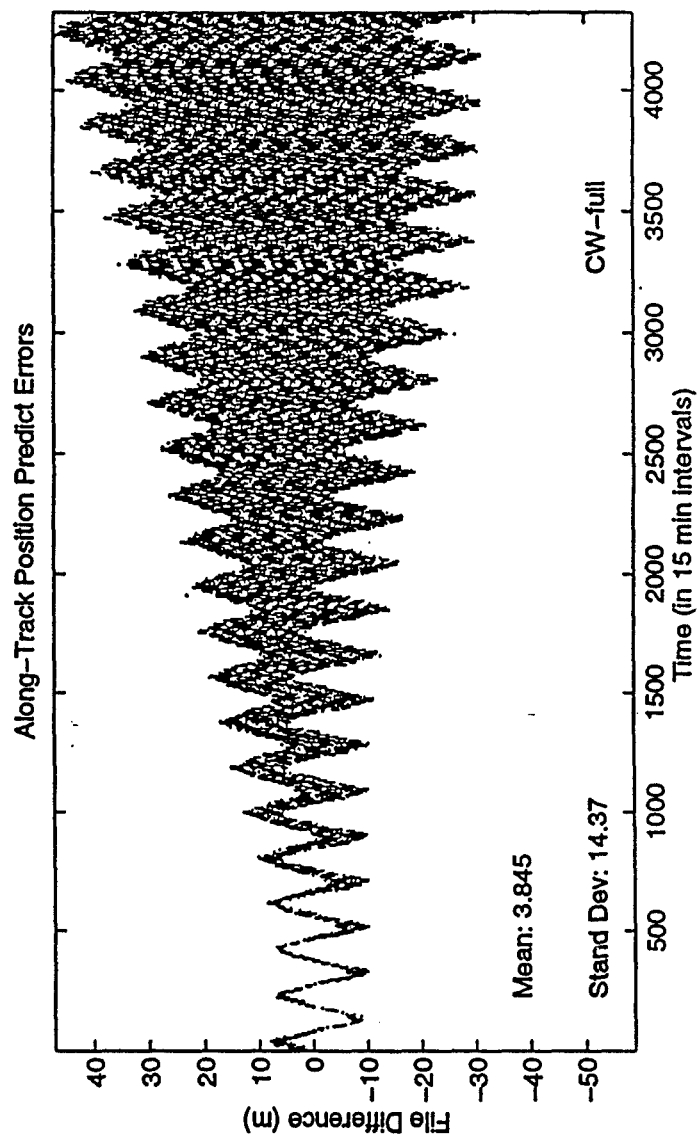
LONGER ARC CASE -- RADIAL PREDICT ERRORS



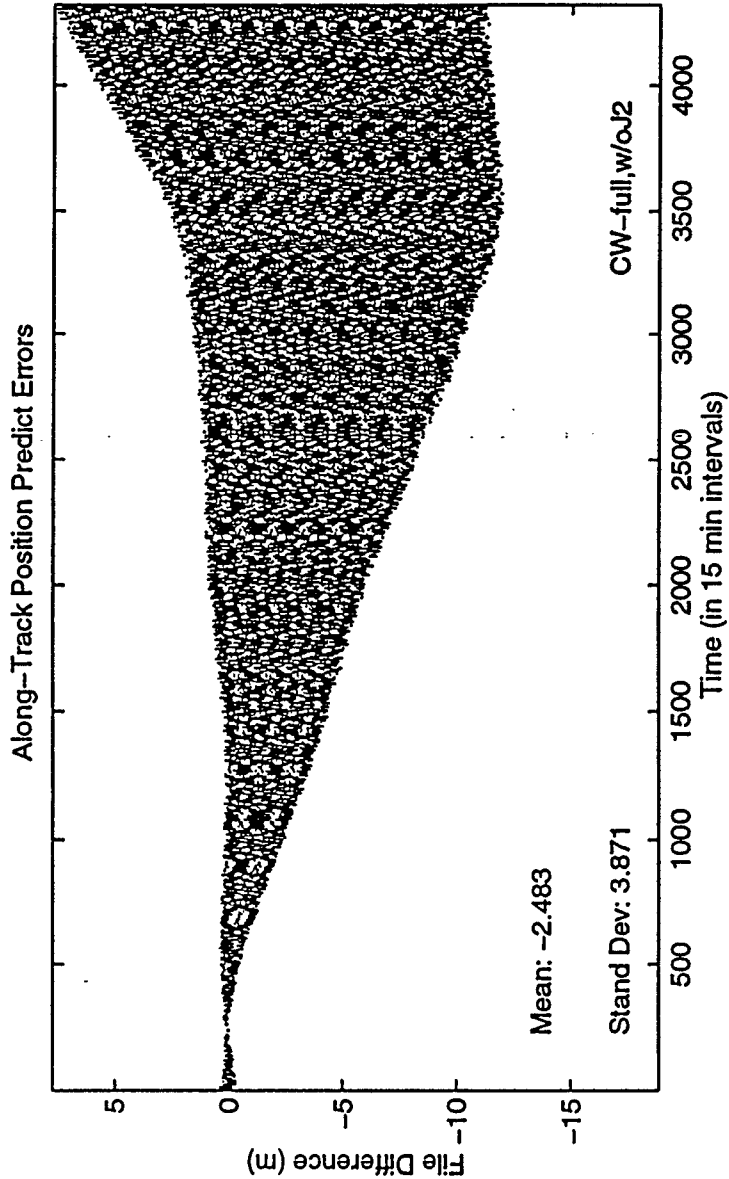
LONGER ARC CASE -- CROSS-TRACK PREDICT ERRORS



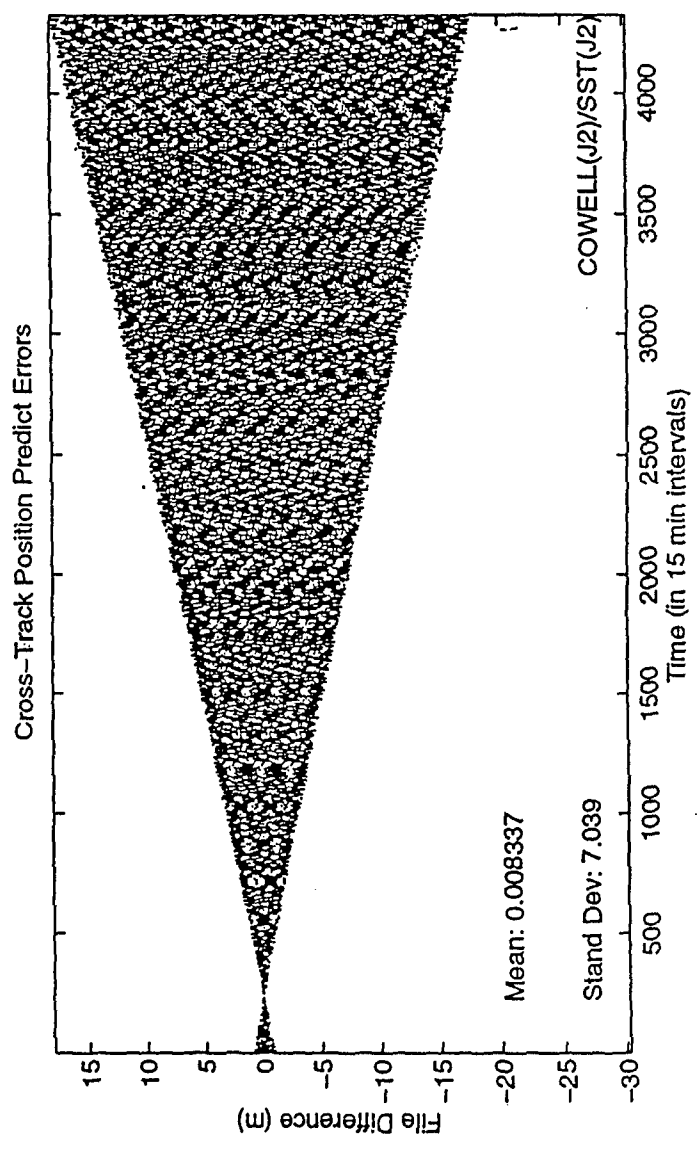
LONGER ARC CASE -- ALONG-TRACK PREDICT ERRORS



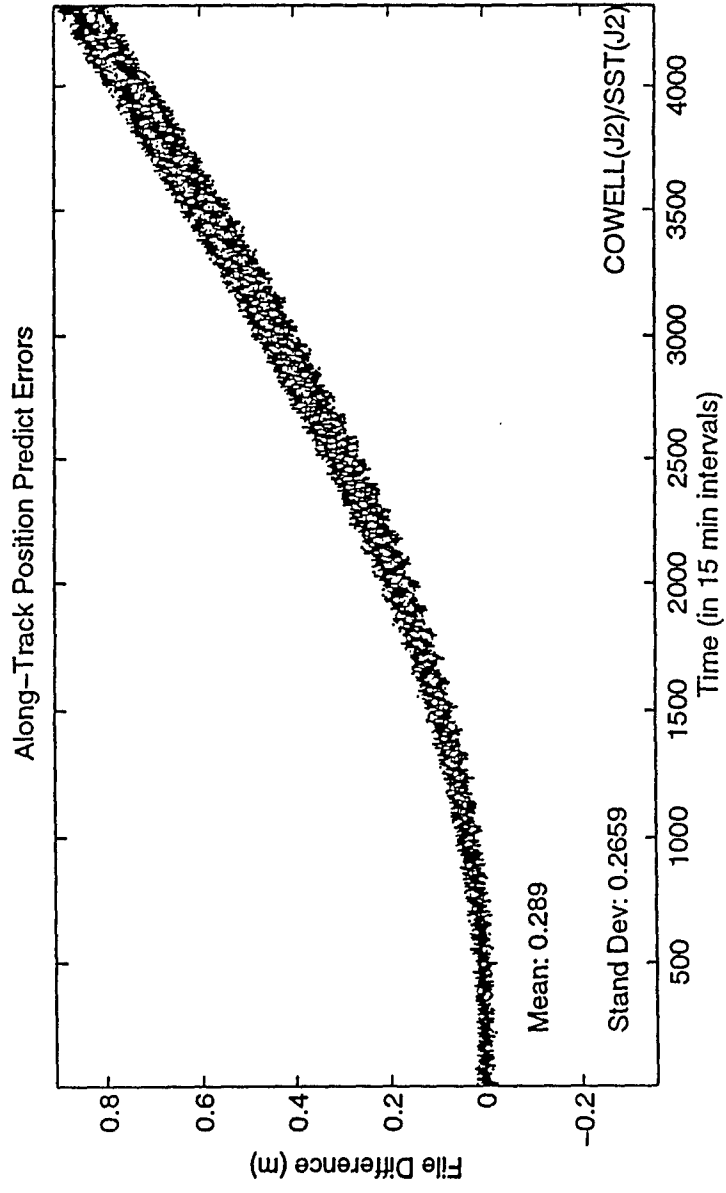
LONGER ARC CASE WITH REDUCED J2 -- ALONG TRACK



LONGER ARC CASE WITH J2 ONLY -- CROSS-TRACK



LONGER ARC CASE WITH J2 ONLY -- ALONG TRACK



SYNERGY BETWEEN SEMIANALYTICAL THEORY AND CANONICAL SATELLITE THEORIES

- Interest in understanding the relation between Analytical (GP) and Semianalytical Satellite Theories (SST)
- GTDS SST Orbit Determination System also hosts versions of SGP, GP4, HANDE, SALT, PPT2
 - Previous results indicated that 12 and 24 hour Tesserall M-Daily terms are a major error source
- Can the periodic models developed for the Semianalytical Theory be employed in enhanced GP Theories?
- Algorithmic approach
 - GP Theory provides at an arbitrary request time:
 - secular Keplerian elements
 - 'single-primed' equinoctial elements
 - osculating equinoctial elements including the J2 short periodics
 - Semianalytical Theory provides:
 - Tesserall M-daily corrections that can be appended to the J2 osculating elements

INTERFACE BETWEEN PPT2 AND SEMIANALYTICAL THEORY

- Expressions for the equinoctial elements in terms of the Lyddane intermediate quantities

$$a = a'' + \delta_2 a$$

$$e \sin(\omega + \Omega) = DE \sin(OS - l'') - DL \cos(OS - l'')$$

$$e \cos(\omega + \Omega) = DE \cos(OS - l'') + DL \sin(OS - l'')$$

$$\tan(i / 2) \sin \Omega = \frac{DI \sin(h'') + DH \cos(h'')}{\sqrt{1 - DI^2 - DH^2}}$$

$$\tan(i / 2) \cos \Omega = \frac{DI \cos(h'') - DH \sin(h'')}{\sqrt{1 - DI^2 - DH^2}}$$

$$M + \omega + \Omega = l'' + g'' + h'' + \delta_1 z + \delta_2 z$$

- Lyddane quantities for the 'single-primed' elements
- Lyddane quantities for the osculating elements

TAOS RADIAL DIFFERENCES VS. POE (PPT2 AND PPT2-MDAILY)

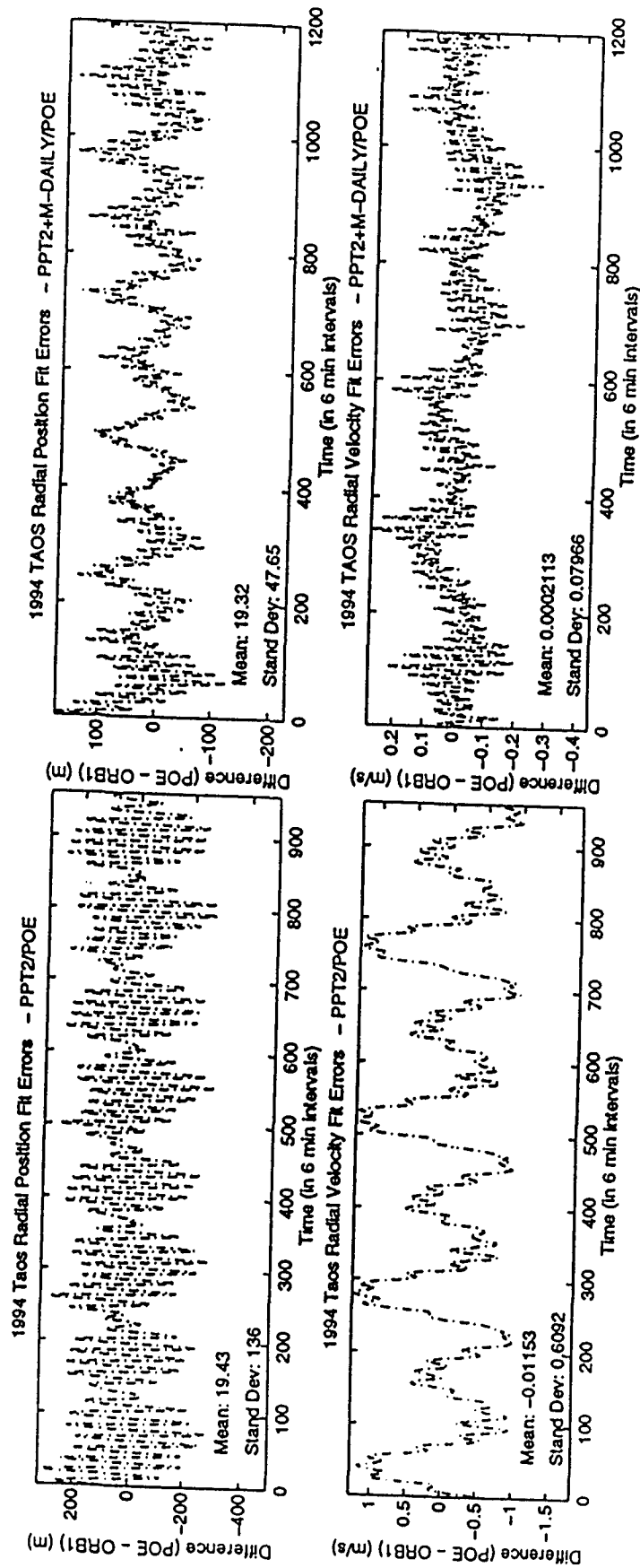


Figure 10. TAOS Radial Differences vs. POE (PPT2 and PPT2-MDAILY)

TAOS CROSS-TRACK DIFFERENCES VS. POE (PPT2 AND PPT2-MDAILY)

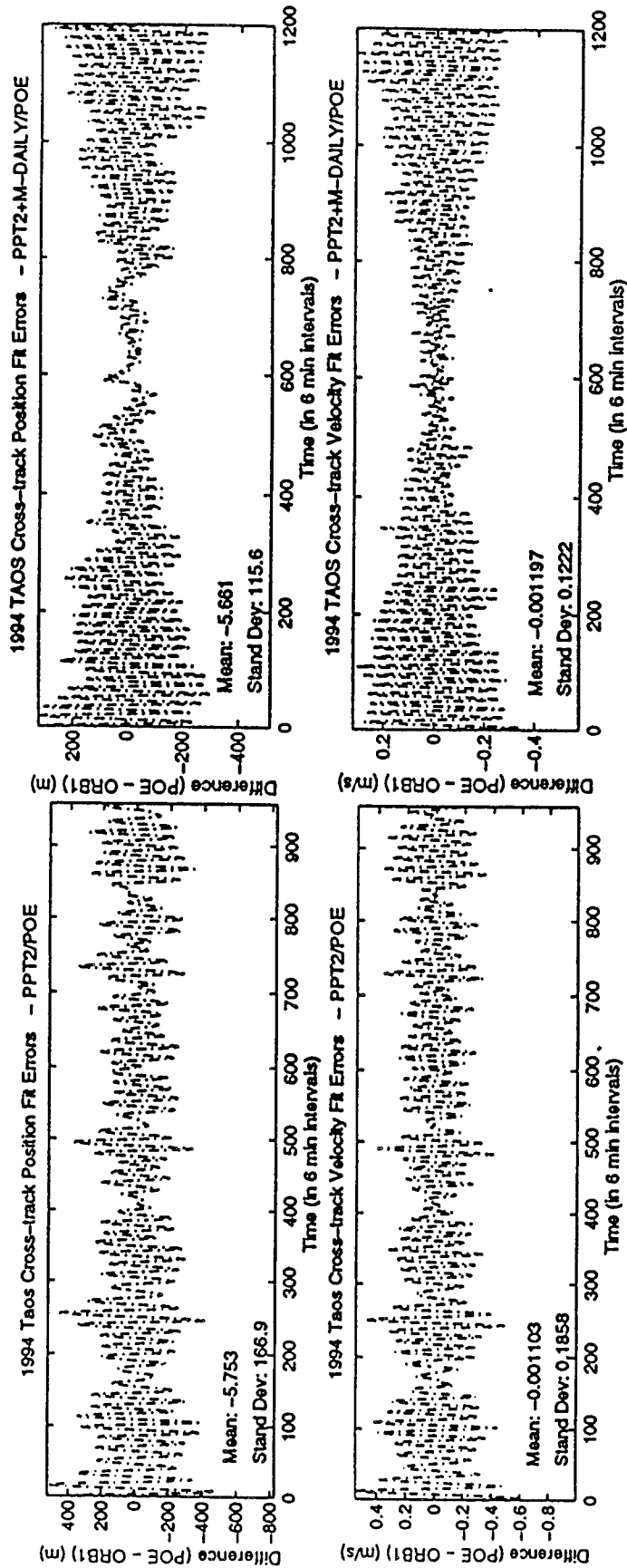


Figure 11. TAOS Cross Track Differences vs. POE (PPT2 and PPT2-MDAILY)

TAOS ALONG-TRACK DIFFERENCES VS. POE (PPT2 AND PPT2-MDAILY)

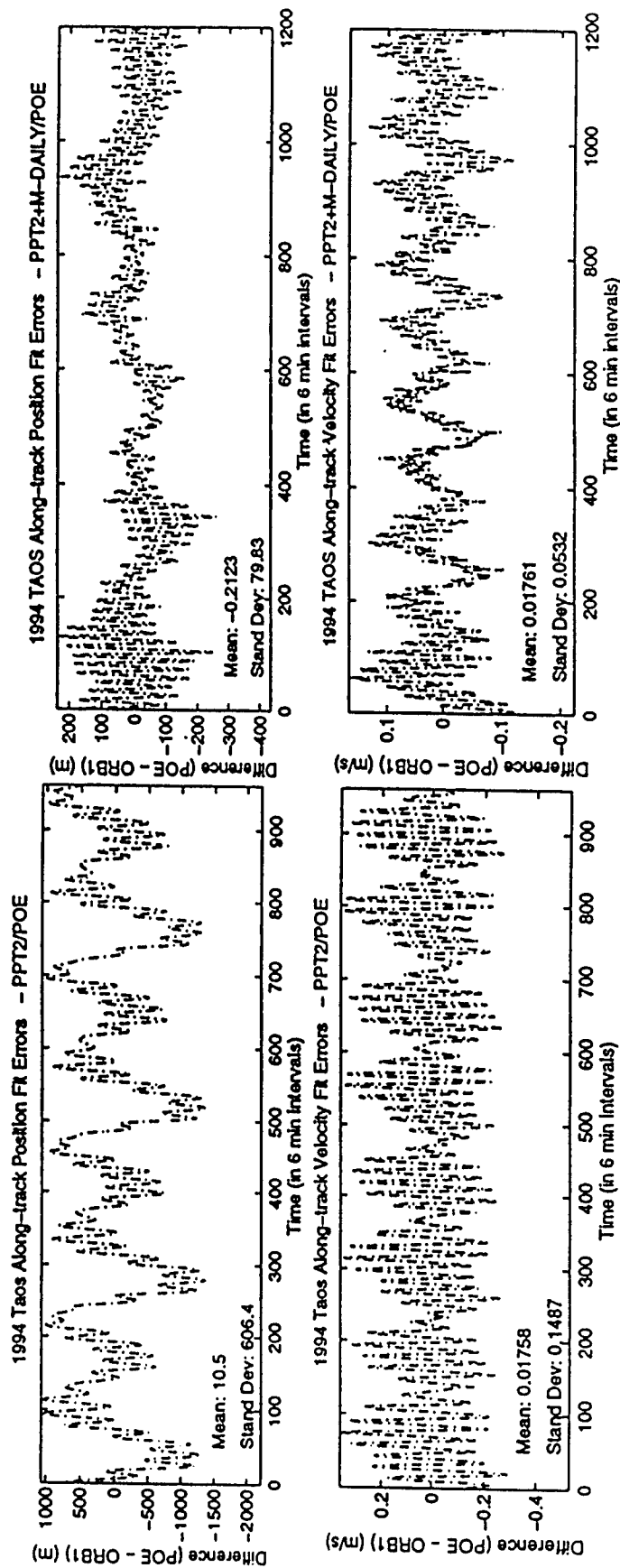


Figure 12. TAOS Along Track Differences vs. POE (PPT2 and PPT2-MDAILY)

TAOS SEMIMAJOR AXIS/ECC DIFFERENCES VS. POE (PPT2 AND PPT2 - MDAILY)

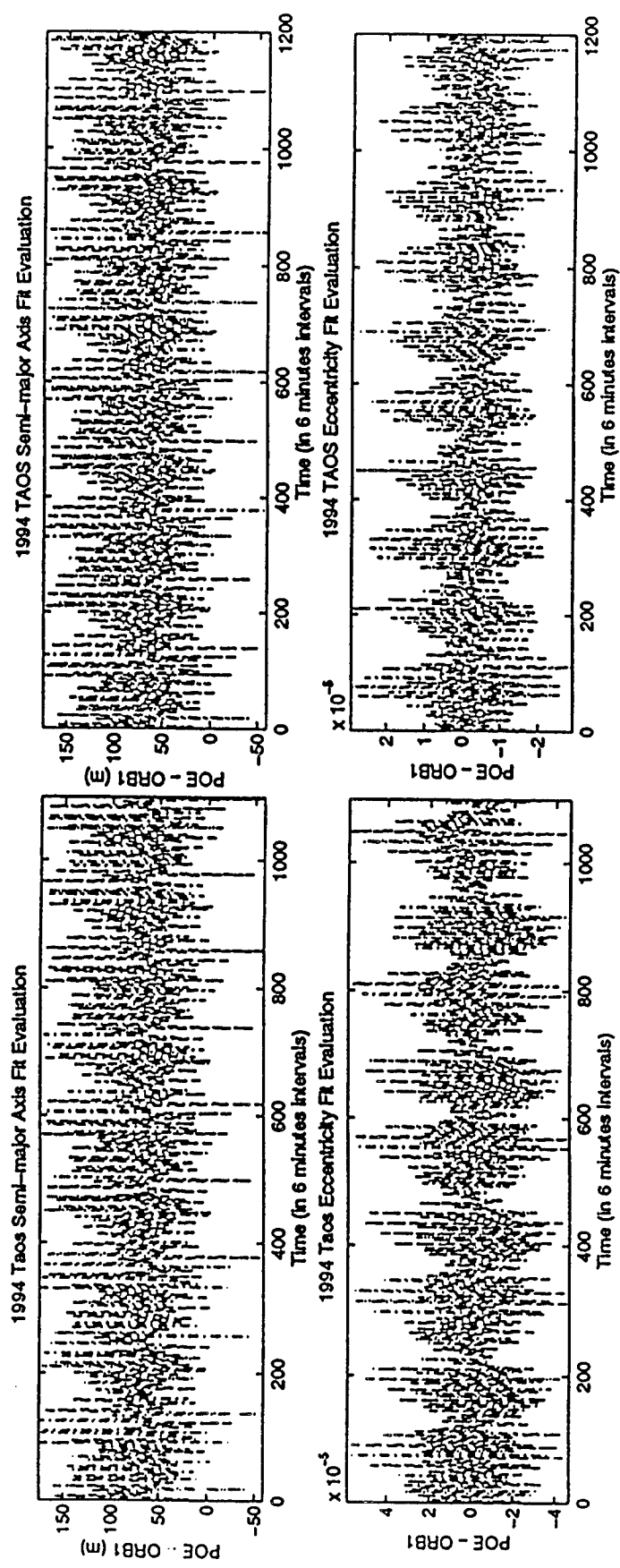


Figure 13 TAOS Semi major axis/eccentricity Differences vs. POE (PPT2 and PPT2-MDAILY)

TAOS INCLINATION / NODE DIFFERENCES VS. POE (PPT2 AND PPT2 - MDAILY)

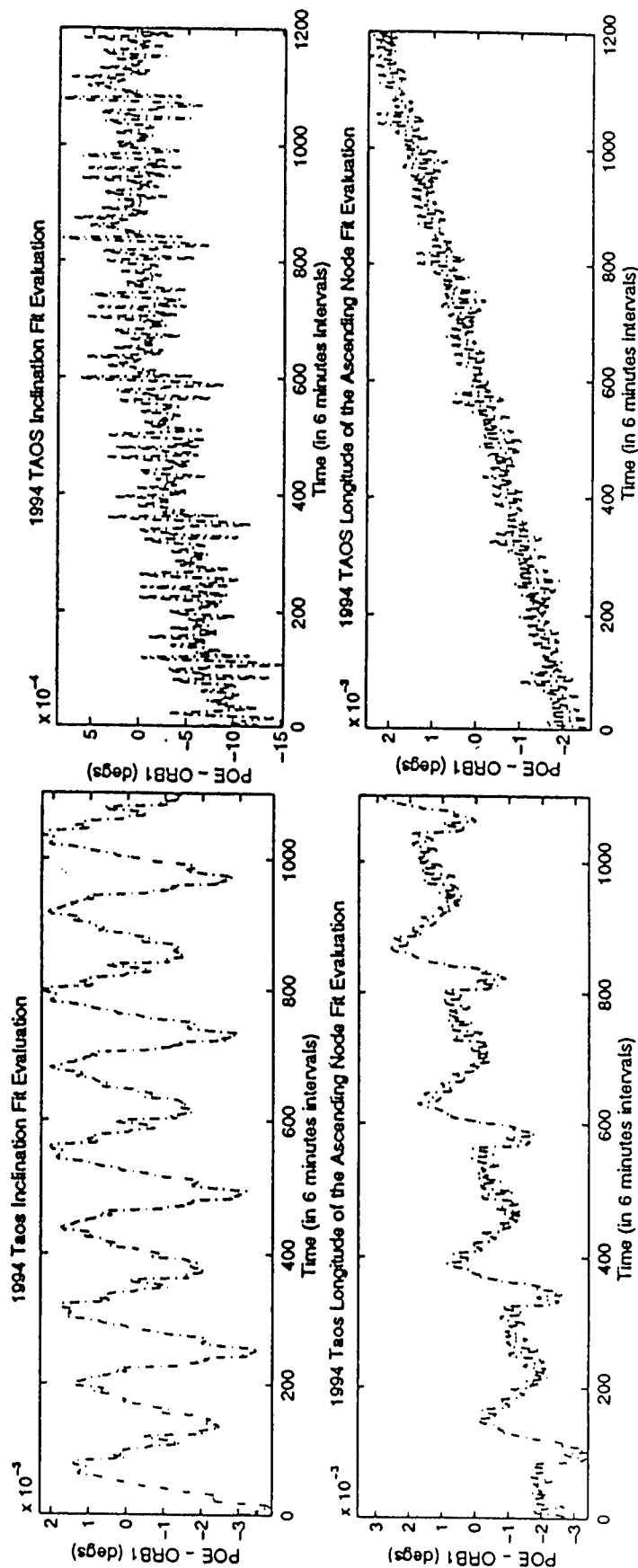


Figure 14. TAOS inclination/node Differences vs. POE (PPT2 and PPT2-MDAILY)

TAOS ARGUMENT OF LATITUDE DIFFERENCES VS. POE (PPT2 AND PPT2 - MDAILY)

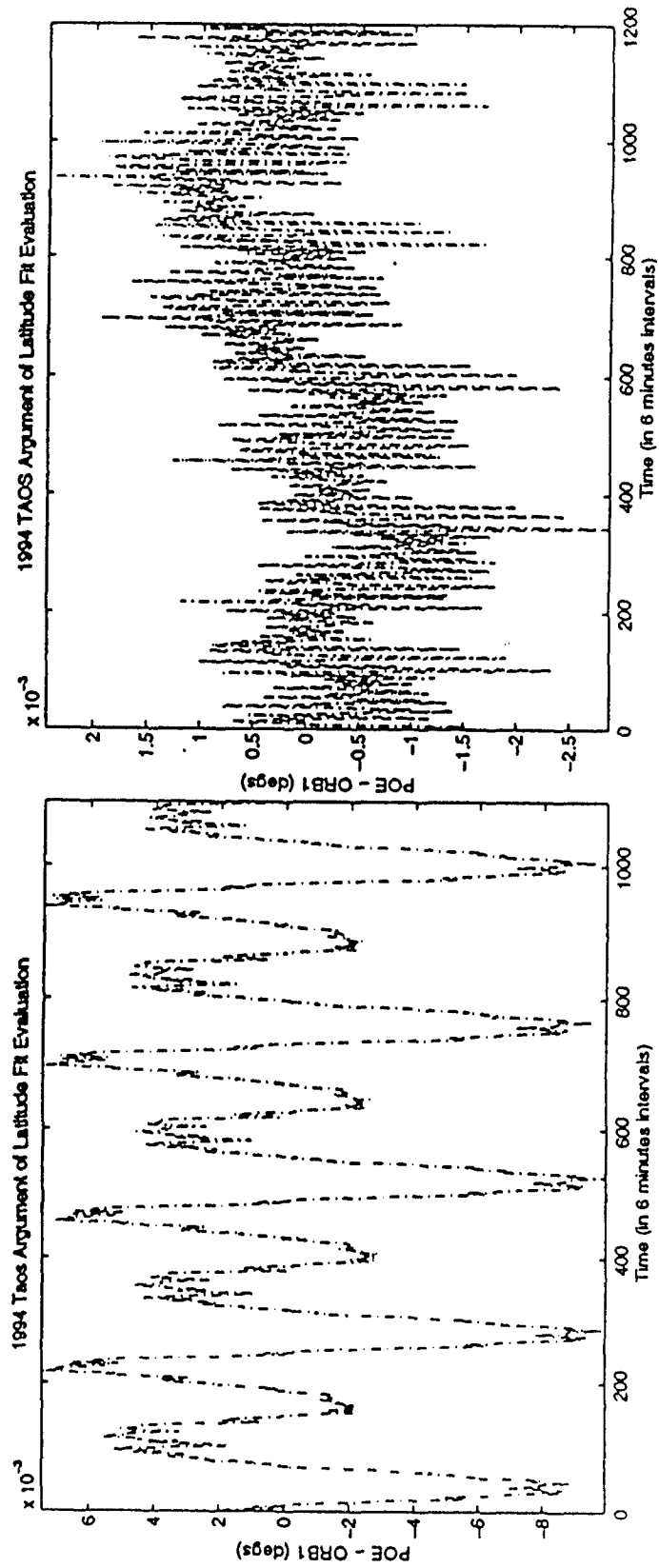
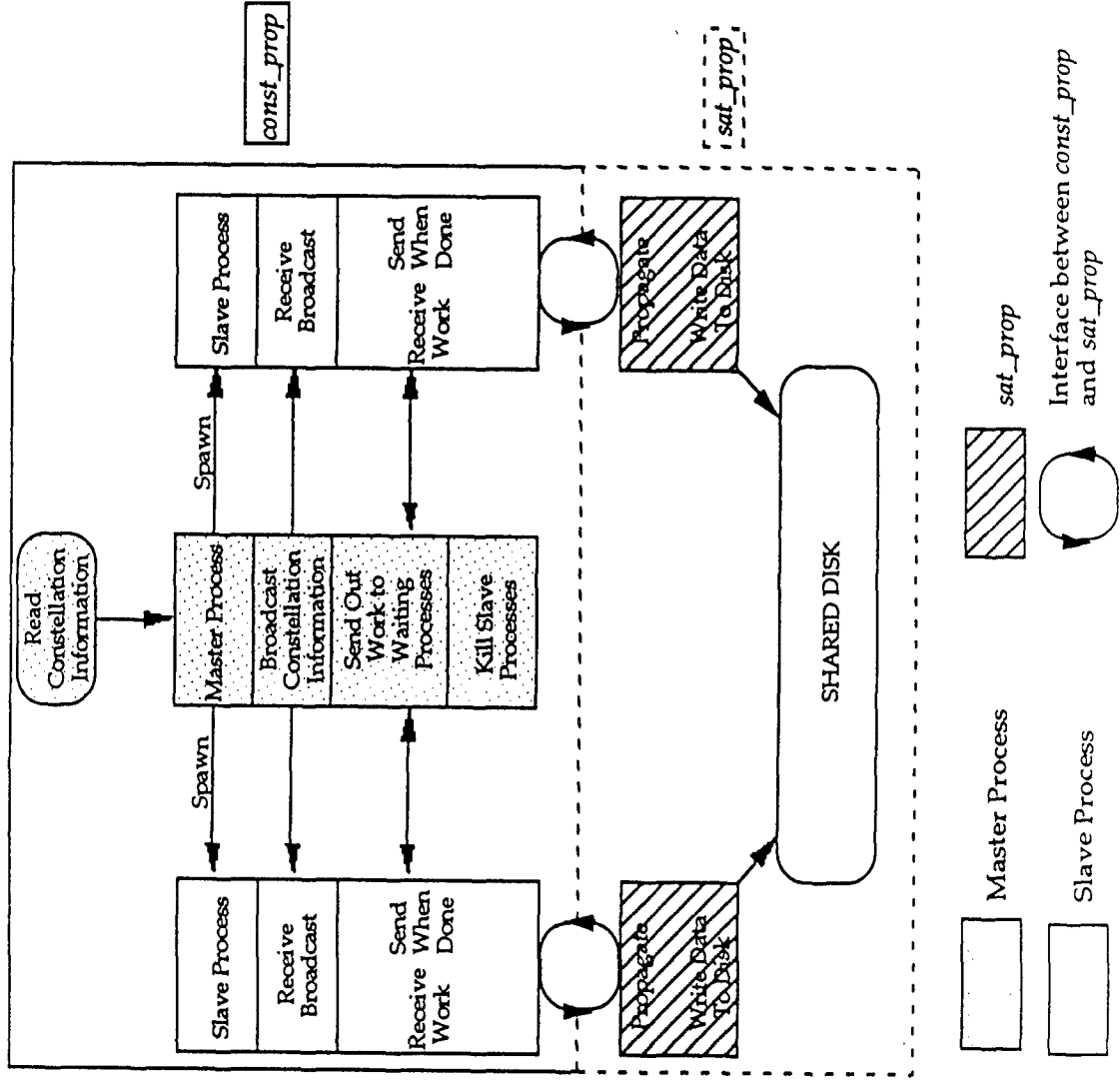


Figure 15. TAOS argument of latitude Differences vs. POE (PPT2 and PPT2-MDAILY)

OPPORTUNITIES FOR PARALLEL PROCESSING WITH SST

- Fine Grain Parallelism (one satellite)
 - Initialization
 - solution of the mean element equations of motion
 - Picard iteration with Chebyshev approximation
 - short-periodic motion
 - all short-periodic coefficients can be computed in parallel once the mean element interpolator has been established
- Output at Request time
 - at one output time,
 - all short-periodic coefficient evaluations can proceed in parallel
 - for multiple output times,
 - all mean element evaluations can proceed in parallel
 - all short-periodic coefficient evaluations can proceed in parallel
 - all osculating element assemblies can proceed in parallel
- Coarse Grain Parallelism (multiple satellite constellation)

PARALLEL VIRTUAL MACHINE / SEMIANALYTIC SATELLITE THEORY (PVM / DSST)



- **PVM / DSST combined with Genetic Algorithm for Optimization**
 - **very precise determination of frozen orbits**
 - **initial applications to constellation design**
 - **5 year propagation for 840 satellite constellation (1994-95)**

CONCLUSIONS

- Comprehensive perturbation theory described
 - comprehensive suite of force models
 - theory is based on the Generalized Method of Averaging
 - mean element and short periodic motion
 - all small parameters are treated as first order
 - some of the coupling between multiple parameters
 - some second order terms
 - multiple phase angle for third body
 - the theory makes extensive use of recursive analytic formulation
 - use of conventional (Jacobi polynomial) and non-conventional (Hansen Coefficients) Special Functions
 - modified Hansen coefficient formulation for high eccentricity
 - stable recursive flows identified for all the models
 - recursions designed for the original 21 x 21 implementation were sufficient for 50 x 50

CONCLUSIONS CONT'D

- Comprehensive theory cont'd
 - theory employs numerical averaging concept for atmospheric drag and solar radiation pressure
 - open to different density models
 - open to spacecraft-specific solar radiation pressure models
 - interpolator structure
- Recent extensions
 - 50 x 50 field
 - Solid earth tides
 - Integration coordinate systems
 - Earth Albedo model in progress
- Relationship between Semianalytical Theory and Canonical Theories is being explored
 - PPT2/Mdaily Theory
- Opportunities for Parallel Processing

FUTURE WORK

- Model refinements
 - J2-squared and J2-cubed
 - Ocean tides
 - additional coupling terms if required
- Continue to explore the interface between Canonical theories and Semianalytical
 - Hybrid PPT2/SSST
 - M-dailies
 - Tesseral Linear Combinations
 - additional Zonal terms in the secular and long periodic portion of theory
 - Application to other GP propagators
 - Open Space Catalog
- Satellite Constellation Control
 - parallel processing
- Software issues

U.S. RUSSIAN SPACE SURVEILLANCE WORKSHOP

SUMMARY AND CONCLUSIONS

In the closing discussion of the workshop, everyone concluded that the presentations were very useful. Both countries are seeking to solve the same problems and the truth is unique; however, different approaches are being taken. The work by the Russians on modeling atmospheric effects and using observations to generate real time corrections for atmospheric drag is particularly interesting. Similarly, the use of workstations and parallel processing by the US was of special interest.

It was suggested that we might identify common problem areas as cases for future discussions and communication between workshops. These are cases where both organizations have difficulty individually, or where cooperation could be immediately beneficial. The following items were identified for future attention:

- 1) Immediate answers concerning breakups or explosions in space.
- 2) Tracking breakups in GEO/GTO orbits.
- 3) Multiple simultaneous or overlapping break ups.
- 4) Calculation of dangerous conjunctions.
- 5) Untrackable hazards to other satellites.
- 6) Comparison of methods of orbit predictions used by Naval Space Command, Air Space Command, and Russian Scientific Research Center "Kosmos", and IAC "Vympel".
- 7) Reentry time and location predictions.
- 8) Comparison of atmospheric density modeling and parameter values.
- 9) Tests of comparable atmospheric models.
- 10) Creation of an observational database for long time periods for geostationary satellites. SRC "Kosmos" and Institute of Theoretical Astronomy (ITA) has initiated this activity in Russia.
- 11) Test methods of evaluating observational accuracies. Some Russian satellites have laser reflectors which could be used for calibration.
- 12) Comparing techniques of uncorrelated target processing.

- 13) Exchange observations of specific passive satellites.
- 14) Regular comparison of catalogs and resolution of differences detected.
- 15) Criteria for including objects in the catalog, especially intrackable or intermittently observed objects.
- 16) Add to catalogs or establish a separate catalog containing more information about objects; history of objects, technical make up of objects, subsystems.
- 17) Compare or develop models of breakups, circumstances that lead to breakups, breakup results analysis.
- 18) Exchange orbit model software for testing purposes.
- 19) More close cooperation between the RSSS and the US SSN in operational works on reentry SO, SO in contingency and other risk SO.

It was agreed that having specific people from each country identified to work on a specific topic would be the best way to accomplish progress between workshops. To accomplish this, it was agreed that communication would be maintained regularly between Dr. Stanislav Veniaminov and Dr. Kenneth Seidelmann and that individuals would be sought from each country to actively pursue cooperation on the given items.

Everyone agreed that the workshops are mutually beneficial. There is a need for the participants to get to know each other better; there are times when we don't understand each other, due to technical, linguistic, and cultural differences. However, from the two workshops it's clear that the communication is improving and that detailed exchanges on specific subjects would be beneficial to both countries.

G. Batyr and S. Veniaminov wrote in the review of joint activity in the proceedings of the workshop of 1994: "One of main and paramount objectives of our cooperation we consider adjusting sound contacts between US and Russian SSS both on the level of technical specialists and on the level of heads and leaders. And generally, it is a sheer abnormality and even indecency in the whole world there exist only two so powerful and unique space surveillance systems - yours and ours and between them there are no interaction. This situation should be urgently corrected".

LIST OF PARTICIPANTS

V. Boikov	ISC Vympel 4th str of 8 March, 4a Moscow 101000, Russia	Fax: 7-095-152-933
P. Cefola	Draper Laboratory Mail Station 86 555 Technology Square Cambridge, MA 02139	Fax: 617-258-1880 Tel: 617-258-1787 cefola@mit.edu cefola@draper.com
G. M. Chernyavskiy	Center for Program Studies 84/32 Profsoyuznaya Ul Moscow 17810 Russia	Fax: 7-095-420-2275 Tel: 7-095-333-1512 solom@febes.msk.su
S. Coffey	Naval Research Laboratory 4555 Overlook Ave. Washington, DC 20375	Fax: 202-404-7785 Tel: 202-767-2818 shannon.coffey@nrl.navy.mil
V. Dicky	SRC Kosmos home address: Apt. 73, 18 Korneychuka str. Moscow 127543, Russia	Fax: 7-095-184-1927 Tel: 7-095-184-1911 Tel: 7-095-406-7607 (home)
B. Kaufman	Naval Research Laboratory Code 8103 4555 Overlook Ave. Washington, DC 20375	Fax: 202-404-7516 Tel: 202-767-0513 kaufman@ssdd.nrl.navy.mil
Z. Khurtovsky	ISC Vympel 4th str of 8 March, 4a Moscow 101000, Russia	Fax: 7-812-272-7968
R. Kiladze	Institute of Theoretical Astronomy Kutuzova Quay 10 St Petersburg 191187, Russia	Fax: 7-812-272-7968 1099@ita.spb.su

A. I. Nazarenko	Center for Program Studies 84/32 Profsoyuznaya Ul Moscow 17810, Russia	Fax: 7-095-420-2275 solom@febes.msk.su
P. Schumacher	Naval Space Command Dahlgren, VA 22448-5180	Fax: 540-653-6148 Tel: 540-653-6170 schumach@nsc.navy.mil
P. K. Seidelmann	U.S. Naval Observatory Washington, DC 20392	Fax: 202-762-1516 Tel: 202-762-1441 Tel: 301-530-7923 (home) pks@spica.usno.navy.mil
S. Veniaminov	SRC Kosmos home address: Apt 282 Tayninskaya str 16-2	Fax: 7-095-184-1927 Tel: 7-095-231-7375 Tel: 7-095-184-1911 (home) sveniami@esoc1.iki.rssi.ru
E. Vovchyk	Lviv State University Ukraine	Tel: 0-322-728083 Tel: 0-322-754849 (home)
S. Wallace	Phillips Lab. VTA 3550 Aberdeen Ave., SE Kirkland AFB, NM 87117-5776	Fax: 505-846-8009 Tel: 505-846-7995 wallace@plk.af.mil
V. Yurasov	SRC Kosmos home address: Apt.59, 10 Magdanskaya Str. Moscow 129345, Russia	Fax: 7-095-184-1927 Tel.: 7-095-184-1911 Tel.: 7-095-184-5935 (home)

Translators

A. Krivov	St Petersburg University Astronomical Institute St. Peterhof St Petersburg 198904, Russia	Fax: 7-812-428-6649 Tel: 7-812-428-4163 krivov@celest.aispbu.spb.su
S. Rudenko	Main Astronomical Observatory Glolsiiv Kiev 252022, Ukraine	Fax: 38-044-266-2147 Tel: 38-044-266-4759 rudenko@mao.gluk.apc.org